THE THERMAL CONDUCTIVITY OF ELECTRICALLY - CONDUCTING LIQUIDS.

A Thesis Submitted To The University Of London

For The Degree Of Doctor Of Philosophy

By

M. Zalaf

B.Sc., M.Sc.

Department Of Chemical Engineering And Chemical Technology

Imperial College Of Science And Technology

LONDON S.W.7

April 1988

Abstract.

A new instrument for the measurement of the thermal conductivity of both electrically insulating and electrically conducting liquids, has been designed, built and commissioned. It is capable of operating in the temperature range of 30° - 100°C and pressure range of 0 - 0.5 GPa, with an associated accuracy of ±0.3% of the absolute thermal conductivity values.

The construction of this instrument, which is based upon the transient hot-wire principle, was implemented in two stages. The first stage was the design and construction of a new computer-controlled Wheatstone Bridge, that is capable of initiating a run, processing the results to yield the thermal conductivity of the liquid of interest. The new bridge was applied to liquids and gases previously measured in the laboratory, to assess and confirm its performance. The results were excellent and showed close agreement with earlier work.

The second phase was the construction of a new high pressure rig housing the purpose built thermal conductivity cells. The cells themselves were made of Inconel 625 alloy, to alleviate corrosion arising from the use with water and saline solutions to be measured. The cells were constructed so as to accomodate tantalum wires in place of the conventional platinum wires, which are not suitable for use with electrically conducting liquids, owing to current leakage. By employing tantalum wires anodically coated with their oxide, the electrically

conducting fluid can be electrically insulated from the wire without inducing an untoward thermal resistance.

Thermal conductivity data for a number of electrically insulating and conducting liquids have been determined over a wide range of pressures up to 500 MPa. They have been used to test a model of transport properties of liquids based upon a hard-sphere theory. For electrically insulating, non-polar fluids, the model represents the density dependence of the experimental data almost within experimental error, and leads to a reliable scheme for the interpolation among and extrapolation of the thermodynamic states and fluids covered in this study. For electrically conducting fluids, the importance of attractive molecular forces, means that the same scheme fails and a new approach becomes necessary.

ACKNOWLEDGEMENT

I would like to express my sincere thanks and gratitude to my supervisors, Prof. W.A. Wakeham and Dr H.J. Michels for their excellent guidance, counsel and patience throughout the course of this work.

Special thanks are due to Prof. C.A.N. de Castro, Dr K.E. Bett, Dr A.M.F. Palavra and Dr G.C. Maitland, all of whom provided invaluable advice during this work.

Special thanks to my colleagues, M. Ross, W. Cole, S.F.Y. Li, T. Retsina, B. Taxis, R. Craven, M. Lubbock and R.D. Trengove, all of whom contributed in their own ways to my progress in this work.

I also wish to extend my gratitude to M. Dix, R. Wood, I.W. Drummond, K. Dougan in the Electronics Workshop, and to the staff in the Chemical Engineering Workshop, K. Gurney,T. Stephenson, R. King and T. Pushman, all of whom contributed immensely to the construction of the thermal conductivity instrument.

TO MY PARENTS

Contents.

		Page
CHAPTER 1	INTRODUCTION.	10
CHAPTER 2	THEORY OF THE TRANSIENT HOT-WIRE METHOD	13
2.1	Theory Of The Experimental Technique	13
2.2	Effects Eliminated Entirely	19
2.2.1	Convection	19
2.3	Corrections Which Are Rendered Negligible	23
2.3.1	Finite Diameter Of The Wire	23
2.3.2	Radiation	24
2.3.3	Viscous Heating	28
2.3.4	Compression Work	29
2.4	Remaining Corrections	30
2.4.1	End Effects	31
2.4.2	The Outer Boundary Correction	32
2.4.3	Finite Heat Capacity Of The Wire	34
2.5	Effects Of An Insulation Layer On The Measurement Of The Thermal Conductivity Of Liquids	38
2.6	Effect Of Thermal Contact Resistance Between Metallic Wire And Insulation Layer	45
2.7	Variable Fluid Properties	47
2.8	Thermal Diffusivity	50
2.9	Summary Of Corrections	56
CHAPTER 3	APPARATUS DESIGN AND USE	60
3.1	Introduction	60

3.2	The Hot-Wire Cells For Electrically Insulating Liquids	61
3.3	The Hot-Wire Cells For Electrically Conducting Liquids	67
3.3.1	Anodization Of The Tantalum Wires	73
3.3.2	Effects Of Pre-existing Film On Adhesion Of Anodic Oxide To Its Substrate	75
3.3.3	Mechanism Of Oxide Formation	76
3.3.4	Cell Mounting	78
3.4	The High Pressure Equipment	79
3.5	Thermostats	87
3.6	Auxiliary Measurements	88
3.6.1	Resistance-Temperature Characteristics Of The Tantalum Wires	88
3.6.2	Wire Diameter Measurements	91
3.7	Filling Procedure	92
3.8	Electronic Apparatus	93
3.8.1	Circuit Analysis	97
3.8.2	Precision Of The Resistors And Temperature Rise	100
3.8.3	Limitation Of R_9 and R_{10} In The Circuit	102
3.8.4	Electrical Noise	102
3.8.5	The Comparator	104
3.8.6	The Working Equations	107
3.8.7	The Heat Flux From The Wires	113
3.9	Testing The Bridge	116
3.10	Data Acquisition And Handling	117
CHAPTER 4	EXPERIMENTAL RESULTS	118
4.1	Introduction	118
4.2	Results	119

4.2.1	The Check Measurements On Toluene	119
4.2.2	Carbon Tetrachloride	125
4.2.3	n-Pentane	126
4.2.4	o-Xylene	128
4.2.5	Oct-1-ene	128
4.2.6	Ethylbenzene	129
4.3	Correlation Of The Experimental Results	155
4.4	Results For Water	171
4.4.1	Accuracy Of The Measurements On Water	172
4.4.2	Comparison With Other Data	180
CHAPTER 5		184
5.1	Introduction	184
5.2	Summary Of Available Methods For The Correlation Of Thermophysical Properties	185
5.2.1	The Monte-Carlo Method	185
5.2.2	The Molecular Dynamics Method	187
5.2.3	Comparison Of Molecular Dynamics Simulations And The Monte-Carlo Methods	191
5.2.4	The Brownian Motion Theory	192
5.3	Van Der Waals Theory	196
5.3.1	Smooth Hard-Sphere Theory	196
5.4	Applications Of Exact Hard-Sphere Expressions	206
5.4.1	Introduction	206
5.4.2	Self-Diffusion	207
5.4.3	Viscosity For Monatomic Fluids At Supercritical Temperatures	210
5.4.4	Thermal Conductivity Coefficients For Monatomic Gases At Supercritical Temperatures	211

5.5	Rough Hard-Sphere Model For Polyatomic Fluids	214
5.5.1	Introduction	214
5.5.2	Application Of The Rough Hard-Sphere Theory To Diffusion	216
5.5.3	Viscosity Coefficients Of Polyatomic Fluids	218
5.5.4	Thermal Conductivity Coefficients For Polyatomic Fluids	222
5.6	The Correlation	232
5.6.1	Experimental Data	233
5.6.2	The Density Dependence Of The Thermal Conductivity	234
5.6.3	n-Pentane	235
5.6.4	Oct-1-ene	241
5.6.5	Carbon Tetrachloride	247
5.6.6	Ethylbenzene	255
5.6.7	The Xylene Isomers	260
5.7	The Universal Correlation	264
CHAPTER 6	CONCLUSION	278
APPENDICES		
Appendix 1		282
Appendix 2		291
Appendix 3		300
REFERENCES		304
LIST OF PUBLICATIONS		316

Chapter 1

Introduction

Data for the thermophysical properties of fluids and, in particular, the transport properties of liquids, are required for the design and operation of many types of process plant. The impossibility of carrying through a measurement programme to determine *all* the properties of *all* the systems of interest over *all* thermodynamic states means that an alternate strategy to fulfil this need must be found. The most efficient strategy is began with the rather careful measurements of high accuracy of the properties of a limited number of selected systems. The subsequent application of available theory to the accurate data then permits refinement and development of the theory and its parameters, so that when the same theory is applied to systems for which no measurements exist, the properties may be predicted reliably. Quite obviously, the accuracy of such predictions can never match that of the best direct measurements, but it can often be sufficient for engineering purposes. At the same time, this strategy leads to an increased understanding of the relationship of the thermophysical properties to the underlying microscopic properties of fluids.

Among the transport properties of fluids, the thermal conductivity has proved the most difficult to measure accurately. Indeed for liquids, it is rather easy to find examples of discrepancies as large as 100% in the thermal conductivity of a single fluid reported by different authors. The inevitable confusion arising from this situation has undoubtedly contributed to the relatively slow development of

theories of transport properties in liquids. The present thesis continues the acquisition of a body of accurate data for the thermal conductivity of electrically insulating liquids over a wide range of conditions, as a contribution to the first part of the strategy set out above. In addition, a new instrumental development is described that makes it possible to begin the same process for electrically conducting liquids. It has also proved possible to begin the application of available theoretical methods to the interpolation and extrapolation of the experimental data obtained according to the second and third parts of the strategy set out above.

The principal difficulties with early measurements of the thermal conductivity of liquids were the neglect of, or improper correction for, the occurence of natural convection and radiative absorption of heat. Both of these processes inevitably accompany the heat conduction process in any measurement made in the earth's gravitational field and invalidate the measurement of the thermal conductivity. In the form in which it has conventionally been employed, the technique is suitable only for fluids that are non-polar and electrically insulating. In an effort to extend the applicability of the technique to electrically conducting liquids, a number of developments have had to be made which are described in this thesis. Such an extension is essential if measurements are to be made on systems auch as aqueous and alcoholic salt solutions, molten salts and liquid metals. Because such materials are receiving increased attention as heat transfer media in fields as varied as refrigeration cycles, nuclear reactors and energy storage systems, [1-10], there is evidently a need for reliable experimental measurements of a few carefully selected systems of each type to

initiate the same predictive process that has proved successful for insulating liquids.

In order to apply the transient hot-wire technique to electrically conducting liquids, it is necessary to modify the apparatus in several respects. In this thesis, these modifications, the adaptation of the theory of the method to encompass them and the application of the new instrument are described in detail. In addition the first measurements with the new instrument on water are presented.

Chapter 2

2.1 Theory Of The Experimental Method.

In the transient hot-wire method, the thermal conductivity of a liquid is deduced from the temperature history of a very thin, vertical, metallic wire, surrounded by the test fluid, which becomes the source of a uniform, radial heat flux as a result of a square voltage step applied across its ends. The temperature rise of the metallic wire is accurately measured as a function of time, and the thermal conductivity of the fluid is established from a theoretically based relationship.

Up to 1970, there was a slow development of the transient hot-wire technique. But with the advent of computers and the advancement of electronics, serious consideration was given to this technique [10].

The starting point for the formulation of the theory of this technique is an "ideal" instrument of this type [11,12]. This ideal instrument consists of an infinitely long, line-source of radial heat flux, q, which is supposed to lose heat only by conduction, initiated at time, t=0, and immersed in a fluid, initially at temperature, T_o, of infinite extent, as illustrated in figure 2.i. The line heat source is coincident with the axis of a cylindrical coordinate system (r,z,θ).

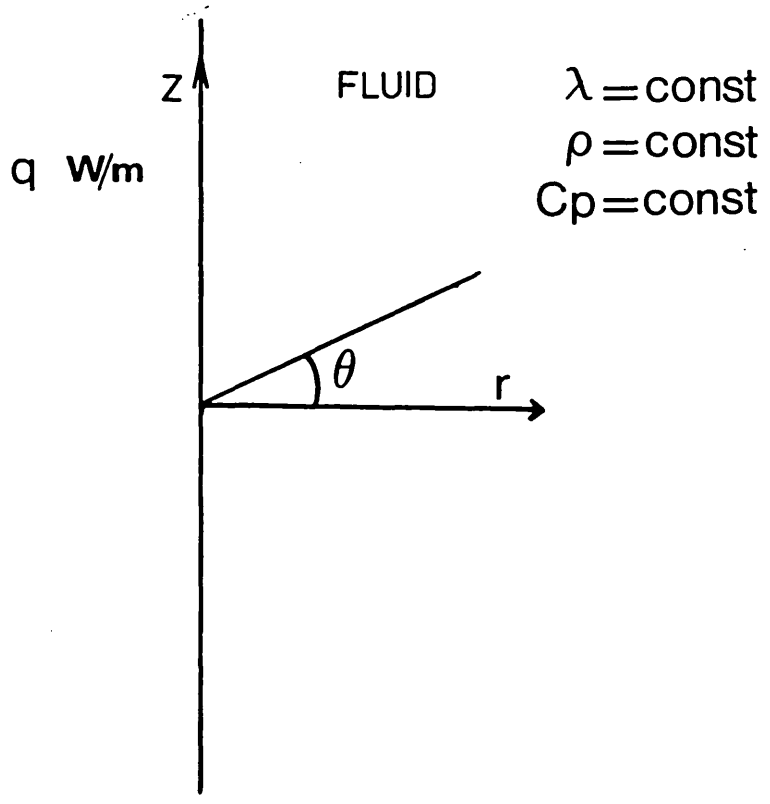


Figure 2.i. The idealized experimental arrangement.

The temperature history of the fluid at a radial position, r, from the axis of the system is given by the solution of the non-steady state conduction equation:

$$\frac{\delta T}{\delta t} = \kappa \nabla^2 T \qquad (2.1)$$

where $\kappa = \lambda / \rho C_p$ is the temperature independent thermal diffusivity of the fluid, together with the definition of the fluid temperature rise :

$$\Delta T(r,t) = T(r,t) - T_o \qquad (2.2)$$

where T_o is the equilibrium temperature of the fluid.

The thermal coductivity of an isotropic fluid is formally defined by the Fourier equation of conductive heat transfer:

$$Q = -\lambda \nabla T \qquad (2.3)$$

where Q is the three-dimensional heat flux and T the local fluid temperature. The solution of the above equation (2.3) is subject to the initial and boundary conditions:

<u>initial conditions</u>:

at $t \leq 0$ and any r position, $\Delta T(r,t) = 0$ (2.4)

boundary conditions:

at $r = 0$ and any $t \geq 0$ $\quad \underset{r\to 0}{\text{Limit}} \; \frac{r\delta T}{\delta r} = -\frac{q}{2\pi\lambda}$ (2.5)

and at $r = \infty$ and any $t \geq 0$ $\quad \underset{r\to \infty}{\text{Limit}} \; \Delta T(r,t) = 0$ (2.6)

with the additional constraint that λ = constant.

The temperature rise of a point in the fluid $\Delta T_{ideal}(r,t)$ is given by [13]:

$$\Delta T_{id}(r,t) = \frac{q}{4\pi\lambda} . E_1\left[\frac{r^2}{4\kappa t}\right] \qquad (2.7)$$

where

$$E_1(x) = \int_x^\infty \frac{e^{-x}}{x}\, dx = -\gamma - \ell n\, x + x + 0(x^2) \qquad (2.8)$$

where

$x = r^2/4\kappa t$ and γ =Euler's constant (0.5772156649)

For small values of $(r^2/4\kappa t)$, the exponential integral E_1 may be expanded to yield, at any radial location a,

$$\Delta T_{id}(a,t) = \frac{q}{4\pi\lambda} \ln\left\{\frac{4\kappa t}{a^2 C} + \frac{a^2}{4\kappa t} + \ldots\right\} \qquad (2.9)$$

In the ideal model of the experimental method, this temperature rise is identified with that of the source of the radial heat flux, q, were it of finite radius a, which is such that, for sufficiently long times, the second term in the above equation is rendered negligible by comparison with the first.

Thus, for sufficiently small values of $(a^2/4\kappa t)$, the thermal conductivity of the fluid can be obtained, from the slope of the experimental line ΔT vs $\ell n\ t$ according to the relation:

$$\Delta T_{id}(a,t) = \frac{q}{4\pi\lambda}\,\ell n\left[\frac{4\kappa t}{a^2 C}\right] \qquad (2.10)$$

without a knowledge of the wire radius or the thermal diffusivity of the test fluid.

When performing transient measurements with a hot-wire instrument, there are inevitable departures in several ways from the ideal model discussed above. It is imperative that the design of the practical instrument deviates as little as possible from the ideal case. This means that all corrections to the working equation of the ideal model should be small and that some should be rendered entirely negligible. In this way, it is possible to retain equation (2.10) as the working equation for the interpretation of the raw experimental data subject to small corrections, which are readily estimated. The retention of equation (2.10) then provides a means of confirming the correct operation of the hot-wire instrument. Only if the heat transfer is

achieved by pure conduction, will the relationship between the temperature rise of the heat source and the time, remain of the form of equation (2.10). Thus, it is possible to detect experimentally the onset and effects of, for example, convective heat transport in the fluid, if a departure from linearity between ΔT and $\ell n\ t$ is observed. The effect of this phenomenon can usually be eliminated from measurements by ensuring that the transient run is of sufficiently short duration, so as to render the additional heat transfer caused by convection negligible. Typically a time of the order of one second is sufficient for this purpose.

To simplify the following analysis of the assumptions and corrections employed, the discussion is separated into three main categories. First, corrections that are eliminated entirely will be discussed. Such corrections are eliminated by careful design and mode of operation of the equipment. Secondly, corrections that are rendered negligible will be presented. It is implied that each particular effect constitutes a correction to ΔT_{id} which is not more than 0.01%. Finally, the remaining corrections will be discussed, generally these corrections will be of a magnitude such that they must be applied to all experiments.

The following analysis will assume that the temperature rise of a finite segment of an infinite wire as a function of time is available from experiments. It has been ascertained that the required corrections to ideality are small [14,15]. The combined effect can be taken to be simply additive:

Hence,

$$\Delta T_{id} = \Delta T + \sum_i \delta T_i \qquad (2.11)$$

where δT_i is a temperature correction due to the physical system in one respect being non-ideal, and ΔT is the measured temperature rise of the finite segment of the wire.

2.2 Effects Eliminated Entirely:

2.2.1 Convection.

Convection, which is a major source of errors in most other methods [16-23] deserves to be examined carefully for this method. It is necessary to distinguish between the two types of convective transfer. One type is due to temperature gradients along the vessel created if the upper regions of the wire enclosures are colder than the lower regions. This kind of convection can be avoided by ensuring that the top part of the wire enclosure is at a slightly higher temperature than its bottom part.

The second type of convection is due to the heat dissipation in the wire. Considering figure 2.ii, the current in the wire induces a heat flow in the fluid such that temperatures T_1 and T_2 are higher than T_1' and T_2'.

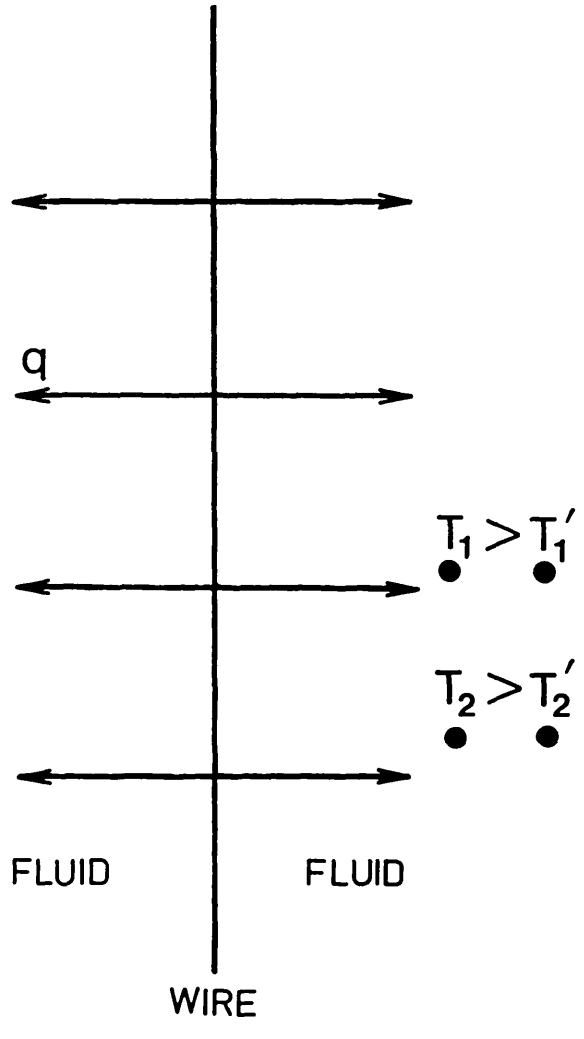


Figure 2.ii. Temperature Profile Around The Wire.

However, this results in temperature T_2 being higher than T_1' and thus the conditions for the onset of convection are established. The experimental conditions can be so arranged that the characteristic time required for the bouyancy forces to accelerate the fluid, and thus appreciably affect the rate of heat loss from the wire, is higher than the experimental times employed. This dictates that the experimental times can be chosen to eliminate convective heat transfer entirely. However, the transient hot-wire method has the additional advantage that should convection occur, it can be immediately detected.

A significant influence from convection causes the wire temperature to increase less rapidly owing to the convective heat transfer mechanism and leads to an appreciably lower plateau than $\Delta T_\infty - \delta T_{OB}$ (δT_{OB} represents the outer boundary correction [section 2.4.2]). Furthermore, this effect results in a sudden increase in the apparent value of the thermal conductivity. This manifests itself, as depicted in figure 2.iii, as a curvature in a plot of the apparent thermal conductivity as a function of time through a run.

Because the phenomenon of convective flow in a transient hot-wire cell is not amenable to exact analysis, conditions for measurements are always chosen so that such curvature is not observed. Thus, the experiment itself is employed to confirm the absence of convective heat transfer.

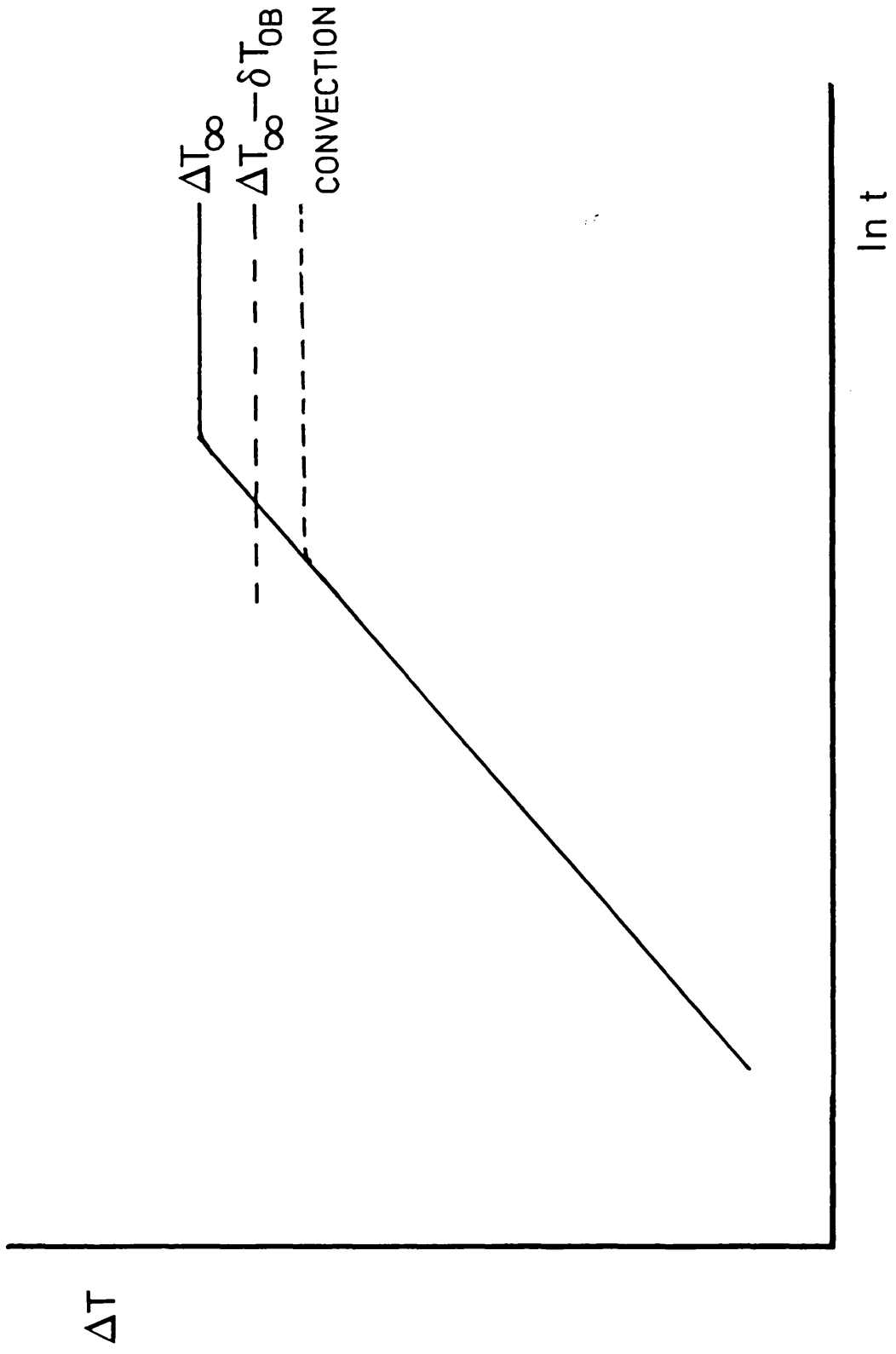


Figure 2.iii. Effect of Convection on Temperature Rise.

2.3 Corrections Which are Rendered Negligible:

2.3.1 Finite Diameter of the Wire.

Evidently, in any real experiment, the wire employed as the heat source must be of a non-zero radius, a. Thus, the previous boundary condition has to be modified to r = a, and at any $t \geq 0$:

$$\frac{\partial T}{\partial r} = - \frac{q}{2\pi\lambda a} \qquad (2.12)$$

The solution of the conduction equation under these conditions (page 338 of Carslow and Jaeger [24]), reads:

$$\Delta T(r,t) = \frac{-q}{\pi^2 a\lambda} \int_0^\infty (1 - e^{-kdu^2 t}) \times \left\{ \frac{J_0(ur).Y_1(ua) - Y_0(ur).J_1(ua)}{u^2(J_1^2(ua) - Y_1^2(ua))} \right\} du \qquad (2.13)$$

For small values of $(r^2/4\kappa_d t)$, the ideal solution is recovered as:

$$\Delta T(r,t) = \frac{q}{4\pi\lambda} \ell n \left[\frac{4\kappa_d t}{r^2 C} \right] + O(a^2/\kappa_d t) \qquad (2.14)$$

The effect of the last term can be made small (0.01%) by employing a wire of small radius.

2.3.2 Radiation:

In deriving the working equation,

$$\Delta T(a,t) = \frac{q}{4\pi\lambda} \ell n\left[\frac{4\kappa t}{a^2 C}\right] \qquad (2.15)$$

it was assumed that heat transfer occured entirely by a conductive mechanism. In reality, there exists two types of heat transfer which take place. These are conductive and radiative heat transfer.

The error incurred due to radiation can be rendered negligible if the test fluid is transparent, and the temperature rise is kept small (<5K). Based on the assumption that the fluid is transparent, the radiative heat flux at the surface can be shown to be:

$$Q_r = A_a E_a F_{ab} - \alpha A_b E_b F_{ba} \qquad (2.16)$$

where A and E refer to the surface area and emmisive power of the wire surface respectively. The subscripts a and b denote the surface of the wire and the surface of the cell. α is the absorptivity of the cell.

Using reciprocity, the view factor F_{ba} is found as:

$$F_{ba} = \frac{A_a}{A_b}.F_{ab} = \frac{A_a}{A_b} \qquad (2.17)$$

with $F_{ab} = 1$

Hence

$$Q_r = A_a \ (E_a - \alpha \ E_b) \qquad (2.18)$$

or

$$q_r = 2\pi a \ (\ \epsilon\sigma T_a^4 - \alpha\sigma T_b^4 \ ) \qquad (2.19)$$

where ϵ is the emissivity of the wire and σ is the Stefan-Boltzmann constant.

If it is assumed that

$$\epsilon \approx \sigma \qquad (2.20)$$

$$q_r = 2\pi a\epsilon\sigma \ (\ T_a^4 - T_b^4 \ ) \qquad (2.21)$$

$$q_r = 8\pi a\epsilon\sigma \ T_o^3 \ \Delta T \ (a,t) \qquad (2.22)$$

and from equation (2.10)

$$\frac{\delta T_R}{\Delta T} = \frac{q_R}{q} = \frac{8\pi a\epsilon\sigma T_o^3}{q} \ \Delta T(a,t) \qquad (2.23)$$

The resulting correction is negligible in the present apparatus.

In the case of fluids which absorb and re-emit radiation, there

has been only one exact solution of the full integro-partial-differential equation governing simultaneous conduction and radiation [14,25]. In addition, there have been a number of approximate analytic treatments of the problem [26-28]. These studies indicate that the effects due to radiation are smaller in the transient measurement techniques than in those operated at steady state [29-39,40]. Since the aim of the present work is to perform thermal conductivity measurements with an accuracy of a fraction of 1%, it is clear that these approximate analyses are inadequate for the present purpose. We therefore make use of the numerical solution of Menashe and Wakeham [25], in the manner described by Nieto de Castro et.al.[41].

Menashe and Wakeham [25] carried out a full numerical solution of the full radiation-conduction heat transfer equation for the transient hot-wire cells, with dimensions similar to these employed here. The study was carried out for a mildly absorbing fluid and in such a manner that the magnitude of each term in the full equation of transfer could be evaluated.

$$\rho C_p \frac{\partial T}{\partial t} = \lambda \nabla^2 T + Q'_{V->dV_i} + Q'_{A_1->dV_L} + Q'_{A_2->dV_i} - 4K_i E_i \qquad (2.25)$$

In this equation, the Q' are the heat flux gradients, V denote the fluid volume, A_1 the inner (wire) surface, A_2 the outer (cell) surface and dV_i a volume element. In addition, K_i is the absorption coefficient of the (grey) fluid and E_i the black body radiative flux.

For cells with the dimensions of those employed here, and for the time scales of interest, Nieto de Castro et.al. [41] showed that the dominant term of these arising from radiation was always the last on the right hand side of the above equation, and demonstrated that this arose from the very large temperature gradients induced in the experiment even though the absolute temperature rise was small. Subsequently they neglected all the terms Q' in equation (2.24) and were able to obtain an analytic solution to the resulting equation. They found that the temperature rise of the wire could be written as:

$$\Delta T = \frac{q}{4\pi\lambda}\left[1 + \frac{Br_1^2}{4\kappa}\right]\ell n\left[\frac{4\kappa t}{r_1^2 C}\right] + \frac{Bqr_1^2}{16\pi\kappa\lambda} - \frac{Bqt}{4\pi\lambda} + O[(Bt)^2, r_1^2/4\kappa t] \qquad (2.25)$$

which implies that for certain values of the radiation parameter B,

$$B = \frac{16\ K\ a^2\ \sigma\ T_o^3}{\rho\ Cp} \qquad (2.26)$$

a curvature of the line ΔT vs $\ell n\ t$ would be observed as a result of radiation.

It is not, in general, possible to evaluate the parameter B from independent optical studies of absorption under all the conditions of interest. Consequently, a different approach has been suggested by

Nieto de Castro et.al. [41] which is followed here - it is similar in spirit to that employed for the examination of convection.

If the radiation parameter B is sufficiently small, then the curvature in the line of ΔT vs ℓn t will be negligible. In which case, it can be seen that the effect of radiation on the thermal conductivity determined from the slope of ΔT_{id} vs ℓn t is negligible. It follows that the absence of any systematic curvature in the line ΔT vs ℓn t implies the absence of any significant radiation effect. This will be shown to be the case for all of the measurements reported here. If there should be a residual curvature, equation (2.26) can of course always be employed to estimate the parameter B, and subsequently used to correct the experimental data.

2.3.3 Viscous Heating.

As mentioned earlier, the temperature gradient in the fluid inevitably gives rise to a velocity field. This velocity field in turn can cause viscous dissipation in the fluid leading to local temperature increases and a consequent reduction in the heat loss from the wire.

Healy et.al., [13] showed, by solving the energy balance equation, and obtaining an approximate formula for the effect of viscous heating on the temperature rise of the wire:

$$\delta T_{visc} = (q/4\pi\lambda)^2\{Pr\}\beta^2 g^2 t^2 \; / \; 2T_0^2 C_p \qquad (2.27)$$

For liquids where the Prandtl number, Pr ≈ 10, $\lambda \approx 0.15$ Wm^{-1} K^{-1}, and $C_p \approx 2000$ J Kg^{-1} K^{-1}, it was shown [14] that for experimental conditions employed in the transient hot-wire measurements, q ≈ 0.5 Wm^{-1}, t ≈ 1s and $T_0 \approx 350$ K, this correction amounts to less than 0.01% of the temperature rise, and is therefore negligible.

2.3.4 Compression Work

In the ideal model, the outer radius b, as well as the axial length L of the cell are assumed to be infinite. In reality, the hot-wire is accommodated in a cylinder of finite dimensions, (constant volume $V = nb^2L$, and constant mass m) and the fact that the heat is introduced into it, causes the pressure, P, to change with time. Thus, elementary cylindrical expansion waves spreading outwards with the velocity of sound result in essentially constant pressure in space but which changes with time.

An approximate analysis of this effect produces a correction to the temperature rise of the wire as [13, 42]:

$$\delta T_c = \frac{q l R t}{\rho C_p C_v V} = -\left[\frac{qR}{\rho C_p C_v}\left\{1 - e^{-b^2/4\kappa t}\right\} + \frac{qR}{4q\lambda} \cdot E_1(b^2/4\kappa t)\right] \qquad (2.28)$$

with R being the universal gas constant, V the volume of the containing vessel, and l the length of the wire. C_p and C_v are the

heat capacities of the fluid at constant pressure and constant volume respectively. The correction may be rendered negligible by employing a sufficiently large container for the gas [13]. In the case of liquids, this effect can be neglected completely because of the much lower compressibility.

2.4. The Remaining Corrections

The final group of corrections that must be considered are those that are sufficiently large to warrant application to the elucidation of the temperature rise of the wire. They arise from the difference between conditions at the inner wall (the wire surface), the outer wall and the temperature dependence of the fluid properties. In part, some of the corrections are connected with the desire to employ the metallic heat source as its own temperature monitor [13, 43–48]. The intention of the design is to make all of these corrections sufficiently small, that they can be estimated with adequate accuracy to ensure that their application has a negligible effect on the thermal conductivity of the fluid.

2.4.1 End Effects.

In the idealised model, the wire is assumed to be infinitely long. In practice, it cannot be infinitely long, since the wires are attached to relatively massive supports at either end, to provide the electrical connections. These connections give rise to departures from ideality, known as end effects. Healy [13], Haarman [49] and Blackwell [50], have provided different approximate analyses of these end effects. Both approaches recommended that such effects are best eliminated experimentally.

The apparatus used employs two wires which are constructed so as to be as near as identical (apart from their lengths) as is practically possible. They are both surrounded by the same fluid, and both are subjected to the same heat dissipation per unit length, due to the same current passing through both wires. The difference in resistance of the two wires, which can be determined experimentally, then gives, to within the required accuracy, a measurement of the temperature of a hypothetical, finite segment of an infinitely long wire. The length of this segment being equal to the difference in the lengths of the two wires. Thus, the end effects of the two wires can be eliminated by a practical cancellation.

This cancellation requires, that apart from their lengths, the wires must be identical. This, in practice, is impossible due to method of manufacture of the wires, their diameter is subject to fluctuation over their lengths. It is also not possible to duplicate the

spot-welded connections (see Chapter 3) to the wire ends, thus introducing further dissimilarities. However, provided the resistances per unit length of the two wires differ from each other by less than 0.8% , then an analysis given by Kestin and Wakeham [46] can be used. From the analysis, the measured temperature rise of the middle portion of the long wire can then be calculated. This temperature rise is shown by Kestin and Wakeham [46] to correspond, within the required accuracy, to the temperature rise of an infinitely long wire.

2.4.2 The Outer Boundary Correction.

The mathematical model used to obtain the idealised temperature rise of the fluid as a function of time, assumes that fluid to be infinite in extent. This is not the case, and an outer concentric cylindrical boundary at r = b exists owing to the need to contain the fluid.

The existence of this outer boundary will alter the temperature field, and a correction to the measured temperature rise is required, in order to recover the necessary idealised temperature rises, through which the thermal conductivity is calculated. It is expected that the correction due to the outer boundary will be small, and will increase with time. This is because, in the idealised model, at small times, the temperatures of elements of the fluid, at the position which would be occupied by the outer boundary in the real system, will be very close to the initial temperature of the fluid. The real and idealised models would therefore be very similar at small times, but, as these elements

in the idealised model increase in temperature with time, the effect is expected to increase.

To obtain the deviation due to the outer boundary, the equation,

$$\frac{\partial T}{\partial t} = \frac{k}{r}\frac{\partial}{\partial r}\left[\frac{r\partial T}{\partial r}\right] \qquad (2.29)$$

must be solved subject to the initial condition:

$$\Delta T(0 \leq r \leq \infty , t \leq 0) = 0 \qquad (2.30)$$

and boundary condition (2.5):

$$\lim_{r\to 0}\left[\frac{r\partial T}{\partial r}\right] = -\frac{q}{2\pi\lambda} = \text{constant} \qquad t \geq 0$$

and

$$\Delta T (r_b , t \geq 0) = 0 \qquad (2.31)$$

The second boundary condition implies that the outer boundary is kept at the initial condition In reality, the boundary cylinder is relatively massive, and made of a metal with a large thermal conductivity, so making this an acceptable and valid approximation. The asymptotic form of the solution as derived by Fischer [51] is:

$$\Delta T(a,t) = \frac{q}{4\pi\lambda}\left\{ 2\ell n(b/a) - \sum_{\upsilon=0}^{\infty} e^{-g_\upsilon \kappa t/b^2} \left[\prod_{\upsilon} Y_0(g_\upsilon)\right]^2 \right\} \tag{2.32}$$

where g_υ are the consecutive roots of $J_0(g_\upsilon) = 0$

This is subject to $b/a >> 1$ and $4\kappa t/a^2 >> 1$.

It can be seen that the ideal solution can again be recovered if an outer boundary correction is used, which results in a correction δT_1 to the idealised temperature rise of:

$$\delta T_1 = -\frac{q}{4\pi\lambda}\left\{ \ell n\left[\frac{4\kappa t}{b^2 C} \right] + \sum_{\upsilon=0}^{\infty} e^{-g_\upsilon^2 \kappa t/b^2} \left[\prod_{\upsilon} Y_0 (g_\upsilon) \right]^2 \right\} \tag{2.33}$$

which in the present apparatus, when performing measurements on liquids, as expected increases in magnitude with time, but ammounts to no more than 0.1% in ΔT_{id}.

2.4.3 Finite Heat Capacity of The Wires Correction.

In the mathematical model from which the idealised temperature rise of the fluid is calculated, heat is assumed to be emitted from a line source, whereas in reality, a hot wire with finite, non-zero physical properties different from those of the fluid is used, thus incurring an error. To account for the error, one requires the solution

of coupled equations for the composite cylinder system (hot-wire and fluid). The following two coupled Fourier equations can be written for the wire and the fluid respectively:

$$(\rho Cp)_w \frac{\partial T_w}{\partial t} = \lambda_w \nabla^2 T_w - \frac{q}{\pi a^2} \qquad 0 \leq r \leq a \qquad (2.34)$$

and for the fluid:

$$\rho\ Cp \frac{\partial T}{\partial t} = \lambda\ \nabla^2 T \qquad r > 0 \qquad (2.35)$$

The continuity condition can also be used giving:

$$T_w(a,t) = T(a,t) \qquad (2.36)$$

and

$$\lambda_w \left[\frac{\partial T_w}{\partial r}\right]_{r=a} = \lambda \left[\frac{\partial T}{\partial r}\right]_{r=a} \qquad (2.37)$$

The initial condition is:

$$T_w(\ r,\ t < 0\ ) = T(\ r,\ t \leq 0\ ) = T_o \qquad (2.38)$$

for all values of r, and the boundary conditions are:

$$\left[\frac{\partial T_w}{\partial r}\right]_{r=0} = 0 \qquad t \geq 0 \qquad (2.39)$$

$$T\ (\ r \rightarrow 0,\ t\ ) = T_o \qquad t \geq 0 \qquad (2.40)$$

$$\left[\frac{\partial T}{\partial r} \right]_{r=a} = -\frac{q}{2\pi\lambda a} \qquad t \geq 0 \qquad (2.41)$$

This is a standard problem (p 379 of [24]) whose solution for large values of $4\kappa_d t/r^2$ is found to be:

$$\Delta T_w(r,t) = \frac{q}{4\pi\lambda} \left\{ \left[1 - \frac{a^2[(\rho C_p)_w - \rho C_p]}{2\lambda t} \right] \ell n \left[\frac{4\kappa t}{r^2 C} \right] \right.$$

$$\left. + \left[\frac{a^2}{2\kappa t} \right] - \left[\frac{a^2}{8\kappa_w t} \right] \right\}$$

$$+ \frac{q}{4\pi\lambda_w} \left[\left[1 - \frac{r^2}{a^2} \right] \left[1 - \frac{a^2\lambda_w}{4\kappa_w \lambda t} \right] \right] \qquad (2.42)$$

During measurements on a fluid, what is measured in the hot-wire method, using the hot-wire as a thermometer, is the average temperature rise over the wire diameter as defined by:

$$\Delta T_w\ (t) = \frac{\int_o^a \Delta T(r,t) r dr}{\int_o^a r dr} \qquad (2.43)$$

so that

$$\Delta T_w(t) = \frac{q}{4\pi\lambda} \ell n\left[\frac{4\kappa t}{a^2 C} \right]\left\{ 1 - \frac{a^2[(\rho C_p)_w - \rho C_p]}{2\lambda t} \right\}$$

$$+ \frac{q}{4\pi\lambda} \left[\frac{a^2}{2\kappa t} - \frac{a^2}{4\kappa_w t} + \frac{\lambda}{2\lambda_w} \right] \qquad (2.44)$$

where

$$\kappa_w = \lambda_w \,/\, (\rho C_p)_w \qquad (2.45)$$

It should be noted that the second term, is usually negligible [13]. The last term in this correction is time-independent and therefore has no influence on the determination of the thermal conductivity from the slope of the line ΔT_{id} vs ℓn t. Consequently, for most runs, the correction to be applied can be written as:

$$\delta T_2 = \frac{q}{4\pi\lambda} \ell n\left[\frac{4\kappa t}{a^2 C} \right]\left[\frac{a^2}{2\lambda t}[(\rho C_p)_w - (\rho C_p)] \right] \qquad (2.46)$$

This term arises solely from the finite heat capacity of the wire, and generally causes the measured temperature rise to fall below the ideal value at short times. By choice of a suitable small radius a, typically a few microns, and long measurement times, t, (greater than 50 ms), the magnitude of the correction may readily be limited to at most 0.5% of the temperature rise, and it falls rapidly with increasing time so that equation (2.46) is entirely adequate for its calculation.

When the diameter of the wire becomes of the same order of magnitude as the mean free path of a molecule of the fluid under observation, the temperature of the fluid at r=a becomes less than the temperature of the wire surface. This is known as the Knudsen effect and is due to a temperature jump existing at the surface of the wire [11,52]. Because the mean free path of a molecule of a liquid is never of the same order of magnitude as that of the hot-wire employed, this effect does not manifest itself and is only applicable to gases at low densities, and therefore the details are omitted from this discussion.

2.5 Effects of an Insulation Layer on the Measurement of the Thermal Conductivity of Liquids.

In order to apply the transient hot-wire technique to fluids that are polar or electrically conducting, additional experimental difficulties must be overcome. This is because a bare metallic wire immersed in such a fluid leads to new electrical effects not present for electrically insulating fluids. To deal with these problems, a thin layer of electrical insulation must be added to the wire and this provides one more difference between the ideal model and the practical instrument.

The transient heat conduction problem arising from the use of a wire coated with an insulation layer has been solved [53,54] by using the appropriate initial and boundary conditions.

The Fourier equations that describe the problem are given as, with reference to figure 2.iv:

$$\frac{\partial^2 \Delta T_1}{\partial r^2} + \frac{1}{r}\frac{\partial \Delta T_1}{\partial r} - \frac{1}{\kappa_1}\frac{\partial \Delta T_1}{\partial t} = -\frac{q}{\pi r_1^2 \lambda_1} \qquad 0 \leq r \leq r_i \quad (2.47)$$

$$\frac{\partial^2 \Delta T_2}{\partial r^2} + \frac{1}{r}\frac{\partial \Delta T_2}{\partial r} - \frac{1}{\kappa_2}\frac{\partial \Delta T_2}{\partial t} = 0 \qquad r_i \leq r \leq r_o \quad (2.48)$$

$$\frac{\partial^2 \Delta T_3}{\partial r^2} + \frac{1}{r}\frac{\partial \Delta T_3}{\partial r} - \frac{1}{\kappa_3}\frac{\partial \Delta T_3}{\partial t} = 0 \qquad r_o \leq r \quad (2.49)$$

where λ is the thermal conductivity, κ the thermal diffusivity, r the radial coordinate measured from the centre of the wire, q the heat generation per unit length of the wire, r_i the radius of the metallic wire and r_o the radius of the insulated wire.

Here, ΔT is the temperature rise of the wire as defined by the equation:

$$\Delta T\,(r,t) = T\,(r,t) - T_o \quad (2.50)$$

where T_o is the initial temperature. The suffixes denote each material according to figure 2.iv.

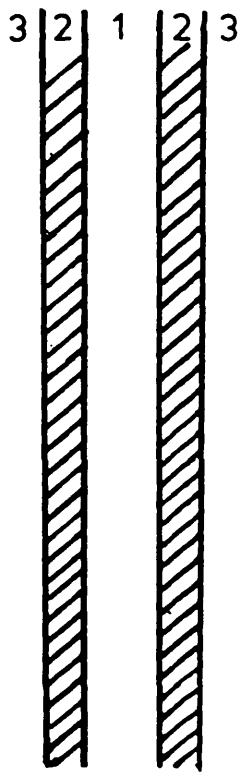


Figure 2.iv. The Hot-Wire Arrangement for Electrically-Conducting Liquids : (1) The Metallic Wire. (2) The Insulating Layer. (3) The Fluid.

The initial condition and boundary conditions are:

$$\Delta T_1 = \Delta T_2 = \Delta T_3 = 0 \qquad t \leq 0 \qquad (2.51)$$

$$\lambda_1 \frac{\partial \Delta T_1}{\partial r} = \lambda_2 \frac{\partial \Delta T_2}{\partial r} \qquad r = r_i \qquad (2.52)$$

$$\Delta T_1 = \Delta T_2 \qquad r = r_i \qquad (2.53)$$

$$\lambda_2 \frac{\partial \Delta T_2}{\partial r} = \lambda_3 \frac{\partial \Delta T_3}{\partial r} \qquad r = r_o \qquad (2.54)$$

$$\Delta T_2 = \Delta T_3 \qquad r = r_o \qquad (2.55)$$

$$\Delta T_3 = 0 \qquad r \to \infty \qquad (2.56)$$

The solution for the problem can be expressed as follows [53-55]:

$$\Delta T_1(r,t) = \frac{q}{4\pi\lambda_3}\left[\ell n \frac{4\kappa_3 t}{r_o^2 C} + 2\frac{\lambda_3}{\lambda_2}\ell n \frac{r_o}{r_i} - \lambda_3\left(\frac{r^2-r_i^2}{r_i^2\lambda_1}\right)\right.$$

$$+ \frac{1}{t}\left\{ \left(\frac{r^2-r_i^2}{4\lambda_1}\right)\left[(\lambda_2-\lambda_3)\left(\frac{1}{\kappa_3}-\frac{1}{\kappa_2}\right)+\frac{\lambda_1}{\kappa_1}\right]\right.$$

$$+ \frac{r_i^2}{2}\left(\frac{1}{\kappa_2}-\frac{1}{4\kappa_1}\right) + \frac{r_o^2}{2}\left(\frac{1}{\kappa_3}-\frac{1}{\kappa_2}\right)$$

$$+ \frac{r_i^2}{\lambda_2}\left(\frac{\lambda_2}{\kappa_2}-\frac{\lambda_1}{\kappa_1}\right)\ell n \frac{r_o}{r_i}$$

$$\left.\left. + \frac{1}{2\lambda_3}\left[r_i^2\left(\frac{\lambda_2}{\kappa_2}-\frac{\lambda_1}{\kappa_1}\right) + r_o^2\left(\frac{\lambda_3}{\kappa_3}-\frac{\lambda_2}{\kappa_2}\right)\right]\ell n \frac{4\kappa_3 t}{r_o^2 C}\right\}\right] \qquad (2.57)$$

and

$$\Delta T_2(r,t) = \frac{q}{4\pi\lambda_3}\left[\ell n \frac{4\kappa_3 t}{r_o^2 C} + 2\frac{\lambda_3}{\lambda_2}\ell n \frac{r_o}{r}\right.$$

$$+ \frac{1}{t}\left\{ \frac{r_i^2}{4}\left(\frac{1}{\kappa_2}-\frac{1}{2\kappa_1}\right)\right.$$

$$+ \frac{r_o^2}{4}\left(\frac{2}{\kappa_3}-\frac{2}{\kappa_2}+\frac{r^2}{\kappa_2 r_o^2}\right) + \frac{r_i^2}{2\lambda_2}\left(\frac{\lambda_2}{\kappa_2}-\frac{\lambda_1}{\kappa_1}\right)\ell n \frac{r_o^2}{r_i r}$$

$$\left.\left. + \frac{1}{2\lambda_3}\left[r_i^2\left(\frac{\lambda_2}{\kappa_2}-\frac{\lambda_1}{\kappa_1}\right) + \left(\frac{\lambda_3}{\kappa_3}-\frac{\lambda_2}{\kappa_2}\right)\right]\ell n \frac{4\kappa_3 t}{r_o^2 C}\right\}\right] \qquad (2.58)$$

where $C = \exp \gamma = 1.7811$ (Euler's constant). The above approximate

solution is valid for large values of ($\kappa_3 t/r^2$), using the expansion method as outlined by Carslaw and Jaeger [24]. It should be noted that these equations include the solution without the insulation layer. Thus, in equation (2.57), if we replace r_o by r_i , suffix 2 by 3 and take an average over the wire radius, we obtain:

$$\Delta T_1(r,t) = \frac{q}{4\pi\lambda_3}\left\{\left[1 - r_i^2\,\frac{(\rho Cp)_1-(\rho Cp)_3}{2\lambda_3 t}\right]\ell n\,\frac{4\kappa_3 t}{r_i^2 C} + \frac{r_i^2}{2\kappa_3 t} - \frac{r_i^2}{4\kappa_1 t} + \frac{\lambda_3}{2\lambda_1}\right\} \qquad (2.59)$$

which is the same solution as Healy et.al.[13]. The measured temperature rise is deduced from the resistance of the wire corresponding to the average integral of $\Delta T_1(r,t)$ in equation (2.57):

$$\Delta T_1 = \int_o^{r_i} \Delta T_1\,\frac{2r}{r_i^2}\,dr$$

So,

$$\Delta T_1 = \frac{q}{4\pi\lambda_3}\left[\ell n\,\frac{4\kappa_3 t}{r_o^2 C} + 2\,\frac{\lambda_3}{\lambda_2}\,\ell n\,\frac{r_o}{r_i} + \frac{\lambda_3}{2\lambda_1} + \frac{1}{t}\left\{\frac{r_i^2}{8}\left[\left(\frac{\lambda_3-\lambda_2}{\lambda_1}\right)\left(\frac{1}{\kappa_1}-\frac{1}{\kappa_2}\right) + \frac{4}{\kappa_2} - \frac{2}{\kappa_1}\right]\right.\right.$$

$$+ \frac{r_o^2}{2}\left(\frac{1}{\kappa_3}-\frac{1}{\kappa_2}\right) + \frac{r_i^2}{\lambda_2}\left(\frac{\lambda_2}{\kappa_2}-\frac{\lambda_1}{\kappa_1}\right)\ell n\,\frac{r_o}{r_i}$$

$$\left.\left. + \frac{1}{2\lambda_3}\left[r_i^2\left(\frac{\lambda_2}{\kappa_2}-\frac{\lambda_1}{\kappa_1}\right) + r_o^2\left(\frac{\lambda_3}{\kappa_3}-\frac{\lambda_2}{\kappa_2}\right)\right]\ell n\,\frac{4\kappa_3 t}{r_o^2 C}\right\}\right] \qquad (2.60)$$

This equation can be re-written in a simplified form using A, B and C which are constant for a particular insulated wire and the test fluid as follows:

$$\Delta T_1 = \frac{q}{4\pi\lambda_3} \left\{ \ell n\ t + A + \frac{1}{t} (B\ \ell n\ t + C) \right\} \qquad (2.61)$$

where

$$A = \ell n \frac{4\kappa_3}{r_o^2 C} + 2 \frac{\lambda_3}{\lambda_2} \ell n \frac{r_o}{r_i} + \frac{\lambda_3}{2\lambda_1} \qquad (2.62)$$

$$B = \frac{1}{2\lambda_3} \left\{ r_i^2 \left(\frac{\lambda_2}{\kappa_2} - \frac{\lambda_1}{\kappa_1} \right) + r_o^2 \left(\frac{\lambda_3}{\kappa_3} - \frac{\lambda_3}{\kappa_2} \right) \right\} \qquad (2.63)$$

$$C = \frac{r_i^2}{8} \left\{ \left(\frac{\lambda_3 - \lambda_2}{\lambda_1} \right) \left(\frac{1}{\kappa_1} - \frac{1}{\kappa_2} \right) + \frac{4}{\kappa_2} - \frac{2}{\kappa_1} \right\}$$

$$+ \frac{r_o^2}{2} \left(\frac{1}{\kappa_3} - \frac{1}{\kappa_2} \right) + \frac{r_i^2}{\lambda_2} \left(\frac{\lambda_2}{\kappa_2} - \frac{\lambda_1}{\kappa_1} \right) \ell n \frac{r_o}{r_i}$$

$$+ \frac{1}{2\lambda_3} \left\{ r_i^2 \left(\frac{\lambda_2}{\kappa_2} - \frac{\lambda_1}{\kappa_1} \right) + r_o^2 \left(\frac{\lambda_3}{\kappa_3} - \frac{\lambda_2}{\kappa_2} \right) \right\} \ell n \frac{4\kappa_3}{r_o^2 C} \qquad (2.64)$$

Thus, for wires coated with an insulating layer, it is possible to discern additional corrections arising from conditions at the inner

surface over and above these arising from the metallic wire itself, δT_2. The additional correction is:

$$\delta T_c = \frac{q}{4\pi\lambda_3}\left[(1 - \frac{\lambda_3}{\lambda_2}) \ell n(r_o/r_i)^2 - \frac{1}{t}\left\{ \frac{r_i^2}{8}\left[(\frac{\lambda_3-\lambda_2}{\lambda_1}) (\frac{1}{\kappa_1}-\frac{1}{\kappa_2}) + 4(\frac{1}{\kappa_2} - \frac{1}{\kappa_1}) + 4(r_o/r_i)^2(\frac{1}{\kappa_1} - \frac{1}{\kappa_2}) + \frac{8}{\lambda_2}[\frac{\lambda_2}{\kappa_2} - \frac{\lambda_1}{\kappa_1}] \ell n(\frac{r_o}{r_i}) + \frac{4}{\lambda_3}\left[(\frac{\lambda_2}{\kappa_2}-\frac{\lambda_3}{\kappa_3})(1-(\frac{r_o}{r_i})^2)\ell n(\frac{4\kappa_3 t}{r_i^2 C}) - \ell n(\frac{r_o}{r_i})^2\{(\frac{\lambda_2}{\kappa_2}-\frac{\lambda_1}{\kappa_1})+(\frac{\lambda_3}{\kappa_3}-\frac{\lambda_2}{\kappa_2})\}\right]\right]\right\}\right] \quad (2.65)$$

2.6 Effect of Thermal Contact Resistance Between Metallic Wire And Insulation Layer.

There may exist a thermal contact resistance between the metallic tantalum wire and the oxide (tantalum pentoxide) layer, which is attributed to the fact that the two exhibit different thermal coefficients of expansion.

To account for this phenomenon, the boundary condition between layer 1 and 2, equation (2.52) is replaced by the following equation:

$$-2\pi\lambda_1 r \frac{\partial \Delta T_1}{\partial r} = \frac{1}{R_T} (\Delta T_1 - \Delta T_2) \qquad r=r_i \qquad (2.66)$$

R_T represents the thermal contact resistance per unit length.

An appropriate solution can be derived, in the same way that was followed to obtain equation (2.60), giving:

$$\overline{\Delta T_1} = \frac{q}{4\pi\lambda_3} \left[\ell n\ t + A + \frac{2\lambda_3\sqrt{\kappa_1 h}}{r_i\sqrt{\kappa_2}} + \frac{1}{t} \left\{ B\ \ell n\ t + C \right.\right.$$

$$\left.\left. + \frac{r_i h}{2} \left[\frac{\sqrt{\kappa_1}}{\sqrt{\kappa_2}} \left(\frac{\lambda_2}{\kappa_2} - \frac{\lambda_1}{\kappa_1} \right) - \left(\frac{\lambda_1}{\sqrt{\kappa_1\kappa_2}} + \frac{\lambda_2}{\kappa_2} \right) \right] \right\} \right] \qquad (2.67)$$

where A, B, and C are the same constants as given by equations (2.62), (2.63), and (2.64), and $h=2r_iR_T$.

To obtain the magnitudes of the thermal contact resistance between the metallic wire and its oxide insulation layer is very difficult <u>in situ</u>. The reason is that the insulated layer is too thin to perform such an experiment.

Several researchers have reported a correlation which is based on the experimental results, so that the thermal contact resistance can be related to contact geometry parameters and contact materials.

According to Vezuroglu [56], he gave a correlation which covers wide ranges of variables; h was estimated to be in the order of 10^{-6}K W^{-1}, by using roughly evaluated parameters, such as the ratio between the actual contact area, apparent contact area C and gap thickness δ.

Therefore, the relative magnitudes of the term involving h in equation (2.67) compared with (B ℓn t + C) can be calculated to about 10%. This yields a negligible effect in the ΔT_{id} vs. ℓn t relation, ($\leq$0.005%).

2.7 Variable Fluid Properties.

A final correction occurs due to the fact that the density and thermal conductivity of the fluid vary with temperature. This results in the observed temperature rises differing from their ideal values, since in the ideal model, the fluid parameters are considered constant.

The thermal conductivity of a test fluid is obtained from the slope of a plot of ΔT vs ℓn t and in the present work, the time domain within which measurements are recorded is between 150 ms and 1 second, and the change in temperature rise during this period is around 4 K. Because the change in thermal conductivity during this period is less than 0.5%, it is sufficiently small to enable the use of the analysis

given by Healy et.al.[13]. It is found that when using this analysis, the temperature rise has the form:

$$\Delta T(t) = \Delta T_{id}.\frac{1}{2} \times(\Delta T)^2 + \{ \frac{q}{4\pi\lambda_o} \}(\times - \varphi) \ell n4 \quad (2.68)$$

where by definition:

$$\lambda (T, \rho) = \lambda_o(1 + \times\Delta T) \quad (2.69)$$

and

$$\rho Cp = \rho_o Cp(1 + \varphi\Delta T) \quad (2.70)$$

The last term in the above equation is time independent and does not influence the slope of ΔT vs ℓn t and is therefore ignored. Now considering the temperature rise at either end of the range of measurement times, $\Delta T_{(t_1)}$ and $\Delta T_{(t_n)}$, (corresponding to the first and final bridge balance conditions,(see Chapter 3)), from their difference it is found:

$$\Delta T_{(t_n)} - \Delta T_{(t_1)} = \frac{q \ \ell n [\ t_n/t_1 \ ]}{4\pi\lambda_o \{ 1 + \frac{1}{2}\times[\Delta T_{(t_1)}+\Delta T_{(t_n)}]\}} \quad (2.71)$$

which using equation (2.71) is identical in the form to the idealised temperature rise with the properties evaluated at:

$$T_r = T_o + \delta T_{fp} \tag{2.72}$$

$$= T_o + \frac{1}{2}\left\{ \Delta T_{id(t_1)} + \Delta T_{id(t_n)} \right\} \tag{2.73}$$

and

$$\rho = \rho_r(T_r, P_o) \tag{2.74}$$

where subscript r refers to the reference temperature, and fp refers to the temperature correction due to variable fluid properties.

It is therefore implied that the fluid thermal conductivity obtained from the slope of the measured ΔT vs $\ell n\ t$ line corresponds to the thermal conductivity at temperature T_r and density $\rho_r(T_r, P_o)$.

In the case where a wire is insulated, the contribution to the reference temperature is rather more involved. However it may be evaluated from the work of Nagashima and Nagasaka [53]. The result is that T_r must be written as:

$$T_r = T_o + \delta T^*_{fp} + \delta T^*_c \tag{2.75}$$

where

$$\delta T^*_c = -\frac{q}{8\pi\lambda_3}\left\{ 2\,\ell n(r_o/r_i)^2 - r_i^2 \left[\{\frac{1}{t_1} + \frac{1}{t_2}\}\left[(\frac{1}{\kappa_2} + \frac{1}{\kappa_1})\right.\right.\right.$$

$$+ (r_o/r_i)^2(\frac{1}{\kappa_3} + \frac{1}{\kappa_2}) + \frac{2}{\lambda_2}(\frac{\lambda_2}{\kappa_2} - \frac{\lambda_1}{\kappa_1})\ell n(r_o/r_i)$$

$$\left.\left.\left. - \frac{2}{\lambda_3}\{(\frac{\lambda_2}{\kappa_2} - \frac{\lambda_1}{\kappa_1}) + (r_o/r_i)^2(\frac{\lambda_3}{\kappa_3} - \frac{\lambda_2}{\kappa_2})\}\ell n(r_o/r_i)\right]\right.$$

$$+ \frac{2}{\lambda_3}\left[\left(\frac{\lambda_2}{\kappa_2} - \frac{\lambda_1}{\kappa_1}\right) + (r_o/r_i)\left[\frac{\lambda_3}{\kappa_3} - \frac{\lambda_2}{\kappa_2}\right]\right]$$

$$x\left\{\left[\frac{1}{t_1} \ell n \frac{4\kappa t_1}{r_i^2 C} + \frac{1}{t_2} \ell n \frac{4\kappa t_2}{r_i^2 C}\right]\right\} \qquad (2.76)$$

2.8 Thermal Diffusivity.

The transient hot-wire technique has now become established as the primary source of accurate data on the thermal conductivity of fluids, over a wide range of thermodynamic states [15,57,58]. This technique, since its conception [59], was capable of yielding the thermal conductivity and thermal diffusivity of the fluid simultaneously. There has been a number of independent investigations into the thermal diffusivity problem [60-62]. The claimed accuracy for the corresponding thermal diffusivity measurements was in the range of $\pm$1% [61], and $\pm$11% [62], and has not been directly linked to the accuracy obtained in the measurement of the thermal conductivity.

Very limited progress has been made until recently [61,63], in attempting to modify and improve existing thermal conductivity instruments, to yield highly accurate thermal diffusivity measurements, complimenting the accuracy ($\pm$0.3%) of the thermal conductivity data. In order to improve the thermal diffusivity evaluation, it is necessary to obtain the fundamental working equation for the thermal diffusivity, equation (2.14), and this can be solved to yield :

$$\kappa = \frac{a^2 C}{4t'} \exp(4\pi\lambda(T_r,\rho_r)\Delta T_{id}(t')/q) \qquad (2.77)$$

where t' is the specific time at which ΔT_{id} is evaluated. In deriving κ from the regression line of ΔT as a function of ℓn t, it has been demonstrated that when t'= 1 second, κ_o can be given by [64]:

$$\kappa_o = \frac{a^2 C}{4x1s} \exp(I/S) \qquad (2.78)$$

where I is the intercept of the regression line, $S=q/4\pi\lambda(T_r,\rho_r)$ is the slope, and κ_o refers to the thermal diffusivity at zero time condition, (i.e. bath temperature), so that:

$$\kappa_o = \kappa(T_o,\rho_o) = \lambda(T_o,\rho_o)/\rho_o(Cp)_o \qquad (2.79)$$

with

$$\rho_o = \rho(P_o,T_o) \qquad (2.80)$$

An error analysis has been carried out [42,65], to give $\delta\kappa_o/\kappa_o$ and the result is:

$$\frac{\delta\kappa_o}{\kappa_o} = 2\left|\frac{\delta a}{a}\right| + \ell n\left[\frac{4\kappa_o}{a^2 C}\right]\left|\frac{\delta[\Delta T_w(t')]}{\Delta T(t')}\right| + \ell n\left[\frac{4\kappa_o}{a^2 C}\right]\left|\frac{\delta S}{S}\right| \qquad (2.81)$$

The prescribed time, t', is chosen to be around one second, to minimize

errors and the onset of convection. It is subsequently found that [65],

$$\frac{\delta\kappa_o}{\kappa_o} = 2\left|\frac{\delta a}{a}\right| + \ell n\left[\frac{4\kappa_o}{a^2 C}\right]\left\{\left|\frac{\delta T_s}{\Delta T_w}\right| + \left[\left|\frac{\delta(R_w(t)-R_{wo}}{R_w(t)-R_{wo}}\right| + \left|\frac{\delta(\Delta T_w)}{\Delta T_w}\right|_t\right] + \left|\frac{\delta a}{a}\right| + \left|\frac{\delta S}{S}\right| + \left|\frac{\delta R_{wo}}{R_{wo}}\right| + \left|\frac{\delta R_{wo}}{(R_w(t)-R_{wo}}\right|\right\} \tag{2.82}$$

In the liquid phase instrument, where a=3.5μm (instrument for electrically non-conducting liquids employing platinum wires), the determination of the wire radius by electron microscopy gives $\delta a/a$ = 0.02. For the same instrument, the statistical estimate of $\delta S/S$ obtained from the linear regression of a set of ΔT versus ℓn t points leads to $\delta S/S = 2\times10^{-4}$. In addition to that, the instrument has been designed [66], so that:

$$\frac{\delta(R_w(t)-R_{wo}}{R_w(t)-R_{wo}} + \left[\frac{\delta\Delta T_w}{\Delta T_w}\right]_t = 5\times10^{-4} \tag{2.83}$$

a figure confirmed by experiment [66]. Thus, if a figure for $\delta a/a = 1\times10^{-4}$ is assigned to the temperature coefficient of resistance of platinum, and take $\delta T_s/\Delta T_w = 1\times10^{-4}$ [65], due to the chosen operating conditions, then the remaining errors are due to the uncertainties in the absolute values of R_{wo} during a transient run. For the liquid phase instrument, the magnitude of $\delta R_w(0) = 7\times10^{-3}$ Ω, while $R_{wo}\approx250\Omega$ and $R_w(t)-R_w(0) = 1.8\Omega$. Equation (2.82) has been evaluated [65] retaining the order of terms and inserting the appropriate values of κ_o, a, and C. The final estimate of the uncertainty in κ_o for the absolute

measurements is:

$$\frac{\delta\kappa_o}{\kappa_o} = 0.04 + 9.5[1\times10^{-4} + 5\times10^{-4} + 1\times10^{-4} + 2\times10^{-4} + 3\times10^{-5} + 4\times10^{-3}] \quad (2.84)$$

or

$$\frac{\delta\kappa_o}{\kappa_o} = 8.7\times10^{-2} \quad (2.85)$$

With this, the error with which the thermal diffusivity can be obtained is about $\pm$9%.

The primary source of the uncertainty in evaluating the thermal diffusivity stems from the difficulty in the measurement of the wire radius itself. The wire radius is difficult to obtain with the high precision required, and varies along the wire length. Another source for concern arises due to the fact the term $\ell n(4\kappa t/a^2C)$ that multiplies the remaining errors, is large and amplifies the individual errors, and this is a direct consequence if the theory of the method is to be complied with. Thirdly, the dominant contribution comes from the uncertainty in $\{\delta R_{wo}/(R_w(t)-R_{wo})\}$. The present bridge design (Chapter 3), makes it rather difficult to reduce the uncertainty in the measurement of the absolute resistance, because it is essential to avoid systematic errors. This feature contributes about $\pm$4% to the uncertainty in the thermal diffusivity.

An improvement in the elucidation of the thermal diffusivity can be achieved by performing relative measurements. It can be seen from the working equation (2.77), that for two fluids, or for two states of the same fluid, denoted by the subscripts 1 and 2, the ratio of the two thermal diffusivities is:

$$\frac{[\kappa_o]_1}{[\kappa_o]_2} = \exp\left\{\left[\frac{\Delta T_{id}(t')}{S}\right]_1 - \left[\frac{\Delta T_{id}(t')}{S}\right]_2\right\} \qquad (2.86)$$

If the thermal diffusivity of one fluid is accurately known under one set of conditions, then the same property may be determined for other liquids as a ratio. The advantages of this arrangement is that some of the errors in equation (2.82) can be neglected, and only the random errors in the determination of ΔT_{id} and S are left outstanding. Thus, it is possible to determine the thermal diffusivities with a precision of about $\pm$4%, but the accuracy of these measurements is invariably worse, owing to the error in the reference value of the thermal diffusivity.

The isobaric heat capacity can be obtained from measurements of the thermal conductivity and thermal diffusivity:

$$\kappa = \frac{\lambda}{\rho C_p} \qquad (2.87)$$

with an error comparable to that of the diffusivity itself. An error of about $\pm$5% in C_p is tolerated, but then the current application of the

transient hot-wire method permits this modest accuracy to be maintained, over a wide range of thermodynamic states.

The analysis presented above has been confirmed by carrying out measurements with the thermal conductivity instrument for electrically insulating liquids [42], in conjunction with the new bridge described later in Chapter 3. The reference datum employed in this analysis was that of toluene at a pressure of 0.1 MPa and a temperature of 28.5K. A reference value was obtained by using the thermal conductivity given by Nieto de Castro et.al. [67], the density reported by Kashiwagi et.al. [68], and the heat capacity data tabulated by Vargaftik [69]. The final value is:

$$\kappa_{ref} = \kappa(P=0.1 \text{ MPa}, T=328.5 \text{ K}) = 8.01 \times 10^{-8} \text{ m}^2 \text{ s}^{-1} \qquad (2.88)$$

Additional transient hot-wire measurements of the thermal diffusivity for toluene and m-xylene over the temperature range of 308 K to 360 K, and for pressures up to 380 MPa have been carried out [70]. They obtained thermal diffusivity values with a standard deviation of $\pm$2.7%, and with a maximum deviation of $\pm$4.9%, which are commensurate with the estimate of the precision of the thermal diffusivity measurements for this instrument. Thermal diffusivity measurements have been performed on toluene over the temperature range 308 K to 345 K at pressures up to 70 MPa. It was estimated [42] that the error in the diffusivity and heat capacity data was in the region of $\pm$6% for toluene.

It may be concluded that under favourable conditions, an error of $\pm 7\%$ to $\pm 9\%$ in absolute measurements of the thermal diffusivity of liquids is the best that can be achieved, in the current state of the art technology. If the wire diameter is very well known, or if relative measurements are performed, then a subsequent improvment in the thermal diffusivity can be readily attained as has been shown.

2.9 Summary of Corrections.

The transient hot-wire technique is based on the idealised solution for the temperature rise of a fluid of infinite extent, initially at thermal equilibrium, through which heat is conducted from an infinitely long line heat source within the medium. The solution at a distance a (the diameter of the hot wire) into the fluid, after truncation, supplies the working equation from which the thermal conductivity is calculated:

$$\Delta T_{id} = \frac{q}{4\pi\lambda_{(T_r)}} \ell n \left[\frac{4\kappa_o t}{a^2 C} \right] \qquad (2.89)$$

From measurements on the hot-wire apparatus, the temperature rises of the wire, $\Delta T_{(t)}$, at a number of times, following the initiation of the ohmic dissipation to the fluid, are found. From these experimentally measured temperature rises, the corresponding idealised temperature rise ΔT_{id} must be calculated in order to use the above equation (2.89) to calculate $\lambda_{(T_r)}$. As stated previously, it has been

assumed that because the error corrections involved, in transforming the measured temperature rises to idealised temperature rises, are small, their combined effect is additive. The idealised temperature rise is therefore, obtained by summing the experimental temperature rise and individual temperature corrections:

$$\Delta T_{id}(t) = \Delta T(t) + \sum_i \delta T_i \qquad (2.90)$$

Similarly, the reference temperature T_r at which the thermal conductivity is obtained:

$$T_r = T_o + \sum_i \delta T_i^* \qquad (2.91)$$

Limiting the inclusion of errors which contribute temperature corrections of greater than 0.01% in ΔT_{id} results in:

$$\Delta T_{id} = \Delta T(t) + \delta T_1 + \delta T_2 + \delta T_c \qquad (2.92)$$

where from (2.33):

$$\delta T_1 = - \frac{q}{4\pi\lambda} \left\{ \ell n \left[\frac{4\kappa t}{b^2 C} \right] + \sum_{\upsilon=0}^{\infty} e^{-g_\upsilon^2 \, \kappa t / b^2} \left[\pi \, Y_o \, (g_\upsilon) \right]^2 \right\}$$

and from (2.46):

$$\delta T_2 = \frac{q}{4\pi\lambda} \ell n \left[\frac{4\kappa t}{a^2 C} \right] \left[\frac{a^2}{2\lambda t} [(\rho Cp)_w - (\rho Cp)] \right]$$

and from (2.65):

$$\delta T_c = \frac{q}{4\pi\lambda_3}\left[(1 - \frac{\lambda_3}{\lambda_2}) \ell n(r_o/r_i)^2 \right.$$

$$- \frac{1}{t}\left\{ \frac{r_i^2}{8}\left[(\frac{\lambda_3-\lambda_2}{\lambda_1})(\frac{1}{\kappa_1} - \frac{1}{\kappa_2})+ 4(\frac{1}{\kappa_2} - \frac{1}{\kappa_1}) \right.\right.$$

$$+ 4(r_o/r_i)^2(\frac{1}{\kappa_1} - \frac{1}{\kappa_2}) + \frac{8}{\lambda_2}[\frac{\lambda_2}{\kappa_2} - \frac{\lambda_1}{\kappa_1}] \ell n(\frac{r_o}{r_i})$$

$$\left.\left.\left. +\frac{4}{\lambda_3}\left[(\frac{\lambda_2-\lambda_3}{\kappa_2\ \kappa_3})(1-(\frac{r_o}{r_i})^2)\ell n(\frac{4\kappa_3 t}{r_i^2 C}) - \ell n(\frac{r_o}{r_i})^2\{(\frac{\lambda_2-\lambda_1}{\kappa_2\ \kappa_1})+(\frac{\lambda_3-\lambda_2}{\kappa_3\ \kappa_2})\}\right]\right]\right\}\right]$$

The reference temperature to which the thermal conductivity calculated from equation (2.46) corresponds, is obtained from equation (2.73) as:

$$T_r = T_o + \delta T_{fp} + \delta T_c^* \qquad (2.93)$$

where δT_{fp} is:

$$\delta T_{fp} = \frac{1}{2}\left\{ \Delta T_{id(t_1)} + \Delta T_{id(t_n)} \right\}$$

and from equation (2.76), δT_c^* is:

$$\delta T_c^* = - \frac{q}{8\pi\lambda_3}\left\{ 2\ell n(\frac{r_o}{r_i})^2 - r_i^2 \left[[\frac{1}{t_1}+\frac{1}{t_2}]\left[(\frac{1}{\kappa_2}-\frac{1}{\kappa_1})\right.\right.\right.$$

$$+ (\frac{1}{\kappa_3}-\frac{1}{\kappa_2}) + \frac{2}{\lambda_2}[\frac{\lambda_2}{\kappa_2}-\frac{\lambda_1}{\kappa_1}]\ell n(r_o/r_i) - \frac{2}{\lambda_3}\left[(\frac{\lambda_2}{\kappa_2}-\frac{\lambda_1}{\kappa_1})\right.$$

$$\left.\left.\left.+(\frac{r_o}{r_i})^2(\frac{\lambda_3}{\kappa_3}-\frac{\lambda_2}{\kappa_2})\right]\ell n(r_o/r_i)\right]$$

$$+ \frac{2}{\lambda_3}\left[\left(\frac{\lambda_2}{\kappa_2}-\frac{\lambda_1}{\kappa_1}\right) + \left(\frac{r_o}{r_i}\right)^2\left(\frac{\lambda_3}{\kappa_3}-\frac{\lambda_2}{\kappa_2}\right)\right]\left[\frac{1}{t_1}\,\ell n\frac{4\kappa_3 t_1}{a^2 C} + \frac{1}{t_2}\,\ell n\frac{4\kappa_3 t_2}{a^2 C}\right]\right\}$$

and the reference density is:

$$\rho_r = \rho(\, T_r,\, P_o\,) \qquad (2.94)$$

where P_o is the initial pressure of a measurement.

Chapter 3

Apparatus Design And Use:

3.1 Introduction:

This chapter is principally devoted to the design, construction, and application of the apparatus for transient hot-wire measurements of the thermal conductivity of electrically conducting liquids, in the pressure range 0.1-700 MPa and temperature range 300-360 K. The equipment has been designed so that it conforms as closely as possible to the mathematical model that it is intended to describe it. In addition, the desire to study electrically conducting, and ultimately, corrosive heat transfer liquids has also been included in the design study. The design of the thermal conductivity cells emerging from this study has itself imposed new requirements for the system employed to determine the transient temperature rises. Consequently, the electronic measurement system itself has been redesigned and reconstructed.

The significance of this apparatus, is that the accuracy of the thermal conductivity obtained is $\pm$0.3% and the precision of the instrument used is $\pm$0.2%. This surpasses anything previously achieved for polar or electrically conducting fluids.

In the following sections, the descriptions of the thermal conductivity cells for electrically conducting liquids, the hot-wires

employed in the new instrument, the pressure system, and the electronic apparatus will be given, together with the working equations used in analysing the data. The experimental procedure will also be described and finally the handling and data processing will be discussed.

In addition to the novel application of the transient hot-wire technique to electrically conducting liquids, some work has also been carried out in parallel on an older instrument for use with electrically insulating liquids. This work has partly been the improvement of the existing instrumentation following the development of the instrument for electrically conducting fluids, and partly the application of the measurement procedure to new fluids. The latter section of work is intended to complement earlier studies [14,71], and to provide a wider range of data for the testing of predictive and correlation schemes for liquid thermal conductivity. Because much of the instrumentation for the apparatus used to study insulating liquids has been described elsewhere [12-14,44,45,71,72], a detailed description is omitted here, and attention is concentrated upon the experimental results. The most important features of the new apparatus for electrically conducting liquids are noted wherever appropriate. To this end, the chapter is begun with a description of the thermal conductivity cells for insulating liquids.

3.2 The Hot-Wire Cells For Electrically Insulating Liquids:

The original form of the transient hot-wire cells for the measurement of the thermal conductivity of electrically insulating

fluids has been described in detail elsewhere [12,14,71]. Here, we describe the form briefly in order to establish its defects and the rationale for the improved version used in most of the work reported here.

In this apparatus, figure 3.i, the two cells are constructed within a stainless steel cylinder (type EN85-M). The cells were made up from two hemi-cylindrical sections. The fixed half of the steel cylinder 1 carries the cell top 2 which connects the cell to the pressure vessel plug; the terminal posts 3 and 4 provide mechanical support for and electrical connections to the two platinum hot-wires 5 of the cells. The removable half of the cells 6 forms a cover and provides a cylindrical outer surface for both cells when fixed in position. A plan view of the complete cylinder assembly is shown in figure 3.i, and this illustrates the channels 7 and 8 used to carry platinum wire connectors (0.5mm diameter) insulated with glass tubing, from each of the terminal posts to the upper end of the cells.

The hot-wires of the cells are made from 7μm nominal diameter platinum wire, (purity $\geq$ 99.9%), supplied by Sigmund Cohn Corporation. At its lower end, the 7μm platinum wire is attached to a gold sphere at one end of a cylindrical platinum weight of about 50mg 9. At its upper end, the weight is electrically connected to the lower terminal by a loop of annealed gold attached at either end with a gold-tin solder 10. The wire, therefore, hangs vertically and is subjected to constant tension due to the weight, this tension being independent of the thermal expansion of the elements of the cell at the

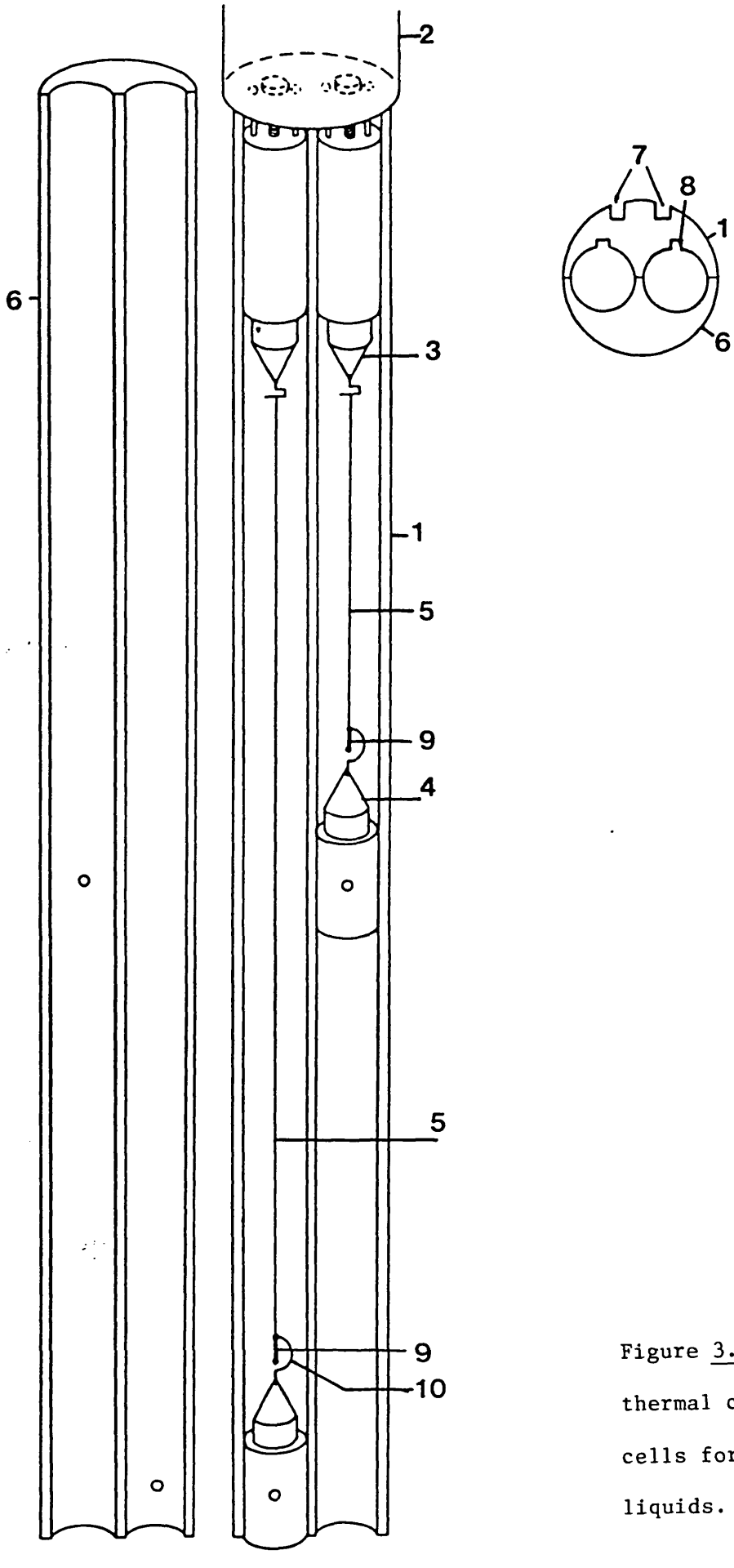


Figure 3.i. The thermal conductivity cells for insulating liquids.

various experimental temperatures used.

The disadvantages of this type of cell, appreciated in hindsight, are thoroughly described elsewhere [73]. The principal point for the present discussion is the fact that the transient heating of the platinum wire causes a thermal expansion of a few microns, so that the tensioning weight 'falls'. This stimulates a mechanical oscillation of the weight in which the wire acts as a spring. This reveals itself through the phenomenon of electro-striction, as an oscillation of the wire resistance, superimposed on the steady rise in resistance owing to heating. Thus, a careful examination of the output of the bridge balance revealed oscillations deriving from this origin. Although the effect on the measured temperature rise of the wire is small, it is systematic. Consequently, it was necessary to adopt an improved cell configuration to remove the effect. Figure 3.ii shows the mechanism adopted in the modified thermal conductivity cells employed in most of this work for insulating liquids. Here, the platinum wires are connected at their upper end to a weak gold spring so designed that its spring constant for linear motion is one-tenth of that of the platinum wire. In this way, the fall of the weight is accomodated mainly by the extension of the spring, and not the wire, and the strain in the platinum wire is much reduced. It was verified by direct measurement [73], that the electrostrictive oscillations in the bridge output were rendered entirely negligible by this technique.

It was felt necessary to confirm that this new cell configuration, did not throw into doubt any of the earlier measurements made with the

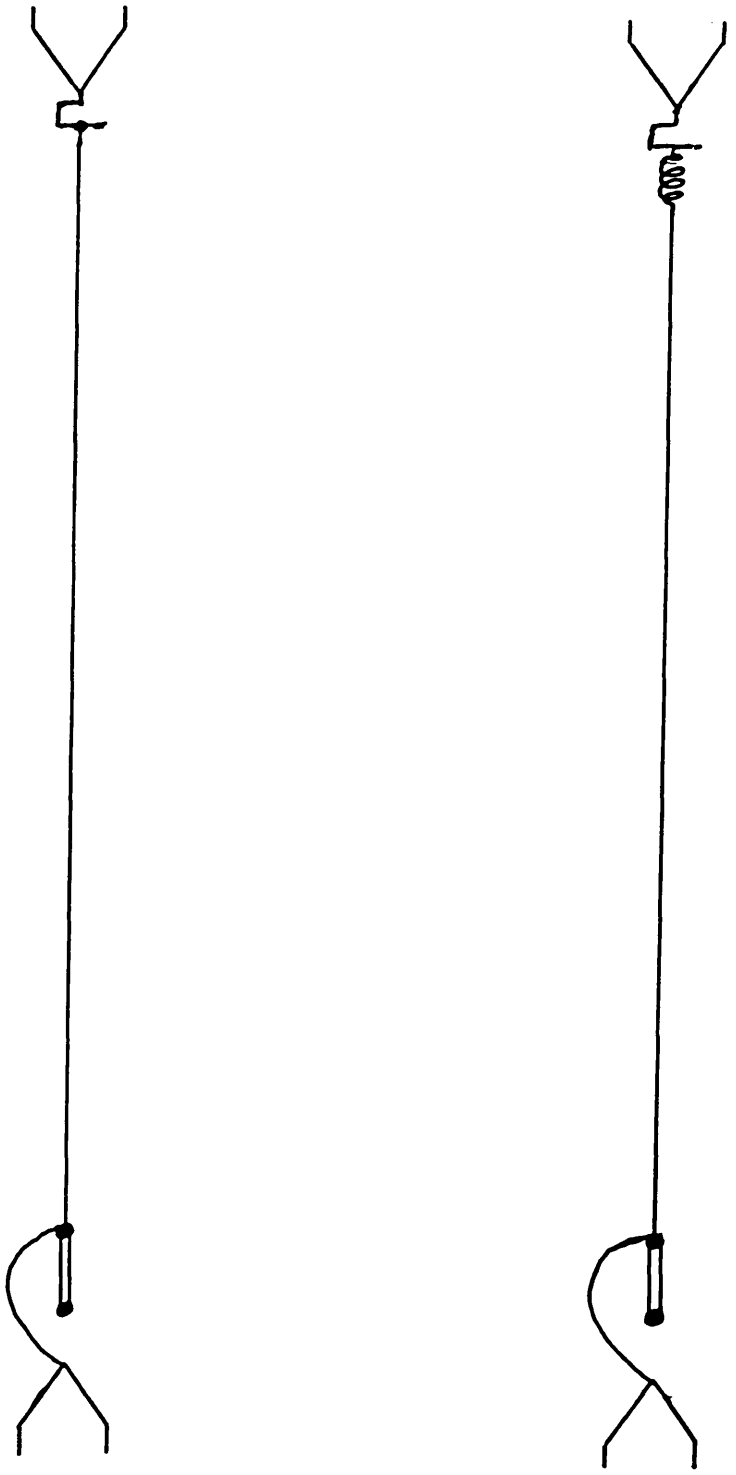


Figure 3.ii. The new arrangement for the installation of the platinum hot-wires in the thermal conductivity cells for non-conducting liquids.

original cell configuration. Consequently, measurements were made of the thermal conductivity of toluene, which had been reported earlier [41,74]. These new results will be presented later together with their comparison with earlier data. It suffices to say that the new data are entirely consistent with the earlier set within their mutual uncertainty, so that all earlier results can be retained together with their associated uncertainty.

The characteristics of the measurement cells for the electrically insulating liquids are given below in table 3.1.

Characteristics of the cell design for electrically insulating liquids, and a typical set of platinum wires, at 302.60K [75].	
Internal diamater of cells	9.90mm ± 0.01mm
Long wire length (platinum)	145.11mm ±0.02mm
Short wire length (platinum)	44.34mm ±0.02mm
Long wire resistance at 4.224MPa	353.67Ω ±0.05Ω
Short wire resistance at 4.224MPa	108.82Ω ±0.05Ω
Platinum wire radius	3.81μm ±0.01μm
Cell material of construction: stainless steel EN85-M.	

Table 3.1.

3.3 The Hot-Wire Cells For Electrically Conducting Liquids:

The problems associated with the use of a bare thin metallic (usually platinum) wire as the sensor in the transient hot-wire instrument for the measurement of the thermal conductivity of electrically liquids and polar liquids are that:

a) Polarisation takes place on the surface of the wire due to the current flowing during the transient run.

b) Part of the current flows through the test liquid and the heat generation of the wires becomes distorted.

c) The electrical system combines with the metallic cell through the test liquid, and the small voltage signals become distorted, and this constitutes the most serious deficiency in the bare metallic wire instrument.

The experience gained with the instrument described above for electrically insulating liquids has been applied to the design of a new set of cells for electrically conducting liquids in order to overcome all of these problems. For this reason, the basic construction of the cells is similar as is shown in figure 3.iii.

The cell-body, 1, consists of two cylindrical cavities machined in

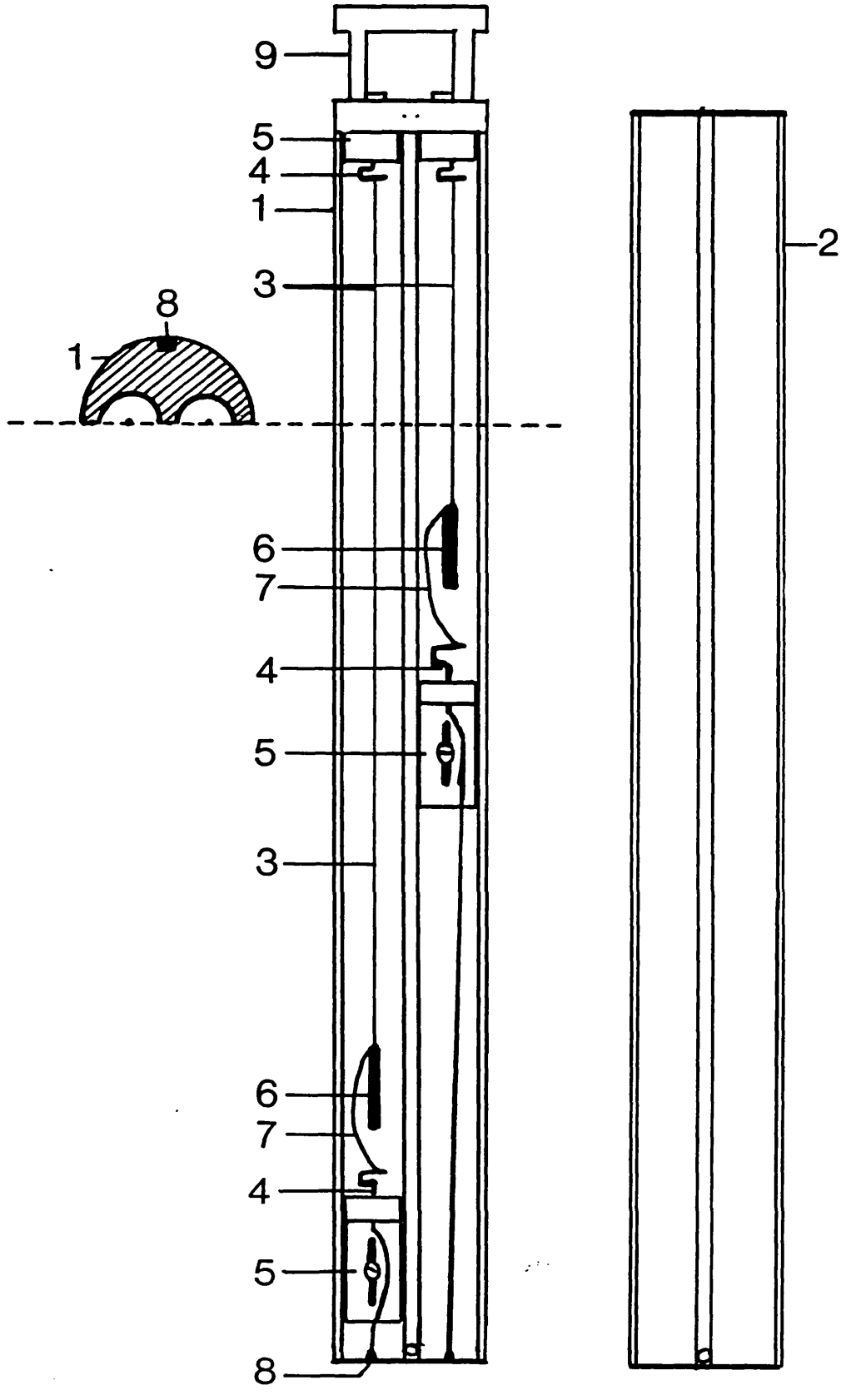


Figure 3.iii. The thermal conductivity cells for electrically conducting liquids.

a cylinder of Inconel 625 alloy, supplied by Wiggin Alloys Ltd., Birmingham. The Inconel 625 has been chosen for the cell body in order to avoid significant corrosion by media to be studied in future work. The single cylinder is divided along a dimetral plane, so that one half, 1, carries the hot-wires, while the other half, 2, forms an easily removable cover to provide access to the interior. The hot-wires 3 are in this case manufactured from 25μm nominal diameter tantalum wire and are affixed at either end to tantalum hooks 4 secured in a machinable ceramic insulator, 5, held in the cell body. There are two such wires of different length, employed to compensate for end effects { sec 2.4.1 }. At the upper end, the wires are secured directly to the hook by a spot weld. At the lower end, the same technique is used to attach the wire to a 100mg tanatalum weight 6 that provides sufficient tension to maintain the wire taut and vertical. The electrical connections to the lower tantalum hook is achieved by means of a thin loop of tantalum 7 arranged so as to exert no lateral force on the weight. At the rear of the cells, a groove was made so as to accomodate the tantalum wires 8 of 0.5mm diameter, which provide the electrical connection to the bridge. These wires were insulated so as to prevent electrical contact with the cell body by covering them in a heat-shrinkable nylon tube. The active half of the cells , carrying the tantalum hot-wires, is attached to an adaptor 9, which screws onto the high pressure vessel cap.

The spot-welding of the various components, that is, the wires to the hooks and weights, were made using an EMIHUS Microcomponents Ltd. Spot-Welder. The tantalum wire, 1, is positioned onto the tantalum hook, 2, was placed over the jaw of the electrode, 4, as shown in

Figure 3.iv. The spot-welding technique for the tantalum wires.

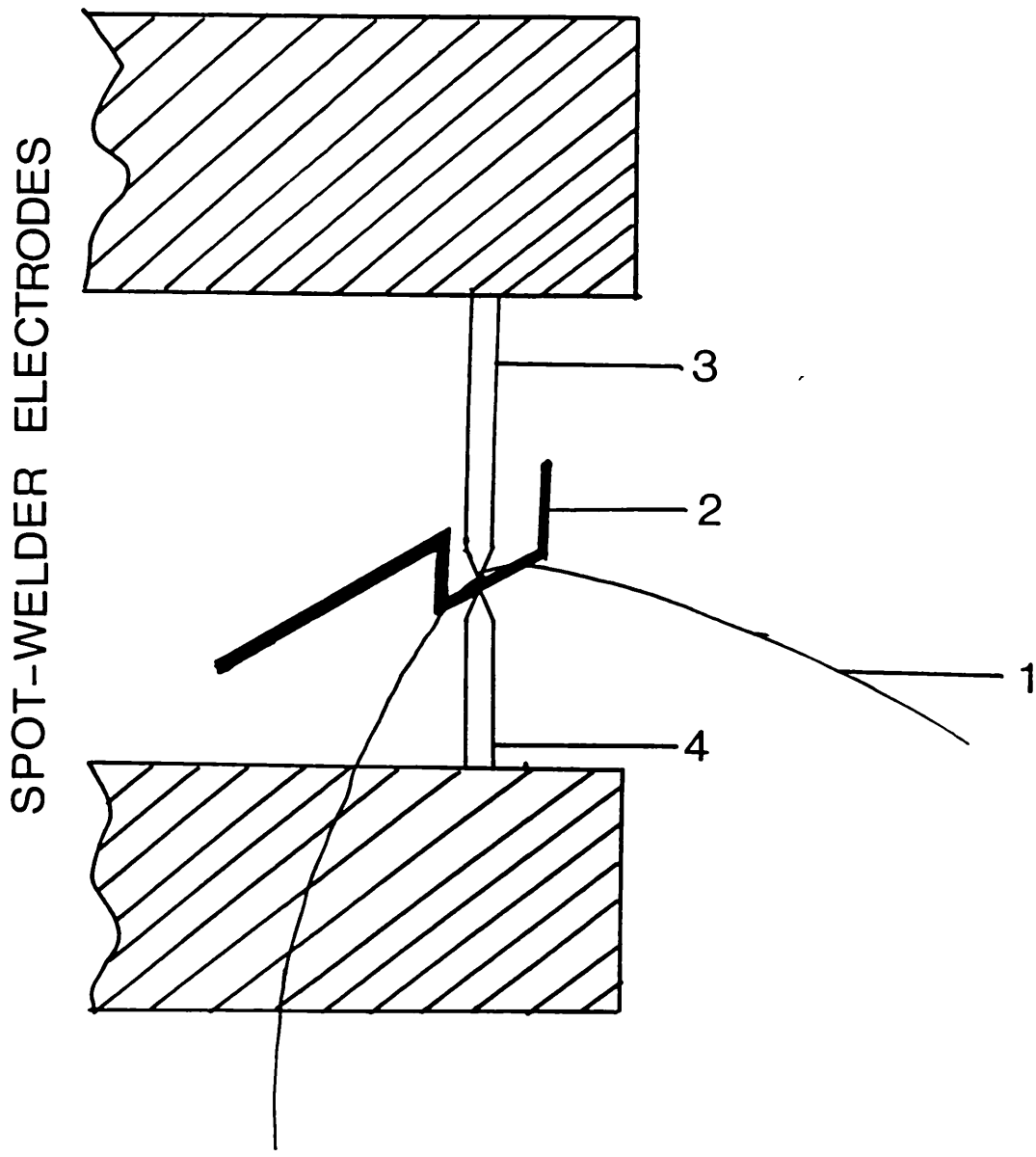


figure 3.iv and the wire was laid above it. The second electrode, 3, was then brought over and the spot-welder was discharged to provide a spot-weld. A large number of attempts were required to give a secure weld between the tantalum wire and the tantalum hooks. Once achieved, the joint was rather secure and robust, and could withstand knocks, unlike the platinum wires employed elsewhere. It is important to note that the electrodes used were made of tantalum, because copper or steel electrodes were found to deposit a dissimilar metal onto the tantalum spot-weld. This was due to the melting of the metal surface of the electrodes onto the tantalum metal during the discharge. Initially, the spot-welding was carried out under water to stop the formation of the metal oxide when employing the copper or steel electrodes. The oxide formation was due to the arcing of the electrodes when discharged in air. By having a disimilar metal deposited onto the tantalum, electrical insulation was virtually impossible, because of current leakage and chemical reaction of a comparatively reactive metal (copper) during electrolysis and anodization.

The characteristics of the thermal conductivity cells employed for the present measurements on electrically conducting liquids, namely water, are given below in table 3.2:

Characteristics of the cell design for electrically conducting liquids, and a typical set of tantalum wires, at 297.62K [66]	
Internal diameter of cells	9.90 mm ± 0.01mm
Length of long wire (tantalum)	144.08mm ± 0.02mm
Length of short wire (tantalum)	46.36mm ± 0.02mm
Long wire resistance at 262.9MPa	42.85Ω ± 0.05Ω
Short wire resistance at 262.9MPa	14.25Ω ± 0.05Ω
Tantalum wire radius	12.7μm ± 0.01μm
Cell material of construction: Inconel-625 Alloy.	

Table 3.2

The cell construction described, in particular the use of tantalum as the primary element, arises from the fact that it permits the insulation of the metallic wire to be accomplished rather simply and *in situ*. This is because it is possible to deposit a very thin layer of tantalum pentoxide on the surface of the tantalum wire by anodization. This oxide layer provides a strongly adherent insulating coating, while its thickness is such that the additional correction required to the measured temperature is very small { chapter 2 }.

The process of anodization is crucial to the success of the present instrument, and so it is described in some detail in what follows.

3.3.1 Anodization of the Tantalum Wires:

Prior to anodization, the wire assembly comprising of the tantalum hooks, wires, and weights as shown below in figure 3.v was chemically polished in a bath containing 98% H_2SO_4, 70% HNO_3 and 40% HF solutions in the ratio 10:4:3 by volume [76] for a few seconds.

Following this period, the tantalum wire assembly was immediately leached in boiling water for around fifteen minutes, to remove the film formed during chemical polishing. Anodic films produced on surfaces prepared in this way have previously been found to be strongly adherent. This treatment removed all scratches and any grease present, and left a surface comparable to that obtainable by electropolishing [76,77], and provided a good surface for the formation of the tantalum pentoxide. The wires were placed in position in the cells and the whole was then immersed in a dilute aqueous electrolyte of 0.2M H_2SO_4. The tantalum wire was connected as the anode of an electrolytic cell, and a 0.5mm diameter platinum wire introduced into the cell as the cathode. An anodizing current density of $2mA.cm^{-2}$ was established in the cell by increasing the applied voltage. When the voltage reached 50V, it was held at this value for three hours until the current density fell to $5\mu A.cm^{-2}$. Under these conditions, a layer of tantalum pentoxide, Ta_2O_5, with a thickness of about 800Å is formed on the surface of the tantalum wire [77]. The equation relating the thickness x(Å), to the voltage, V, was found to be:

$$x = 19 + 16.32\ V \qquad (3.1)$$

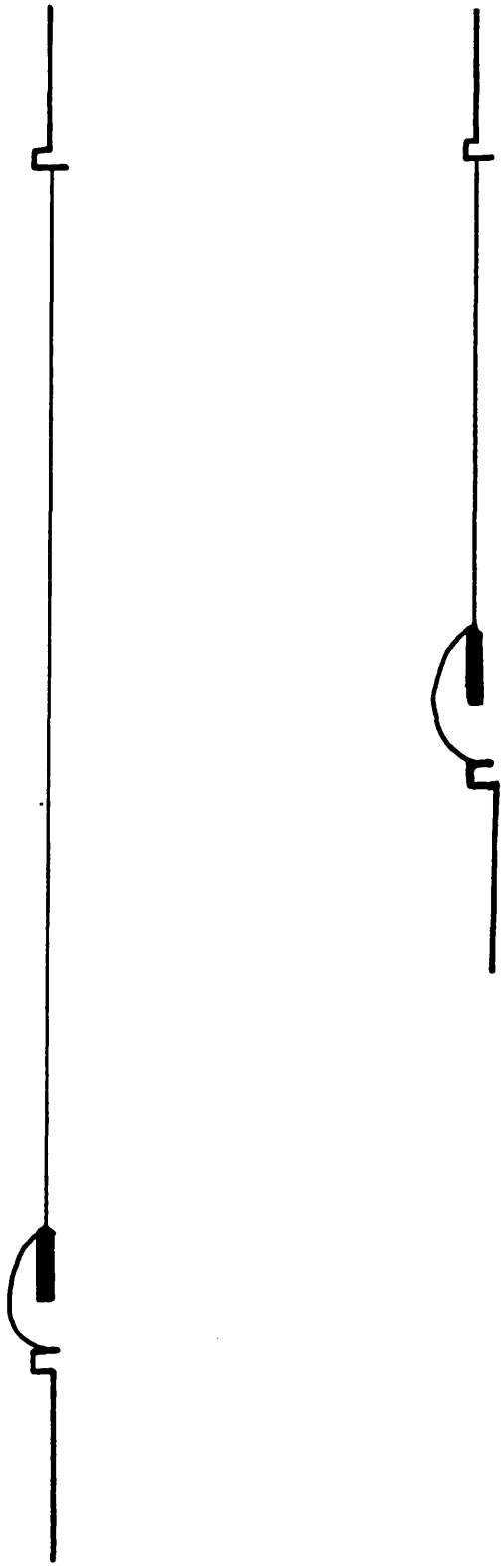


Figure 3.v. The tantalum wires' assembly prior to placing in the Inconel thermal conductivity cells.

When the anodization was complete, the electrolyte was removed, and the cells were cleaned and washed with distilled water several times, to remove traces of the electrolyte. The cells were then placed into a special housing that would contain the test fluid of interest, in this case, water. The water would then be introduced into the cells under vacuum and this will be described in a later section.

3.3.2 Effects of Pre-existing Film on Adhesion of Anodic Oxide to Its Substrate:

Films formed on chemically polished tantalum were initially found to be poorly adherent. The degree of adhesion depends to a large extent on the precise way in which the chemical polishing is done.

If the anodized metal is stretched, the oxide becomes detached in flakes of a size which depends on the method and materials used in chemical polishing. The oxide is detached in diagonal bands where slip occurs. If the anodized metal is cathodically polarized in dilute acid, hydrogen is liberated from under the film and separates it from the metal.

The reason for the initial poor adhesion on chemically polished tantalum was to be sought in the effect of the film left by chemical polishing. This was confirmed by leaching in distilled boiling water for longer than initially was thought necessary after chemical

polishing and before anodizing. In fact, on stretching the metal, such as when making the hooks, the oxide changed colour, indicating a decrease of thickness. The oxide does not become detached even where the fracture eventually occurs. It transpired that the time required for leaching for good adhesion, depends on the precise way in which the metal is chemically polished. One minute in boiling water is stated to be normally sufficient [78], but for metal " polished " in a cold bath, (as it was done here), up to thirty minutes were required.

3.3.3 Mechanism of Oxide Formation:

The chemical reaction that accmpanies the oxide deposition onto the metal surface is:

$$2\ Ta + 5\ H_2O \longrightarrow Ta_2O_5 + 10H^+ + 10e^- \qquad E_o = -0.81\ V \qquad (3.2)$$

In detail, this takes place initially:

$$2\ H_2O + 2e^- \longrightarrow H_2(g) + 2\ OH^- \qquad (3.3)$$

$$Ta \longrightarrow Ta^{5+} + 5e^- \qquad (3.4)$$

then:

$$2\ Ta^{5+} + 10\ OH^- \longrightarrow Ta_2O_5 + 5H_2(g) \qquad (3.5)$$

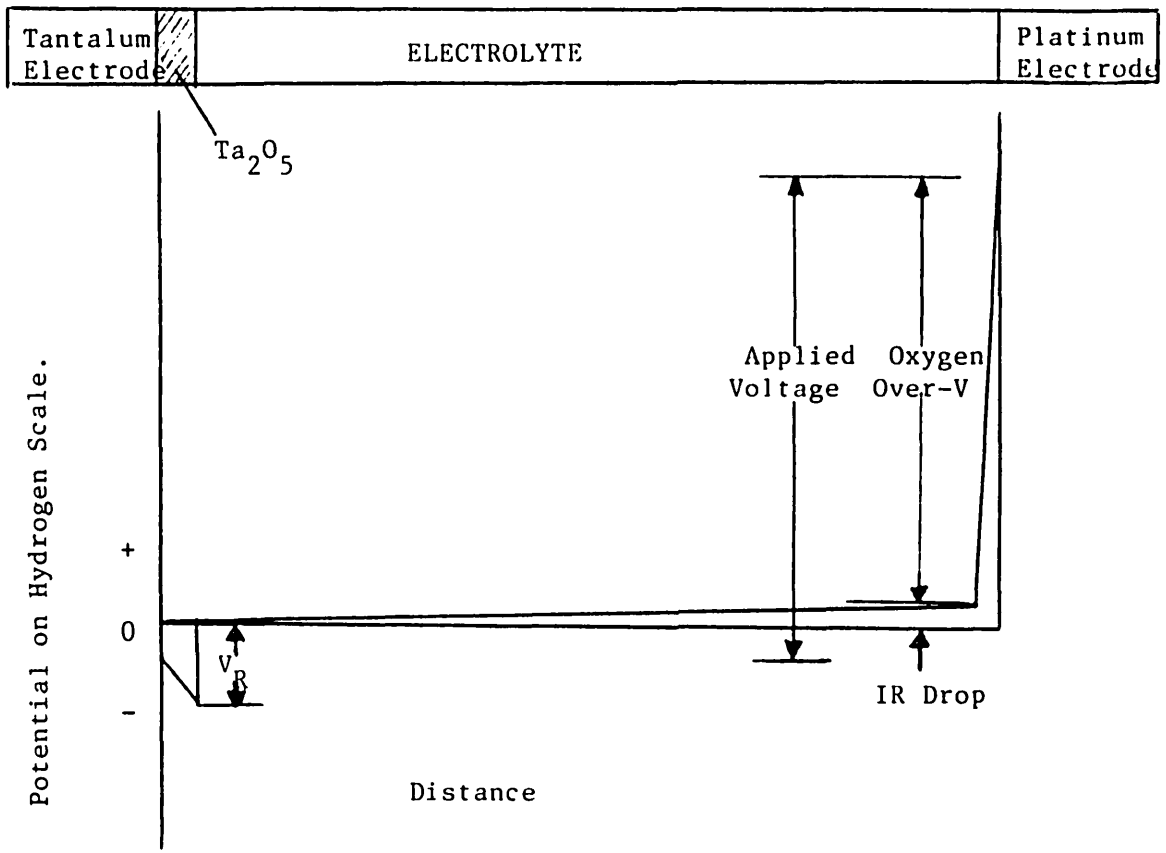


Figure 3.vi. Postulated distribution of potential during anodic oxidation of tantalum.

At the tantalum electrode, two reactions are possible; evolution of hydrogen and formation of tantalum oxide. When the tantalum is covered with an oxide film, as it is in this case, activity of the metal is very small, so that the electrode potential will be less negative than 0.81V and is designated in figure 3.vi by V_R. It is supposed that this potential difference occurs across a very thin double layer in the solution next to the tantalum pentoxide film.

It may be seen from figure 3.vi that although tantalum is negative with respect to the bulk of the solution, it is positive with respect to the solution immediately in contact with the tantalum pentoxide film, so that the field in the oxide film is in a direction to cause tantalum ions to move out through it to react with the water, and form the tantalum pentoxide layer.

3.3.4 Cell Mounting:

The cell is mounted on the top closure of a 1000MPa pressure vessel, 1, within a two component sheath as shown in figure 3.vii. The inner part of the sheath 2 is an inconel support section, whereas the outer part 3, is a thin walled, flexible heat shrinkable polymeric material, which forms a seal to the inconel at either end by using specially supplied adhesives. This polymer sheath provides the enclosure for the test fluid 4, and separates it from the hydraulic fluid 5, which is pressurised using an external hand pump. This separating sheath is sealed to the upper cap of the pressure vessel by a lead gasket 6. The enclosure may be filled with the test fluid under

vacuum through the ports 7 and 8 prior to insertion in the pressure vessel.

The polymeric material 3, DR-25, was supplied by Raychem (UK) Ltd. This tubing is capable of operating from -75°C to +150°C, and has a number of suitable properties for application to the work undertaken in this work. These properties include flexibility, chemical resistance and abrasion resistance. It is made from a radiation cross-linked elastomeric material formulated for optimum high temperature fluid resistance and long term heat resistance.

3.4 The High Pressure Equipment.

A schematic diagram of the pressure vessel employed for the measurement of thermal conductivity is shown in figure 3.vii. The pressure vessel was manufactured by Harwood Engineering Company Inc. from aircraft quality steel, designed to the following specifications:

Working Pressure	10000 Kg cm^{-2}.
Working Cavity	0.205m Long and 0.0381m i.d.
Outside Diameter	0.21m.
Overall Length	0.5m.

Table 3.3 High Pressure Vessel Specifications.

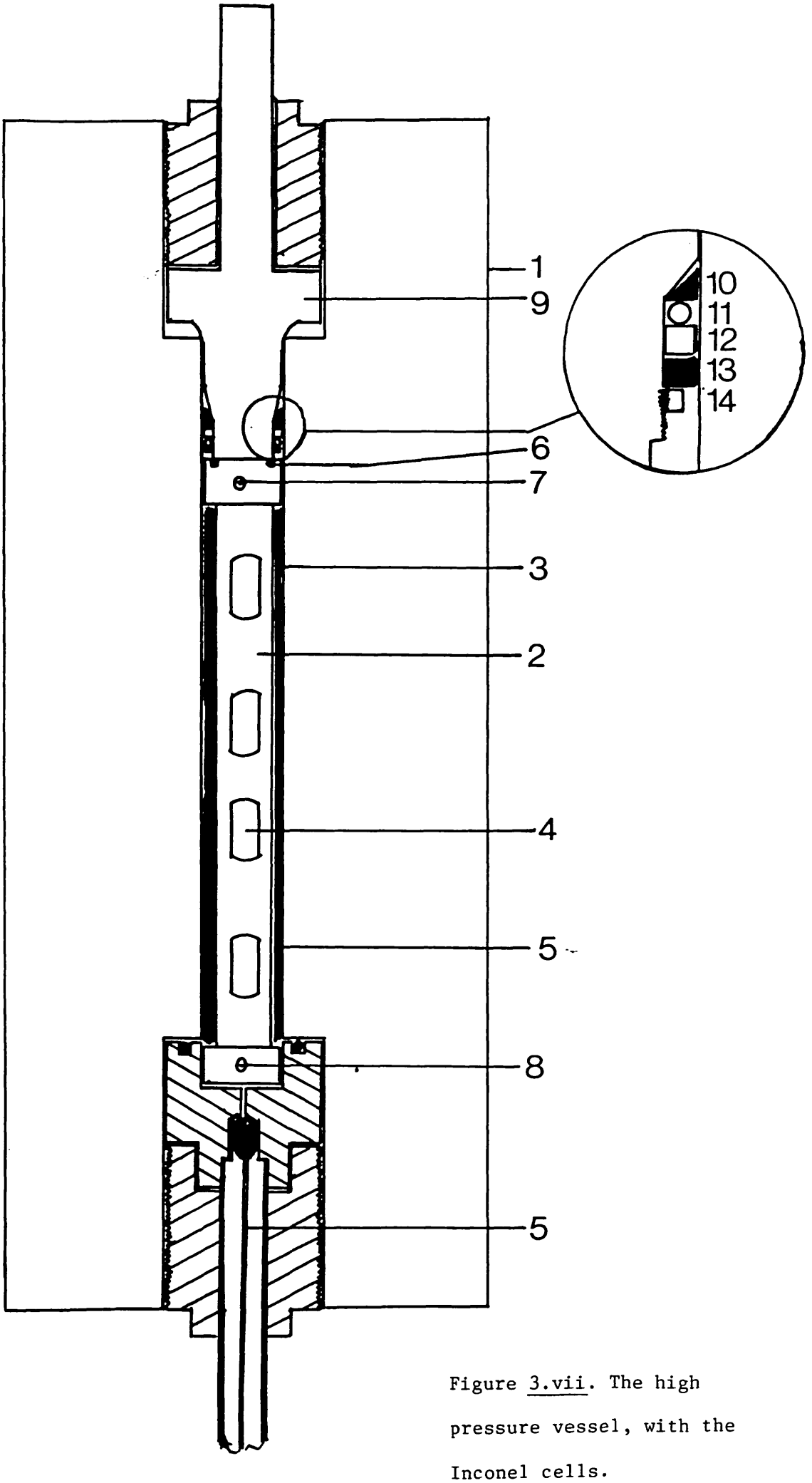


Figure 3.vii. The high pressure vessel, with the Inconel cells.

With reference to figure 3.vii, the pressure vessel, 1, is sealed at its upper end by plug 9, which carries a phosphor bronze sealing ring 10, together with a rubber O-ring 11, supported by a teflon primary sealing ring 12. These rings are all secured in position by a retaining ring 14, separated by a phosphor bronze washer ring, 13. The top plug 9, is bored with four holes to enable the connection of the electrical leads to the inside of the pressure vessel. The four feed-throughs consist of Invar cones lapped into ceramic cones, which themselves are lapped into the plug body. Thus, the electrical leads are connected to the Invar cones and are passed through the holes in the plug body to the exterior of the vessel and straight to the measurement bridge.

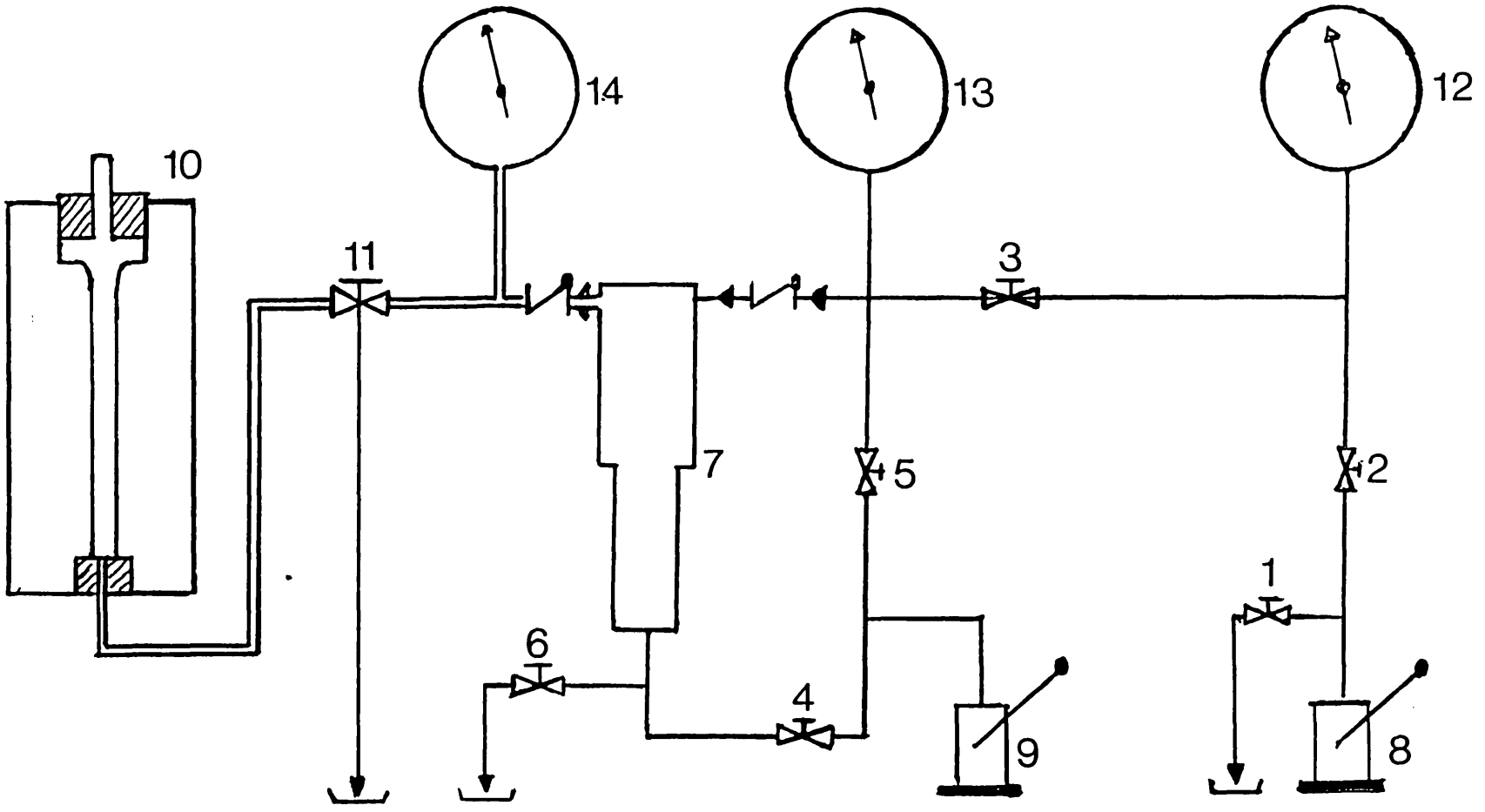
It is, of course, not possible to insulate the Invar cones by means of the anodization process applied to the tantalum components of the cells. Consequently, a different method had to be applied, and it proved rather difficult to insulate both the connections between the tantalum wires and the Invar, as well as the surface of the Invar cones. After many trials, the greatest degree of success was achieved with an electronic component potting resin, a polyurethane flexible Encapsulant 555-106, supplied by Radio Spares Components, Corby. This compound proved both sufficiently strongly adherent and flexible to withstand pressures as high as 300MPa and temperatures up to 90°C. This material completely filled the cavity indicated by 9, between the bottom of the pressure vessel plug, and the top of the cells as indicated in figure 3.iii.

At its lower end, the pressure vessel is connected through high pressure piping to a hydraulic system. The thermal conductivity cells are mounted onto the pressure vessel sealing plug as shown in figure 3.vii, then inserted within the cylindrical housing which contains the liquid under test. The housing 2 is sealed to the pressure vessel cap by means of a lead gasket 6. At its lower end, the housing carries the heat shrinkable polymeric sheath. The housing containing the thermal conductivity cells, is filled with the test liquid under vacuum, to ensure complete filling of all the voids, before insertion into the pressure vessel.

A schematic representation of the pressurizing system is shown in figure 3.viii. The system is essentially divided into a low pressure and a high pressure side. The low pressure side is for pressurization of the pressure vessel and the high pressure side up to 25MPa. After this initial pressurization, the high pressure side, when isolated from the low pressure side by valve 5, pressurizes the autoclave via an intensifier 7 from 25MPa up to 700 MPa.

The specifications of the individual components of the pressurizing system employed in this apparatus are given below:

1 Relief valve, non-rotating, spindle type, model number V-110-20, made by Pressure Products Inc. Ltd. and rated to 20,000 psi (150 MPa approx.).



High Pressure Tubing.

Low Pressure Tubing.

Figure 3.viii The pressurizing system.

2 Low pressure isolation valve, non-rotating, spindle type, model number V-110-30, made by Pressure Products Inc. Ltd. and rated to 30,000 psi (200 MPa approx.).

3 Low pressure isolation valve, non-rotating, spindle type, model number V-110-60, made by Pressure Products Inc. Ltd. and rated to 60,000 psi (400 MPa approx.).

4 Low pressure isolation valve, specification as 3.

5 Low pressure isolation valve, specification as 3.

6 Relief valve, specification as 1.

7 Intensifier model number A2.SJ, manufactured by Harwood Engineering Company Inc. USA, with intensification factor of 15 and rated to 200,000 psi (1400MPa approx).

8 Hand-operated low pressure pressurizing pump manufactured by Blackhawk Hydraulic, model number P76, rated at 10,000 psi, (75 MPa approx.).

9 Hand-operated high pressure pressurizing pump manufactured by Enerpac model number P228, rated at 40,000 psi.(300 MPa approx.)

10 Pressure vessel manufactured by Harwood Engineering Company Inc., USA, designed to sustain a working pressure of 10,000 MPa.

11 Vent valve, non-rotating spindle spindle type, made by Harwood Engineering Company Inc. USA, and rated to 10,000 MPa.

12 1500 Atmosphere gauge made by the Budenberg Gauge Company, accurate to ± 1% of full-scale deflection.
For calibration, see appendix 3.

13 3000 Atmosphere gauge, same as 12.

14 5000 Atmosphere gauge, same as 12.

The tubing used in the low pressure line was 1/4" o.d. and 1/16" i.d., type 304S stainless steel seamless tubing, supplied by Nova-Swiss Ltd.

The tubing used in the high pressure side was 3/4" o.d. and 1/16" i.d., type 12H-1* composite, type 316 stainless steel core with alloy shroud and with a working pressure of 200,000 psi.

The entire pressurizing system, apart from the two hand-operated pumps 8 and 9, is enclosed within, but electrically insulated from, a steel cabinet with 1/4" mild steel plate sides. This was made for two primary reasons, (i) safety - in case of pipe or fitting rupture or failure due to the high pressures attained, and (ii) electrical noise pick-up that may be introduced to the highly sensitive electronic

measuring apparatus, connected to the pressure vessel via the leads to the wires. It has been an ardious task to insulate the entire system from external sources of electrical interference, and to stop the whole apparatus from acting as an aerial for picking up stray signals from within and outside the building.

The test liquid in the autoclave is pressurized by initially pumping on the low pressure side pump 8 until about 1000 bar is attained within the system and the pressure vessel. The low pressure side is then isolated with isolation valve 5 and then further pressurization is performed using pump 9. The pressure in the system was determined by one of the three Budenberg gauges depending on the pressure. The first gauge 12 had a range to 150 MPa, the second 13 to 300 MPa and the third 14 to 500 MPa. Each pressure gauge was independently calibrated against a dead-weight tester certified by the National Physical Laboratory. The detailed results of the calibration are given in appendix 3.

The entire pressurizing system was mounted on pneumatic anti-vibration supports to isolate the entire instrument from building vibrations, which are rather easily transmitted to the hot-wire assembly. Such vibrations, appear as low frequency noise on the bridge output, as a result of strain induced fluctuations in the resistances of the tantalum wires.

The pressure vessel and pressuring system for the work with

insulating liquids, is essentially the same as that described here and the full details may be found elsewhere [14,71].

3.5 Thermostats.

The pressure vessel itself is contained within a well-stirred oil bath, whose temperature is controlled by a three-term control system with a platinum resistance thermometer sensor operating on a distributing immersion heater network. The stirrers of the thermostat bath are mounted independently of the pressure vessel, so as to avoid the transmission of vibrations to cell-wires. The oil employed in the bath was Thermia B, manufactured by the Shell Oil Company, which which can be maintained at a temperature up to 150°C without any significant degradation.

A temperature differential, (0.25°C) increasing upwards, was maintained along the length of the pressure vessel by means of a small auxilliary heater. This ensures that convective currents cannot be established in the thermal conductivity cell under steady state conditions. The absolute temperature of the liquid within the thermal conductivity cells was determined using a Degussa platinum resistance thermometer, in good thermal contact with the presure vessel. The resistance of the Degussa element was measured with a Comark Microprocessor Thermometer type 6800, and was converted to temperature using an independent calibration. In this way, it was estimated that the temperature of the test liquid was determined with an uncertainty of no more than $\pm$0.01K. Tests of the stability and uniformity of the

temperature in the oil bath indicated that the variation of the temperature was no more than $\pm$0.03K over a six hour period. Because the duration of a single experiment is of the order of one second, this stability is more than sufficient for accurate measurements.

The thermostat system employed for the measurements on the electrically insulating liquids, differs only in detail from that described here, and a complete description is given elsewhere [14,71].

3.6 Auxilliary Measurements.

Two auxilliary measurements are necessary in order to be able to make absolute thermal conductivity measurements. The first is the determination of the temperature-resistance characteristics of the metallic wire, and the second is its diameter. The first result contributes directly to the accuracy of the thermal conductivity data, whereas the second need be known with only moderate accuracy to permit the application of small corrections. { Chapter 2 }.

3.6.1 Resistance-Temperature Characteristics Of The Wires.

A literature survey was conducted to obtain the physical properties of the tantalum wires employed here as temperature rise sensors. There proved to be conflicting sets of values for the temperature-coefficient of resistances of this material, that ranged from 0.0031 to 0.00383. Because the final, reported thermal

conductivity depends directly on this temperature coefficient, it was decided to determine the temperature coefficient independently, for a sample of wire employed in the thermal conductivity studies.

A sample of tantalum wire was mounted in a stainless steel frame, so that it was free from tension. The frame and wire were immersed in a glass cell full of toluene, which itself was mounted in a thermostat oil bath. A standard platinum resistance thermometer (Tinsley), was immersed in the toluene, in order to determine the absolute temperature of the sample. The resistance of the tantalum wire was determined at ten degree intervals in the range 20°C to 90°C using an A.C. resistance bridge, (ASL) with a resolution of 0.00001Ω. From a statistical analysis of the data, the correlating equation:

$$R_T/R_0 = 1 + 3.3738E\text{-}3(T-273.15) + 3.17669E\text{-}7(T-273.15)^2 \qquad (3.6)$$

was established. Figure 3.ix shows the deviations of the experimental data for this correlation, and demonstrates that the deviations are commensurate with the accuracy of the resistance measurements. It is estimated that the uncertainty in the temperature coefficient of resistance of tantalum at any temperature is no more than ±0.2% [66].

In the case of the platinum wires employed for the measurements on electrically insulating liquids, there is considerably less difficulty in obtaining the resistance-temperature characteristics. This is

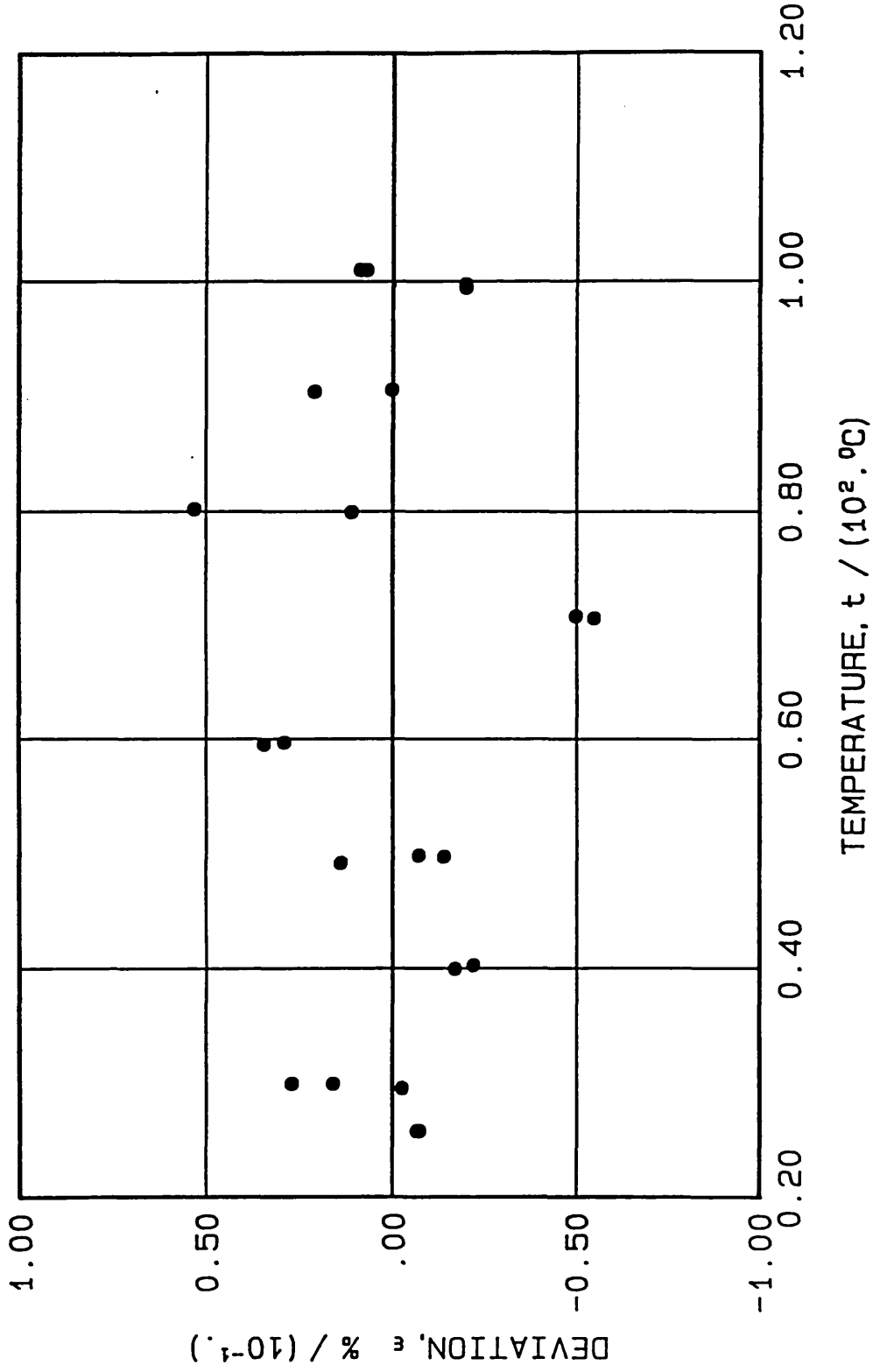


Figure 3.ix. Deviations of measurements of the resistance of tantalum wire, as a function of temperature from the correlation of equation (3.6). $\epsilon = [(R_{expt} - R_{calc})/R_{calc}] \times 100$.

because the platinum employed for the measurements, supplied by Sigmund Cohn Ltd. has a purity in excess of 99.99%. Thus, it is possible to use the formulation of the resistance-temperature characteristics of platinum which forms the basis of the International Practical Temperature Scale [79]. Thus, for platinum, we employ:

$$R_{(T)}/R_0 = 1 + A(T-273.15) + B(T-273.15)^2 \qquad (3.7)$$

where, $A = 3.98471 \times 10^{-3} K^{-1}$ and $B = -5.874557 \times 10^{-7} K^{-2}$.

This has been shown to be adequate for the platinum wires employed for measurements in the gas phase [80], where the absolute value of the thermal conductivity determined depends on this calibration, can be checked independently.

3.6.2 Wire Diameter Measurements.

The diameter of samples of the platinum and tantalum wires were determined by electron microscopy. For this purpose, samples of different sections of each wire were mounted in specially manufactured potassium bromide blocks. From the electron micrographs it was possible to determine the diameter of each wire. Accounting for magnification errors in the measurement, as well as the inevitable non-uniformity of the wire diameters, the final results, together with their uncertainty are:

for platinum

$$a = 3.82\ \mu m \pm 0.1\ \mu m,$$

for tantalum

$$a = 12.7\ \mu m \pm 0.1\ \mu m.$$

These quoted uncertainties are relevent to the estimation of the error incurred in applying many of the corrections listed in Chapter 2. However, the values quoted above are sufficiently small to ensure that the effect on the final reported thermal conductivity is negligible.

3.7 Filling Procedure.

The test liquid is first distilled, so as to satisfy the requirement that it is as pure as possible. This purity was invariably verified with a gas chromatogram test, and was usually greater than 99.9%. To facilitate introduction into the cell enclosure, so as to ensure complete filling without any voids - as these voids tend to lead to possible rupture under pressure due to air entrapment - the liquid is introduced under a vacuum through ports 7 and 8, see figure 3.vii, via a special filling rig, specifically designed to perform such tasks [71]. Because the liquid is filled in such a manner, it is necessary to degas the fluid. The liquid of interest is at first frozen and the air above it in the flask is evacuated until a good vacuum is achieved. The frozen mass is allowed to melt, and hence, evolution of air bubbles dissolved in the liquid is observed, which will occupy the evacuated space above the liquid. The liquid is then refrozen and the volume of air above the solid is evacuated again. This process is repeated until no more air is observed in the space above the liquid. This is confirmed by using sensitive Pirani and Penning Vacuum Gauges.

3.8 Electronic Apparatus.

The main purpose of the electronic components in the apparatus is to determine the temperature rise of the tantalum hot-wires in the thermal conductivity cells, as a function of time during their transient heating.

The use of 25μm diameter tantalum wire in place of the 7μm platinum wire of earlier instruments [14,71], means that the resistance of the temperature-sensing elements in the thermal conductivity hot-wire instrument, is drastically reduced, by a factor of five compared with the earlier instruments. Since it is desired to retain the same precision in a temperature rise measurement of no more than 3 - 5K, it has been necessary to design a new measurement system, to improve the resolution of the automatic Wheatstone bridge employed. At the same time, a similar, new bridge has been applied to the cells in the instrument for electrically insulating liquids. This is because, in addition to its other advantages, the new bridge allows automatic data-acquisition and greater flexibility in operation.

The bridge provides a means of determining the times, following initiation of transient heating, at which the resistance difference of the long and short tantalum wires attains certain preset values. Thus, on the one hand, it provides a means of automatically compensating for end effects in the wires [12,13,45], and, on the other hand, it allows the temperature rise of the wire as a function of time, to be

determined from the resistance-temperature characteristics of the metal.

The symbols R_L and R_S represent the long and short wires of the thermal conductivity cells respectively. The left-hand arm of the bridge is identical with that of previous arrangements [14,71]. However, the right-hand arms of the bridge used earlier are replaced by a different arrangement, in which V_E is a source voltage, which can be arranged to provide accurate preset values, to a programmed sequence. This element is, in practice, a digital to analogue convertor.

The other resistive elements of the bridge are high precision decade or fixed resistors. The bridge power supply V_o is a stable, high precision source of a direct current voltage, used to provide the wire heating current and as a reference voltage for the digital to analogue convertor, V_E. S_1 is a mercury-wetted reed relay. C is a very high impedence null-detector (comparator).

Both the digital to analogue convertor and the comparator are interfaced to a microcomputer, which controls the entire measurement cycle. Prior to the initiation of a measurement, a sequence of values for V_E are stored in the microcomputer. A first value of V_E is established and the bridge is set out of balance. Upon initiation of a run by closure of relay S_1, a timer is started, and the current in R_L and R_S would cause their temperature to rise, at a rate determined by the thermal conductivity of the fluid in the surrounding cell. The

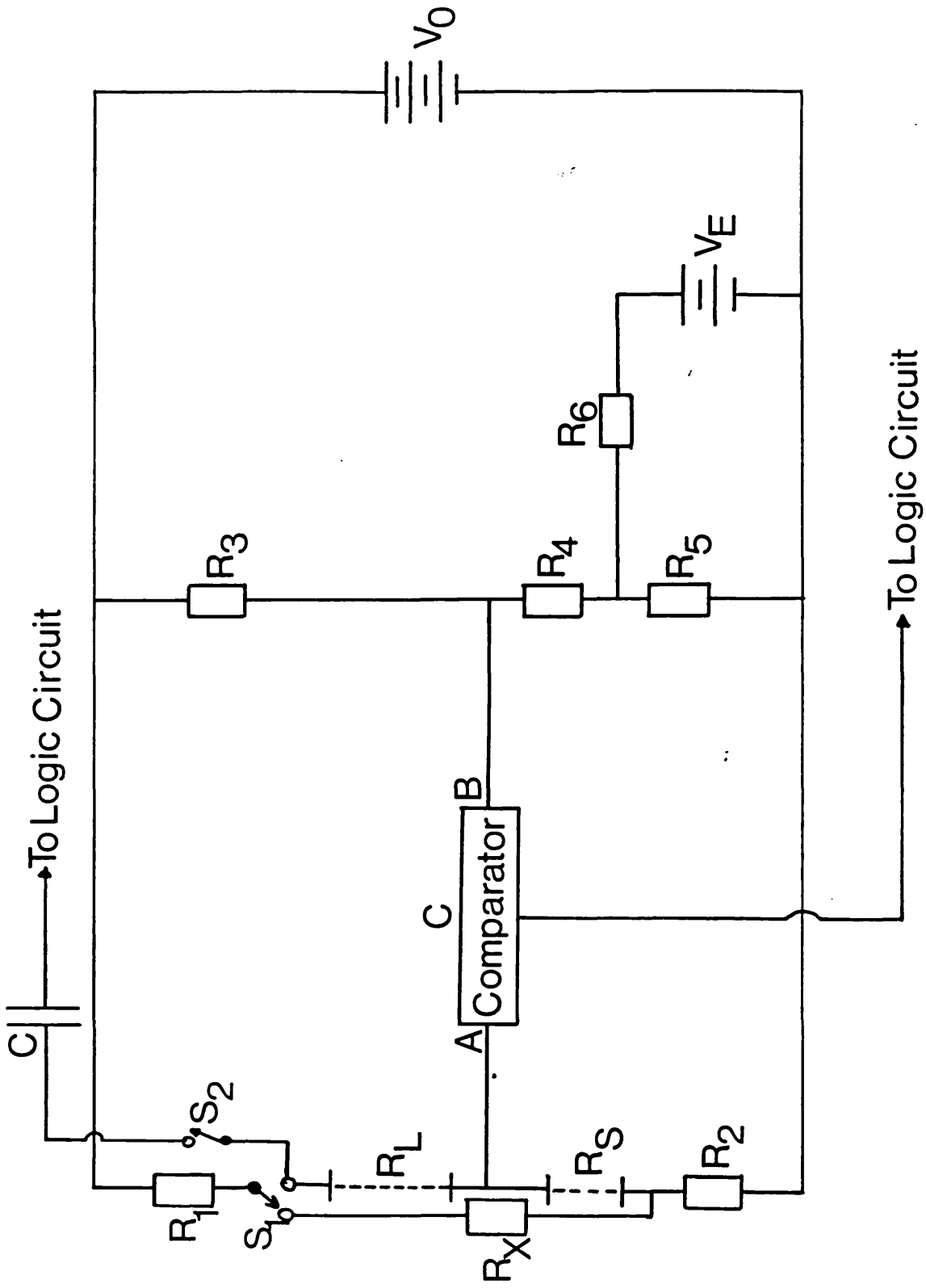


Figure 3.x. A schematic diagram of the new bridge arrangement, for the measurement of the thermal conductivity of liquids[81].

temperature of the wires increases according to:

$$\Delta T_{id} = \Delta T_w + \sum_i \delta T_i \qquad (3.8)$$

where $$\Delta T_{id} = \frac{q}{4\pi\lambda} \ell n \frac{4\kappa t}{a^2 C} \qquad (3.9)$$

and at some time later, the bridge balances. This balance is detected by the zero crossing of the comparator, and the time at which this occurs is recorded for the first preset value of V_E. From the balance condition, the resistance difference ($R_L - R_S$) at this time may be determined. Subsequently, the microcomputer downloads the second value of V_E so that the bridge is unbalanced, from which a second balance condition is achieved later in the cycle. By repetition of this process, up to 1024 (ΔT, t) points may be acquired in a single run with a duration of one second. A description of the comparator is given in a later section, together witha diagram of the comparator employed in this bridge.

In order to use this bridge to measure the transient resistance difference of R_L and R_S, a complete circuit analysis is necessary. The same analysis then permits the selection of the various resistors in the circuit to achieve the required precision in the temperature rise measurements.

3.8.1 Circuit Analysis.

With reference to figure xi, the following equations can be established:

$$i_1 = i_2 + i_3 \tag{3.10}$$

$$i_1 = i_7 - i_6 \tag{3.11}$$

$$i_5 = i_6 + i_4 \tag{3.12}$$

$$i_7 = i_5 + i_{11} \tag{3.13}$$

$$V_o = i_3R_3 + i_4R_4 + i_5R_5 \tag{3.14}$$

$$V_o = i_2(R_1 + R_L) + i_8(R_2 + R_S) \tag{3.15}$$

$$V_E = i_6R_6 + i_5R_5 \tag{3.16}$$

These equations may be solved to yield the out-of-balance voltage across A-B as:

$$\frac{V_{AB}}{V_o} = \frac{R_1+R_L}{(R_1+R_L+R_2+R_S)} - \left[\frac{\left[\left(\frac{R_3}{R_5} + \frac{R_3}{R_6}\right] - \frac{V_E}{V_o}\frac{R_3}{R_6}\right.}{1 + \left[\frac{R_3}{R_5} + \frac{R_4}{R_5}\right]\left[\frac{R_5}{R_6} + 1\right]}\right] \tag{3.17}$$

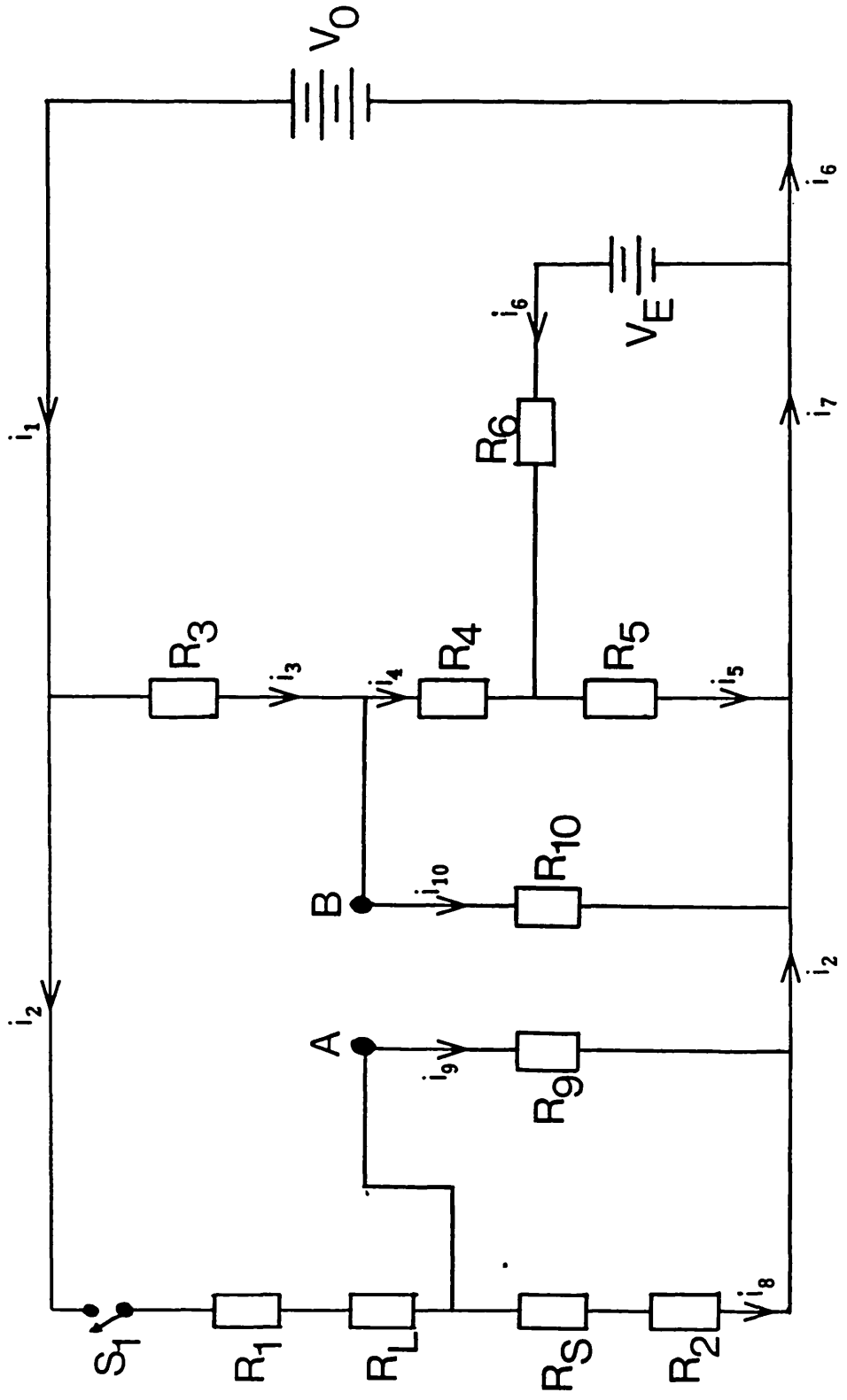


Figure 3.xi. The automatic bridge for the measurement of thermal conductivity, showing the currents for the circuit analysis.

At balance, $V_{AB} = 0$, and this leads to the result:

$$\frac{R_1+R_L}{R_1+R_L+R_2+R_S} = \frac{\left[\frac{R_3}{R_5} + \frac{R_3}{R_6}\right] + \frac{V_E}{V_o}\frac{R_3}{R_6}}{\left[1 + \left[\frac{R_3}{R_5} + \frac{R_4}{R_5}\right]\left[\frac{R_5}{R_6} + 1\right]\right]} \qquad (3.18)$$

so that:

$$R_L - R_S = \frac{\left[\frac{R_L}{R_S} - 1\right]\left[CR_2 - (1-C)R_1\right]}{\frac{R_L}{R_S}(1-C) - C} \qquad (3.19)$$

where C is

$$C = \frac{\left[\frac{R_3}{R_5} + \frac{R_3}{R_6}\right] - \frac{V_E}{V_o}\frac{R_3}{R_6}}{\left[1 + \left[\frac{R_3}{R_5} + \frac{R_4}{R_5}\right]\left[1 + \frac{R_5}{R_6}\right]\right]} \qquad (3.20)$$

Equation (3.19) therefore forms the working equation for the interpolation of the bridge measurements. It will be noted that the equation for the resistance difference of the two wires, contains the ratio of R_L and R_S. However, this ratio is almost independent of time, so that the equation is (almost) explicit in (R_L-R_S).

3.8.2 Precision of The Resistors and The Temperature Rise.

In order to determine the thermal conductivity of a fluid with a precision of $\pm 0.1\%$, it has already been shown [57], that the temperature rise measurements should be made with a precision of $\pm 0.05\%$. This implies tolerances for all of the resistors in the bridge as well as the voltage V_E. In addition, V_o should be known with an uncertainty of less than $\pm 0.05\%$. Because the precision in the temperature rise is identical to that in the value of

$$\{[R_L(t) - R_S(t)] - [R_L(0) - R_S(0)]\} \qquad (3.21)$$

so far as the thermal conductivity is concerned, equation (3.19) forms the basis for the calculation of the tolerances in each of the bridge components, as well as their absolute values. In this manner, it is found that to achieve the specified uncertainty, the resistors R_3, R_4, R_5 and R_6 should all have a tolerance of $\pm 0.01\%$, while V_E/V_o should have a tolerance of $\pm 0.01\%$. The absolute values of the resistances selected are listed in table 3.3. For R_1, R_2, and R_6, decade resistors were employed to retain the greatest flexibility.

Resistor	Make/Model	Resistance Value (Ω)	Temperature Coefficient per °C	Tol.
R_1,R_2	H.Tinsley & Co. Ltd. Model 5690	10x10 ,10x1 10X0.1,10x0.01	Not Available	±0.01%
R_3	Vishay Welwyn 4812	2x1000	0.0025%	±0.01%
R_4	Vishay Welwyn 4812	1x1000	0.0025%	±0.01%
R_5	Vishay Welwyn 4812	1x1000	0.0025%	±0.01
	Muirhead Vac	2x1	N/A	±0.1%
	Pye Manganin	1x1		±0.1%
R_6	Muirhead Vac D 805-F	10x10000	<±0.001%	±0.05%
	D 805-G/I	10x100000	<±0.001%	±0.05%
R_D	Muirhead Vac	10x10	0.002%	±0.05%
D.C. Power Supply: Hewlett Packard Output 0-40 volts at 0-500 mA, Model Number 6112 A.				
Switches: S_1 One Mercury-Wetted Reed Relay Type Switch.				

Table 3.3 Bridge Components.

The circuit described above has also been repeated for the case when the input impedance of the comparator is finite and not infinite as assumed in section {3.8.1}. The comparison of this calculation with the earlier one, enables the definition of the comparator input impedance necessary to introduce a negligible effect, ($< 1x10^{-5}$) into the evaluation of (R_L-R_S). It is found that an impedance of 10^9 Ohm is sufficient for this purpose which is rather easily achieved.{ Section 3.8.3 }.

3.8.3 Limitation of R_9 and R_{10} Resistances In The Circuit.

It has been shown that, if R_9 and R_{10} exceed 10^9 Ohm - that is essentially the conribution from the input impedance of the comparator - then an error in the evaluation of (R_L-R_S) is only $1x10^{-5}$% . An input impedance of 10^9 Ohm is easily achieved.

3.8.4 Electrical Noise.

A final consideration in the design of the electronic circuitry concerns the level of electrical noise at the bridge output. Any such noise manifests itself as a scatter in the temperature rise measurements. Consequently, the noise level must be maintained as low as possible. The tolerable level, consistent with the precision aimed for, can be deduced from the circuit analysis given earlier, and it transpires that the value needs to be of the order of 1 μV. This is one order of magnitude less than that necessary, and achieved in early versions of the automatic bridge. This is because of the much lower signal to be observed in the case of the tantalum wires. The problem is exacerbated by a further factor associated with the case of an electrolytically deposited oxide film for insulation. Figure 3.xii(a) shows a schematic diagram of the earthing arrangement used in earlier automatic bridges to reduce noise. In essence, the center point of the bridge (the comparator) is maintained at earth potential, which is also the potential of the outer walls ot the thermal conductivity cells and the pressure vessel. This arrangement ensures the lowest interference pick up by the comparator.

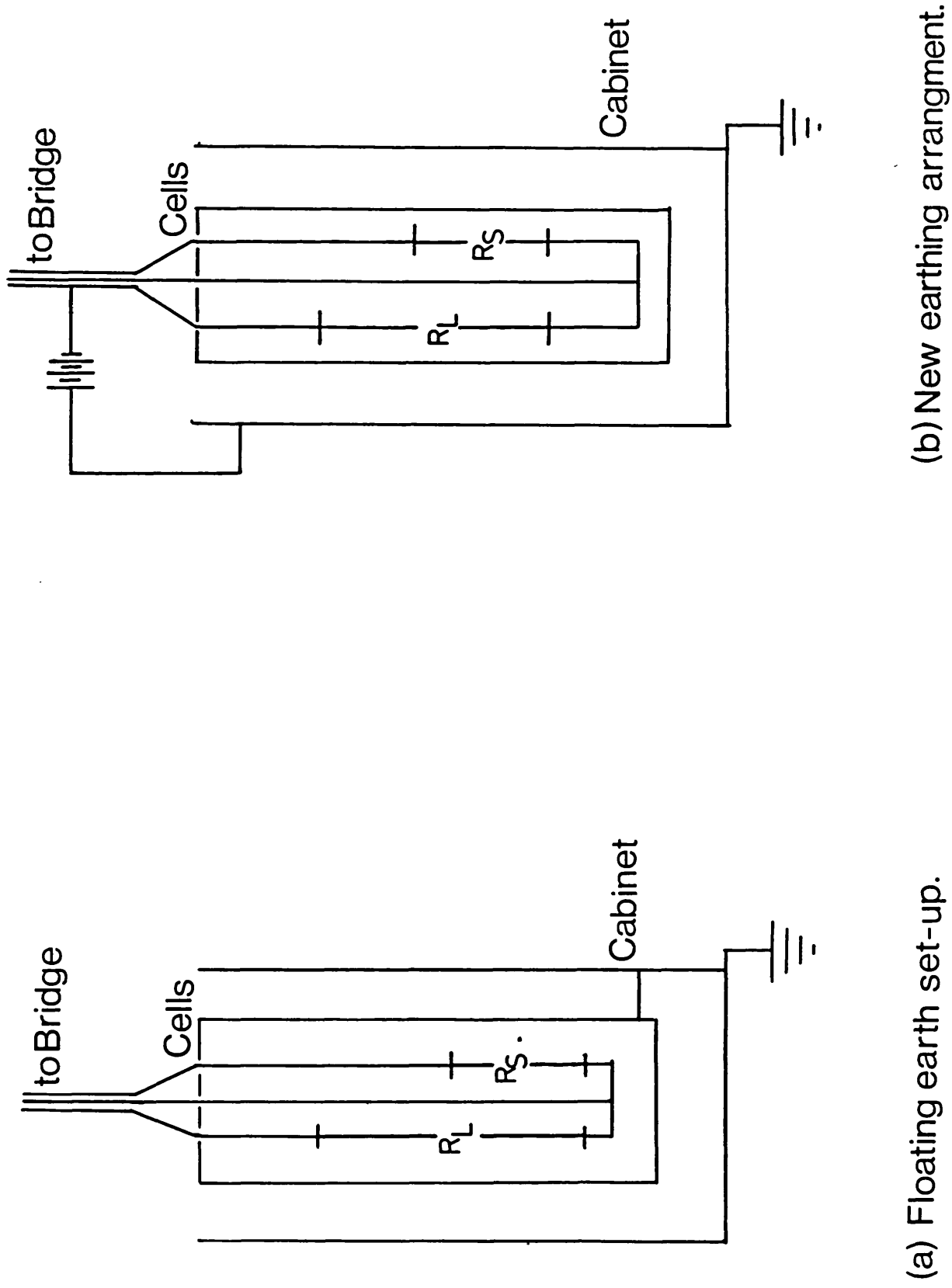


Figure 3.xii. The different earthing arrangements for the thermal conductivity apparatus, for both electrically conducting and insulating liquids.

In the case of the tantalum wires, the same scheme cannot be adopted, because the structure would be maintained at a negative potential with respect to the vessel wall and the fluid achieved within it, and so the insulating oxide film will be destroyed by electrolysis. Consequently, the configuration shown in figure 3.xii(b) has to be adapted, in which the tantalum wire is biased by a d.c. voltage supply with respect to the ground potential. Although this arrangement obviated the dissolution of the oxide film, it means that the center point of the bridge is no longer at earth potential, and the pick-up of electrical noise is made worse.

For these reasons, great care had to be taken with the location of each element of the automatic bridge system, to minimize such pick-ups. Thus, the comparator was built into a screened box and both it and the bridge resistors were mounted inside a hermetically sealed enclosure. The latter could be mounted very close to the pressure vessel containing the cells, so as to keep the connecting leads to the hot-wires as short as possible. Furthermore, it was necessary to select very carefully the position of the computer, in order to avoid pick-up of its radiation. After a considerable amount of trial and error, suitable positions and conditions were found, so that the noise level at the bridge output attained a value of 1 μV.

3.8.5 The Comparator.

From the preceding discussion, it should be clear that the

comparator forms a vital element in the circuit. This is because the device must possess a high input impedance, a high common-mode rejection ratio and a high gain, while maintaining an internal noise level below that intrinsic to the bridge itself. The times at which the bridge balances during transient heating are determined by recording the times at which the voltage across points A and B in figure 3.x. This is achieved by using a comparator which is in essence a very sensitive electronic galvanometer. The circuit diagram of the comparator employed is shown in figure 3.xiii. It consists of two input buffer amplifiers (type OP37) which are balanced in a cross-coupled mode, so as to attain a very high input impedance (greater than 10^9 ohms), and a common mode rejection ratio of better than 96 dB.

The cross-coupled mode implemented, ensures that common mode signals are passed at unit gain, while differential signals are amplified. The outputs of the two buffers feed a conventional differential circuit, that is provided with a zeroing adjustment and a meter to allow offset adjustment.

In this apparatus, the specifications of the comparator are a band width of 100 kHz, and a peak to peak noise level of approximately $3nV/\sqrt{Hz}$ at input. These parameters are consistent with the inherent noise level from the resistors used in the bridge, and the time scale of the measurements.

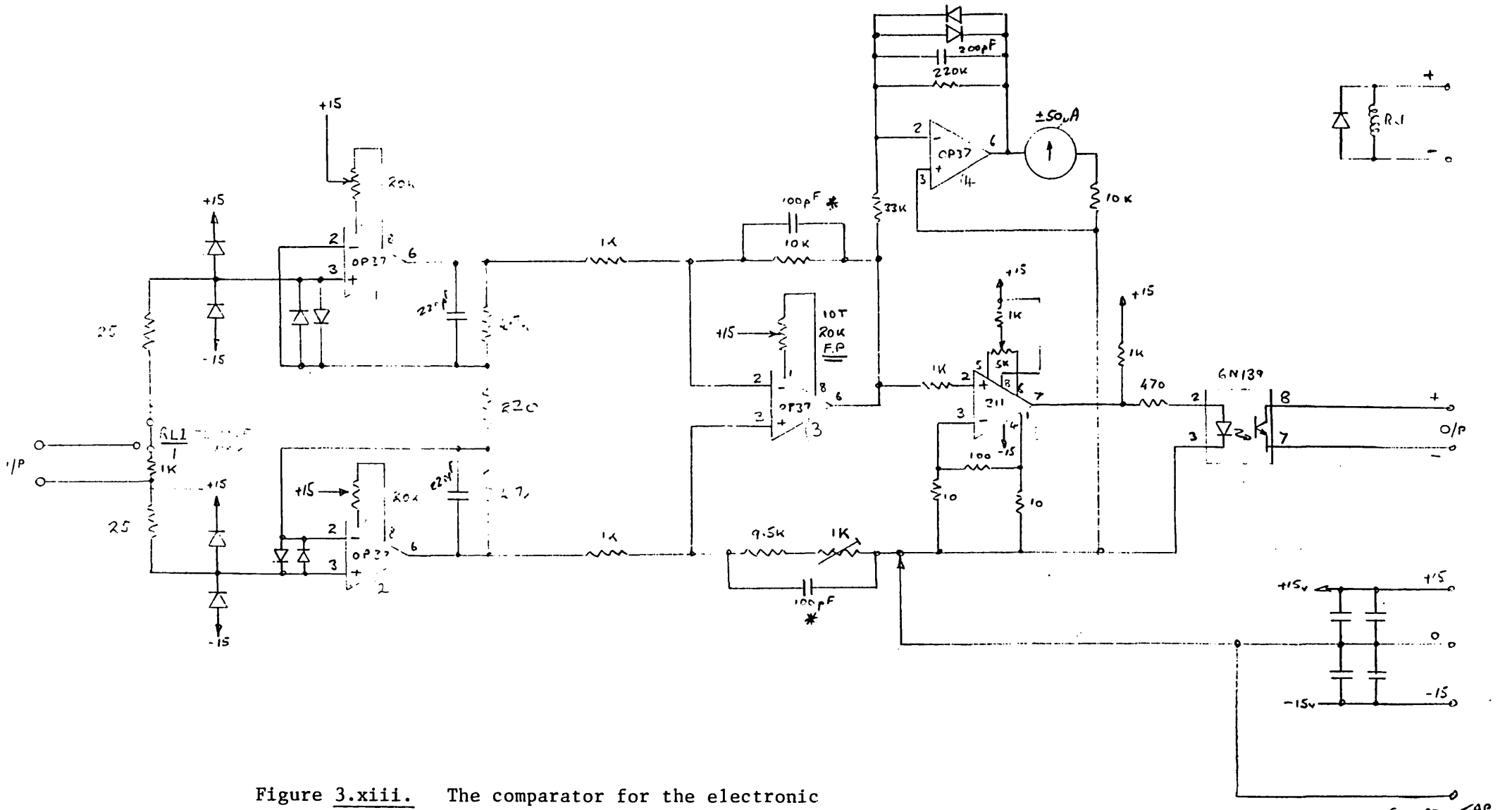


Figure 3.xiii. The comparator for the electronic bridge, for the measurement of the thermal conductivity.

3.8.6 The Working Equations.

It was shown in a previous section how the difference in the resistance of the wires ($R_L - R_S$) can be obtained during an experimental run. In this section, it will be shown how the actual temperature rise of the middle portion of a wire which acts as a finite segment of an infinitely long wire, can be obtained from this resistance difference.

For this purpose, it is necessary to use the resistance-temperature characteristics of the hot-wires, and it is convenient to employ a psuedo-linear temperature coefficient of resistance for any wire, defined by the equation:

$$R_{(T)} = R_{(T_o)}\left\{ 1 + \alpha'(T,T_o)(T-T_o) \right\} \qquad (3.22)$$

where $R_{(T)}$ is the resistance of the wire at a temperature T and T_o refers to the equilibrium bath temperature prior to a measurement. The advantage of this definition is that the full quadratic expression for the resistance of a wire given by this equation:

$$\frac{R_{(T)}}{R_{(273.15)}} = 1 + A(T-273.15) + B(T-273.15)^2 \qquad (3.23)$$

has been substituted by a linear relation,

$$\alpha'(T,T_o) = \frac{A + B\{2(T_o-273.15) + (T-T_o)\}}{1 + A(T_o-273.15) + B(T_o-273.15)^2} \qquad (3.24)$$

The main purpose of employing two wires in the opposite arms of the automatic bridge, is to eliminate the effects of axial heat transfer in them, which occur at the point of connection to the cell terminals, i.e. the hooks. In the ideal case, when the two wires and their supports are identical except for their length, this compensation works exactly and it is possible from the resistance difference of the two wires, to calculate the temperature rise of a central portion of one of them directly [13]. However, due to the manufacturing process of the wires, it is almost impossible to ensure uniformity in the radius of the tantalum wire, thus it is necessary to use a different approach to calculate the wire temperature rise.

It is necessary to ascribe to each wire a different average radius and heat flux per unit length, denoted by a_l and q_l for the long wire, and a_s and q_s for the short wire. Then, if each wire behaved as a finite portion of an infinitely long wire, the temperature rise of each wire would be:

$$(\Delta T)_l = \frac{q_l}{4\pi\lambda} \ell n \left\{ \frac{4\kappa t}{a_l^2 C} \right\} \qquad (3.25)$$

and

$$(\Delta T)_s = \frac{q_s}{4\pi\lambda} \ell n \left\{ \frac{4\kappa t}{a_s^2 C} \right\} \qquad (3.26)$$

All corrections due to the heat capacity and outer boundary and

the effect due to the insulation layer, are ignored for the purpose of this analysis, since it is assumed that the effects that are being discussed are small and so their coupling to other small effects is one order smaller.

Experimentally, the temperature rise for the wire is inferred from its resistance change. Thus it is possible to describe an "experimental" temperature rise for the long wire $\overline{\Delta T}_l$ defined by the equation:

$$R_l - R_{l(0)} = \alpha(T_o).R_{l(0)}.\overline{\Delta T}_l \qquad (3.27)$$

and for the short wire:

$$R_s - R_{s(0)} = \alpha(T_o).R_{s(0)}.\overline{\Delta T}_s \qquad (3.28)$$

Here, R_l and R_s represent, as before, the resistance of the long and short wires at a time t, whereas $R_{l(0)}$ and $R_{s(0)}$ the resistances of the long and short wires at t = 0 (i.e. the bath temperature prior to the initiation of the current, so that $R_{l(0)} = R_{l(T_o)}$).

The "experimental" temperature rise $\overline{\Delta T}_l$ differs from the ideal temperature rise $(\Delta T)_l$ by an amount dependent on the axial heat conduction at the ends of the wire. Therefore, this can be written as:

$$\overline{\Delta T}_l = (\Delta T)_l - \frac{q_l}{l_l}.F_l(G_l, a_l, t, k_d, \lambda_w) \qquad (3.29)$$

and for the short wire:

$$\overline{\Delta T}_s = (\Delta T)_s - \frac{q_s}{l_s}.F_s(G_s, a_s, t, k_d, \lambda_w) \qquad (3.30)$$

where G is a function of the wires' respective radii, thermal diffusivity, and thermal conductivity, together with the wires' geometry as well as being a function of time.

A further temperature rise $\Delta T'$ is now defined, (the experimentally measured temperature rise), which is:

$$\Delta T' = \frac{(R_l - R_s) - (R_{l(0)} - R_{s(0)})}{\alpha(T_o)(R_{l(0)} - R_{s(0)})} \qquad (3.31)$$

Substituting equations (3.26) to (3.29) in the above equation (3.31), we obtain:

$$\Delta T' = (\Delta T)_l \left\{ 1 + \frac{R_{s(0)}}{R_{l(0)} - R_{s(0)}} \left[1 - \frac{(\Delta T)_s}{(\Delta T)_l} \right] - \frac{1}{R_{l(0)} - R_{s(0)}} . \right.$$

$$\left. (q_l.\bar{\sigma}_l.F_l - q_s.\bar{\sigma}_s.F_s) \right\} \qquad (3.32)$$

where $\bar{\sigma}_l = R_{l(0)}/l_l$ and $\bar{\sigma}_s = R_{s(0)}/l_s$.

It can be seen that if the radii of the two wires were exactly the same, their resistances per unit length would have been equal and so would the heat dissipation within them and the temperature rise in each wire. In this case, equation (3.32) would read as:

$$\Delta T' = (\Delta T)_1 \tag{3.33}$$

The first term in equation (3.32) accounts for the difference in the temperature rise of each wire. The second term represents the consequent incomplete cancellation of the end effects of the two wires. Because the end effects for each wire constitutes at most only about 2% of the temperature rise, the difference between them at most can usually be neglected [46]. Therefore, the temperature rise of a portion of the long wire acting as a segment of an infinitely long wire may be obtained from the temperature rise $\Delta T'$ as:

$$(\Delta T)_1 = \Delta T' \left\{ 1 + \frac{R_{s(0)}}{R_{l(0)} - R_{s(0)}} \left[1 - \frac{(\Delta T)_s}{(\Delta T)_1} \right] \right\}^{-1} \tag{3.34}$$

By manipulating equation (3.34) together with equations (3.29) to (3.32), it can be shown that the required temperature rise $(\Delta T)_1$ can be obtained from entirely experimental parameters by the following expression:

$$(\Delta T)_1 = \frac{\Delta T'}{1 + \epsilon_3} \tag{3.35}$$

where $\Delta T'$ is given by the equation (3.31) and

$$\epsilon_3 = \frac{R_{s(0)}}{(R_{l(0)} - R_{s(0)})} \cdot \epsilon_2 \qquad (3.36)$$

$$\epsilon_2 = \frac{\epsilon_1 \left\{ 1 + \ell n \left[\frac{4\kappa t}{a_s^2 C} \right] \right\}}{\ell n \left[\frac{4\kappa t}{a_s^2 C} \right]} \qquad (3.37)$$

and

$$\epsilon_1 = 1 - \bar{\sigma}_s / \bar{\sigma}_l \qquad (3.38)$$

The difference ($R_l - R_s$) in equation (3.31) is obtained from the bridge balance equations (3.17-3.20). There, it was stated that to zeroth order, the ratio R_l/R_s which is required for the evaluation, may be equated to $R_{l(0)}/R_{s(0)}$. A more rigorous approach is to calculate the corrected value of R_l/R_s with the aid of the following equations:

$$\frac{R_l}{R_s} = \frac{R_{l(0)}}{R_{s(0)}} \left[1 + \alpha(T_o).[(\Delta T)_l - (\Delta T)_s] \right] \qquad (3.39)$$

$$\frac{R_l}{R_s} = \frac{R_{l(0)}}{R_{s(0)}} \left[1 + \alpha(T_o).\Delta T_l.\epsilon_2 \right] \qquad (3.40)$$

where ϵ_2 is defined by equation (3.37) and $\alpha(T_o)$ is the effective temperature coefficient of resistance of the tantalum wire given by:

$$\alpha(T_o) = \alpha'(T,T_o) - (1 - \epsilon_1) \qquad (3.41)$$

An approximate value for $(\Delta T)_1$ may be obtained from the zeroth order approximation ($R_1/R_s = R_{1(0)}/R_{s(0)}$), which can then be used in equation (3.40) to generate a better estimate of R_1/R_s which can be returned to the bridge balance equations for a better estimate of $(\Delta T)_1$. Normally, one iteration of this type is sufficient.

3.8.7 The Heat Flux From The Hot-Wire.

Having obtained the temperature rise of the middle portion of the long wire, the final quantity required to arrive at the thermal conductivity of the surrounding fluid, is the heat flux per unit length from this portion of the wire.

The present bridge configuration, as depicted in figure 3.x, ensures that equal current flows in both wires. However this alone does not guarantee that an equal rate of dissipation per unit length in the wires; this is mainly due to their physical construction. It is difficult to ensure exact radial uniformity along the wire. Therefore, this limitation is overcome by treating the heat flux per unit length of the middle portion of the long wire, q, written in terms of experimental quantities as:

$$q = \frac{q^*}{(1 - \epsilon_4)^2(1 + \epsilon_5)} \qquad (3.42)$$

where

$$q^{*} = \frac{V^2 \left(R_1 - R_s \right) / \left(l_1 - l_s \right)}{\left\{ R_1 + R_2 + \left(R_1 - R_s \right)\left(l_1 + l_s \right) / \left(l_1 - l_s \right) \right\}^2} \tag{3.42}$$

and

$$\epsilon_4 = \frac{2\sigma_1 . \epsilon_1 . l_1 . l_s}{\left(l_1 - l_s \right)\left(R_1 - R_s \right) + \left(R_1 - R_s \right)\left(l_1 + l_s \right)} \tag{3.43}$$

with

$$\epsilon_5 = \frac{l_s . \epsilon_1}{\left(l_1 - l_s \right)} \tag{3.44}$$

Here, V is the applied bridge voltage, and R_1 and R_2 are the bridge resistances as defined previously.

It is necessary to correct for the temperature difference of the performed measurement and room temperature when the wire lengths are measured at about 295K, by introducing a further small correction owing to the linear coefficient of expansion of the metallic wire. This correction is expressed as:

$$l_{(T_o)} = l_{(T_m)} \left\{ 1 + \gamma \left(T_o - T_m \right) \right\} \tag{3.45}$$

where γ is the temperature coefficient of expansion of tantalum metal,

(6.5×10^{-6} K^{-1}), T_m is the temperature at which the wire measurements were performed, and l is the length of the wires.

The heat flux emitted from the tantalum hot-wires during a transient run was initially found to be greater than expected. This effect was present from the beginning when the tantalum wires were employed in the new thermal conductivity cells. The thermal conductivity values obtained for test runs in the initial period for toluene were not correct. After careful reanalysis of the results, it was found that the leads resistances made a profound effect on the calculated thermal conductivity. The reason for this was the use of 25μm diameter tantalum wires in place of the thinner 7μm platinum wires, resulted in an eight-fold decrease in the resistance of the hot-wires. This meant that a decrease in the resolution of the bridge circuitry was inevitable. To overcome this handicap, the bridge had to be built with an enhanced sensitivity in order to give a higher resolution, and the ability to perform the said measurements with a lower temperature rise. The comparator can then detect the much smaller out of balance conditions due to the reduced wire resistances. It transpired that the connecting electrical leads from the hot-wires to the bridge played a significant part in the evaluation of the heat flux emitted from the hot-wires. Because the heat flux forms the basis of the thermal conductivity calculation, it was necessary to take into account the contributions that these lead resistances made in the final bridge balance equations.

In the platinum hot-wire cells, the lead resistance connecting the

long wire to the bridge was measured to be 0.065Ω, and the long wire itself had a resistance of 350Ω. But in the tantalum case, the same lead resistance of 0.065Ω has a greater effect when the long wire resistance is only 41Ω. Therefore, it was deemed necessary to re-measure all the wires and leads' resistances. This was carried out by using an accurate milliohmeter. The analysis of the temperature rise of the hot-wires is given in detail in appendix 2.

3.9 Testing The Bridge

Once all the preliminary tests have been made in order to ascertain the correct operation of all the bridge components, that is, the bridge relays, the various resistors (fixed and variable), the timers and finally, the software of the computer that handles the operation and execution of the entire measurement of the thermal conductivity of fluids, it was necessary to test the instrument as a whole.

The new automatic bridge for the measurement of the thermal conductivity of liquids has been constructed so as to perform the transient run in one second with a reasonable number of balance points (> 50), unlike the previous instrument [14,71] which could only muster six balance points at a time in one second. The various components that make up the bridge were tested seperately, to ensure the correct performance of the relays that initiate the transient heating, the internal clock and the timers which record the balance times and their corresponding voltages, when the zero crossing of the

comparator takes place. The fluid employed for the testing of the instrument was a reference standard the IUPAC commission have selected as a reference for the measurement of thermal conductivity. The deviations of the new results were entirely consistent with those of the previous measurements, which indicated that the bridge was working with the required accuracy and precision. These experiments were carried out in parallel with the 'old' bridge, and the platinum wires [14,71,75], so that the operating conditions were identical, i.e. the pressure at one atmosphere and 302.65 K. The maximum deviations amounted to $\pm$0.7% , while the standard deviation was one of $\pm$0.15%.

3.10 Data Acquisition and Handling.

The hardware employed for the data acquisition and handling was a BBC microcomputer model B. This machine was capable of running a programme that initiates the transient heating of the hot-wires in the thermal conductivity cells, storing the voltages and times at each balance point onto a floppy disk, so that these could be retrieved at a later date-if desired-to perform an analysis of the run. The software was written in basic and assembler machine code for the controlling of the bridge. The analysis programme was written in basic.

CHAPTER 4

RESULTS

4.1 Introduction:

This chapter is devoted to a presentation of the experimental results of the thermal conductivity measurements performed with the instruments described in the earlier sections. We begin with a presentation of the results for toluene which has been adopted [82] as a reference standard for liquid thermal conductivity. Accurate measurements of the thermal conductivity of toluene have been made in this laboratory [41,67,70,83,84] and elsewhere [68,85] by the transient hot-wire technique, so that the present measurements serve to confirm the correct operation of the two instruments employed here following their modification.

First, we present the results of measurements on toluene made in the instrument for insulating liquids, following the introduction of the new automatic bridge described in the previous chapter. Secondly, the results of a similar series of measurements on toluene performed in the new instrument for electrically insulating liquids are presented. This latter series serves to confirm the correct operation and theory of the new cells, as well as the new automatic bridge.

In subsequent sections, the results of measurements of the thermal conductivity of five electrically insulating liquids,

tetrachloromethane, n-pentane, ethylbenzene, oct-1-ene, and o-xylene are presented. These measurements extend over the temperature 300-370K, and for pressures upto 500MPa or the freezing pressure, whichever is the smaller. Finally, we present the thermal conductivity of water determined in the instrument designed for use with electrically conducting liquids. Table 4.1 shows the details of the sources and purities of all liquid samples used. Generally, the samples been redistilled in the laboratory before use, and the improved purity confirmed by chromatography.

In a final section of the chapter, a simple correlation of all the experimental data as a function of pressure is given, to aid interpretation of the data. A discussion of the more theoretically based density dependence is given in the next chapter.

4.2 Results.

4.2.1 The Check Measurements on Toluene.

The thermal conductivity of toluene has been measured in the platinum wire cells, designed for operation with electrically-insulating liquids, along three isotherms at pressures up to 100MPa. These measurements were performed with the new automatic Wheatstone bridge described earlier. The results of the new measurements are listed in table 4.2 corrected to nominal isotherms at

Liquid	Purity (as stated by manufacturer.)	Purity (after distillation)	Supplier
n-Pentane	99.0%	99.9%	BDH Chemicals Ltd.
o-Xylene	99.0%	99.9%	Aldrich Chem. Company.
Ethylbenzene	99.0%	99.9%	Koch-Light Laboratories.
Carbon Tetrachloride	99.5%	99.9%	BDH Chemicals Ltd.
Oct-1-ene	99.0%	99.9%	BDH Chemicals Ltd.
Toluene	99.5%	99.9%	Hopkin and Williams Ltd.
Water	99.0%	99.9%	Imperial College.

Table 4.1 Summary of the Liquids Employed for the Measurement of the Thermal Conductivity, their purities and sources.

p/MPa	(T,p)/mW m^{-1} K^{-1}	p/MPa	(T,p)/mW m^{-1} K^{-1}	p/MPa	(T,p)/mW m^{-1} K^{-1}
T=306.15K		T=319.15K		T=343.15K	
0.1	129.6	1.7	126.3	3.3	119.4
0.3	129.9	8.5	128.2	3.3	119.4
10.0	133.0	18.9	131.8	14.9	123.5
30.5	139.2	52.0	142.1	29.8	129.6
53.1	146.5	101.6	155.1	29.6	129.5
73.0	151.5			52.3	135.9
73.2	151.5			78.1	144.0
113.3	160.8				

Table 4.2 Thermal Conductivity of Toluene.

306.15K, 319.15K, and 343.15K in the manner described by Menashe and Wakeham [25]. Because the correction never exceeded ±0.3%, the additional uncertainty introduced in the final results is negligible.

Figure 4.i is a plot of the thermal conductivity, λ, of the newly measured toluene, against pressure. Figure 4.ii compares the set of results with the correlation of the earlier data presented by Nieto de Castro et.al. [41,67]. The deviations do not exceed the mutual uncertainty of the two independent determinations, which is ±0.3%. The fact that the deviations are systematic, reflects the general result that the precision of the thermal conductivity measurements is superior to their accuracy. We may deduce from this comparison that the new automatic bridge and its theory are satisfactory.

Table 4.3 presents the results for the thermal conductivity of toluene obtained in the new Inconel cells designed for use with electrically conducting liquids. In this case, the measurements have been carried out only at a pressure of 0.1MPa at a reference temperature of 299.8K. The table also contains the values recommended as standard reference data at one atmosphere by IUPAC [82]. The latter values have an estimated uncertainty of ±1%. The measurements with the new cells are entirely consistent with the values, and we conclude that the new instrument operates successfully.

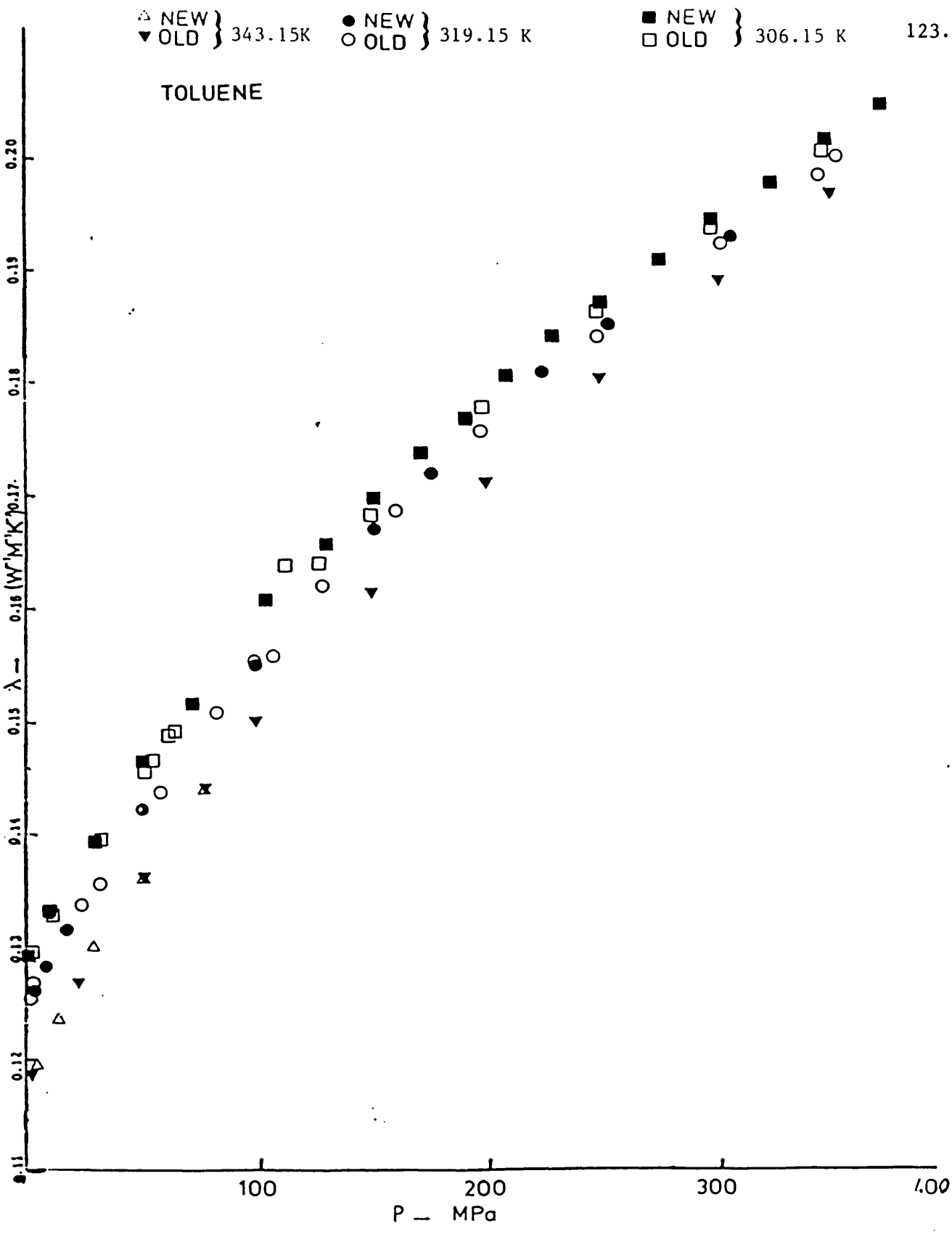
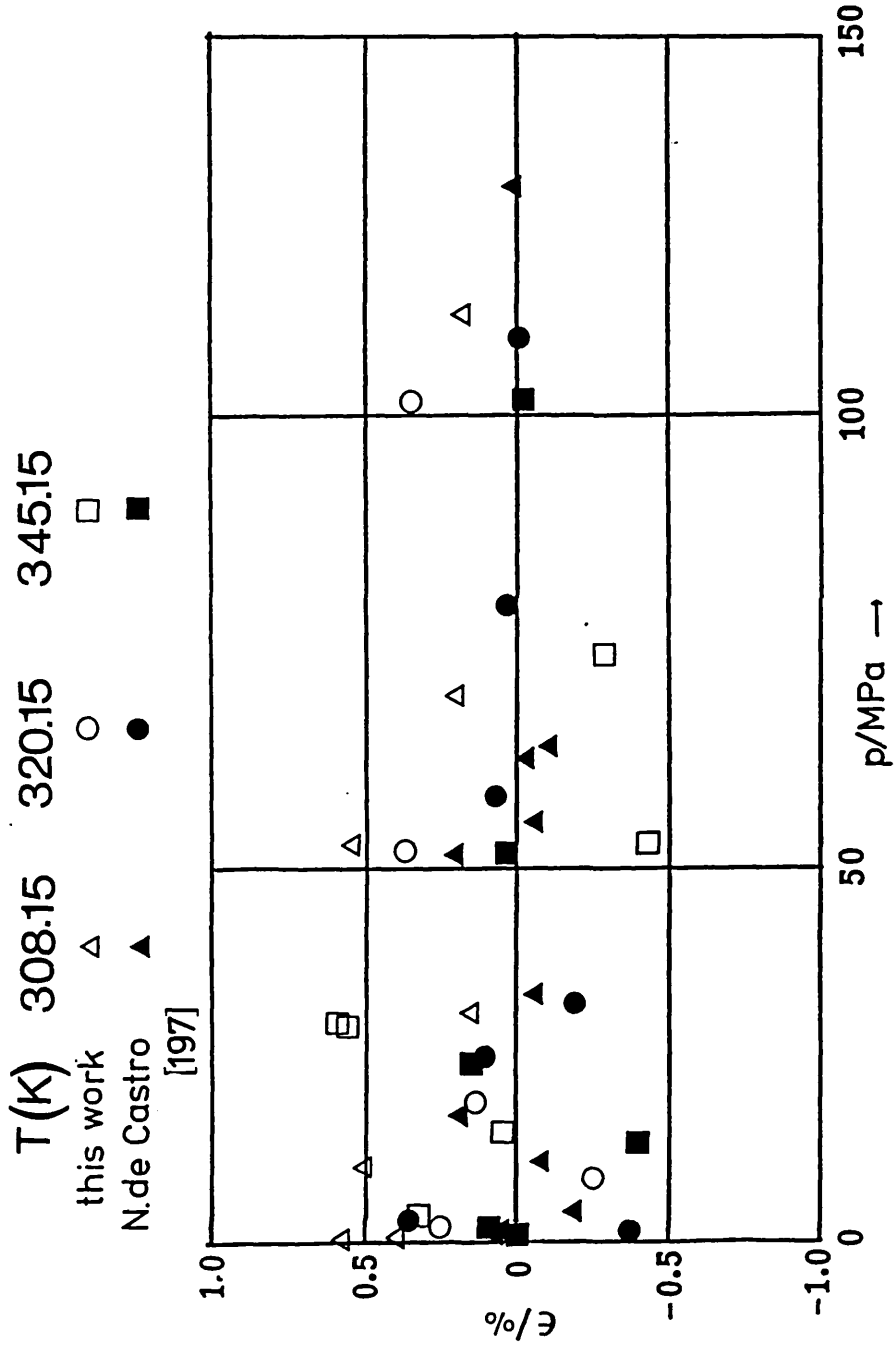


Figure 4.i. The thermal conductivity of toluene as a function of pressure, for three isotherms.

Figure 4.ii.


T(K) 308.15 320.15 345.15
this work
N.de Castro [197]
1.0
0.5
0
-0.5
-1.0
ε/%
0
50
100
150
p/MPa

T(K)	P/MPa	This Work λ/mW m^{-1} K^{-1}	IUPAC Standard[82] λ/mW m^{-1} K^{-1}
299.8	0.1013	131.1 ± 0.4	130.6 ± 1.3
299.3	0.1013	130.9 ± 0.4	130.6 ± 1.3

Table 4.3 The thermal Conductivity of Toluene.

4.2.2 Carbon Tetrachloride.

In the case of carbon tetrachloride (tetrachloromethane), the measurements extended from 310.15K to 364.15K, and included five isotherms. This liquid freezes at relatively moderate pressures, and thus the ranges were rather restricted. Also owing to the relative unreliability of the density data available at the higher temperatures, the thermal conductivity was listed as a function of density, $\lambda(T_{nom},\rho_r)$ only for the three lowest isotherms. At the higher temperatures, a tabulation of the thermal conductivity as a function of $\lambda(T_{nom},P)$ is given. In addition to that, the data in every case have been corrected to the nominal temperature by the application of a linear correction, which never ammounted to more than ±0.1%, so that the process made a negligible contribution to the error in the thermal conductivity [57]. The uncertainty in the reported thermal conductivity data of carbon tetrachloride is estimated to be one of ±0.3%, and the

uncertainty in the tabulated density is estimated to be no more than $\pm$0.2%.

The density of carbon tetrachloride was measured over a part of the range of states appropriate to this work by Easteal and Woolf [86], and their data has been represented by a modified form of the Tait equation:

$$1 - \frac{V_p}{V_{0.1}} = C \, \ell og\left[\frac{B + P}{B + 0.1}\right] \qquad (4.1)$$

The heat capacity of the liquid required for the data processing were taken from the tables of Vargaftik [69]. It is also necessary to record here that none of the experimental measurements revealed any evidence of the effects of radiation absorption [41], so that the results reported are " radiation-free ".

Tables 4.4 to 4.8 list the experimental values obtained for carbon tetrachloride.

4.2.3 N-Pentane.

For n-pentane, the experimental data for the thermal conductivity along four isotherms at 305.8K, 322.8K, 342.5K and 359.5K are given in tables 4.9 to 4.12. In each table, the listed thermal conductivity data are adjusted to a nominal temperature by means of a linear correction, at both the experimental pressure, P, and the reference density, ρ. The

correction never exceeded ±0.2%, and hence the extra uncertainty introduced is negligible.

The density of normal pentane has been measured by a number of investigators under the conditions of interest [86,87]. For the purposes of applying small corrections in the analysis of the thermal conductivity data, the results of Bridgman [87], have been employed together with heat capacity data from Vargaftik [69]. However, for the purposes of representing the thermal conductivity data of n-pentane as a function of density, it was preferable to employ the more accurate, although less extensive, data of Easteal and Woolf [86]. These new results cover the temperature range 278.15K to 338.15K, and pressures up to 280MPa and have an estimated uncertainty of ±0.2%. These densities were not entirely consistent with earlier data [87-89] in the overlapping range of states; their deviations exceeding 1% in some cases. Some doubt is therefore cast on the older results. Consequently, in the tabulation of the results, the densities only for those conditions are included which have been obtained by interpolation or a modest extrapolation of those covered by Easteal and Woolf.

Tables 4.9 to 4.12 list the thermal conductivities of n-pentane as a function of pressure and density, together with the corrected values of the thermal conductivity to the nominal temperatures at constant pressure and density.

4.2.4 O-Xylene.

Measurements on the thermal conductivity of ortho-xylene were carried out at four isotherms, 308.15K, 318.15K, 337.65K, and 360.15K and pressure ranges up to 419MPa, or the solidification pressure. For the application of small corrections in the data reduction, the density data by Mamedov et.al.[90], have been employed for the o-xylene. For this liquid, the highest pressure for which the density has been measured is 50MPa. Consequently, solely for the purpose of making these corrections, it has been necessary to extrapolate the equation of state fitted to these data for the higher pressures. The effect of this extrapolation on the reported thermal conductivity data is negligible. The data here have been also corrected to the nominal temperatures as mentioned earlier [57], and this correction never amounted to more than $\pm$0.3%, so that the additional uncertainty in the reported data is negligible. It is estimated that the overall error in the tabulated thermal conductivity is one of $\pm$0.3%. The corresponding density is also quoted whenever it lies within the range of direct measurements [90]. No extrapolated density data have been included.

Tables 4.13 to 4.16 list the data for the thermal conductivity of o-xylene, together with the pressure and density values available.

4.2.5 Oct-1-ene.

Measurements of the thermal conductivity of oct-1-ene have been carried out along the four isotherms at 307.65K, 320.65K, 344.15K, and

360.15K, and at pressures up to 500MPa. The density of oct-1-ene in the appropriate temperature range for pressures up to 260MPa has been determined by Isdale [91]. These data, together with the heat capacity data compiled by Vargaftik [69], have been employed to make small corrections during the analysis of the measurements. It is worthwhile again to mention here that there was no evidence of radiation absorption in any measurement [41], so that the data reported here are also "radiation-free" values.

Tables 4.17 to 4.20 list the experimental data for the thermal conductivity of oct-1-ene, along the four isotherms, as a function of pressure and density. At the higher pressures, the density is not quoted, since the pressures lie beyond the range of the density measurements. The corrections of the experimental data to uniform nominal temperatures has been accomplished in the manner described elsewhere [57]. In this case, no correction amounted to more than $\pm$0.2%, so that the additional uncertainty introduced is negligible. The uncertainty in the reported thermal conductivity is estimated to be one of $\pm$0.3%, whereas in the associated density is $\pm$0.2%.

4.2.6 Ethylbenzene.

Measurements on the thermal conductivity have been carried out on ethylbenzene at four isotherms 304.65K, 319.15K, 339.65K, and 357.15K, and at pressures up to 500MPa. The value of the density of ethylbenzene, which was required to make small corrections in the data, was taken from the results of Mamedov et.al.[90], and the heat capacity

T_r (K)	P (MPa)	$(\frac{\partial\lambda}{\partial T})_{\rho_r}$ (mW m^{-1} K^{-2})	$(\frac{\partial\lambda}{\partial T})_P$ (mW m^{-1} K^{-2})	$\lambda(T_r,\rho_r)$ (mW m^{-1} K^{-1})	$\lambda(T_n,\rho_r)$ (mW m^{-1} K^{-1})	$\lambda(T_n,P)$ (mW m^{-1} K^{-1})	ρ_r (Kg m^{-3})
310.126	5.376	0.882E-01	-0.289E+00	97.49	97.49	97.49	1573.30
309.947	8.329	0.861E-01	-0.283E+00	98.52	98.51	98.47	1578.20
309.931	14.440	0.846E-01	-0.224E+00	100.33	100.34	100.28	1587.70
310.236	17.282	0.850E-01	-0.212E+00	101.02	101.02	101.04	1591.70
309.820	22.853	0.871E-01	-0.191E+00	102.44	102.47	102.37	1600.50
310.076	29.251	0.908E-01	-0.177E+00	104.12	104.13	104.11	1609.60
309.963	36.257	0.958E-01	-0.170E+00	105.89	105.90	105.88	1619.50
309.983	42.091	0.100E+00	-0.168E+00	107.29	107.31	107.26	1627.40
308.896	47.583	0.104E+00	-0.171E+00	108.54	108.56	108.48	1634.60
309.968	53.278	0.107E+00	-0.176E+00	109.94	109.96	109.91	1641.60
309.877	58.837	0.109E+00	-0.183E+00	111.28	111.31	111.28	1648.50
311.303	63.749	0.108E+00	-0.186E+00	111.77	111.64	111.96	1652.50
310.085	68.234	0.109E+00	-0.198E+00	113.27	113.26	113.26	1658.80
310.104	72.708	0.108E+00	-0.207E+00	114.20	114.20	114.19	1663.60

Table 4.4 Thermal Conductivity of Carbon Tetrachloride at T_{nom}=310.15K

T_r (K)	P (MPa)	$(\frac{\partial\lambda}{\partial T})_{\rho_r}$ (mW m^{-1} K^{-2})	$(\frac{\partial\lambda}{\partial T})_P$ (mW m^{-1} K^{-2})	$\lambda(T_r,\rho_r)$ (mW m^{-1} K^{-1})	$\lambda(T_n,\rho_r)$ (mW m^{-1} K^{-1})	$\lambda(T_n,P)$ (mW m^{-1} K^{-1})	ρ_r (Kg m^{-3})
322.574	1.367	0.128E+00	-0.201E+00	93.41	93.42	93.40	1548.10
322.619	5.271	0.113E+00	-0.208E+00	94.41	94.41	94.40	1555.10
322.566	9.805	0.101E+00	-0.214E+00	95.75	95.75	95.73	1563.20
322.617	15.072	0.918E-01	-0.217E+00	97.51	97.51	97.50	1571.90
322.514	20.332	0.868E-01	-0.216E+00	99.31	99.32	99.28	1580.50
322.584	24.743	0.849E-01	-0.215E+00	100.78	100.78	100.76	1587.20
322.666	26.421	0.848E-01	-0.214E+00	100.81	100.81	100.81	1589.60
322.810	27.051	0.846E-01	-0.214E+00	100.82	100.81	100.85	1590.40
322.480	32.391	0.854E-01	-0.210E+00	102.33	102.34	102.30	1598.60
322.491	37.717	0.878E-01	-0.205E+00	104.04	104.06	104.01	1606.10
322.609	44.377	0.915E-01	-0.198E+00	105.51	105.52	105.51	1614.90
322.520	52.665	0.978E-01	-0.188E+00	107.62	107.64	107.60	1625.90
322.589	61.397	0.103E+00	-0.177E+00	109.80	109.80	109.79	1636.20
322.752	68.844	0.107E+00	-0.168E+00	111.45	111.44	111.47	1644.70
322.686	77.383	0.109E+00	-0.160E+00	113.24	113.23	113.24	1654.30
322.688	81.446	0.110E+00	-0.156E+00	114.31	114.30	114.31	1658.70
322.793	84.492	0.110E+00	-0.153E+00	114.95	114.93	114.97	1661.80
322.902	91.393	0.108E+00	-0.149E+00	116.17	116.14	116.21	1668.80
322.733	95.145	0.107E+00	-0.147E+00	116.28	116.28	116.30	1672.80
322.563	101.125	0.103E+00	-0.146E+00	118.15	118.15	118.13	1678.90
322.644	105.889	0.989E-01	-0.146E+00	119.13	119.13	119.13	1683.50
322.482	112.883	0.909E-01	-0.149E+00	120.31	120.33	120.29	1690.20

Table 4.5 Thermal Conductivity of Carbon Tetrachloride at T_{nom} = 322.65K

T_r (K)	P (MPa)	$(\frac{\partial\lambda}{\partial T})_{\rho_r}$ (mW m^{-1} K^{-2})	$(\frac{\partial\lambda}{\partial T})_P$ (mW m^{-1} K^{-2})	$\lambda(T_r,\rho_r)$ (mW m^{-1} K^{-1})	$\lambda(T_n,\rho_r)$ (mW m^{-1} K^{-1})	$\lambda(T_n,P)$ (mW m^{-1} K^{-1})	ρ_r (Kg m^{-3})
342.302	6.220	0.220E+00	-0.533E-01	90.71	90.76	90.69	1519.40
342.171	10.964	0.179E+00	-0.104E+00	92.35	92.43	92.30	1529.30
342.128	14.861	0.154E+00	-0.135E+00	93.33	93.44	93.26	1536.80
342.181	21.488	0.123E+00	-0.169E+00	95.59	95.65	95.51	1548.70
341.932	30.089	0.994E-01	-0.182E+00	98.10	98.17	97.96	1563.70
342.148	38.551	0.883E-01	-0.197E+00	100.22	100.27	100.13	1576.50
342.272	44.896	0.851E-01	-0.185E+00	101.95	101.99	101.88	1585.60
342.301	49.766	0.847E-01	-0.192E+00	102.35	102.38	102.28	1592.40
342.200	55.751	0.861E-01	-0.188E+00	104.73	104.77	104.65	1600.60
342.128	62.113	0.890E-01	-0.183E+00	106.41	106.46	106.32	1609.00
342.274	68.844	0.928E-01	-0.178E+00	108.08	108.12	108.02	1617.10
342.046	74.639	0.966E-01	-0.175E+00	109.36	109.42	109.26	1624.40
342.053	80.431	0.100E+00	-0.173E+00	110.55	110.61	110.45	1631.00
342.351	86.015	0.103E+00	-0.172E+00	111.63	111.65	111.58	1636.90
342.172	89.871	0.105E+00	-0.172E+00	112.58	112.63	112.50	1640.60
342.139	94.739	0.107E+00	-0.173E+00	113.98	114.03	113.89	1641.30
342.223	101.429	0.109E+00	-0.174E+00	115.13	115.18	115.06	1653.40
342.680	108.626	0.110E+00	-0.177E+00	117.05	117.04	117.05	1660.00
342.585	113.896	0.109E+00	-0.178E+00	118.14	118.15	118.13	1665.30
342.584	121.598	0.107E+00	-0.178E+00	119.49	119.50	119.46	1672.70
342.703	126.057	0.104E+00	-0.178E+00	120.54	120.53	120.55	1676.70
342.466	132.643	0.994E-01	-0.174E+00	121.57	121.59	121.54	1683.00
342.667	138.419	0.938E-01	-0.169E+00	122.91	122.91	122.92	1687.90
342.746	146.824	0.834E-01	-0.154E+00	123.92	123.92	123.94	1695.00
342.802	152.893	0.742E-01	-0.138E+00	124.92	124.91	124.94	1700.00
342.741	156.128	0.684E-01	-0.128E+00	125.65	125.64	125.66	1702.90

Table 4.6 Thermal Conductivity of Carbon Tetrachloride at T_{nom} = 342.65K

T_r (K)	P (MPa)	$(\frac{\partial\lambda}{\partial T})_{\rho_r}$ (mW m^{-1} K^{-2})	$(\frac{\partial\lambda}{\partial T})_P$ (mW m^{-1} K^{-2})	$\lambda(T_r,\rho_r)$ (mW m^{-1} K^{-1})	$\lambda(T_n,\rho_r)$ (mW m^{-1} K^{-1})	$\lambda(T_n,P)$ (mW m^{-1} K^{-1})	ρ_r (Kg m^{-3})
359.400	6.115	--	--	--	--	86.18	--
359.418	13.176	--	--	--	--	88.57	--
359.342	25.058	--	--	--	--	92.73	--
359.229	37.300	--	--	--	--	96.27	--
359.378	48.456	--	--	--	--	99.79	--
359.331	59.245	--	--	--	--	102.30	--
360.171	70.064	--	--	--	--	105.16	--
360.148	77.586	--	--	--	--	106.88	--
360.007	86.421	--	--	--	--	108.68	--
359.936	93.218	--	--	--	--	110.54	--
359.915	103.456	--	--	--	--	112.38	--
359.534	112.173	--	--	--	--	114.33	--
359.706	120.990	--	--	--	--	116.22	--
359.844	130.921	--	--	--	--	118.32	--
359.569	141.559	--	--	--	--	120.00	--
359.628	153.398	--	--	--	--	122.40	--
359.568	163.995	--	--	--	--	124.41	--
359.602	173.967	--	--	--	--	125.94	--
359.394	184.333	--	--	--	--	128.00	--
359.292	194.185	--	--	--	--	129.68	--
359.311	204.357	--	--	--	--	131.51	--
359.258	214.622	--	--	--	--	133.47	--
359.252	224.586	--	--	--	--	135.22	--

Table 4.7 Thermal Conductivity of Carbon Tetrachloride at T_{nom} = 359.65K

T_{nom} = 364.15K

Pressure P/MPa	Thermal Conductivity λ /mW m^{-1} K^{-1}
3.478	84.26
9.277	86.60
19.81	90.10
34.90	94.64
47.70	98.67
63.75	102.9
76.37	105.8
87.84	108.5
100.9	111.6
118.0	115.1
128.8	117.2

Table 4.8 Thermal Conductivity Of Carbon Tetrachloride at T_{nom}=364.5K

T_r (K)	P (MPa)	$(\frac{\partial\lambda}{\partial T})_{\rho_r}$ (mW m^{-1} K^{-2})	$(\frac{\partial\lambda}{\partial T})_P$ (mW m^{-1} K^{-2})	$\lambda(T_r,\rho_r)$ (mW m^{-1} K^{-1})	$\lambda(T_n,\rho_r)$ (mW m^{-1} K^{-1})	$\lambda(T_n,P)$ (mW m^{-1} K^{-1})	ρ_r (Kg m^{-3})
307.024	1.790	0.897E-01	-0.340E+00	110.12	110.01	110.54	614.71
306.898	5.693	0.878E-01	-0.342E+00	112.95	112.86	113.33	619.76
305.598	14.124	0.818E-01	-0.350E+00	118.05	118.07	117.98	630.67
306.208	24.743	0.737E-01	-0.355E+00	123.10	123.07	123.25	640 91
305.918	35.422	0.638E-01	-0.366E+00	128.28	128.28	128.33	650.70
305.937	47.282	0.525E-01	-0.378E+00	133.47	133.46	133.52	660.11
306.021	58.629	0.414E-01	-0.391E+00	137.90	137.89	137.99	668.14
306.106	62.829	0.374E-01	-0.396E+00	139.13	139.12	139.26	670.88
305.982	69.352	0.308E-01	-0.404E+00	142.36	142.35	142.43	675.15
305.977	80.431	0.199E-01	-0.416E+00	146.07	146.07	146.15	681.79
305.823	91.088	0.925E-02	-0.428E+00	150.84	150.84	150.85	687.84
305.823	102.240	-0.157E-02	-0.438E+00	154.11	154.11	154.12	693.67
305.811	112.072	-0.110E-01	-0.446E+00	157.35	157.35	157.35	698.52
305.811	122.612	-0.210E-01	-0.461E+00	160.68	160.68	160.68	703.45
305.720	134.062	-0.318E-01	-0.477E+00	163.84	163.84	163.80	708.59
305.678	143.179	-0.403E-01	-0.490E+00	167.14	167.14	167.08	712.50
305.882	145.104	-0.418E-01	-0.493E+00	166.86	166.86	166.90	713.17
306.007	153.600	-0.493E-01	-0.504E+00	170.37	170.38	170.47	716.57
305.888	167.522	-0.621E-01	-0.521E+00	173.48	173.49	173.53	722.13
305.600	180.810	-0.744E-01	-0.535E+00	177.60	177.58	177.49	727.32

Table 4.9 Thermal Conductivity of n-Pentane at T_{nom} = 305.8K

T_r (K)	P (MPa)	$(\frac{\partial\lambda}{\partial T})_{\rho_r}$ (mW m^{-1} K^{-2})	$(\frac{\partial\lambda}{\partial T})_P$ (mW m^{-1} K^{-2})	$\lambda(T_r,\rho_r)$ (mW m^{-1} K^{-1})	$\lambda(T_n,\rho_r)$ (mW m^{-1} K^{-1})	$\lambda(T_n,P)$ (mW m^{-1} K^{-1})	ρ_r (Kg m^{-3})
305.772	197.817	-0.892E-01	-0.555E+00	182.02	182.02	182.00	733.37
305.824	213.414	-0.103E+00	-0.573E+00	186.62	186.62	186.63	738.75
305.756	229.964	-0.117E+00	-0.591E+00	190.13	190.12	190.10	744.33
305.823	243.432	-0.129E+00	-0.607E+00	192.95	192.95	192.96	748.66
305.875	262.454	-0.145E+00	-0.631E+00	197.49	197.51	197.54	754.61
305.764	283.081	-0.162E+00	-0.655E+00	202.08	202.07	202.05	760.94
305.838	303.132	-0.179E+00	-0.685E+00	206.11	206.12	206.14	766.78
305.825	332.898	-0.203E+00	-0.734E+00	209.81	209.82	209.83	775.19
305.910	342.446	-0.211E+00	-0.753E+00	214.32	214.34	214.40	777.74
305.890	362.719	-0.227E+00	-0.794E+00	217.85	217.87	217.92	783.18
305.911	382.617	-0.242E+00	-0.840E+00	222.02	222.05	222.11	788.31
305.973	402.439	-0.257E+00	-0.891E+00	225.29	225.33	225.44	793.23
305.877	427.563	-0.276E+00	-0.960E+00	230.28	230.31	230.36	799.35
306.151	453.060	-0.294E+00	-0.102E+01	233.93	234.03	234.29	804.91
306.131	476.390	-0.310E+00	-0.112E+01	238.21	238.31	238.58	809.98
306.110	501.194	-0.326E+00	-0.121E+01	242.05	242.16	242.43	815.06

Table 4.9 Thermal Conductivity of n-Pentane at T_{nom}=305.8K (continued)

T_r (K)	P (MPa)	$(\frac{\partial\lambda}{\partial T})_{\rho_r}$ (mW m^{-1} K^{-2})	$(\frac{\partial\lambda}{\partial T})_P$ (mW m^{-1} K^{-2})	$\lambda(T_r,\rho_r)$ (mW m^{-1} K^{-1})	$\lambda(T_n,\rho_r)$ (mW m^{-1} K^{-1})	$\lambda(T_n,P)$ (mW m^{-1} K^{-1})	ρ_r (Kg m^{-3})
323.282	3.689	0.915E-01	-0.303E+00	106.06	106.01	106.20	600.99
322.998	4.849	0.916E-01	-0.302E+00	106.96	106.95	107.02	602.95
323.155	14.861	0.892E-01	-0.304E+00	112.97	112.94	113.08	615.98
322.900	24.848	0.838E-01	-0.306E+00	118.12	118.11	118.15	627.49
322.814	37.926	0.743E-01	-0.309E+00	124.47	124.47	124.47	640.27
322.764	52.349	0.620E-01	-0.311E+00	130.66	130.66	130.65	652.28
322.690	65.382	0.503E-01	-0.313E+00	135.97	135.98	135.94	661.79
322.886	70.268	0.460E-01	-0.316E+00	137.38	137.37	137.40	664.95
322.661	81.040	0.358E-01	-0.316E+00	142.02	142.03	141.98	671.89
322.540	94.435	0.233E-01	-0.317E+00	146.75	146.75	146.67	679.73
322.707	112.173	0.715E-02	-0.322E+00	151.37	151.37	151.34	688.99
322.625	124.435	-0.415E-02	-0.322E+00	155.19	155.19	155.13	695.01
322.696	142.268	-0.204E-01	-0.326E+00	161.53	161.53	161.50	703.11
322.937	155.823	-0.323E-01	-0.329E+00	165.50	165.50	165.54	708.81
322.967	173.161	-0.487E-01	-0.330E+00	170.15	170.16	170.21	715.87
322.933	173.363	-0.480E-01	-0.330E+00	170.29	170.30	170.33	715.97
322.987	187.352	-0.604E-01	-0.329E+00	173.05	173.06	173.11	721.39
322.860	203.351	-0.747E-01	-0.327E+00	177.28	177.29	177.30	727.44
322.891	217.441	-0.871E-01	-0.325E+00	181.10	181.10	181.13	732.53
322.787	236.891	-0.104E+00	-0.319E+00	185.53	185.53	185.52	739.39

Table 4.10 Thermal Conductivity of n-Pentane at T_{nom}= 322.8K

T_r (K)	P (MPa)	$(\frac{\partial\lambda}{\partial T})_{\rho_r}$ (mW m^{-1} K^{-2})	$(\frac{\partial\lambda}{\partial T})_P$ (mW m^{-1} K^{-2})	$\lambda(T_r,\rho_r)$ (mW m^{-1} K^{-1})	$\lambda(T_n,\rho_r)$ (mW m^{-1} K^{-1})	$\lambda(T_n,P)$ (mW m^{-1} K^{-1})	ρ_r (Kg m^{-3})
322.742	257.557	-0.123E+00	-0.313E+00	189.99	189.98	189.97	746.39
322.811	277.865	-0.140E+00	-0.305E+00	194.66	194.67	194.67	753.03
322.734	300.330	-0.160E+00	-0.287E+00	199.75	199.74	199.73	760.18
322.735	322.105	-0.179E+00	-0.270E+00	203.56	203.55	203.55	766.87
321.632	342.346	-0.197E+00	-0.244E+00	208.14	207.91	207.85	772.99
322.801	368.069	-0.218E+00	-0.229E+00	212.65	212.65	212.65	780.35
323.344	394.305	-0.240E+00	-0.202E+00	217.20	217.33	217.31	787.68
323.291	417.014	-0.259E+00	-0.176E+00	220.95	221.08	221.04	793.74
323.279	441.459	-0.278E+00	-0.146E+00	225.39	225.52	225.46	799.99
323.210	465.417	-0.296E+00	-0.115E+00	228.90	229.02	228.94	805.78
323.268	497.781	-0.319E+00	-0.706E-01	234.09	234.24	234.14	813.10

Table 4.10 Thermal Conductivity of n-Pentane at T_{nom} = 322.8K (continued)

T_r (K)	P (MPa)	$(\frac{\partial\lambda}{\partial T})_{\rho_r}$ (mW m^{-1} K^{-2})	$(\frac{\partial\lambda}{\partial T})_P$ (mW m^{-1} K^{-2})	$\lambda(T_r,\rho_r)$ (mW m^{-1} K^{-1})	$\lambda(T_n,\rho_r)$ (mW m^{-1} K^{-1})	$\lambda(T_n,P)$ (mW m^{-1} K^{-1})	ρ_r (Kg m^{-3})
342.357	4.638	0.867E-01	-0.278E+00	101.46	101.47	101.42	582.84
342.329	14.019	0.912E-01	-0.259E+00	107.31	107.32	107.27	597.16
342.247	24.743	0.906E-01	-0.245E+00	112.98	113.01	112.92	611.01
342.652	25.058	0.906E-01	-0.242E+00	113.10	113.09	113.14	611.07
342.234	35.422	0.864E-01	-0.235E+00	117.99	118.02	117.93	622.76
342.397	46.971	0.796E-01	-0.226E+00	123.51	123.52	123.49	633.70
342.437	57.294	0.723E-01	-0.221E+00	127.95	127.95	127.93	642.44
342.349	72.403	0.602E-01	-0.217E+00	134.04	134.05	134.00	653.85
342.281	87.842	0.471E-01	-0.214E+00	139.14	139.15	139.10	664.13
342.340	102.544	0.343E-01	-0.212E+00	144.14	144.15	144.11	672.91
342.767	117.038	0.217E-01	-0.206E+00	148.77	148.76	148.82	680.71
342.934	133.049	0.745E-02	-0.205E+00	153.15	153.15	153.24	688.83
342.491	148.241	-0.660E-02	-0.212E+00	157.60	157.60	157.60	696.28
342.458	162.382	-0.195E-01	-0.214E+00	161.49	161.49	161.48	702.72
342.472	182.722	-0.381E-01	-0.219E+00	166.62	166.62	166.62	711.51
342.559	202.048	-0.559E-01	-0.225E+00	171.57	171.58	171.59	719.44
342.522	223.386	-0.758E-01	-0.234E+00	176.15	176.15	176.16	727.89
342.531	243.331	-0.946E-01	-0.243E+00	180.45	180.46	180.46	735.51
342.546	263.353	-0.114E+00	-0.254E+00	184.27	184.27	184.28	742.95

Table 4.11 Thermal Conductivity of n-Pentane at T_{nom} = 342.5K

T_r (K)	P (MPa)	$(\frac{\partial\lambda}{\partial T})_{\rho_r}$ (mW m^{-1} K^{-2})	$(\frac{\partial\lambda}{\partial T})_P$ (mW m^{-1} K^{-2})	$\lambda(T_r,\rho_r)$ (mW m^{-1} K^{-1})	$\lambda(T_n,\rho_r)$ (mW m^{-1} K^{-1})	$\lambda(T_n,P)$ (mW m^{-1} K^{-1})	ρ_r (Kg m^{-3})
342.687	283.282	-0.132E+00	-0.271E+00	189.44	189.47	189.50	750.08
342.647	303.632	-0.152E+00	-0.285E+00	192.63	192.66	192.68	757.31
342.851	327.960	-0.176E+00	-0.302E+00	196.09	196.15	196.19	765.75
342.719	328.457	-0.176E+00	-0.301E+00	197.19	197.23	197.26	765.95
342.666	353.366	-0.201E+00	-0.317E+00	202.00	202.03	202.05	774.44
342.729	378.065	-0.225E+00	-0.334E+00	205.87	205.92	205.94	782.63
342.675	402.935	-0.249E+00	-0.350E+00	209.92	209.96	209.98	790.68
342.727	426.876	-0.367E+00	-0.376E+00	213.98	214.04	214.06	798.19
342.708	450.200	-0.295E+00	-0.381E+00	217.47	217.53	217.55	805.28
342.727	475.996	-0.319E+00	-0.396E+00	221.40	221.48	221.49	812.80
342.772	500.218	-0.340E+00	-0.409E+00	224.88	224.97	224.99	819.54

Table 4.11 Thermal Conductivity of n-Pentane at T_{nom} = 342.5K (continued)

T_r (K)	P (MPa)	$(\frac{\partial\lambda}{\partial T})_{\rho_r}$ (mW m^{-1} K^{-2})	$(\frac{\partial\lambda}{\partial T})_P$ (mW m^{-1} K^{-2})	$\lambda(T_r,\rho_r)$ (mW m^{-1} K^{-1})	$\lambda(T_n,\rho_r)$ (mW m^{-1} K^{-1})	$\lambda(T_n,P)$ (mW m^{-1} K^{-1})	ρ_r (Kg m^{-3})
358.921	4.005	0.732E-01	-0.183E+00	98.41	98.45	98.30	565.03
359.265	4.216	0.733E-01	-0.181E+00	97.96	97.98	97.92	565.14
359.259	14.440	0.874E-01	-0.148E+00	104.13	104.15	104.10	584.34
359.144	25.268	0.915E-01	-0.125E+00	109.52	109.55	109.47	600.42
358.960	35.422	0.901E-01	-0.110E+00	114.58	114.63	114.52	613.01
359.515	46.971	0.853E-01	-0.965E-01	119.50	119.50	119.50	624.95
359.481	57.499	0.789E-01	-0.886E-01	123.48	123.48	123.47	634.72
359.537	67.216	0.719E-01	-0.825E-01	127.43	127.43	127.44	642.81
359.585	82.157	0.601E-01	-0.754E-01	133.12	133.11	133.12	653.99
359.671	97.983	0.466E-01	-0.703E-01	137.99	137.99	138.01	664.51
359.542	112.680	0.335E-01	-0.691E-01	142.85	142.85	142.86	673.40
359.722	127.475	0.202E-01	-0.691E-01	147.29	147.29	147.31	681.57
359.706	142.471	0.657E-02	-0.732E-01	151.83	151.83	151.85	689.31
359.728	158.448	-0.804E-02	-0.810E-01	155.99	155.99	156.01	697.01
359.742	174.168	-0.224E-01	-0.926E-01	159.92	159.93	159.94	704.14
359.656	188.896	-0.359E-01	-0.107E+00	163.90	163.90	163.91	710.50
359.696	205.665	-0.512E-01	-0.128E+00	166.65	166.66	166.67	717.39
359.663	205.464	-0.510E-01	-0.128E+00	166.27	166.27	166.29	717.31

Table 4.12 Thermal Conductivity of n-Pentane at T_{nom}= 359.5K

T_r (K)	P (MPa)	$(\frac{\partial\lambda}{\partial T})_{\rho_r}$ (mW m^{-1} K^{-2})	$(\frac{\partial\lambda}{\partial T})_P$ (mW m^{-1} K^{-2})	$\lambda(T_r,\rho_r)$ (mW m^{-1} K^{-1})	$\lambda(T_n,\rho_r)$ (mW m^{-1} K^{-1})	$\lambda(T_n,P)$ (mW m^{-1} K^{-1})	ρ_r (K_{ℓ}; m^{-3})
359.670	205.665	-0.512E-01	-0.128E+00	166.41	166.42	166.43	717.39
359.646	209.187	-0.544E-01	-0.133E+00	168.63	168.64	168.65	718.80
359.938	224.495	-0.682E-01	-0.156E+00	173.47	173.50	173.54	724.72
359.808	253.357	-0.943E-01	-0.211E+00	178.48	178.51	178.54	735.41
359.750	273.556	-0.112E+00	-0.254E+00	182.73	182.76	182.79	742.51
359.747	292.914	-0.130E+00	-0.298E+00	186.43	186.46	186.50	749.03
360.439	314.572	-0.148E+00	-0.357E+00	190.44	190.58	190.78	755.88
360.937	337.937	-0.169E+00	-0.426E+00	194.78	194.87	195.02	763.37
360.214	362.719	-0.190E+00	-0.503E+00	199.34	199.48	199.70	770.82
360.231	363.314	-0.191E+00	-0.505E+00	199.12	199.26	199.49	770.98
360.089	363.512	-0.191E+00	-0.505E+00	199.44	199.55	199.74	770.12
360.048	383.013	-0.208E+00	-0.568E+00	202.67	202.79	202.98	776.87
360.067	407.399	-0.229E+00	-0.646E+00	207.20	207.33	207.57	783.81
359.918	427.563	-0.246E+00	-0.710E+00	210.13	210.23	210.43	789.49
359.898	446.951	-0.262E+00	-0.770E+00	213.32	213.42	213.63	794.72
359.916	466.506	-0.278E+00	-0.829E+00	216.38	216.49	216.72	799.81
359.825	486.004	-0.293E+00	-0.883E+00	219.23	219.32	219.52	804.84
359.755	505.502	-0.309E+00	-0.934E+00	222.14	222.22	222.38	809.71

Table 4.12 Thermal Conductivity of n-Pentane at T_{nom}= 359.5K (continued)

T_r (K)	P (MPa)	$(\frac{\partial\lambda}{\partial T})_{\rho_r}$ (mW m^{-1} K^{-2})	$(\frac{\partial\lambda}{\partial T})_P$ (mW m^{-1} K^{-2})	$\lambda(T_r,\rho_r)$ (mW m^{-1} K^{-1})	$\lambda(T_n,\rho_r)$ (mW m^{-1} K^{-1})	$\lambda(T_n,P)$ (mW m^{-1} K^{-1})	ρ_r (Kg m^{-3})
307.551	0.310	0.109E+00	-0.169E+00	130.82	130.88	130.72	869.51
307.503	8.901	0.117E+00	-0.161E+00	133.72	133.79	133.62	875.66
307.461	24.061	0.125E+00	-0.155E+00	138.23	138.31	138.12	885.62
307.398	43.291	0.126E+00	-0.149E+00	143.51	143.61	143.40	896.98
307.369	58.330	0.123E+00	-0.143E+00	147.24	147.33	147.12	905.06
307.237	76.570	0.118E+00	-0.134E+00	151.84	151.95	151.72	914.14
307.271	93.375	0.114E+00	-0.126E+00	155.93	156.03	155.82	921.82
307.329	122.916	0.109E+00	-0.108E+00	161.05	161.14	160.97	934.14
307.266	147.836	0.109E+00	-0.873E-01	165.54	165.64	165.46	943.62
307.238	169.234	0.112E+00	-0.669E-01	169.96	170.06	169.90	951.18
307.302	194.295	0.121E+00	-0.401E-01	174.02	174.12	173.98	959.42
307.342	224.696	0.138E+00	-0.139E-02	178.60	178.71	178.60	968.73
307.385	244.235	0.154E+00	-0.260E-01	181.53	181.65	181.55	974.34
307.193	143.484	0.108E+00	-0.907E-01	165.18	165.29	165.09	942.05

Table 4.13 Thermal Conductivity of o-Xylene at T_{nom} = 308.15K

T_r (K)	P (MPa)	$(\frac{\partial\lambda}{\partial T})_{\rho_r}$ (mW m^{-1} K^{-2})	$(\frac{\partial\lambda}{\partial T})_P$ (mW m^{-1} K^{-2})	$\lambda(T_r,\rho_r)$ (mW m^{-1} K^{-1})	$\lambda(T_n,\rho_r)$ (mW m^{-1} K^{-1})	$\lambda(T_n,P)$ (mW m^{-1} K^{-1})	ρ_r (Kg m^{-3})
318.038	2.721	0.961E-01	-0.245E+00	128.23	128.24	128.21	863.17
318.236	15.991	0.114E+00	-0.219E+00	132.03	132.02	132.05	872.74
318.049	26.043	0.121E+00	-0.205E+00	135.57	135.58	135.55	879.66
318.053	41.324	0.126E+00	-0.191E+00	139.59	139.61	139.57	889.15
318.092	57.100	0.125E+00	-0.181E+00	143.73	143.74	143.72	898.08
318.013	76.977	0.121E+00	-0.173E+00	148.82	148.83	148.79	908.42
317.952	96.868	0.116E+00	-0.167E+00	153.58	153.61	153.55	917.86
317.926	122.206	0.111E+00	-0.158E+00	158.92	158.94	158.88	928.80
317.970	148.241	0.108E+00	-0.148E+00	164.21	164.22	164.18	938.99
317.837	150.163	0.108E+00	-0.147E+00	164.50	164.53	164.45	939.78
317.937	173.665	0.111E+00	-0.134E+00	168.84	168.86	168.81	948.19
317.851	203.955	0.120E+00	-0.112E+00	174.25	174.29	174.22	958.31
317.833	228.830	0.133E+00	-0.889E-01	178.09	178.14	178.07	966.01
317.824	228.830	0.133E+00	-0.889E-01	177.89	177.94	177.87	966.01
317.793	253.257	0.151E+00	-0.622E-01	181.74	181.80	181.72	973.12
317.798	253.257	0.151E+00	-0.624E-01	181.81	181.86	181.79	973.12
317.812	279.671	0.174E+00	-0.291E-01	185.28	185.34	185.27	980.36

Table 4.14 Thermal Conductivity of o-Xylene at T_{nom} = 318.15K

T_r (K)	P (MPa)	$(\frac{\partial\lambda}{\partial T})_{\rho_r}$ (mW m^{-1} K^{-2})	$(\frac{\partial\lambda}{\partial T})_P$ (mW m^{-1} K^{-2})	$\lambda(T_r,\rho_r)$ (mW m^{-1} K^{-1})	$\lambda(T_n,\rho_r)$ (mW m^{-1} K^{-1})	$\lambda(T_n,P)$ (mW m^{-1} K^{-1})	ρ_r (Kg m^{-3})
337.783	8.692	0.577E-01	-0.318E+00	125.44	125.44	125.48	850.83
337.760	8.692	0.578E-01	-0.318E+00	125.32	125.31	125.36	850.85
337.696	24.896	0.967E-01	-0.262E+00	130.80	130.80	130.81	863.43
337.700	30.523	0.105E+00	-0.249E+00	132.22	132.21	132.23	867.43
337.643	41.221	0.116E+00	-0.229E+00	135.81	135.81	138.81	874.66
337.643	41.221	0.116E+00	-0.229E+00	135.73	135.73	135.73	874.66
337.576	57.510	0.125E+00	-0.210E+00	140.29	140.30	140.27	884.76
337.454	77.180	0.126E+00	-0.197E+00	145.55	145.57	145.51	895.81
337.413	98.591	0.123E+00	-0.191E+00	150.85	150.88	150.80	906.62
337.637	123.726	0.116E+00	-0.188E+00	156.32	156.32	156.32	917.92
337.351	148.949	0.111E+00	-0.186E+00	161.63	161.66	161.57	928.51
337.275	173.762	0.108E+00	-0.183E+00	166.14	166.18	166.07	937.95
337.348	184.232	0.108E+00	-0.180E+00	167.77	167.80	167.71	941.66
337.247	204.760	0.111E+00	-0.173E+00	171.58	171.62	171.51	948.74
337.171	234.877	0.112E+00	-0.158E+00	176.99	177.05	176.92	958.39
337.177	263.653	0.134E+00	-0.140E+00	181.84	181.90	181.77	966.92
337.177	295.120	0.157E+00	-0.112E+00	186.17	186.24	186.12	975.62
337.195	306.525	0.167E+00	-0.101E+00	187.59	187.66	187.54	978.62
337.128	319.726	0.181E+00	-0.864E-01	189.65	189.75	189.61	982.05
337.099	352.966	0.218E+00	-0.448E-01	194.33	194.45	194.31	990.23

Table 4.15 Thermal Conductivity of o-Xylene at T_{nom} = 337.65K

T_r (K)	P (MPa)	$(\frac{\partial\lambda}{\partial T})_{\rho_r}$ (mW m^{-1} K^{-2})	$(\frac{\partial\lambda}{\partial T})_P$ (mW m^{-1} K^{-2})	$\lambda(T_r,\rho_r)$ (mW m^{-1} K^{-1})	$\lambda(T_n,\rho_r)$ (mW m^{-1} K^{-1})	$\lambda(T_n,P)$ (mW m^{-1} K^{-1})	ρ_r (Kg m^{-3})
360.455	5.696	-0.714E-01	-0.430E+00	118.26	118.28	118.39	827.99
360.638	16.122	-0.925E-02	-0.358E+00	121.97	121.98	122.15	837.18
360.481	23.957	0.274E-01	-0.316E+00	124.90	124.89	125.00	843.94
360.515	42.360	0.819E-01	-0.249E+00	130.86	130.83	130.95	857.89
360.497	42.360	0.820E-01	-0.249E+00	130.75	130.72	130.83	857.90
360.435	56.792	0.106E+00	-0.218E+00	135.07	135.04	135.14	867.69
360.292	74.842	0.121E+00	-0.195E+00	140.30	140.29	140.33	878.79
360.267	97.375	0.126E+00	-0.182E+00	146.15	146.14	146.18	891.10
360.196	123.118	0.124E+00	-0.177E+00	152.29	152.28	152.30	903.67
360.166	150.669	0.117E+00	-0.177E+00	158.01	158.00	158.01	915.70
360.017	171.349	0.113E+00	-0.178E+00	162.19	162.21	162.17	924.04
359.982	176.282	0.112E+00	-0.178E+00	163.01	163.03	162.98	925.95
360.037	203.854	0.109E+00	-0.176E+00	168.41	168.42	168.39	935.93
359.977	233.668	0.109E+00	-0.171E+00	173.84	173.86	173.81	945.91
359.954	262.554	0.116E+00	-0.162E+00	178.64	178.66	178.61	954.85
359.872	291.610	0.127E+00	-0.147E+00	183.30	183.33	183.26	963.25
359.875	325.775	0.148E+00	-0.123E+00	188.38	188.42	188.35	972.42
359.954	338.037	0.157E+00	-0.113E+00	189.95	189.99	189.93	975.52
359.943	354.764	0.171E+00	-0.968E-01	192.16	192.20	192.14	979.68
359.349	382.716	0.199E+00	-0.671E-01	196.04	196.09	196.03	986.35
359.955	419.192	0.243E+00	-0.215E-01	200.55	200.60	200.55	994.54

Table 4.16 Thermal Conductivity of o-Xylene at T_{nom} = 360.15K

T_r (K)	P (MPa)	$(\frac{\partial\lambda}{\partial T})_{\rho_r}$ (mW m^{-1} K^{-2})	$(\frac{\partial\lambda}{\partial T})_P$ (mW m^{-1} K^{-2})	$\lambda(T_r,\rho_r)$ (mW m^{-1} K^{-1})	$\lambda(T_n,\rho_r)$ (mW m^{-1} K^{-1})	$\lambda(T_n,P)$ (mW m^{-1} K^{-1})	ρ_r (Kg m^{-3})
307.629	7.173	0.146E+00	-0.281E+00	124.61	124.61	124.60	709.60
307.523	14.743	0.149E+00	-0.265E+00	128.15	128.17	128.11	716.12
307.523	14.743	0.149E+00	-0.265E+00	128.42	128.44	128.39	716.12
307.420	21.441	0.153E+00	-0.252E+00	131.17	131.20	131.11	721.52
307.189	42.232	0.171E+00	-0.214E+00	138.98	139.06	138.88	736.31
308.003	45.519	0.173E+00	-0.210E+00	140.39	140.33	140.47	737.82
307.129	59.543	0.186E+00	-0.190E+00	145.00	145.09	144.90	746.78
307.944	70.971	0.194E+00	-0.176E+00	148.86	148.80	148.91	752.49
307.362	80.111	0.202E+00	-0.165E+00	152.10	152.16	152.05	757.49
307.642	97.476	0.213E+00	-0.152E+00	156.67	156.67	156.67	765.50
307.746	104.673	0.218E+00	-0.145E+00	158.61	158.59	158.62	768.62
307.658	147.735	0.235E+00	-0.125E+00	168.08	168.08	168.08	785.43
308.109	201.138	0.241E+00	-0.124E+00	180.94	180.83	181.00	802.51
307.889	249.352	0.232E+00	-0.136E+00	190.24	190.18	190.27	816.33
307.789	288.299	0.214E+00	-0.153E+00	197.33	197.30	197.35	826.63

Table 4.17 Thermal Conductivity of Oct-1-ene at T_{nom} = 307.65K

T_r (K)	P (MPa)	$(\frac{\partial\lambda}{\partial T})_{\rho_r}$ (mW m^{-1} K^{-2})	$(\frac{\partial\lambda}{\partial T})_P$ (mW m^{-1} K^{-2})	$\lambda(T_r,\rho_r)$ (mW m^{-1} K^{-1})	$\lambda(T_n,\rho_r)$ (mW m^{-1} K^{-1})	$\lambda(T_n,P)$ (mW m^{-1} K^{-1})	ρ_r ($K\ell$ m^{-3})
321.546	8.352	0.145E+00	-0.224E+00	121.36	121.23	121.56	699.60
321.413	14.645	0.145E+00	-0.231E+00	124.77	124.66	124.94	705.39
321.300	24.794	0.148E+00	-0.234E+00	129.42	129.33	129.58	713.88
320.911	48.213	0.164E+00	-0.224E+00	138.72	138.67	138.78	730.83
320.778	70.058	0.181E+00	-0.207E+00	145.90	145.87	145.92	743.85
320.589	91.389	0.198E+00	-0.188E+00	152.97	152.98	152.96	754.85
321.059	147.634	0.228E+00	-0.148E+00	167.08	166.98	167.14	777.79
320.732	187.251	0.239E+00	-0.128E+00	175.77	175.75	175.78	791.36
320.888	199.528	0.241E+00	-0.123E+00	178.88	178.82	178.90	795.11
320.491	279.269	0.230E+00	-0.108E+00	194.48	194.52	194.47	817.84
321.103	298.327	0.222E+00	-0.108E+00	197.81	197.71	197.86	822.52
320.915	343.048	0.196E+00	-0.115E+00	205.53	205.28	205.36	834.04
320.791	399.661	0.143E+00	-0.137E+00	213.80	213.78	213.82	848.28
320.713	447.738	0.764E-01	-0.174E+00	220.84	220.83	220.85	860.59
320.570	492.138	-0.593E-02	-0.225E+00	227.51	227.51	227.49	872.25

Table 4.18 Thermal Conductivity of Oct-1-ene at T_{nom} = 320.65K

T_r (K)	P (MPa)	$(\frac{\partial\lambda}{\partial T})_{\rho_r}$ (mW m^{-1} K^{-2})	$(\frac{\partial\lambda}{\partial T})_P$ (mW m^{-1} K^{-2})	$\lambda(T_r,\rho_r)$ (mW m^{-1} K^{-1})	$\lambda(T_n,\rho_r)$ (mW m^{-1} K^{-1})	$\lambda(T_n,P)$ (mW m^{-1} K^{-1})	ρ_r (Kg m^{-3})
343.969	29.734	0.145E+00	-0.142E+00	128.29	128.31	128.26	700.95
343.775	53.416	0.151E+00	-0.199E+00	134.91	134.96	134.83	718.27
344.259	97.679	0.180E+00	-0.219E+00	149.93	149.91	149.96	742.75
343.820	151.073	0.213E+00	-0.201E+00	164.21	164.28	164.14	765.45
344.223	203.452	0.233E+00	-0.179E+00	176.49	176.47	176.50	782.96
344.053	248.250	0.241E+00	-0.163E+00	185.86	185.88	185.85	796.30
344.688	302.832	0.237E+00	-0.145E+00	196.23	196.11	196.31	810.88
344.434	345.053	0.223E+00	-0.141E+00	203.68	203.62	203.72	821.97
344.264	393.611	0.194E+00	-0.145E+00	211.97	211.95	211.99	834.46
344.162	449.215	0.140E+00	-0.159E+00	220.31	220.31	220.31	848.86
344.084	496.807	0.707E-01	-0.186E+00	227.31	227.31	227.30	861.50

Table 4.19 Thermal Conductivity of Oct-1-ene at T_{nom} = 344.15K

T_r (K)	P (MPa)	$(\frac{\partial\lambda}{\partial T})_{\rho_r}$ (mW m^{-1} K^{-2})	$(\frac{\partial\lambda}{\partial T})_P$ (mW m^{-1} K^{-2})	$\lambda(T_r,\rho_r)$ (mW m^{-1} K^{-1})	$\lambda(T_n,\rho_r)$ (mW m^{-1} K^{-1})	$\lambda(T_n,P)$ (mW m^{-1} K^{-1})	ρ_r (Kg m^{-3})
360.491	22.427	0.159E+00	-0.136E+00	118.59	118.53	118.63	683.13
360.143	55.020	0.145E+00	-0.155E+00	132.27	132.27	132.27	709.12
360.486	100.213	0.169E+00	-0.129E+00	147.44	147.39	147.49	734.86
360.226	154.712	0.203E+00	-0.872E-01	162.46	162.44	162.47	758.20
360.598	205.062	0.226E+00	-0.351E-01	174.50	174.40	174.51	775.48
360.501	241.018	0.236E+00	0.471E-02	182.59	182.51	182.59	786.70
360.629	298.828	0.241E+00	0.831E-01	193.61	193.49	193.57	803.40
360.774	351.065	0.229E+00	0.163E+00	203.27	203.13	203.17	817.98
360.595	399.561	0.202E+00	0.237E+00	211.80	211.71	211.70	831.65

Table 4.20 Thermal Conductivity of Oct-1-ene at T_{nom} = 360.15K

T_r (K)	P (MPa)	$(\frac{\partial\lambda}{\partial T})_{\rho_r}$ (mW m^{-1} K^{-2})	$(\frac{\partial\lambda}{\partial T})_P$ (mW m^{-1} K^{-2})	$\lambda(T_r,\rho_r)$ (mW m^{-1} K^{-1})	$\lambda(T_n,\rho_r)$ (mW m^{-1} K^{-1})	$\lambda(T_n,P)$ (mW m^{-1} K^{-1})	ρ_r (Kg m^{-3})
306.261	4.014	0.420E-01	-0.305E00	131.52	131.46	132.02	859.01
306.262	4.225	0.421E-01	-0.305E00	131.26	131.19	131.75	859.17
305.358	8.559	0.435E-01	-0.298E00	133.26	133.23	133.47	863.17
305.363	8.559	0.435E-01	-0.298E00	132.94	132.91	133.15	863.16
305.225	15.949	0.456E-01	-0.291E00	135.19	135.17	135.36	868.58
305.137	25.848	0.484E-01	-0.281E00	137.99	137.96	138.12	875.32
305.141	36.018	0.514E-01	-0.273E00	141.39	141.37	141.53	881.75
305.095	49.756	0.555E-01	-0.260E00	145.03	145.00	145.14	889.86
304.918	60.473	0.588E-01	-0.253E00	147.90	147.89	147.97	895.86
304.835	85.305	0.663E-01	-0.235E00	154.00	153.99	154.05	908.41
304.864	92.204	0.684E-01	-0.229E00	155.16	155.14	155.21	911.63
304.821	100.922	0.711E-01	-0.223E00	157.82	157.81	157.86	915.60
304.704	126.462	0.789E-01	-0.206E00	163.10	163.10	163.11	926.48
304.580	162.685	0.899E-01	-0.183E00	170.30	170.31	170.29	940.31
304.636	184.232	0.962E-01	-0.173E00	174.46	174.46	174.46	947.76
304.494	204.257	0.102E+00	-0.162E00	177.82	177.83	177.79	954.37
304.438	233.265	0.111E+00	-0.147E00	182.63	182.65	182.59	963.29
304.465	263.653	0.119E+00	-0.133E00	187.30	187.32	187.28	971.94
304.466	293.516	0.127E+00	-0.119E00	191.93	191.96	191.91	979.89
304.444	324.187	0.136E+00	-0.106E00	196.11	196.14	196.09	987.59
304.478	352.966	0.143E+00	-0.940E-1	199.68	199.71	199.67	994.38
304.415	360.637	0.146E+00	-0.913E-1	200.77	200.80	200.75	996.17
304.499	382.815	0.151E+00	-0.820E-1	203.65	203.67	203.64	1001.08
304.409	421.761	0.161E+00	-0.663E-1	208.83	208.87	208.82	1009.37
304.482	460.471	0.171E+00	-0.532E-1	212.88	212.91	212.87	1017.06
304.465	501.096	0.181E+00	-0.393E-1	217.32	217.35	217.31	1024.72

Table 4.21 Thermal Conductivity of Ethylbenzene at T_{nom} = 304.65K

T_r (K)	P (MPa)	$(\frac{\partial\lambda}{\partial T})_{\rho_r}$ (mW m^{-1} K^{-2})	$(\frac{\partial\lambda}{\partial T})_P$ (mW m^{-1} K^{-2})	$\lambda(T_r,\rho_r)$ (mW m^{-1} K^{-1})	$\lambda(T_n,\rho_r)$ (mW m^{-1} K^{-1})	$\lambda(T_n,P)$ (mW m^{-1} K^{-1})	ρ_r (Kg m^{-3})
356.588	3.501	0.329E-01	-0.273E+00	115.06	115.08	114.90	813.69
357.702	5.494	0.330E-01	-0.271E+00	116.26	116.25	116.41	814.76
356.221	8.031	0.333E-01	-0.274E+00	117.73	117.76	117.47	818.63
357.538	13.522	0.337E-01	-0.271E+00	118.50	118.49	118.61	822.80
359.096	18.901	0.342E-01	-0.268E+00	120.36	120.30	120.88	826.46
357.304	24.692	0.352E-01	-0.270E+00	121.96	121.96	122.00	832.96
358.845	34.344	0.366E-01	-0.265E+00	125.37	125.30	125.81	839.63
357.189	41.029	0.381E-01	-0.265E+00	127.02	127.02	127.03	845.96
358.737	49.652	0.395E-01	-0.260E+00	129.93	129.86	130.34	851.05
357.091	56.672	0.414E-01	-0.261E+00	132.09	132.09	132.08	856.98
358.416	65.892	0.431E-01	-0.256E+00	135.19	135.13	135.51	862.04
358.325	82.259	0.468E-01	-0.250E+00	139.46	139.40	139.75	871.91
357.003	96.969	0.509E-01	-0.246E+00	142.88	142.89	142.85	880.82
358.714	97.273	0.505E-01	-0.244E+00	143.84	143.76	144.22	879.93
358.270	121.801	0.569E-01	-0.234E+00	149.33	149.27	149.59	892.47
356.595	145.103	0.635E-01	-0.227E+00	154.39	154.43	154.27	903.92
358.111	147.431	0.636E-01	-0.224E+00	155.06	155.00	155.28	904.08
358.179	147.431	0.636E-01	-0.224E+00	155.58	155.52	155.81	904.04
358.228	173.665	0.705E-01	-0.214E+00	161.04	160.97	161.27	914.70
356.640	174.067	0.712E-01	-0.216E+00	160.51	160.54	160.40	915.70
358.227	204.156	0.786E-01	-0.203E+00	166.81	166.73	167.03	925.99
356.526	202.747	0.788E-01	-0.204E+00	166.94	166.99	166.81	926.36
356.741	232.055	0.865E-01	-0.193E+00	171.98	172.02	171.90	936.19
356.730	262.154	0.944E-01	-0.182E+00	177.87	177.91	177.79	945.62
356.731	262.154	0.944E-01	-0.182E+00	177.98	178.02	177.91	945.62
356.639	293.917	0.103E+00	-0.171E+00	183.38	183.43	183.29	954.87
356.597	321.609	0.110E+00	-0.161E+00	188.05	188.11	187.96	962.40
355.651	352.166	0.118E+00	-0.151E+00	192.88	193.06	192.66	970.62
356.479	383.211	0.125E+00	-0.140E+00	197.35	197.44	197.26	977.71
356.441	422.845	0.135E+00	-0.128E+00	202.55	202.64	202.46	986.67
356.489	462.350	0.144E+00	-0.115E+00	207.54	207.64	207.47	994.98
356.336	501.780	0.153E+00	-0.103E+00	212.54	212.66	212.46	1002.88

Table 4.22 Thermal Conductivity of Ethylbenzene at T_{nom} = 319.15K

T_r (K)	P (MPa)	$(\frac{\partial\lambda}{\partial T})_{\rho_r}$ (mW m^{-1} K^{-2})	$(\frac{\partial\lambda}{\partial T})_P$ (mW m^{-1} K^{-2})	$\lambda(T_r,\rho_r)$ (mW m^{-1} K^{-1})	$\lambda(T_n,\rho_r)$ (mW m^{-1} K^{-1})	$\lambda(T_n,P)$ (mW m^{-1} K^{-1})	ρ_r (Kg m^{-3})
340.420	6.234	0.348E-01	-0.336E+00	121.81	121.78	122.07	830.95
340.384	16.371	0.366E-01	-0.321E+00	125.47	125.44	125.71	839.86
340.590	23.745	0.380E-01	-0.312E+00	127.77	127.74	128.06	845.65
340.430	24.271	0.382E-01	-0.311E+00	127.42	127.39	127.66	846.19
340.305	25.217	0.384E-01	-0.310E+00	128.16	128.14	128.37	847.03
340.336	40.090	0.417E-01	-0.294E+00	132.78	132.75	132.98	857.90
340.328	54.200	0.451E-01	-0.282E+00	136.95	136.95	137.14	867.25
340.235	65.994	0.480E-01	-0.273E+00	140.37	140.34	140.53	874.51
340.114	82.157	0.523E-01	-0.261E+00	144.48	144.45	144.60	883.71
340.034	99.402	0.570E-01	-0.250E+00	149.39	149.37	149.49	892.69
339.902	105.483	0.587E-01	-0.247E+00	150.48	150.47	150.55	895.76
339.916	105.483	0.587E-01	-0.247E+00	150.42	150.40	150.48	895.75
339.876	123.118	0.636E-01	-0.237E+00	154.79	154.78	154.84	903.98
340.205	148.140	0.704E-01	-0.225E+00	159.77	159.73	159.90	914.50
340.231	148.140	0.703E-01	-0.225E+00	160.21	160.17	160.34	914.48
339.849	150.770	0.712E-01	-0.225E+00	160.41	160.39	160.45	915.77
340.050	173.866	0.776E-01	-0.214E+00	165.72	165.69	165.81	924.65
340.001	204.357	0.860E-01	-0.202E+00	171.54	171.51	171.61	935.56
339.961	204.357	0.860E-01	-0.201E+00	171.46	171.43	171.52	935.58
339.905	232.156	0.936E-01	-0.192E+00	176.69	176.67	176.74	944.74
339.958	263.054	0.102E+00	-0.181E+00	180.46	180.43	180.51	954.11
339.741	293.917	0.110E+00	-0.172E+00	186.15	186.14	186.17	962.93
339.972	354.664	0.126E+00	-0.154E+00	194.92	194.88	194.97	978.38
339.840	383.508	0.133E+00	-0.147E+00	198.92	198.90	198.95	985.22
339.696	383.508	0.133E+00	-0.147E+00	199.10	199.10	199.11	985.28
339.408	423.239	0.143E+00	-0.137E+00	205.50	205.54	205.47	994.19
339.374	462.544	0.153E+00	-0.127E+00	210.67	210.72	210.64	1002.35
339.221	500.706	0.162E+00	-0.119E+00	215.23	215.30	215.18	1009.87

Table 4.23 Thermal Conductivity of Ethylbenzene at T_{nom} = 339.65K

T_r (K)	P (MPa)	$(\frac{\partial\lambda}{\partial T})_{\rho_r}$ (mW m^{-1} K^{-2})	$(\frac{\partial\lambda}{\partial T})_P$ (mW m^{-1} K^{-2})	$\lambda(T_r,\rho_r)$ (mW m^{-1} K^{-1})	$\lambda(T_n,\rho_r)$ (mW m^{-1} K^{-1})	$\lambda(T_n,P)$ (mW m^{-1} K^{-1})	ρ_r (Kg m^{-3})
319.967	3.697	0.384E-01	-0.362E+00	126.57	126.54	126.87	847.03
319.773	15.949	0.413E-01	-0.339E+00	130.71	130.69	130.92	856.89
319.723	16.160	0.414E-01	-0.338E+00	130.40	130.38	130.59	857.09
319.633	29.524	0.448E-01	-0.316E+00	134.84	134.82	135.00	866.71
319.422	46.230	0.494E-01	-0.296E+00	139.88	139.86	139.96	877.63
319.488	60.678	0.535E-01	-0.280E+00	143.99	143.97	144.08	886.05
319.353	77.790	0.585E-01	-0.265E+00	148.27	148.26	148.32	895.36
319.183	77.891	0.586E-01	-0.264E+00	148.52	148.52	148.53	895.52
319.767	96.767	0.638E-01	-0.251E+00	152.93	152.89	153.09	904.46
318.043	97.679	0.648E-01	-0.249E+00	153.80	153.87	153.52	905.99
319.774	118.153	0.701E-01	-0.236E+00	157.99	157.95	158.14	914.14
319.594	144.294	0.778E-01	-0.221E+00	163.47	163.43	163.56	925.05
319.434	172.457	0.861E-01	-0.208E+00	169.02	168.99	169.08	935.73
319.584	203.150	0.949E-01	-0.194E+00	174.69	174.65	174.77	946.19
319.485	234.172	0.104E+00	-0.183E+00	180.04	180.01	180.11	956.04
319.295	263.853	0.112E+00	-0.172E+00	184.67	184.65	184.70	964.82
319.530	293.014	0.120E+00	-0.164E+00	189.16	189.11	189.22	972.67
319.666	323.790	0.128E+00	-0.154E+00	193.60	193.54	193.68	980.50
319.778	352.466	0.136E+00	-0.147E+00	196.35	196.27	196.45	987.39
319.602	354.165	0.136E+00	-0.146E+00	197.77	197.71	197.83	987.87
319.507	382.320	0.143E+00	-0.139E+00	201.39	201.34	201.44	994.37
319.754	421.958	0.153E+00	-0.130E+00	207.81	207.72	207.89	1002.82
319.888	421.662	0.153E+00	-0.131E+00	207.71	207.60	207.81	1002.70
319.875	463.043	0.164E+00	-0.121E+00	212.75	212.63	212.84	1011.10
319.694	501.096	0.173E+00	-0.113E+00	217.34	217.25	217.41	1018.46

Table 4.24 Thermal Conductivity of Ethylbenzene at T_{nom} = 357.15K

required for the same purpose was obtained from the compilation of Vargaftik [69]. For ethylbenzene, the measured thermal conductivity has been corrected to the nominal temperature, in the manner described by Menashe and Wakeham [57]. In no case did the correction exceed ±0.3%, so that the additional error incurred by using this correction is negligible. It is estimated that the uncertainty in the tabulated data is ±0.3%. For ethylbenzene, a tabulation of the thermal conductivity as a function of density is included in tables 4.21 to 4.24 over the range for which direct measurements of the volumetric properties are available ($P \leq 50MPa$) Mamedov et.al.[90]. It is claimed [90] that the uncertainty in the density data is within the range of ±0.2% to ±0.5%.

4.3 Correlation Of The Experimental Results.

For the purposes of correlating the experimental data, the thermal conductivity obtained at the nominal temperature and reference density, $\lambda(T_n, \rho_r)$, and the thermal conductivity at the nominal temperature and experimental pressure, were fitted to polynomials. The pressure dependence of the thermal conductivity, λ, of all the liquids along each isotherm, has been represented for the purposes of interpolation, by an equation of the form:

$$\lambda = \lambda' \left\{ 1 + \sum_{i=1}^{n} a_i \left[(P - P') / P' \right]^i \right\} \qquad (4.2)$$

The coefficients which secure the optimum representation of the data for all the liquids are listed in tables 4.25 to 4.29.

T(K)	p'/MPa	λ'/mW m^{-1} K^{-1}	$10a_1$	10^2a_2	10^2a_3	10^2a_4
310.15	50	109.09	1.041	-0.79	9.00	-0.26
322.65	50	107.05	1.146	-1.71	2.09	1.081
342.65	50	103.09	1.236	-1.03	3.79	-1.722
359.65	50	99.87	1.355	-1.95	4.19	-0.472
364.15	50	99.16	1.381	-1.88	4.72	-1.183

Table 4.25 Coefficients of the Correlation for the Pressure Dependence of the Thermal Conductivity of Carbon Tetrachloride. (Eq. (4.2)).

T(K)	p'/MPa	λ'/mW m^{-1} K^{-1}	$10a_1$	10^2a_2	10^2a_3	10^2a_4
305.8	250	194.36	2.892	-6.256	4.971	-3.026
322.8	250	188.38	2.927	-5.873	4.968	-4.183
342.5	250	181.79	2.821	-6.377	6.138	-4.409
359.5	250	177.39	2.963	-5.954	5.558	-4.486

Table 4.26 Coefficients of the Correlation for the Pressure Dependence of the Thermal Conductivity of n-Pentane. (Eq. (4.2)).

T(K)	p'/MPa	λ'/mW m^{-1} K^{-1}	$10a_1$	10^2a_2	10^2a_3	10^2a_4
308.15	250	182.39	1.9512	-7.7619	-6.1889	-7.2386
318.15	250	181.22	1.9957	-7.9077	-1.4013	-3.3111
337.65	250	179.29	2.2372	-4.8354	0.30786	-4.2433
360.15	250	176.40	2.3554	-4.8825	2.1394	-3.4978

Table 4.27 Coefficients of the Correlation for the Pressure Dependence of the Thermal Conductivity of o-Xylene. (Eq. (4.2)).

T(K)	p'/MPa	λ '/mW m^{-1} K^{-1}	$10a_1$	10^2a_2	10^2a_3	10^2a_4
307.65	200	180.337	2.358	-3.089	-1.229	-7.372
320.65	200	179.120	2.279	-5.689	3.952	-1.464
344.15	200	175.689	2.556	-5.957	1.773	-0.251
360.15	200	173.468	2.577	-6.108	4.034	-1.644

Table 4.28 Coefficients of the Correlation for the Pressure Dependence of the Thermal Conductivity of Oct-1-ene. (Eq. (4.2)).

T(K)	p'/MPa	λ'/mW m^{-1} K^{-1}	$10a_1$	10^2a_2	10^2a_3	10^2a_4
304.65	250	185.24	2.0902	-5.0071	2.4829	-1.1205
319.15	250	182.39	2.1728	-4.3991	3.5221	-1.5883
339.65	250	179.13	2.3033	-5.2290	3.6199	-1.1947
357.15	250	175.65	2.5455	-5.3766	2.4115	-1.7728

Table 4.29 Coefficients of the Correlation of the Pressure Dependence of the Thermal Conductivity of Ethylbenzene. (Eq. (4.2)).

Figures 4.iii to 4.vii contain the deviations of the thermal conductivity of the five electrically insulating fluids from the optimum correlation of equation (4.2). The same figures contain the results of earlier measurements of the thermal conductivity of the same liquids for comparison.

Figure 4.iv illustrates the deviations of the experimental data of n-pentane from the correlation. In no case do the deviations exceed $\pm$1.0%, the standard deviations of the entire set being $\pm$0.2%. This figure also includes a comparison with earlier measurements of the thermal conductivity of n-pentane [92-94]. The earlier results generally deviate from the present correlation by more than the mutual uncertainty. The data of Carmichael et.al.[92] are systematically lower than the reported ones by about 6%, as well as Bogatov et.al.[94] which are also systematically lower than the current values by 2%. Those of Mukhamedzyanov and Usmanov [93] are systematically higher by about two to five percent. Owing to the higher precision of the present data, they are to be preferred to the earlier results.

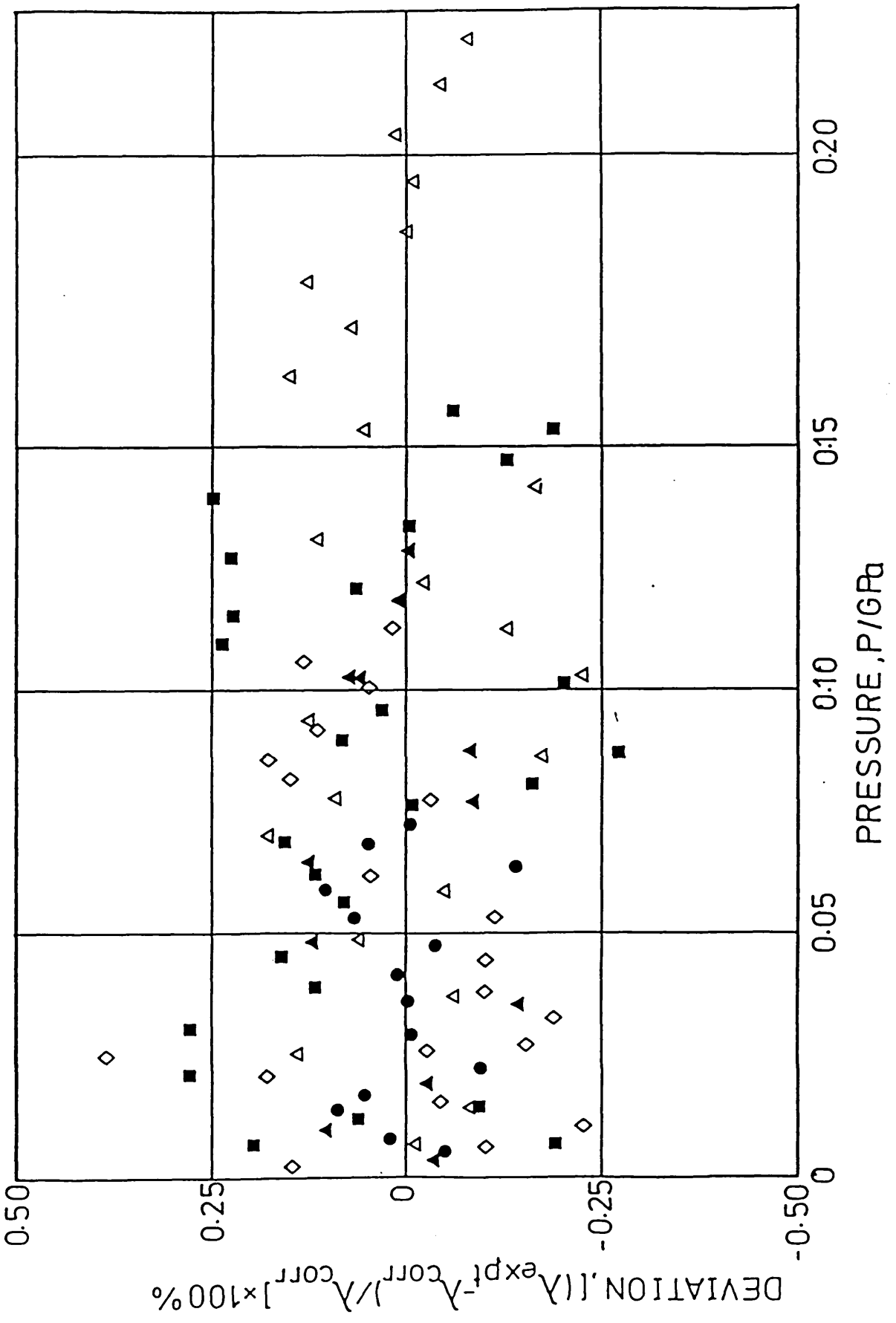
Figure 4.vii represents the pressure dependence of the thermal conductivity , λ, of ethylbenzene over the entire range of the measurements. The figure contains a plot of the deviations from the above correlation (4.2), which reveals that the maximum deviation is $\pm$0.61%, while the standard deviation is $\pm$0.13%. The same figure

includes a comparison with the earlier results of Rastorguev and Pugach [95]. The significant systematic departure of the earlier results from the correlation of the present values is outside the claimed uncertainty of the two sets of results. However, the present results are to be preferred owing to their accuracy.

Figure 4.iii shows the deviations of the experimental data of carbon tetrachloride from the correlation of (4.2). It can be seen that they do not exceed ±0.5%; the standard deviation over the entire set being one of ±0.15%. There appears to have been no previous measurements of the thermal conductivity of carbon tetrachloride under pressure against which to compare the present results.

Figure 4.v contains the deviations of the experimental data of o-xylene from equation (4.2) that secures the optimum representation of the pressure dependence on the thermal conductivity. The standard deviation of the data from the correlation is about ±0.1%, while the maximum deviation is ±0.4%. Accurate data on the thermal conductivity of o-xylene is lacking. Mamedov et.al.[90], gives the equation of state of the said liquid for the density dependence on temperature and pressure, but with a very restricted range, up to 500 bar.

Figure 4.vi gives the pressure dependence of the thermal conductivity of oct-1-ene along each isotherm based on the correlation of equation (4.2). The figure illustrates the deviations of the present experimental data from this correlation and includes the results of the


0.50
0.25
0
-0.25
-0.50
0
0.05
0.10
0.15
0.20
PRESSURE, P/GPa
DEVIATION, [(λexpt-λcorr)/λcorr]×100%

5.0
0
-5.0
0
200
400
600
PRESSURE, P/MPa
DEVIATION, [(λexpt-λcorr)/λcorr]×100 %

Figure 4.iv.

Figure 4.v.

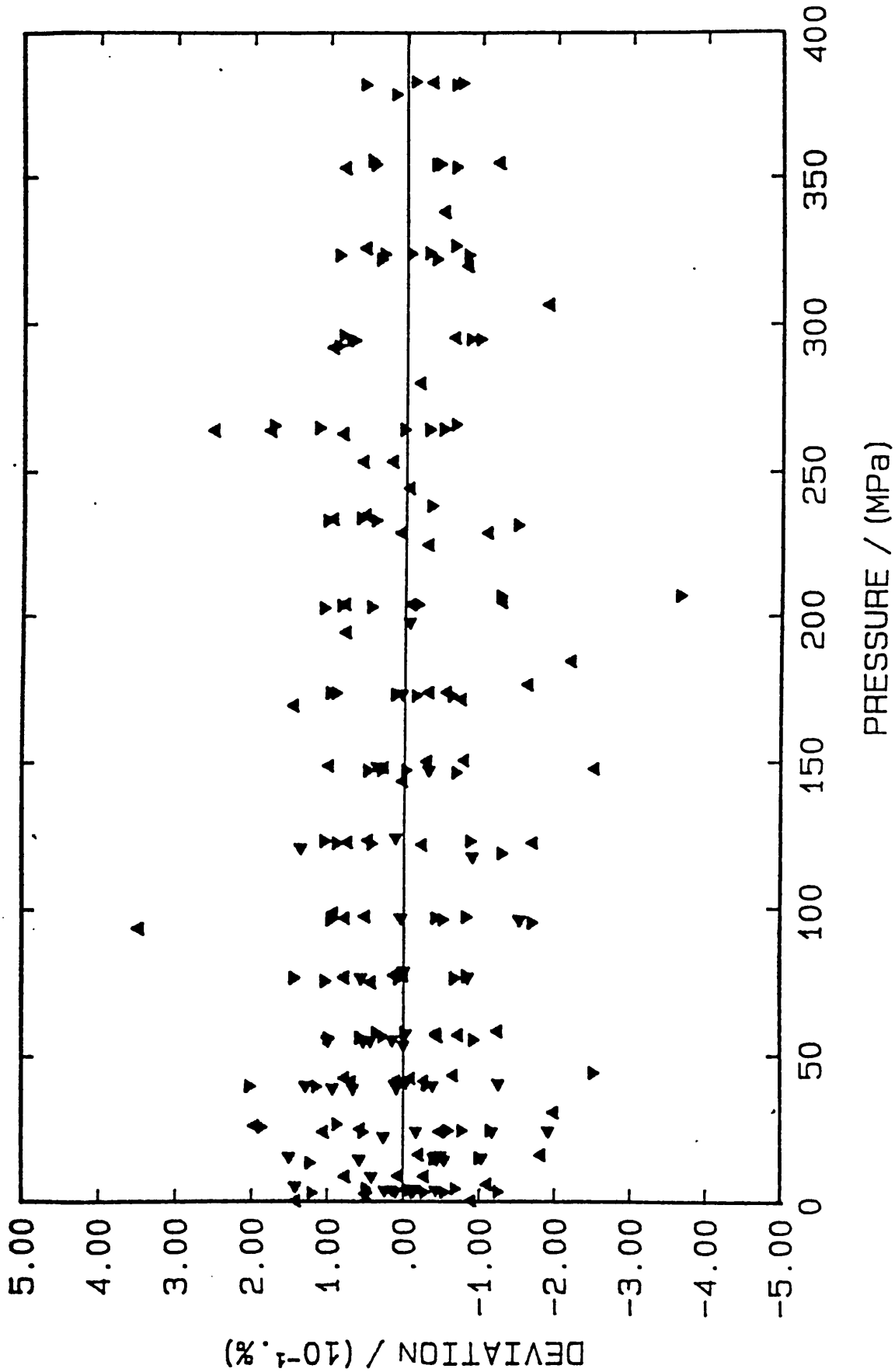

5.00
4.00
3.00
2.00
1.00
.00
-1.00
-2.00
-3.00
-4.00
-5.00
DEVIATION / (10⁻⁴.%)
0
50
100
150
200
250
300
350
400
PRESSURE / (MPa)

Figure 4.vi.

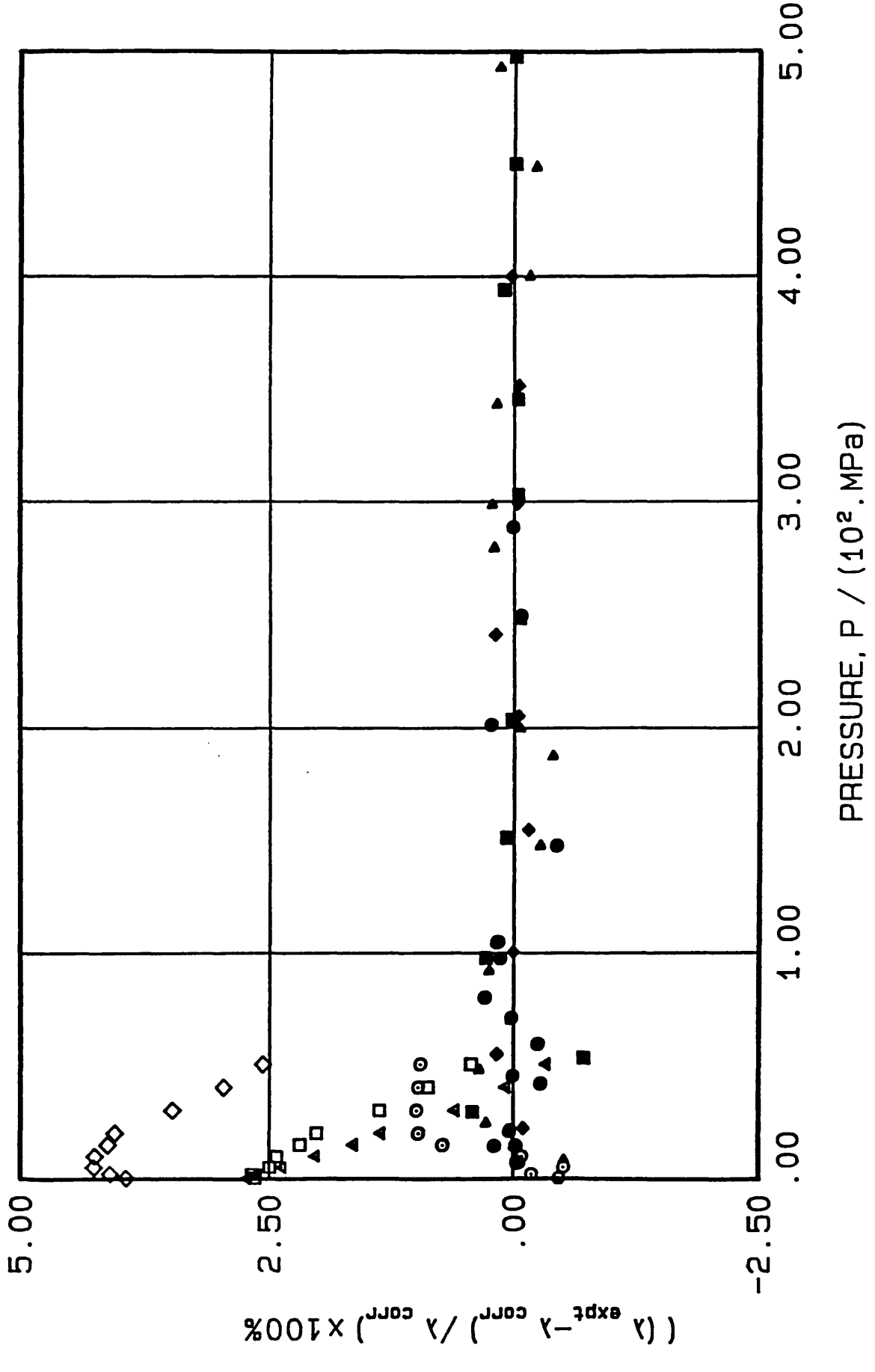

5.00
4.00
3.00
2.00
1.00
.00
PRESSURE, P / (10² .MPa)
5.00
2.50
.00
-2.50
((λ expt − λ corr) / λ corr) x100%

Figure 4.vii.

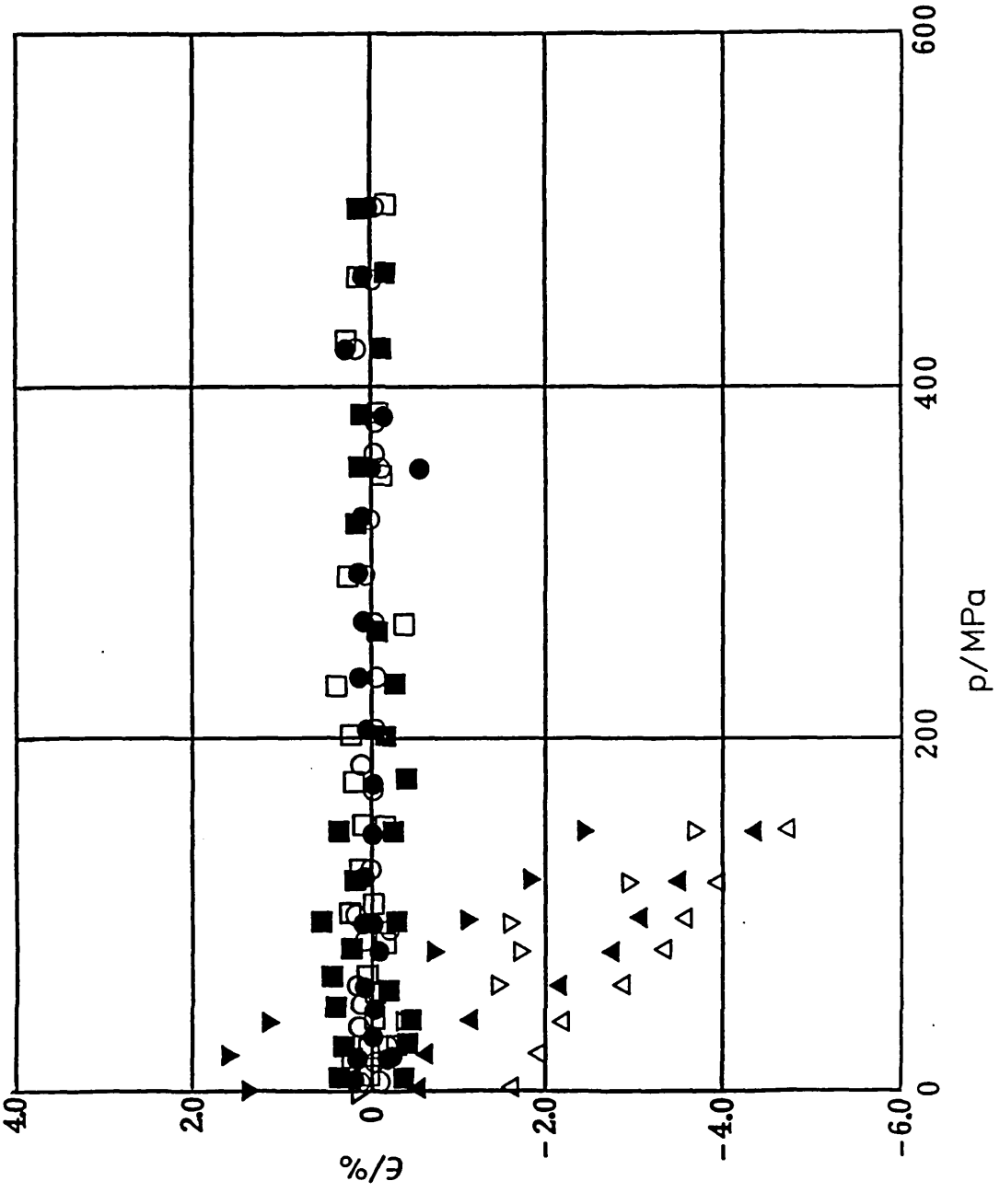


Figure 4.iii The deviations of the thermal conductivity data from their correlation as a function of pressure by equation (4.2), for liquid carbon tetrachloride.

● 310.15 K

◇ 322.65 K

■ 342.65 K

△ 359.65 K

▲ 364.15 K

Figure 4.v The deviations of the thermal conductivity data from their correlation as a function of pressure by equation (4.2), for liquid o-xylene, m-xylene and p-xylene.

▲ o-xylene

▼ m-xylene

◀ p-xylene

Figure 4.vi. The deviations of the experimental thermal conductivity of oct-1-ene, from the correlation of equation (4.2).



Figure 4.iv The deviations of the experimental thermal conductivity of n-pentane, from the correlation of equation (4.2).

Present work:

○ 305.8 K; ● 322.8 K; ◑ 342.5 K; ◐ 359.5 K.

[92] : △ 305.8 K; ▽ 342.5 K.

[93] : □ 305.8 K; ■ 342.5 K.

[94] : ◪ 305.8 K; ◪ 342.5 K.

Figure 4.vii The deviations of the experimental thermal conductivity of ethylbenzene, from the correlation of equation (4.2).

This work:

○ 304.65 K; ● 319.15 K; □ 339.65 K; ■ 357.15 K.

[95] :

△ 304.65 K; ▲ 319.15 K; ▽ 339.65 K; ▼ 357.15 K.

only earlier set of measurements at pressures up to 50MPa [96]. The present data do not depart from the correlation by more than ±0.7% over the entire range of pressures. The agreement with the results of Naziev and Abasov [96] is within the mutual uncertainty of the two sets of data in the limited range of overlapping pressures, although the present results are of higher accuracy.

4.4 Water.

Water is a highly polar fluid and whilst it is possible to obtain the material with an extremely low electrical conductivity, this cannot be maintained in the presence of the metallic walls of the thermal conductivity cells. Thus, in any practical instrument, the water will contain a very low concentration of ions. This low concentration is most certainly not enough to cause any change in the thermal conductivity of water, but has a profound effect upon the electrical conductivity. Water is therefore a suitable prototype fluid for the first test measurements for the new thermal conductivity instrument for electrically-conducting fluids. Water has also the peculiar advantage over other electrically conducting liquids in that it has been the subject of many earlier studies of the thermal conductivity, which have been critically reviewed by the International Association of the Properties of Steam. As a result, there is a quite accurate and wide ranging correlation of the thermal conductivity against which to test the results of new instruments.

For these reasons, we report here measurements of the thermal

conductivity of water as a proof that the new instrument operates correctly and in accordance with the theory of it. The measurements have been carried out at four isotherms of 302.65K, 312.55K, 324.15K and 341.65K at pressures up to 100MPa. A further set of measurements was carried out in the extended pressure range up to 300MPa. The thermodynamic properties of water required for the application of the corrections detailed in Chapter 2 have been taken from the work of Haar et.al.[97,98], and these for tantalum pentoxide required for the same purpose taken from [99].

Tables 4.30 to 4.33 list the experimental data for water. As well as the thermal conductivity at the reference conditions $\lambda(T_r,\rho_r)$ we list the values corrected to the nominal temperature at the same density and the experimental pressure. The thermal conductivity has been converted to a nominal temperature by the application of a small, linear correction based upon the I.A.P.S. formulation for the thermal conductivity of the water substance [100,101]. The quoted density is, in each case, based upon the equation of state of Haar et.al. [96,98]. These tables include check measurements carried out at the end of each isotherm.

4.4.1 Accuracy of the Measurement of Water.

In order to demonstrate that the apparatus operates in accord with the theoretical model of it outlined earlier, it is essential to ascertain that the experimental term ΔT_w vs. ℓn t line with ΔT

T_o (K)	T_r (K)	Pressure (MPa)	$\lambda(T_r, \rho_r)$ (mW m^{-1} K^{-1})	$\rho_r(P, T_r)$ (kg m^{-3})	$\lambda(T_{nom}, \rho_r)$ (mW m^{-1} K^{-1})	$\lambda(T_{nom}, P)$ (mW m^{-1} K^{-1})
297.57	302.71	0.1013	611.7	995.7	611.7	611.7
297.52	302.68	0.1013	613.5	995.7	613.4	613.5
297.52	302.67	3.74	614.7	997.4	614.7	614.7
297.60	302.73	9.72	616.1	1000.0	615.9	617.0
297.57	302.69	16.01	618.0	1002.7	617.9	617.9
297.62	302.73	20.75	620.9	1004.7	620.7	620.8
297.62	302.76	25.49	623.6	1006.6	623.4	623.4
297.62	302.80	25.49	623.7	1006.6	623.5	623.5
297.62	302.83	28.99	624.6	1008.1	624.2	624.3
297.57	302.67	41.96	628.5	1013.4	628.5	628.5
297.57	302.67	41.96	630.6	1013.4	630.6	630.6
297.57	302.59	52.15	634.0	1017.5	634.1	634.1
297.57	302.61	52.15	635.6	1017.5	635.7	635.7
297.62	302.69	62.63	638.9	1021.6	638.8	638.8
297.62	302.70	62.63	638.2	1021.6	638.1	638.1
297.60	302.67	70.44	644.9	1024.6	644.9	644.9
297.57	302.54	82.14	648.5	1029.1	648.7	648.7
297.60	302.56	92.82	651.8	1033.1	652.0	652.0
297.60	302.58	92.82	652.6	1033.1	652.7	652.7
297.62	302.57	102.66	655.4	1036.7	655.6	655.5
297.60	302.79	0.1013	613.5	995.7	613.3	613.3

Table 4.30 Thermal Conductivity of Water at T_{nom} = 302.65K

T_o (K)	T_r (K)	Pressure (MPa)	λ (T_r, ρ_r) (mW m^{-1} K^{-1})	ρ_r(P, T_r) (kg m^{-3})	λ (T_{nom}, ρ_r) (mW m^{-1} K^{-1})	λ (T_{nom}, P) (mW m^{-1} K^{-1})
319.58	324.29	0.1052	645.4	987.5	645.2	645.2
319.55	324.30	6.22	648.5	990.1	648.3	648.3
319.55	324.32	6.22	649.6	990.1	649.4	649.4
319.55	324.29	9.00	649.6	991.3	649.4	649.4
319.50	324.20	19.82	655.6	995.9	655.5	655.5
319.50	324.16	19.82	655.3	995.9	655.3	655.3
319.50	324.23	19.82	654.0	995.8	654.0	654.0
319.53	324.15	33.52	658.3	1001.4	658.3	658.3
319.53	324.15	33.52	659.5	1001.4	659.5	659.5
319.55	324.22	41.55	663.0	1004.6	662.9	662.9
319.55	324.11	50.91	668.2	1008.3	668.2	668.2
319.55	324.14	61.29	672.2	1012.3	672.2	672.2
319.55	324.14	61.29	673.1	1012.3	673.1	673.1
319.55	324.20	72.70	676.9	1016.5	676.8	676.8
319.55	324.15	72.70	677.3	1016.5	677.3	677.3
319.50	324.07	82.76	681.6	1020.3	681.7	681.6
319.55	324.29	92.82	687.8	1023.8	687.8	687.8
319.55	324.18	92.82	686.4	1023.9	686.4	686.4
319.55	324.23	92.82	686.5	1023.9	686.4	686.5
319.53	324.18	102.56	689.5	1027.4	689.5	689.5
319.53	324.08	102.56	688.8	1027.4	688.9	688.8
319.50	324.12	38.77	663.6	1003.6	663.6	663.6
319.53	324.32	0.1052	644.0	987.5	644.0	644.0

Table 4.31 Thermal Conductivity of Water at T_{nom} = 324.15K

T_o (K)	T_r (K)	Pressure (MPa)	$\lambda(T_r, \rho_r)$ (mW m^{-1} K^{-1})	$\rho_r(P, T_r)$ (kg m^{-3})	$\lambda(T_{nom}, \rho_r)$ (mW m^{-1} K^{-1})	$\lambda(T_{nom}, P)$ (mW m^{-1} K^{-1})
337.34	341.78	0.1013	661.8	978.6	661.6	661.7
337.394	341.82	5.39	664.1	980.9	663.8	663.9
337.29	341.87	10.34	666.8	983.0	666.5	666.6
337.37	341.63	14.16	667.7	984.6	667.7	667.7
337.29	341.89	14.67	670.7	984.6	670.3	670.5
337.29	341.85	14.67	669.1	984.6	668.8	668.9
337.32	341.84	17.97	672.5	986.1	672.2	672.4
337.32	341.86	17.97	674.9	986.1	674.6	674.7
337.29	341.74	32.18	676.7	992.1	676.6	676.6
337.32	341.81	41.34	678.7	995.7	678.5	678.6
337.29	341.84	51.01	686.1	999.5	685.6	685.9
337.34	341.69	62.12	692.9	1003.8	692.9	692.9
337.32	341.63	73.11	695.7	1007.9	695.7	695.7

Table 4.32 Thermal Conductivity of Water at T_{nom} = 341.65K

T_o (K)	T_r (K)	Pressure (MPa)	$\lambda(T_r, \rho_r)$ (mW m^{-1} K^{-1})	$\lambda_r(P, \rho_r)$ (kg m^{-3})	$\lambda(T_{nom}, \rho_r)$ (mW m^{-1} K^{-1})	$\lambda(T_{nom}, P)$ (mW m^{-1} K^{-1})
297.70	302.64	0.1013	613.7	995.8	613.8	613.8
297.65	302.73	3.95	616.6	997.5	616.5	616.5
297.65	302.48	9.52	617.4	999.9	617.8	617.7
297.73	302.53	16.11	619.5	1002.8	619.8	619.7
297.65	302.43	22.61	621.4	1005.5	621.9	621.8
297.67	302.51	36.51	628.3	1011.3	628.8	628.7
297.65	302.35	51.84	635.2	1017.5	635.8	635.7
297.73	302.31	67.15	640.4	1023.5	641.1	641.0
297.73	302.31	67.15	640.2	1023.5	640.9	640.8
297.67	302.27	82.56	647.6	1029.4	648.3	648.2
297.67	302.21	100.41	655.2	1036.0	656.1	655.9
297.65	302.25	110.65	660.0	1039.7	660.9	660.7
297.20	302.24	125.20	665.1	1044.8	665.9	665.8
297.67	302.31	125.20	666.2	1044.8	666.9	666.8
297.67	302.14	147.29	672.7	1052.4	673.8	673.6
297.65	302.11	172.83	682.2	1060.8	683.4	683.2
297.62	302.12	200.87	691.6	1069.6	692.8	692.6
297.62	302.12	200.87	690.4	1069.6	691.5	691.3
297.62	302.15	219.71	703.4	1075.2	704.5	704.3
297.62	302.07	262.90	710.9	1087.6	712.2	712.0
297.62	302.19	285.72	718.3	1093.7	719.4	719.2

Table 4.33 Thermal Conductivity of Water at T_{nom} = 302.65K up to 300MPa.

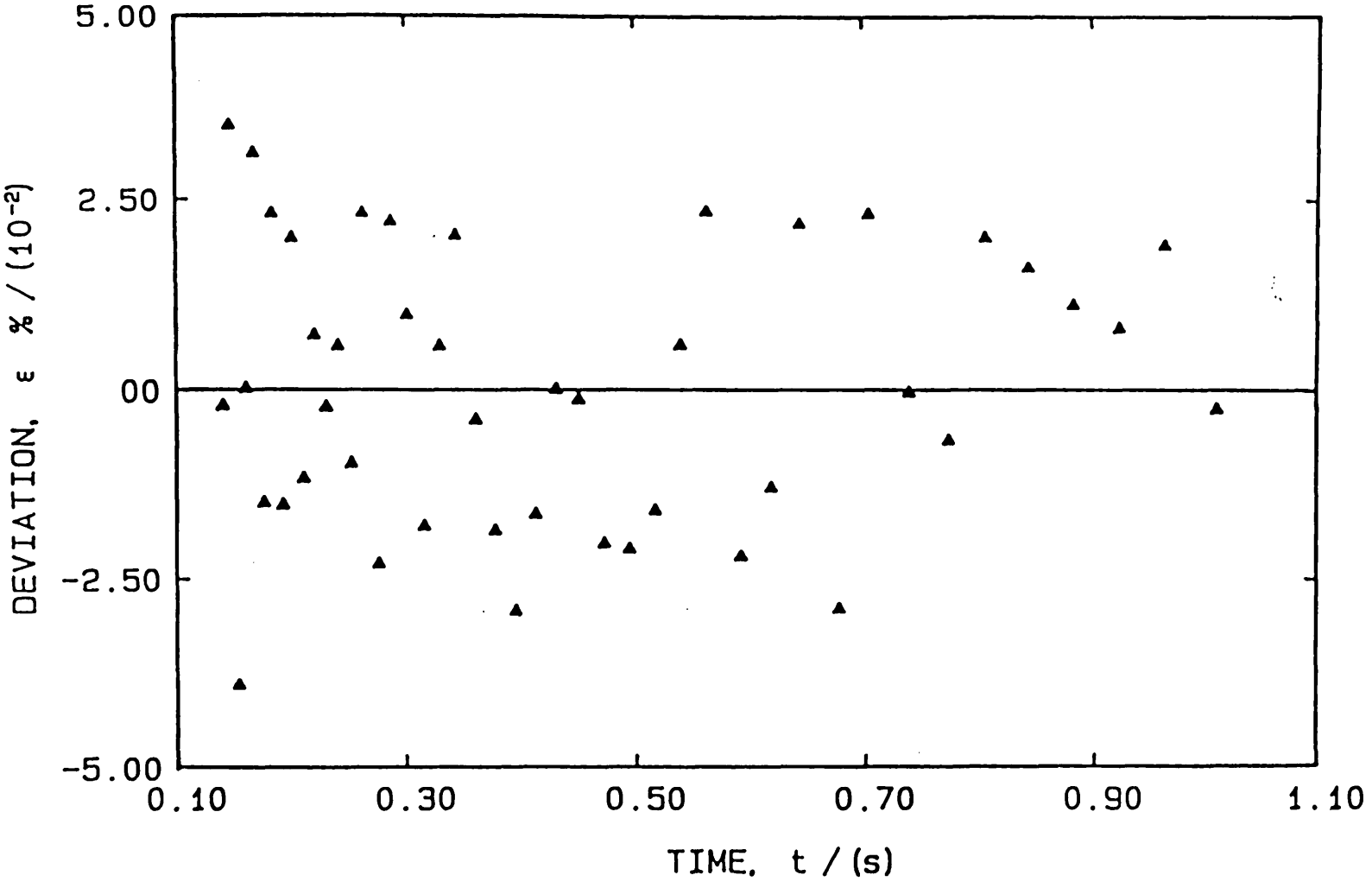
corrections as outlined in Chapter 2, is linear. This serves also to establish that the measurement of the thermal conductivity is free of convection and radiation effects.(Chapter 2).

In consequence, figure 4.viii displays a plot of the deviation of the corrected, experimental measured temperature rises as a function of time from a linear fit to the data, for a run in water at a temperature of 302K, and a pressure of 102.7 MPa. Figure 4.ix contains a plot of the absolute temperature rise itself, for a run in water at 298K and 0.1 MPa. It can be seen that no point deviates by more than $\pm$0.04% from the linear fit, while the standard deviation is one of $\pm$0.02%, which is consistent with the estimated precision of the measurements. Furthermore, there is no evidence of any systematic curvature in the data.

This figure is typical of these encountered under all conditions, and can be taken as proof that the experiment operates in a manner consistent with the theory of it.〈4.viii〉

The precision of the measurement of thermal conductivity, based upon the statistical uncertainty in the slope of the line ΔT vs. $\ell n\ t$ is $\pm$0.1%. However, the accuracy is rather worse, because it involves the uncertainty in the temperature coefficient of resistance of tantalum. It is estimated that the overall accuracy of the data is one of $\pm$0.3%.

Figure 4.viii. Deviations of the corrected, experimental temperature rise as a function of time, from a linear fit in ln t, for a measurement in water at T=302.65 K, P=102.7MPa.



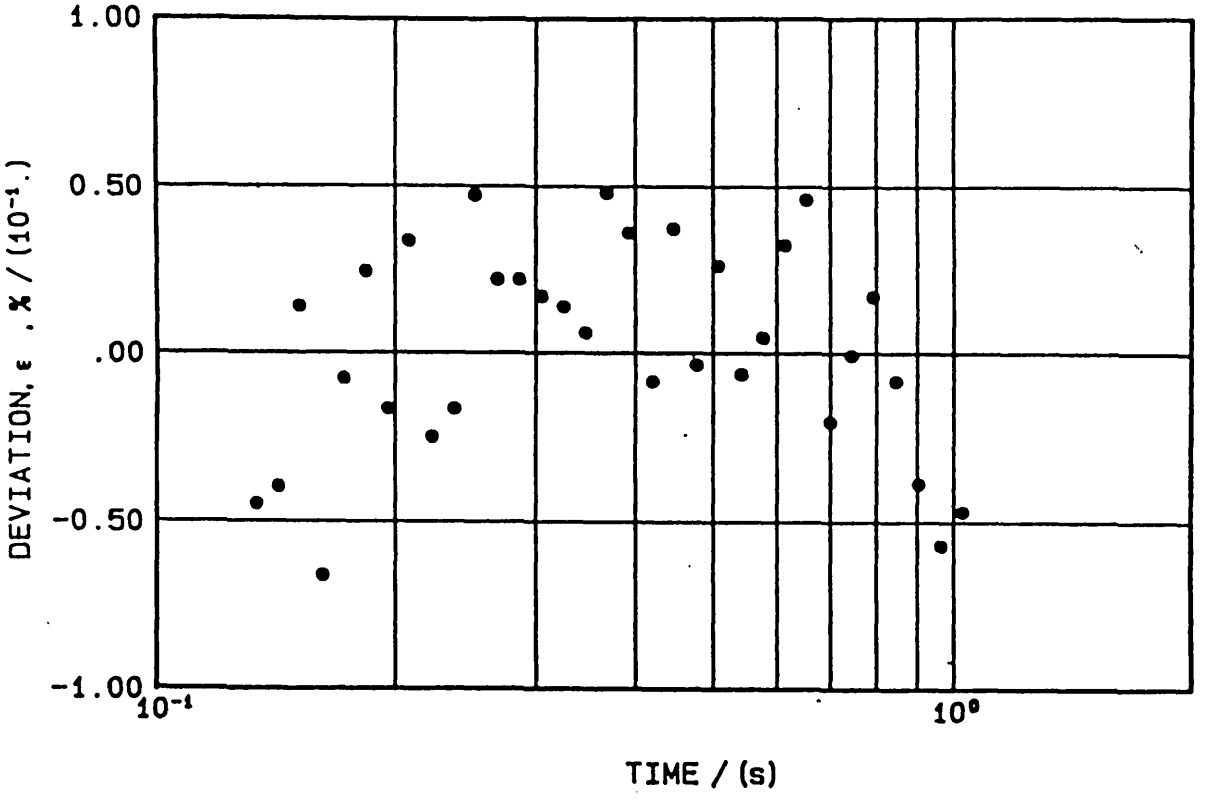


Fig. 4.ix. Deviations of the experimentally measured temperature rise of the tantalum wire from a linear fit vs ℓn t for a run in water at a temperature of 298 K and a pressure of 0.1 MPa.
$\epsilon = [(\Delta T_{exp} - \Delta T_{fit})/\Delta T_{fit}] \times 100$

4.4.2 Comparison With Other Data.

The International Association for the Properties of Steam have prepared a correlation of the thermal conductivity of water substance for scientific use. The correlating equation has the form [100,101] :

$$\lambda = \lambda_o \exp\left\{ \frac{\rho}{\rho^*} \sum_{i=0}^{4} \sum_{j=0}^{5} b_{ij} \left[\frac{T^*}{T} - 1 \right]^i \left[\frac{\rho}{\rho^*} - 1 \right]^j \right\} + \Delta\lambda \qquad (4.3)$$

where

$$\lambda_o = \left[\frac{T}{T^*} \right]^{1/2} \left[\sum_{k=0}^{3} a_k \left[\frac{T^*}{T} \right]^k \right]^{-1} , \qquad (4.4)$$

$$\Delta\lambda = \frac{C}{\mu} \left[\frac{T\rho^*}{T^*\rho} \right]^2 \left[\frac{\partial(P/P^*)}{\partial(T/T^*)} \right]_\rho^2 \aleph_T^\omega \left[\frac{\rho}{\rho^*} \right]^{1/2}$$

$$\exp\left\{ - A \left[\frac{T}{T^*} - 1 \right]^2 - B \left[\frac{\rho}{\rho^*} - 1 \right]^4 \right\} \qquad (4.5)$$

Numerical values of the constants

$T^* = 647.27$ K

$\rho^* = 317.763$ kg/m^3

$P^* = 22.115$ MPa

$C = 3.7711 \times 10^{-8}$ W Pa s/K m

$\omega = 0.4678$

$A = 18.66$

$B = 1.00$

Here,

λ denotes the thermal conductivity ($W\ m^{-1}K^{-1}$),

ρ denotes the density,

T denotes the absolute temperature on the 1968 Practical Temperature Scale,

P denotes the pressure,

μ denotes the dynamic viscosity as defined in the I.A.P.S. Release on the International Representation of Dynamic Viscosity of Water Substance, 1975, as amended in 1982 (Pa.s),

$$\kappa_T = \left[\frac{\rho}{\rho^*} \right] \left[\frac{\partial(\rho/\rho^*)}{\partial(P/P^*)} \right]_T \qquad (4.6)$$

is the reduced isothermal compressibility, T^*, P^*, and ρ^* denote numerical constants which are close to, but do not represent the corresponding critical constants. C, ω, A, B, a_k, b_{ij} are numerical constants listed above.

In figure 4.x, this correlation is used as the basis for a comparison with the results of the present work, as well as a selection of the most accurate earlier measurements covering the same range of conditions as we have studied here. In this region of states, the I.A.P.S. correlation has an estimated uncertainty of ±1.5-2.5%, and it can be seen that the present data lie within this band. For the lower isotherm at 302.65K, the present data are systematically approximately 0.4% below the correlation. At a temperature of 324.15K, the data are distributed about the correlation. In neither case does the deviation exceed ±0.7% while the standard deviation over the entire set of data is ±0.3%.

The I.A.P.S. formulation [100,101] therefore provides a reasonable representation of the present data, although the latter are more accurate. Other measurements are in progress to extend the ranges of temperature and pressure of the present measurements, which should eventually allow the improvement of the international correlation.

It should be noted that the accuracy claimed for the present measurements is superior to that associated with any earlier measurements, or indeed the I.A.P.S. correlation itself.

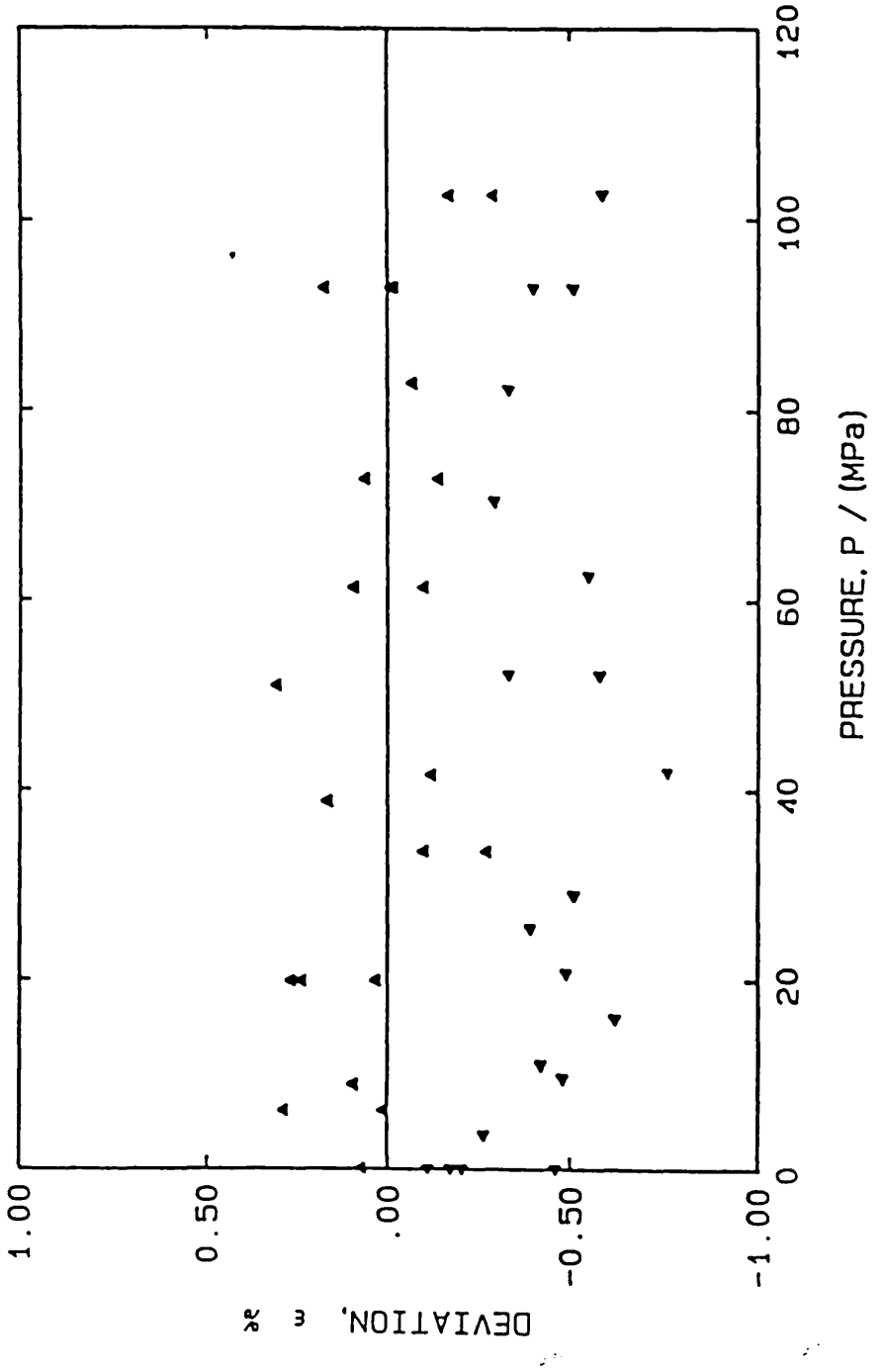


Figure 4.x. Deviations of the present experimental data for the thermal conductivity of water from the IAPS correlation.

◀ : 302.65 K; ▲ : 324.15 K.

Chapter 5.

TRANSPORT THEORY IN LIQUIDS

5.1 Introduction.

A substantial effort has been expended into the accurate measurement of the transport properties of fluids [102,103]. The reasons are two-fold; first, the industrial need for accurate data of the transport properties, which is geared to efficient running and optimizing manufacturing processses [104], and equally as important, the fundamental molecular information that can be gained from such high quality measurements [105,106].

Reliable predictions of the transport of dense and/or polyatomic fluids cannot be made ab initio for a number of reasons. First, there is no solution of a suitably generalised Boltzmann equation [107-111], nor are the necessary intermolecular potentials, either pair and many-body known. It is true that there exists a formal statistical mechanical theory for the transport coefficients, but its application for use to calculate physical properties for real fluids, has only been accomplished by obtaining approximations based on uncertain physical assumptions. In addition to that, transport coefficients calculations of simple fluids based on these approximations do not yield results with the desired accuracy and are frequently in poor agreement with experimental data. In such circumstances, it is necessary to use the approximate theories carefully, as a guide to the development of

prediction methods, and not as the prediction methods themselves. Among the most successful of the approximate theories is known as the Van der Waals model. It is to the application of this theory to the present experimental data and to the development of a refined prediction method for the transport properties, namely, the thermal conductivity of dense polyatomic systems that the present chapter is devoted.

5.2 Summary of Available Methods for the Calculation of Thermophysical Properties.

At this point, it is desirable to consider briefly the methods that have been used to evaluate certain thermophysical properties, such as transport phenomena, which includes thermal conductivity, thermal diffusion and viscosity. A number of moderately successful theories and models were postulated to describe transport phenomena, but each of these models had serious deficiencies ascribed to them. They could not adequately represent the entire thermodynamic ranges of density or temperature required, and most importantly, these theories could not fully support one another, thereby contradicting some aspects of the predicted properties and evaluations of the calculated results. The following sections are devoted to brief descriptions of these models, and then lead to the more concise theories of the smooth hard-sphere and the rough hard-sphere models.

5.2.1 The Monte-Carlo Method.

In this method, the configurational thermodynamic properties of a

model are calculated by the method of statistical mechanics. The model comprises a specification of the intermolecular potential for the fluids and their masses. The particular form of the Monte-Carlo method used in liquid state physics, is that devised by Metropolis et.al [112,113].

The Monte-Carlo method consists in generating a set of molecular configurations of the N particles in the model. A configuration N_j is accepted or rejected according to a criterion which ensures that in the limit of an infinite number of transition, a given configuration occurs with a probability proportional to the Boltzmann factor, $\exp(-\Phi_N/kT)$ for that configuration.

A criterion is required for the acceptability of the new configurations, such that they develop with the correct Boltzmann weighting: when the thermodynamic and configurational characteristics of the assembly may be determined as actual canonical averages in the true statistical mechanical state:

$$\langle f \rangle = \int f(x)P(x)dx / \int P(x)d(x) \qquad (5.1)$$

The thermodynamic average, $\langle f \rangle$ is thus determined as a weighted phase average where P(x) is the weighting function. A commonly used prescription for the acceptability of a trial configuration is the following: a particle of the system is selected, either serially or at random, and given a random displacement from state i to state j. The increase in the total configurational energy is then assumed to be

$\Delta\phi_N^{ij}$, then if $\Delta\phi_N^{ij}$ is negative, the move is accepted and the new configuration replaces the old one - the new configuration is evidently more probable than the former one. If $\Delta\phi_N^{ij}$ is positive, the move is accepted only with the probability that $P_{ij}=\exp(-\Delta\phi_N^{ij}/kT)$, the machine then selects a random decimal number in the range 0 to 1 and compares it to $\exp(-\Delta\phi_N^{ij}/kT)$. If the exponential is the greater, the move is allowed, otherwise the move is rejected. If a move is rejected, the previous configuration is counted again. The distribution in the configuration space develops as the Boltzmann factor $\exp(-\phi_N/kT)$. The overall chain average of any function therefore converges to the canonical ensemble as the number of steps in the chain approaches infinity. This technique cannot be used for the transport properties, because they involve a time dependence for the system.

5.2.2 The Molecular Dynamics Method.

Molecular dynamics simulation has proved to be extremely effective in predicting the physical properties of systems ranging from simple liquids and plasmas to systems governed by more complex potentials such as liquid metals and gases. A number of investigators have studied the dynamics of particles interacting through hard sphere (short range) potentials [114-122]. Such systems are easy to analyse, because the particles stream freely between collisions. The time evolution can be treated as a sequence of binary, elastic collision events. The essential idea is to integrate the equations of motion characterising the particles as they interact, moving about in an arbitrary cell of a fixed volume. In this method, the Classical Newtonian equation of motion of an assembly of particles are solved numerically and

integrated to yield the evolution of the configurational and velocity distributions. The particles are released from an arbitrary (non-overlapping) configuration within the fundamental cell, either from rest or with a random distibution of velocities. The system evolves rapidly, attaining a Maxwellian velocity distribution after about six collisions per particle in the case of hard-spheres, in which the energy of the assembly is purely kinetic - rather more for realistic interactions in which configurational adjustment must accompany the potential-kinetic energy exchange in attaining the equilibrium velocity distribution.

The position and velocity coordinates are stored as a function of time, and after the transient effects of the initial starting configuration have died out, the data may be analysed for the microstructure of the assembly. The net force on an atom i may be determined classically by taking the vector sum over the neighbouring particles:

$$-\sum_{j}^{N-1} \nabla\phi(ij) \qquad (5.2)$$

presupposing a knowledge of the distribution of atomic centres and the interaction potentials $\phi(ij)$. If the configurational and momentum coordinates of each atom at some time t are stored, then the classical trajectory of atom i over a period of time Δt may be determined by solution of the Newtonian equation as a sequence of discrete linear steps. The new position coordinate in the absence of any external fields will be:

$$q_i(t+\Delta t) = v_i(t)\Delta t - \frac{1}{2m_i}\sum_{j}^{N-1} v\phi(ij)(\Delta t)^2 + q_i(t) \qquad (5.3)$$

whilst the new velocity coordinate will be:

$$v_i(t+\Delta t) = v_i(t) - \frac{1}{m_i}\sum_{j}^{N-1} v\phi(ij)(\Delta t) \qquad (5.4)$$

Short life-time vibratory modes are interdispersed with diffusive motions, and the phonon spectrum of a liquid shows these two components quite clearly. The simulation proceeds sequentially determining the net force trajectory of each of the N particles in the assembly, and the system executes an implicitly pairwise evolution.

The second general application of the molecular dynamics method is the simulation of assemblies of molecules, interacting with somewhat over-simplified forms of potential energy function, in order to establish a sound physical basis for the development of a successful theory of transport properties in dense fluids. For example, the computations of Alder and Einwohner [118,119], on the free path distribution for hard-spheres, which interact according to :

$$U(r) = 0 \quad r > \sigma$$

$$U(r) = \infty \quad r \leq \sigma$$

and square-well molecules, for which the interaction potential is:

$$U(r) = 0 \quad r \geq R\sigma$$

$$U(r) = -\epsilon \quad \sigma < r < R\sigma$$

$$U(r) = \infty \quad r \leq \sigma$$

showed that molecular motion proceeds by a succession of small diffusive steps, and not by relatively small number of jumps, whose length is approximately equal to the intermolecular spacing, as is implicit in the model of Eyring [123]. Furthermore, they showed [118,119] that the Brownian motion approximation, which postulates that the molecules undergo many collisions involving the attractive part of the potential, between successive repulsive interactions, and which was used by Rice et.al.[124], as a basis for a theory of transport properties, is unsatisfactory even at high pressure and low temperature.

Such simulations have been performed for systems characterised by a variety of short range interaction potentials, including the Lennard-Jones potential and exponential repulsive potentials. The simulation of systems interacting by way of long range forces-particularly Coulomb forces-is a bit more difficult, since a very large number of particles may interact (10^5 to 10^6) to produce "self-consistent" fields that act on the particles [125].

The conflicting interests of computational expediency, and significance of the calculated result, restrict the time graining

$\Delta t \approx 10^{-14}$ seconds. If coarser time graining is used, overlapping configurations of atoms will develop, and the particles will subsequently separate with infinite or near-infinite velocities, depending upon the details of the repulsive core of the interaction potential.

5.2.3 Comparison of Molecular Dynamics Simulations and the Monte Carlo Methods.

Many of the essential limitations of the computer schemes discussed earlier, apply to both the principal simulation methods. The restriction to small, finite assemblies (N = 100 to 1000) is inevitable in both procedures and periodic boundary conditions are introduced to eliminate surface effects. In neither case is pairwise additivity of the potential function an essential restriction; although it is generally employed because of the great simplification that ensues.

The great advantage of the Molecular Dynamics approach lies in its ability to deal with non-equilibrium and transport phenomena, provided the relaxation time for the process is significantly smaller than the computation time. Since the maximum temporal extent for which a dynamic event can be followed is 10^{-11}s, the process is therefore limited to microscopic non-hydrodynamic events.

The equivalence of the asymptotic results of the Monte Carlo configurational averages for the thermodynamic quantities, and molecular dynamics results obtained as time averages over phase-space trajectories depends essentially on the passage to the asymptotic limit $N \to \infty$, $V \to \infty$, $N/V \to$ constant. The two methods should produce results in agreement to order N^{-1} , and one would generally expect agreement of the two approaches within statistical error.

One particular advantage of the Monte Carlo method is that it may be relatively easily extended to quantum-mechanical system, in which the exchange symmetry of the single-particle wavefunction must be preserved. Neither these models are easily applied to calculations involving real fluids, because the pair-potential in not known.

5.2.4 The Brownian Motion Theory.

The classical theory of Brownian motion as developed by Einstein in 1905 [126], can provide the basis for a theory of transport in fluids, with an application to dense fluids, in which the particles interact through realistic intermolecular potential. The configurational diffusion of particles in a fluid, may be interpreted at a macroscopic or a microscopic level.

The approach to equilibrium is regarded as a relaxation of a concentration gradient, c, with time, or alternatively, the individual particles may be imagined to execute random trajectories (Brownian

motion), until they have spread uniformly throughout the accessible volume.

In the macroscopic case, the evolution is determined by the diffusion equation:

$$\frac{\partial c}{\partial t} = Dv^2c = D\left\{ \frac{\partial^2 c}{\partial x^2} + \frac{\partial^2 c}{\partial y^2} + \frac{\partial^2 c}{\partial^2 z} \right\} \qquad (5.5)$$

where D is the coefficient of self-diffusion and it is straight-forward to show that $D=kt/\beta_{(1)}$. The result is important, first, in that it describes an irreversible configurational evolution towards equilibrium in the fluctuating soft force field, and second, that the diffusion equation can usually be readily solved for given initial and boundary conditions, to yield the concentration as a function of the coordinates and the time. The natural extension of this equation is towards the molecular interpretation.

Smoluchowski showed that the corresponding generalization of Brownian motion in an external field X, with c replaced by $n_{(1)}$, the simple particle distribution function, is:

$$\partial n_{(1)}/\partial t = \text{div} \left\{ \frac{kT}{\beta_{(1)}} \text{ grad } n_{(1)} - \frac{X}{\beta_{(1)}} n_{(1)} \right\} \qquad (5.6)$$

in vector notation. This is the Smoluchowski equation.

(Setting X=0, the right hand-side becomes (kT/α)div grad $n_1=(kT/\alpha)\nabla^2 n_1$, which with $D = (kT/\alpha)$, reduces to the original diffusion equation). Clearly, equilibrium is characterized by the absence of generalized fluxes in the system:

$$\partial n_{(1)}/\partial t = \text{div} \left\{ \frac{kT}{\beta_{(1)}} \text{grad } n_{(1)} - \frac{X}{\beta_{(1)}} n_{(1)} \right\} = 0 \qquad (5.7)$$

There is one important modification which has to be made to this treatment, before it can be used to describe the configurational evolution in a dense fluid. As it has been described thus far, the Brownian particles are regarded as being independent, as in a dilute gas, so that all the structural information is continued in the single-particle distribution $n_{(1)}$. In a dense fluid assembly, it is known that there are well-developed spatial correlations, and the evolution of the hierachy of higher-order distributions need to be known. In a better approximation, the evolution of the two-particle function $n_{(2)}$ needs to be known.

The necessary modifications of equation (5.6) have been made by Kirkwood and Eisenschitz [127]. The representative pair of molecules are now considered as the Brownian particle moving in the fluctuating soft force field of the remaining (n-2) particles. The irreversible progress towards equilibrium is now expressed in terms of a two-body friction constant $\beta_{(2)}$, given by the force autocorrelation acting on the representative pair:

$$\beta_{(2)} = \frac{1}{3mkT} \int_0^T \langle F_{(2)}(0).F_{(2)}.(t) \rangle_{(N-2)} dt \qquad (5.8)$$

The upper limit is set at τ rather than infinity to avoid difficulties, and irreversibility is ensured by time smoothing over the period of decay of the force autocorrelation, τ. The remaining question is the evaluation of $\beta_{(2)}$. Assuming $\beta_{(2)}$ is large enough, the configurational projection of the two-body Fokker-Planck equation, sometimes called the Kramers-Chandrasekhar equation, [128] is regained:

$$\frac{\partial n_{(2)}}{\partial t} = \text{div} \left\{ \frac{kT}{\beta_{(2)}} \text{grad } n_{(2)} - \left[- \frac{\text{grad } \psi}{\beta_{(2)}} \right] n_{(2)} \right\} \qquad (5.9)$$

which is the two-body Smoluchowski equation. Instead of the external force acting on a Brownian particle, the mean relative force of one molecule on the other is then obtained, -grad $\psi_{(12)}$, where $\psi_{(12)}$ is the potential of the mean force.

To apply the theory to viscosity, the bulk velocity vector C is given an appropriate form for the steady laminar flow, where the velocity gradient can be chosen to be small, since the liquid is assumed to be Newtonian. As the flow is steady, i.e., not time-dependent, the slightly distorted radial distribution function is also independent of time, and the left hand-side of equation (5.9) diminishes. The small perturbation of the equilibrium distribution can be solved and inserted in equation (5.9). On expressing the operators

in spherical planar coordinates, the angular functions can be cancelled throughout. The outcome was evaluated by Kirkwood and Eisenschitz [127], and its solution furnished a value for the viscosity, provided the numerical value of the friction constant was known.

At equilibrium, $\partial n_{(2)}/\partial t = 0$, and the generalized current:

$$J_{(2)} = \text{div} \left\{ \frac{kT}{\beta_{(2)}} \text{grad } n_{(2)} - \left[- \frac{\text{grad } \psi}{\beta_{(2)}} \right] n_{(2)} \right\} \tag{5.10}$$

is zero; i.e.

$$\frac{kT}{\beta_{(2)}} \text{grad } n_{(2)} = - n_{(2)} \frac{\text{grad } \psi}{\beta_{(2)}} \tag{5.11}$$

which follows directly from the definition of the potential mean force, $n_{(2)} = \exp(-\psi/kT)$.

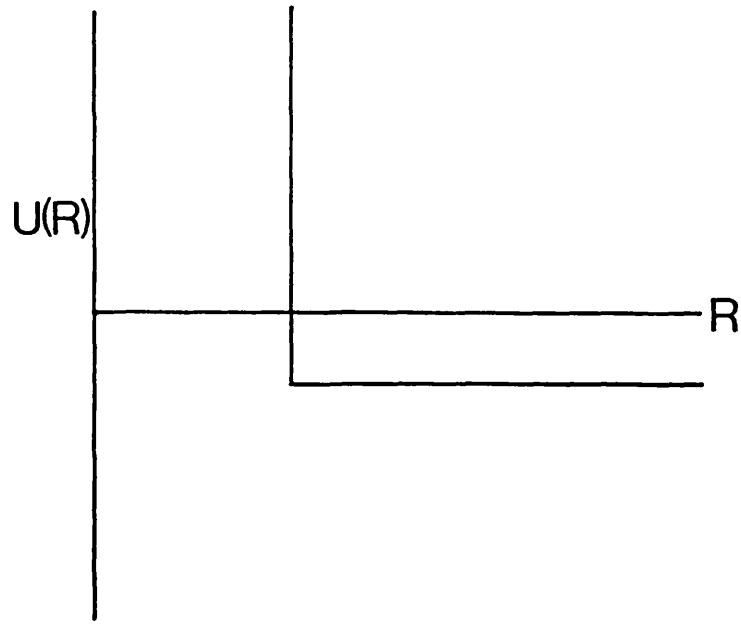
5.3 Van der Waals Model.

5.3.1 Smooth Hard Sphere Theory.

The Van der Waals model replaces the rigorous view of a dense fluid as an assembly of molecules each interacting with the others through an intermolecular pair potential with separation dependent repulsive and attractive regions. Figure 5.i(a) depicts the simple model which assumes that an assembly of molecules possess a weak

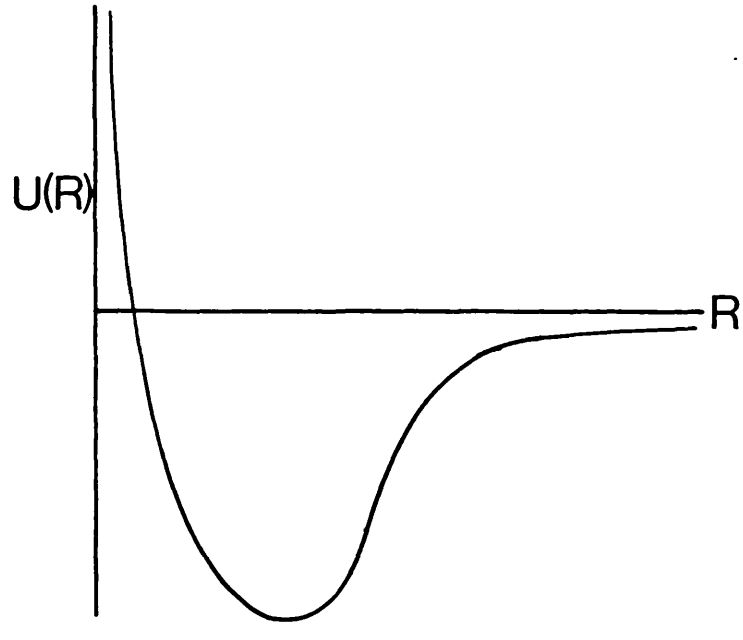
long-range attractive energy and a hard-core repulsive energy. For real systems, the dependence of the pair interaction potential energy on molecular separation is shown in Figure 5.i(b). The molecules are there seen to interact with a hard-core (infinitely steep) repulsion at a fixed distance, and to move otherwise, in a uniform attractive field. This means that the dynamics of molecules comprise hard-core interactions, between which the molecules move in straight lines. The model is expected to be most applicable at high temperatures, when the real repulsive forces dominate collisions, and at elevated densities when the view of uniform attractive potential is most realistic. Thus, the Van der Waals model, at sufficiently high densities and temperatures, becomes equivalent to the hard-sphere model. Significant progress towards a successful molecular theory of transport properties of dense fluids has been made as a result of computer simulation studies by the molecular dynamics method [118,119]. These studies clearly indicate that this description of molecular motion based on the Van der Waals model is physically much more realistic for real fluids than descriptions based upon the activation energy model [123,129], or the Brownian motion approach [124,130].

For real systems, the potential does have a steep repulsive part and the range of attractive force can be considered large relative to the interparticle spacing at densities greater than the critical density. Furthermore, the attractive potential energy can be considered weak relative to the kinetic energy whenever the temperature is greater than the well depth or, roughly, the critical temperature. As a result, for densities and temperature greater than critical, real systems are found [131] to obey the Van der Waals equation of state, provided that



(a) Van der Waal's Model.

Figure 5.i(a): Van der Waals model.



(b) Realistic Pair Potential.

Figure 5.i(b): Realistic Pair Potential Function.

the core size is allowed to diminish as the temperature increases, a consequence of the relatively soft repulsive energy of real molecular systems.

An extremely important consequence of the Van der Waals theory for the transport properties is that the particles move in straight lines before core collisions, because the attractive potential forms a uniform surface. This so-called "free-flight" approximation is in direct opposition to the Brownian motion approximation, which postulates that there are many collisions involving the attractive part of the potential (soft-collision), between hard-core collisions.

The effect of Brownian motion would be to break the velocity correlation between successive core collisions of a particle. So far as transport properties are concerned, one important difference between the Brownian motion and the hard-sphere models is that the former prohibits correlations of the velocity of a molecule beyond a simple collision, whereas the latter allows them. Because molecular dynamics does indicate that relatively long time velocity correlations exist, the hard-sphere theory is to be preferred. However, significant velocity correlations do not persist for more than three or four collisions even in pure hard-sphere systems [132], and so the numerical consequences of the Brownian approximation may not be great. On the other hand, the opposite model of a straight-line path for a particle between hard-core collisions is approximate, because non-uniformities in the potential surface cause the linear trajectory to be diverted. In so far, as these deviations caused by soft collisions are small, they

can be treated by perturbation theory [133], and the Van der Waals theory is a good approximation. The real situation clearly lies somewhere between these two extreme approximations. At high temperatures and densities, the Van der Waals model is more realistic. However, it does not follow that the Brownian motion concept is the better approximation at low temperatures and high densities. Molecular dynamics simulations of the number of soft and hard collisions for a realistic potential showed, that they were compatible in number in the region of ordinary liquid conditions, indicating that the Van der Waals model is still the better concept or approximation.

The Van der Waals theory can be said to give the better approximation for transport properties whenever it can explain the equilibrium properties satisfactorily. Before stating this fact, two effects have to mentioned. The first one concerns the magnitude of the effect on a given property of a non-uniformity in the potential surface. It is conceivable that the transport properties are much more sensitive to these non-unifomities than are equilibrium properties. After all, a small change in a trajectory can alter the whole subsequent history of the system. This can be analytically investigated by perturbation theory. The second factor concerns the quantitative failure of the Van der Waals theory under ordinary liquid conditions, not because of any conceptual failure of the Van der Waals model, but because of a cancellation of terms which make the pressure respond more sensitively to the higher-order deviations from the Van der Waals theory. For the transport coefficients in the liquid phase, such a cancellation does not occur, hence the first-order perturbation theory from the van der Waals approximation is likely to provide reasonably good results.

In the treatment that follows, the perturbation is neglected, and only the hard-sphere contribution is treated in order to estimate over what region of temperature and density the transport coefficients are insensitive to deviations from linear trajectories. For this purpose, it is first necessary to establish under what conditions the equation of state can be adequately described by the Van der Waals equation. From this analysis, an effective hard-sphere diameter is obtained, which must be independent of density, but can depend in a reasonable way on temperature.

In addition to the restriction of the validity of the Van der Waals model to high temperatures and densities, another constraint is to be considered, which is the fact that a hard-sphere fluid exhibits a solid-like transition at densities where the molar volume is less than $1.5V_o$, where V_o is the volume of close packing of the hard spheres. Despite these limitations, it has been found empirically that correlations based on this model, may be reliably extended to higher densities and lower temperatures within the liquid phase. The perturbation theory has been usefully employed [133] to extend the van der Waals model to even lower densities, so that the increasing influence of attractive forces could be accounted for.

Enskog has derived a kinetic theory for transport in a dense hard-sphere fluid [134], and this version was complimentary to the Van

der Waals model. In the Enskog theory, modifications to the Boltzmann theory were made to provide a first approximation to the behaviour of dense systems. The mechanism for the transport of momentum across a plane occurs via the movement of the molecules themselves across a reference plane. If density or temperature is raised, a molecule will then transfer its momentum across the plane to another neighbouring molecule, but without moving across the plane. This is referred to as the collisional transfer of flux. In a dense system, the collision rate is higher than in a dilute system, because the inter-particle distance becomes significant compared to the diameter of the molecules. The Enskog theory of diffusion [134] assumes that the high density system behaves exactly as a low density system, except that the collision frequency is increased by a factor of $g(\sigma)$, where $g(\sigma)$ is the radial distribution function of contact for hard spheres of diameter σ, and the difference in position between the two colliding molecules is no longer neglected. The solution of the Boltzmann equation valid at low density is merely scaled in time to give the ratio of the diffusion coefficient D_E at high number density n relative to that at low density, subscript zero:

$$nD_E/n_oD_o = 1/g(\sigma) \qquad (5.12)$$

where $g(\sigma)$ is obtained from computer simulation studies, and is given by the Carnahan-Starling equation [135]

$$g(\sigma) = (1-0.5\zeta) / (1-\zeta)^3 \qquad (5.13)$$

where $\zeta = b/4V$ for a molar volume V, and

$$b = 2\pi N\sigma^3/3 = \frac{3}{2}\pi\sqrt{2}V_o \qquad (5.14)$$

D_o is related to the number density n_o at temperature T by the expression:

$$D_o = \left(\frac{3}{8} n_o \pi\sigma^2 \right)(\pi kT/m)^{0.5} \qquad (5.15)$$

where m is the molecular mass, and k is the Boltzmann constant, and

$$V_o = N_A\sigma^3/\sqrt{2} \qquad (5.16)$$

For diffusion, the particles themselves must move, but for viscosity and thermal conductivity, there is the additional mechanism of collisional transfer whereby momentum and energy can be passed to another molecule upon collision. The Enskog theory for the viscosity η_E and the thermal conductivity λ_E , in terms of the low density coefficients accordingly contains additional terms:

$$\eta_E/\eta_o = \left[\frac{1}{g(\sigma)} + 0.800\frac{b}{V} + 0.761g(\sigma)\left(\frac{b}{V}\right)^2 \right] \qquad (5.17)$$

$$\lambda_E/\lambda_o = \left[\frac{1}{g(\sigma)} + 1.200\frac{b}{V} + 0.755g(\sigma)\left(\frac{b}{V}\right)^2 \right] \qquad (5.18)$$

where the low density coefficients are given to first order approximation by:

$$\eta_o = \left(\frac{5}{16} \pi\sigma^2 \right)(\pi mkT)^{0.5} \qquad (5.19)$$

$$\lambda_o = \left(\frac{25C_v}{32} \pi\sigma^2 \right)(\pi kT/m)^{0.5} \qquad (5.20)$$

where C_v is the molar heat capacity at constant volume.

In order to apply equations (5.12), (5.17) and (5.18), for the calculation of dense fluid transport coefficients, it is necessary to assign a value to the core size. In the original application of this method [136], values for σ for the rare gases were obtained by fitting pVT data to the Van der Waals equation of state, and $g(\sigma)$ was taken from results of computer simulation for hard spheres [135]. It was found that the calculated high density transport coefficients differed by less than ten percent from the experimental values.

Now the Enskog theory is based on the molecular chaos approximation, and neglects all correlations of molecular velocities in the evaluation of the transport coefficients. A sphere is considered as always colliding with other spheres approaching from random directions, with random velocities from a Maxwell-Boltzmann distribution for the appropriate temperature. However, molecular dynamics calculations [137,138] have shown that there are correlated molecular motions in hard-sphere systems. These corrections may be ascribed to in the form of ratios of the exact hard sphere results (subscript MD) to the Enskog results, (subscript E), so that:

$$\frac{nD}{(nD)^o} = \left[\frac{D_E}{D^o}\right]\left[\frac{D_{MD}}{D_E}\right] \tag{5.21}$$

$$\frac{\eta}{\eta_E} = \left[\frac{\eta_E}{\eta^o}\right]\left[\frac{\eta_{MD}}{\eta_E}\right] \tag{5.22}$$

and

$$\frac{\lambda}{\lambda^o} = \left[\frac{\lambda_E}{\lambda^o}\right]\left[\frac{\lambda_{MD}}{\lambda_E}\right] \tag{5.23}$$

where the superscript ^{o} indicates the low density results.

At high densities, the principal correlation effect is back-scattering, whereby a sphere closely surrounded by a shell of surrounding spheres, is most likely to have its velocity reversed on collision with its neighbours, and this leads to a decreased diffusion coefficient. At intermediate densities, there is a different correlation effect associated with an unexpected persistence of velocities, which leads to an enhanced diffusion coefficient. The resulting corrections to the Enskog transport coefficients have been computed by Alder [120] and correlated as functions of molar volume by Dymond [139] for systems of 108 and 500 particles, with the diffusion coefficients extrapolated to infinite systems on the basis of hydrodynamic theory.

For V_o/V up to 0.5, corresponding to dense gases at densities up

to 2.5 the critical density, the corrections to the Enskog theory for the viscosity and thermal conductivity coefficients are less than 10%, but for diffusion, the corrected coefficient is significantly greater than the Enskog value at densities corresponding to 1.5 to 2 times the critical density. At the highest densities, approaching the onset of solidification, the corrections arising from back-scattering result in the exact hard sphere diffusion coefficient being lower by about 40%, and the viscosity coefficient being higher by a similar amount. To obtain exact expressions for the dense hard-sphere transport coefficients in terms of the low density coefficients, equations (5.12), (5.17) and (5.18) must be multiplied by an appropriate correction factor at the given reduced volume. With core sizes determined from equilibrium data by extrapolation to infinite temperatures, quantitative evidence for the existence of these correlated motions in real systems was obtained of self-diffusion coefficients of methane [140] and of carbon dioxide [141].

5.4 Applications of Exact Hard Sphere Expressions.

5.4.1 Introduction.

Dymond [102] has discussed a number of ways of applying the corrected Enskog theory, to the evaluation and correlation of the transport properties of dense fluids. The following section will outline these methods for the smooth hard-sphere fluids.

5.4.2 Self-Diffusion.

The determination of the core size from equilibrium data [102], was not satisfactory, and different methods were proposed [142] for comparing calculated and experimental transport coefficients, without a prior estimation of core size. A quantity D^* which is independent of molecular diameter was defined as:

$$D^* = (nD/n_oD_o)(V/V_o)^{2/3} \qquad (5.24)$$

D^* can be calculated from theory by expressing:

$$D^* = (\frac{1}{g(\sigma)})(D/D_E)(V/V_o)^{2/3} = f(V/V_o) \qquad (5.25)$$

where (D/D_E) is the computed correction to the Enskog theory. D^* can also be calculated from experimental data on the assumption that the real fluid exhibits a behaviour like an assembly of hard spheres, since on substitution for hard-spheres expressions for n_oD_o and V_o leads to:

$$D^* = F_D(V/V_o) = 5.030x10^8(M/RT)^{1/2} D/V^{1/3} \qquad (5.26)$$

from equation (5.25), D^* is a function of (V/V_o); from equation (5.26), D^* is a function of V for a given substance at a given temperature. To test whether this smooth hard-sphere theory can adequately account for the density dependence of the experimental measurements at a given temperature, D^* from theory, equation (5.25), is plotted against the logarithm of (V/V_o), and D^* from experiment, equation (5.26) is plotted against the logarithm of (V). If these curves are superimposable laterally, then the hard-sphere theory does represent the density

dependence of the data, and the range of applicability of the theory can be established. Furthermore, V_o can be obtained from points where the curves coincide.

In the absence of extensive accurate diffusion coefficient measurements for rare gases, accurate methane data [142,143] obtained using nuclear magnetic resonance spin-echo technique have been used [102,142,143,144,145] to test the applicability of the smooth hard sphere theory. It was assumed initially, and subsequently confirmed, that methane is a polyatomic molecule to which the rough-hard sphere model applies, but with a minor correction necessary. It was shown that the experimental points at these temperatures from 1.7 times the critical temperature T, down to 1.2T, lie within 5% of the smooth hard-sphere values down to densities about 0.8 times the critical density. A subsequent experimental study was proposed by Harris and Trappeniers [144] on methane at 110, 140 and 160K. They found the reduced diffusivity D^* isotherms fell on a common curve when plotted against reduced density n^* $(=n\sigma^3)$, in agreement with the smooth hard sphere predictions, except at the highest densities ($n^* > 0.86$), where the experimental values are significantly higher. A similar conclusion was reached by analysis of the self-diffusion data for ethene obtained by Arends, Prins and Trappeniers [146].

The discrepancy at high density cast some doubt on the validity of the model. However, a recent molecular dynamics study by Easteal, Woolf and Jolly [147] of the self-diffusion coefficient in a hard-sphere system, concluded that although the computed corrections to the Enskog

theory were dependent on the number of molecules considered in the calculations, the number dependence was significantly lower than that previously reported by Alder, Gass and Wainwright [120]. By taking small increments in density, the dependence of (D/D_E) on reduced density was obtained, and their results were compared with previous computations.

The result is given by the following equation, where the coefficients have been rounded off to give significant figures only:

$$D/D_E = 0.7144 + 2.878\xi - 0.8223\xi^2 - 10.93\xi^3 \qquad (5.27)$$

Using this correction to the Enskog theory, Easteal, Woolf and Jolly [147] found that D for methane obtained from experiment was in good agreement with the smooth hard sphere predictions over the whole density range.

The smooth hard-sphere model has been used [148] as a basis for the calculation of rare gas self-diffusion coefficients. Core sizes were derived from densities at freezing temperatures close to the triple point. The calculated values generally agree with the experimental results to within the large experimental uncertainties of the measurements, and in fact provide a more reliable estimate of this property for these substances.

5.4.3 Viscosity for Monatomic Fluids at Supercritical Temperatures.

Analysis of dense gas viscosity coefficient data on the basis of the hard-sphere model can be carried out in an analogous manner to the analysis of diffusion coefficient data described earlier. A quantity η^* is defined by:

$$\eta^*_{SHS} = F_\eta(V/V_o) = (\eta/\eta_E)(\eta_E/n_o)(V/V_o)^{2/3} \qquad (5.28)$$

where η_E is the Enskog dense gas value, (η/η_E) is the computed correction [120] to the Enskog theory, and (η_E/η_o) is given by equation (5.17). Values of η^* can be obtained from experimental data by substitution of the hard-sphere expression to give:

$$\eta^* = (16/5)(2N_A)^{1/3}(\pi/MRT)^{1/2}\eta V^{2/3} =$$

$$6.035\times10^{8}\eta V^{2/3}/(MRT)^{1/2} \qquad (5.29)$$

The range of applicability of this model is tested by superimposing curves of η^* against $\log(V/V_o)$ from theory, equation (5.28), and η^* versus $\log(V)$ from experiment, equation (5.29). Using extensive measurements at the above critical densities for neon [149], argon [150,151,152], krypton [151,153], and xenon [151], it was shown that the density dependence of the data above the critical temperatures was very satisfactorily represented by the hard-sphere theory at densities from above twice the critical density down to about 1.2 times the critical density. Although the computed corrections to the Enskog

theory are less well known than the corresponding corrections to the diffusion coefficient, nevertheless, it can be concluded that the smooth hard-sphere theory gives an adequate fit to the viscosity coefficient data at densities down to 1.2 times the critical density. Deviations obtained as a function of reduced density demonstrate that the fit is generally better than the uncertainties in the measured viscosity coefficients [149-153].

5.4.4 Thermal Conductivity Coefficients for Monatomic Gases at Supercritical Temperatures.

The applicabilty of the smooth hard-sphere theory for interpolation of thermal conductivity data has been conveniently tested by considering the function λ^* defined by:

$$\lambda^* = (\lambda/\lambda_E)(\lambda_E/\lambda_0)(V/V_0)^{2/3} \qquad (5.30)$$

where (λ/λ_E) gives the computed correction to the Enskog theory [118,119,134], (λ_E/λ_0) is the ratio of Enskog dense hard-sphere thermal conductivity coefficient to the dilute hard-sphere value, equation (5.18) and λ^* is core size independent.

Theoretical values of λ_{th} may be obtained from the molecular dynamics simulation results, and experimental values from equation (5.31):

$$\lambda^*_{exp} = \frac{64}{75}\left[\frac{\pi m}{k^3 T}\right]^{1/2} \frac{2^{1/3}}{N_A^{2/3}} .\lambda V^{2/3} \qquad (5.31)$$

so that whenever the Van der Waals model is applicable, i.e. dense monatomic fluids, it should be possible to superimpose plots of λ^*_{th} against $\log(V/V_o)$, and λ^*_{exp} against $\log(V)$.

The Van der Waals model for the transport properties of fluids incorporates a hard-sphere theory for dense fluids, with a temperature dependent core size, V_o, [102,139,154]. Its basis and application to liquids have been attempted with some success [139]. It has been shown recently, that the thermal conductivity of liquid argon and liquid methane can be adequately described by this model [58,155] to within $\pm$2%. The main result of the model results in a definition of a reduced thermal conductivity, λ^*. Substitution of the hard-sphere expressions [58,102] leads to the following relationship for a monatomic fluid, which behaves as an assembly of hard spheres:

$$\lambda^* = F_\lambda(V/V_o) = \lambda/\lambda_o(V/V_o)^{2/3}$$

$$= [1.02 + 0.1(x-0.3).\left[\frac{(1-0.7405x)^3}{(1-0.3702x)} + 3.554\ x\right.$$

$$\left. + 6.624\ x^2\left[\frac{(1-0.3702x)}{(1-0.7405x)^3}\right]\right] x^{-2/3}$$

where $x = V/V_o$, so:

$$\lambda^* = 1.610\times10^{8}\lambda V^{2/3}(M/R^3T)^{1/2} \qquad (5.32)$$

This theory can be treated using the extensive experimental measurements at high pressures and temperatures above the critical temperature for argon [156,157], and krypton [157], for which the values for the core sizes have been obtained by application of the rough hard-sphere theory to viscosity coefficient data. There are thus, no adjustable parameters, and λ^* from experiment, equation (5.32), can be compared directly with λ^* from theory, equation (5.30) by plotting versus $\log(V/V_0)$. At higher densities, the experimental results are lower than the hard-sphere predictions. This is unlikely to be due to errors in the computed corrections to the Enskog theory, since recent calculations for 108 particle system [158] agree closely with the earlier results [120], and the number dependence of the results would not account for this significant discrepancy. The difference may be due to uncertainties in the density at these high pressures.

New values for the thermal conductivity of liquid argon were presented [159] over a range of densities, 23 to 36 $mol.L^{-1}$. The precision of these results was $\pm$0.5% at the 2σ level, and the accuracy of the measurements was better than $\pm$1%. Earlier, a set of measurements was performed [58] and the agreement between the two sets of data was $\pm$0.5% at the 1σ level. The extrapolation of the later results to the saturated liquid line confirmed the earlier results to better than $\pm$0.5%, and those of the correlation scheme employed by the IUPAC [160], to better than 1%. The authors concluded that their experimental results in the range of 110K to 140K, did not conform to the hard-sphere theory.

A comparison of calculated thermal conductivities with experimental values at densities below 0.8 times the critical density, shows the predicted values to be lower, and this difference increases as the density is decreased. This is attributable to neglect of intermolecular attractions, which become significant at lower densities. These differences can be related [161] to the reduced temperature and the reduced volume.

There is an additional factor with regard to the thermal conductivity and that is the anomalous behaviour in the critical region. The smooth hard-sphere theory, modified to account for the effects of intermolecular attractions [161], is unable to reproduce this behaviour. It is worthwhile to note that deviations begin to occur at temperatures as high as $1.7T_c$ and this has been shown to be true in a recent accurate experimental study [162].

5.5 Rough Hard Sphere Model for Polyatomic Fluids.

5.5.1 Introduction.

Polyatomic fluids exhibit three major differences from monatomic ones. The most important being the physical shape of the molecules, in that they are invariably non-spherical in shape, and the second regards the fact that these molecules possess internal energy, due to their

structural nature. The third difference is attributed to the energy transfer by virtue of the coupling that occurs between the translational and rotational motions. These three phenomena could not be accounted for by the smooth hard-sphere theory. To overcome these difficulties, a different approach was necessary. The rough hard-sphere theory was therefore introduced, to complement the description of the transport properties of such fluids.

The rough hard-sphere model considers the molecules to be rigid spheres, each of diameter σ and mass m, possessing a moment of inertia I, associated with the spherically symmetric distribution of the aforesaid mass about the molecular center of gravity. Therefore, the molecules exhibit rotational degrees of freedom, and a collision between two rough hard spheres, is of zero duration. At the points of impact during collision, the relative velocity of the two spheres is completely reversed, and thus, one sphere can transfer linear and angular momentum to the impacted sphere.

The model accounts for the basic characteristics of a polyatomic fluid in a concise concept. The model is useful because the radial distribution function is the same as that for the smooth hard-spheres, and in addition to that, many of the integrals occuring in the relevant theory have already been evaluated. But there is a pitfall to the model, in that it tends to overemphasise the role of inelastic collisions, and does not take into account the molecular configuration.

There are two approaches to the calculations of the transport coefficients of dense polyatomic fluids by the rough hard-sphere model. Chandler's approach [163] was based upon the correlation function formation, and this has been studied extensively by Dymond. The second formulation was founded upon a kinetic description involving the solution of an appropriate kinetic equation, which was essentially a follow-up to Dahler's work.

Chandler's rough hard-sphere model is merely an extension of the smooth hard-sphere model for the determination of the transport coefficients of polyatomic fluids. The change introduced to the smooth hard-sphere concept was done by incorporating a parameter referred to as the "roughness" of the hard-sphere, which is the degree of coupling between the rotational and translational modes of motion. The value of the roughness is deduced from experimental data for the transport coefficient of interest.

5.5.2 Application of the Rough Hard-Sphere Theory to Diffusion.

The motion of a polyatomic molecule in a real fluid has been shown by Chandler [163,164] to be related to the motion of a particle in a rough hard-sphere fluid. It is assumed that the motion is determined primarily by those parts of the intermolecular potential that are short-ranged and steeply repulsive. This is considered valid at densities about twice the critical density, where attractive interactions will play only a minor role. For polyatomic molecules, there is a possibility of changes in angular momentum, as well as in

translational momentum upon collision. Chandler [163,164] showed that coupling between translational and rotational motions led to the result that the diffusion coefficient for a rough hard-sphere fluid D_{RHS} was related to that for a smooth hard-sphere fluid D_{SHS}:

$$D \approx D_{RHS} \approx AD_{SHS} \qquad (5.33)$$

where $0 < A \leq 1$.

A represents a translational-rotational coupling factor, and was assumed to be rigorously independent of density and furthermore, assumed to be temperature independent. There is thus a lowering of the self-diffusion coefficient as coupling produces an additional mechanism for molecular velocity relaxation.

On the basis of the rough hard-sphere theory, the reduced self-diffusion coefficient D^*_{RHS} is given by:

$$D^*_{RHS} = 5.030x10^8(M/RT)^{1/2}\, D/V^{1/3} \qquad (5.34)$$

If the coupling factor is density dependent and temperature independent, D^*_{RHS} is just a function of molar volume for a given fluid at a constant temperature. Plots of D^*_{SHS} (or log D^*_{SHS}) versus log(V) for different isotherms will therefore be superimposable laterally, and the amount by which the curve at a given temperature has to be moved to superimpose it on a curve at a reference temperature, T_R, leads to a value for $V_o(T)/V_o(T_R)$ [145].

The initial application of the rough hard-sphere theory was to carbon tetrachloride data [164]. The temperature dependent core size was determined by matching along isotherms of the logarithmic derivative of the experimental diffusion coefficient, with respect to that predicted by the theory. For ease of application, D_E was calculated using the Alder, Gass and Wainwright [120] correction to Enskog, and was represented by an analytical quadratic expression in reduced density $n\sigma^3$. A satisfactory fit to the high pressure measurements of McCool and Woolf [165] at different temperatures was given with a constant value of A of 0.54 and with core sizes given by:

$$\sigma/\text{nm} = 0.5270[\ 1 - 0.051\{(T/K - 283.2)/283.2\}] \qquad (5.35)$$

Since then, accurate measurements of self-diffusion coefficients have been made for several polyatomic fluids, by n.m.r. spin-echo technique, and the data interpreted in terms of the rough hard-sphere model.

5.5.3 Viscosity Coefficients of Polyatomic Fluids.

For a system of fairly spherical polyatomic molecules at densities greater than twice the critical density, Chandler [164] showed that the viscosity coefficient is approximate to the rough hard-sphere viscosity coefficient η_{RHS}. When account is taken of the effect of changes in the angular momentum as well as changes in the linear momentum of a particle upon collision, then it was found that the rough hard-sphere

coefficient is directly related to the smooth hard-sphere coefficient:

$$\eta \approx \eta_{RHS} \approx C\eta_{SHS} \qquad (5.36)$$

where C is assumed to be constant. It obeys the inequality $C \geq 1$, and equals one when coupling between angular and translational motion is absent.

Most tests of the rough hard-sphere model for viscosity have been performed using the full equation:

$$\eta = C(\eta/\eta_E)\eta_E \qquad (5.37)$$

where (η/η_E) is the Alder, Gass and Wainwright [120] computed correction to the Enskog theory. Values of the core sizes were obtained either from fitting the high density diffusion coefficient data for the fluids, or from plots of $\log(1/\eta)$ vesus $\log(\rho)$, from which the slope was determined and σ, the core size, was derived by using the smooth hard-sphere expressions for fluidity, given by Dymond [166]. Values for the core diameters agreed closely with values obtained from self-diffusion coefficient data.

The coupling factor, C, is practically independent of density or pressure for those molecules which can be considered pseudospherical, but shows a marked temperature dependence, where there is a significant departure from spherical shape, or where the molecules can hydrogen bond.

The rough hard-sphere model of transport properties has been treated in a different way by Dahler, with the derivation [167,168] and solution [169,170] of an appropriate kinetic equation. The transport coefficients depend on the internal mass distribution, characterised by the moment of inertia in reduced form, is given by:

$$k = \frac{4I}{m\sigma^3} \qquad (5.38)$$

The dimensionless moment of inertia can have values from zero when the mass is evenly distributed over the surface of the sphere. The coefficient of viscosity can be written [71] in terms of k and the reduced volume V/V_0. It is found that (η_{RHS}/η_{SHS}) has a maximum value of 1.64, and more important, it is constant to within 2% for a given value of k over the range of V/V_0 from 1.5 to 2.5. This supports the result obtained by Chandler [164], that the rough hard-sphere coefficient is proportional to the smooth hard-sphere coefficient, though in Chandler's theory, there is no way of evaluating the proportionality constant. The disadvantage of the Dahler theory, is that it over emphasises the role of inelastic collisions, in the same way as the other rough hard-sphere theories.

Generally, the values derived for the translational-rotational coupling factor derived from viscosity, are greater than unity as postulated by Chandler [164]. However, for chlorotrifluoromethane, Harris [171] obtained the figure of 0.77 for C, which he showed to be reasonable, since application of the slip and stick boundary conditions

of the Stokes-Einstein equation leads to the inequality:

$$2/3 \leq AC \leq 1 \qquad (5.39)$$

where A is the coupling factor from self-diffusion.

Recently, Easteal and Woolf [148] have used their calculated corrections to the approximate Enskog theory, based on methane data, to determine the density and temperature dependence of the translational-rotational coupling factor for relatively simple polyatomic fluids. They found that the coupling factor may have a strong density dependence; the shear viscosity data (tabulated by McCool and Woolf [148]), gave the value of A_η, which is the translational-rotational coupling factor for viscosity, and it appeared to be a temperature-independent function of density. This must throw some doubt on the physical validity of the rough sphere model, but in view of its success for predictive purposes in other areas, it is evidently worthy of retention.

A method analogous to that described above for self-diffusion coefficients can bu used for the successful correlation and prediction of viscosity coefficients over the whole density range. A quantity η' was defined [172]:

$$\eta' = 9.118\times10^{7}\eta V^{2/3}/(MRT)^{1/2} \qquad (5.40)$$

For the density region where the rough hard-sphere theory is applicable, η' will be proportional to $(\eta_{SHS}/\eta_0)(V/V_0)^{2/3}$, and so will

depend only on (V/V_o) for a given fluid at a given temperature. This holds true providing that the translational-rotational coupling factor for viscosity is density and temperature independent. Plots of η' or $\log(\eta')$ versus $\log(V)$ using data for a given compound at different temperatures, should be superimposable on the curve obtained for any reference temperature. The amount of adjustment gives a value for $V_o(T)/V_o(T_R)$. Results obtained [145,165,173,174,175] for carbon tetrachloride and tetramethylsilane showed that the curves were superimposable, not only over the density range for which the rough hard-sphere theory was applicable, but over the whole density range. This method has been successfully applied to the correlation of viscosity data for liquid normal alkanes, aromatic hydrocarbons and their binary mixtures. The system also works for n-alkanes, such as n-octane and n-dodecane [176], n-hexane and cyclohexane [177], and benzene and hexafluorobenzene [178]. It was found that the internal energy had a profound effect on the thermal conductivity coefficients, and simple expressions for providing correlations for the thermal conductivities of monatomic fluids could not be formulated with confidence. This is due to the presence of direct internal energy transport, and the coupling between motions. Therefore, Chandler's approach could not provide a similar basis for the problem of the thermal conductivity as it did for viscosity and diffusion.

5.5.4 Thermal Conductivity Coefficients for Polyatomic Fluids.

The application of equations (5.30) and (5.32) to polyatomic fluids required a fundamental modification introduced by Menashe [179]. It is well known that polyatomic molecules possess internal energy in

addition to the translational energy. The contribution of the internal degrees of freedom to the thermal conductivity was assumed to have the same density dependence as the translational part. Therefore, the quantity:

$$\lambda' = \frac{\lambda}{\lambda^o}(V/V_o)^{2/3} \qquad (5.41)$$

was made by analogy with the monatomic case, and should be a function of (V/V_o), but λ^o is the zero density total thermal conductivity of the fluid.

The sound foundation of the kinetic theory description of the rough hard-sphere theory, with a proven result for the viscosity of real dense polyatomic liquids, implies that the same can be extended to provide a basis for the analysis of the thermal conductivity of the aforementioned systems. The thermal conductivity for a rough hard-sphere fluid has been treated by Theodosopulu and Dahler [167,169,170]. Li [71] has evaluated their expressions and shown that the translational and rotational contributions vary quite significantly with changes in the moment of inertia. According to them, the thermal conductivity of a rough hard sphere fluid is given by the sum of a translational and internal contribution as:

$$\lambda^D_{RHS} = \lambda^{tr}_{RHS} + \lambda^{int}_{RHS} \qquad (5.42)$$

where

$$\lambda_{RHS}^{tr} = \lambda_{k1}\left[1 + \frac{1}{5}\frac{(5K+3)}{(K+1)}\,bng\right] + \lambda_{k2}\frac{1}{3}\frac{(3K+2)}{(K+1)}\,bng$$

$$+ \lambda_{k3}\left[\frac{kT}{\pi I}\right]^{1/2}\frac{K^{1/2}}{(K+1)}\,bng + \left[\left[\frac{k^3T}{\pi m}\right]^{1/2} n^2\sigma bg\left[\frac{(2K+1)}{(K+1)}\right]\right] \tag{5.43}$$

and

$$\lambda_{RHS}^{int} = \lambda_{k2}\left[1 + \frac{2}{3}\frac{bng}{(K+1)}\right] + \left[\frac{kT}{\pi I}\right]^{1/2}\frac{K^{1/2}}{(K+1)}\,bng$$

$$+ \left[\left[\frac{k^3T}{\pi m}\right]\frac{n^2\sigma bg}{(K+1)}\right] \tag{5.44}$$

The coefficients λ_{ki} are defined in terms of the determinant:

$$A = \begin{vmatrix} \frac{4}{15}\alpha\frac{(34K+8)}{(K+1)^2} & -\frac{40}{9}\frac{\alpha K}{(K+1)^2} & 0 \\ -\frac{8}{3}\alpha\frac{K}{(K+1)^2} & \frac{8}{3}\alpha\frac{(2K^2+2K+1)}{(K+1)^2} & -\frac{kT}{I}\gamma\frac{K}{K+1} \\ 0 & \frac{2}{3}\gamma\frac{K}{(K+1)} & \frac{16}{3}\alpha \end{vmatrix} \tag{5.45}$$

as

$$\lambda_{ki} = -\frac{A_i}{A} \tag{5.46}$$

where A_i is the determinant obtained by replacing the i^{th} column of A by the column vector:

$$\begin{bmatrix} -\frac{kP}{2m}\left[5 + \left[\frac{5K+3}{(K+1)}\right]\tau\right] \\ -\frac{3}{2}\frac{\kappa\rho}{m}\left[1 + \frac{2\tau}{3(K+1)}\right] \\ \frac{16}{3}\frac{P\alpha}{mT}\frac{I}{(K+1)} \end{bmatrix} \tag{5.47}$$

Here,

$$P = nkT \tag{5.48}$$

$$\tau = bng \tag{5.49}$$

$$\alpha = ng\sigma^2(\pi kT/m)^{1/2} \tag{5.50}$$

$$b = \frac{2}{3}\pi N_A \sigma^3 \tag{5.51}$$

where n, k, N_A, and m are the number density, Boltzmann constant, Avogadro constant and molecular mass, respectively.

In order to evaluate the thermal conductivity of the rough hard-sphere fluid, we employ the radial distribution function for

hard-spheres at contact, given by Carnahan and Starling [135]:

$$g = (1-0.5\xi)(1-\xi)^3 \qquad (5.52)$$

where

$$\xi = \frac{2^{1/2}\pi V_o}{6V} \qquad (5.53)$$

and V_o, the close packed volume of the hard-sphere system, where b is obtained from equation (5.14).

Following some laborious algebra [71], and using the earlier results for g and σ in terms of the characteristic volume V_o, and the molar volume V, it can be shown that the ratio:

$$(\lambda^D_{RHS}/\Lambda^o)(V/V_o)^{2/3} = \lambda^*(V/V_o, K) \qquad (5.54)$$

is a function only of the relative molar volume (V/V_o), and the dimensionless parameter K. Here,

$$\Lambda_o = 75(k^3T/\pi m)^{1/2}/64\sigma^2 \qquad (5.55)$$

is the thermal conductivity of a fluid of smooth spheres of diameter σ at zero density.

Recently, the thermal conductivity of liquid methane [155,180], was measured with an accuracy of better than 0.5%. It was found that the excess thermal conductivity is a function of density alone, within the range of experimental conditions of 110K and 180K, with pressures up to 10MPa. A reliable correlation scheme for accurate interpolation and extrapolation was devised based upon an empirical modification of the dense hard-sphere theory. The corrected dense hard-sphere theory was able to represent the data with a standard deviation better than $\pm$0.5% and a maximum deviation of $\pm$1%. The model is capable of being used to predict the thermal conductivity of liquid methane along the saturation line, and an equation was found to reproduce the extrapolated data to within $\pm$0.3%. The accuracy of the correlation scheme is believed to be better than $\pm$1.0%.

Unlike the case of viscosity, direct calculations show that the dependence of the thermal conductivity upon the parameter K, cannot be factorized from equation (5.54) in any range of densities. Therefore, the technique used by Dymond [181,182] cannot be used to examine the applicability of the rough fard-sphere model for the description of viscosity.

The density dependence of the viscosity for n-hexane and n-octane at 25°C were analysed using Chandler's result,[164] (equation (5.36)) for the rough hard-sphere by means of the method proposed by Dymond [181,182]. For neither n-hexane nor n-octane is the range of thermodynamic states for which the rough hard-sphere model is strictly applicable to the viscosity, very extensive, because of the importance

of the attractive forces in the low temperature region, characteristic of the liquid phase. In fact, for n-hexane, the range is limited to pressures below 150MPa and for n-octane it is even smaller.

Since the theories of Chandler and Dahler are mutually consistent for viscosity of rough hard-sphere systems, a value of dimensionless moment of inertia, k, can be derived from C and the thermal conductivity calculated and compared with experiment. Li [71] applied this method to n-hexane at 298K, for which he found that C = 1.45, V_o = 78×10^{-6} $m^3 mol^{-1}$, k = 0.44 and n-octane at 298K for which C = 1.77, V_o = 105×10^{-6} $m^3 mol^{-1}$ and k = 0.66. The calculated thermal conductivity coefficients agreed [176] with measured values for n-hexane to within 5% over the density range for which the smooth hard-sphere model is stable. For n-octane, the differences were somewhat greater [183], but still less than 10%, which is good in view of the simplicity of the model.

On the basis of the rough hard-sphere theory of Dahler [169,170], the thermal conductivity coefficient of a fluid can be represented by the general equation:

$$\frac{(\lambda_{RHS})_D}{\Lambda_o} = C_1\left[\frac{1}{g(\sigma)}\right] + C_2\left[\frac{b}{V}\right] + C_3\left[\frac{1}{g(\sigma)}(b/V)^2\right] \qquad (5.56)$$

where Λ_o is given by equation (5.55), and C_1, C_2 and C_3 are algebraic functions of the dimensionless moment of inertia k. As shown by Li

[71], the dependence of the thermal conductivity on k is weak. For this model system, k is temperature independent, and for a real fluid the temperature dependence is likely to be small.

Substitution for Λ_0 and V_0 in equation (5.54) allows λ^* to be calculated from experimental results:

$$\lambda^* = (64/75)(\pi^{1/2}(2N_A)^{1/3}/R)\lambda V^{2/3}(RT/M)^{-1/2}$$

$$= \frac{64}{75}\left[\frac{m\pi}{k^3T}\right]^{1/2}\frac{2^{1/3}}{N_A^{2/3}}\lambda V^{2/3}$$

and $$\lambda^* = 1.936\times10^{7}\lambda V^{2/3}(M/RT)^{1/2} \qquad (5.57)$$

with all the quantities in SI units, where M is the molecular weight, R the Universal gas constant, and V the molar volume, λ the experimental thermal conductivity, and T the temperature, so that

$$\lambda^*_{SHS} = F_\lambda(V/V_0) \qquad (5.58)$$

Again, the available data for monatomic gases confirm the validity of equation (5.58), and the values of V_0 for them derived from an analysis of viscosity through equation (5.28), or the thermal conductivity through equation (5.58) are mutually consistent [139,161].

For polyatomic fluids, the situation is rather more complicated than the viscosity, because the internal energy is very much more

important for the thermal conductivity. The first attempt to account for the internal energy, within the spirit of the hard-sphere model, proposed an ad hoc modification to equation (5.58), so that for polyatomic fluids [179]:

$$\lambda^* = B\ F_\lambda(V/V_o) \qquad (5.59)$$

with

$$B = \{1 + 0.352\ C^o_{v,int}/R\}^{-1} \qquad (5.60)$$

where $C^o_{v,int}$ is the internal energy contribution to the ideal gas molar heat capacity of the fluid. The thermal conductivity of a number of normal alkanes can be represented quite accurately by equations (5.59) and (5.60), although the values of V_o derived are not consistent with those derived from an analysis of viscosity data [71].

An alternative scheme to correlate the same set of data was envisaged by Dahler et.al. [169,170] , employing the rough hard-sphere theory. This approach led to a different functional form for $F_\lambda(V/V_o)$ and an expression for B which relates it a single parameter of the rough hard-sphere model [71,184]. An analysis based upon their idea was successful in providing a somewhat reliable correlating scheme. But, whereas the derived values of the characteristic volume were closer to those obtained from an analysis of the viscosity, they were not entirely consistent with them [71,169,170,184]. In addition to that, the use of a rough hard-sphere model meant that the internal energy of the molecules is species independent, $C^o_{v,int} = 3R/2$, which is not realistic.

By analogy with D^* for diffusion and η' for viscosity, λ^* is expected to be a function only of (V/V_o). Plots of λ^* versus log(V) at different temperatures for a given fluid should therefore be superimposable on the curve for a reference temperature. The relative shift along the log(V) axis provides a value for the ratio of V_o values at different temperatures. Li [71] has tested this approach using accurate measurements on n-hexane, n-octane, benzene and cyclohexane, using the lowest isotherm as the reference in each case. A very satisfactory correlation was obtained with values for $V_o(T)/V_o(T_R)$ in close agreement with values obtained by Dymond [176,178,185] for the same liquids.

Since λ^* is so weakly dependent on k, there is the possibility of deriving a universal correlation for λ^*. This was studied and concluded by Li [71], using accurate thermal conductivity measurements on eleven hydrocarbons over a wide range of pressures and temperatures. This earlier study was complimented here by new accurate thermal conductivity measurements performed on five additional liquids [70,75,186,187,188].

Analysis of the experimental thermal conductivity data has led to a successful means for interpretation. This may be understood from the viewpoint that the data for all the normal alkanes studied conform to

the general equation:

$$\ell n\, \lambda^* = a_0 + a_1 \ell n V^* \qquad (5.61)$$

where $V^* = V/V_0$, with essentially universal values of a_1 [179,184]. Thus, the problem of the determination of B and V_0 from such data is basically one of finding the shifts, parallel to the axes to the $\ell n\lambda^*$ and ℓnV^*, which superimpose a number of parallel, straight lines.

5.6 The Correlation.

The rough hard-sphere theory as it stands, is not capable of providing a rigorous and accurate means of predicting the thermal conductivity of polyatomic fluids. But according to the discussion in the previous sections, there are some indications that such a scheme is possible to form the basis of a reliable interpolation and extrapolation procedure. In order to present such a procedure, it is necessary to define λ^* in equation (5.54), according to the rough hard-sphere model for one particular fluid, a quantity K is constant, so that $\lambda^* = \lambda^*(V/V_0)$ only. This means that it should be possible to superimpose plots of λ^* against ℓnV for one fluid along several isotherms upon one another, merely by shifts along the ℓnV axis. The amount of the relative shift for two isotherms then determines the ratio of the core volume V_0 at the two temperatures. As mentioned above, this method is similar to that adopted by Dymond and Brawn [172] for viscosity and diffusion, and to that put forward by Menashe [179]. However, there are two fundamental differences between the current formulation and that which was introduced by Menashe [179]. First, the

definition of λ^* adopted here is somewhat different from the heuristic proposal put earlier. Secondly, the current formulation is founded upon a model which includes the essential features of transport in dense polyatomic systems, albeit in a simplified manner, which the former proposal did not.

In order to ascertain the proposition found in equation (5.57), the precondition that the function λ^* should itself be accurately predicted by the rough hard-sphere model , and with it the constraint on the range of densities to which it applies, is waived. First, the function λ^* is determined empirically for each fluid, by assigning an arbitrary, but realistic, value to the core volume V_o at the lowest temperature for which accurate thermal conductivity data exists. This is followed by evaluating the function λ^* according to equation (5.54) for all the available isotherms. The plots of λ^* against ℓnV for the higher temperatures are then superimposed upon that for the lowest temperature, by translation along the ℓnV axis only. In this way, values of $V_o(T)$ are evaluated for each isotherm.

5.6.1 Experimental Data.

Since the earlier analyses of transport coefficient data for liquid normal alkanes were performed, new measurements on a further set of liquids, namely, ethylbenzene, carbon tetrachloride, n-pentane, oct-1-ene, and ortho-xylene over a wider range of thermodynamic states have been performed within the scope of this work [70,75,186-188]. Diller et.al. [189-191] have measured the viscosity of ethane, propane

and n-butane in the temperature range 90-300K at pressures up to 30MPa; Dymond, Isdale et.al [176,185] have reported data on n-hexane and n-octane in the temperature range 300-400K at pressures up to 500MPa. Both sets of measurements have an estimated uncertainty of ±1 to ±2%.

In the case of thermal conductivity, Roder et.al [192,193] have reported results for ethane and propane in the temperature range 110K to 300K at pressures up to 70MPa. de Castro et.al. [194] have reported data for liquid n-butane in the temperature range 300-413K at pressures up to 70MPa. Again, the accuracy of these results is estimated to be in the range of ±1 to ±2%. Li et.al. [183] have reported thermal conductivity data for n-hexane and n-octane in the temperature range 300-400K and pressures up to 700MPa, with an associated uncertainty of ±0.3%. To complete the study on the n-alkanes series, we have performed thermal conductivity measurements on n-pentane in the temperature range of 300-370K at pressures up to 500MPa, with an accuracy of ±0.3% [186].

5.6.2 The Density Dependence of the Thermal Conductivity.

For the normal alkanes, a correlation scheme based upon the ideas of the rough hard-sphere model of a dense fluid, has proved successful [179]. The basic idea of this scheme is that the experimental group, λ^*,

$$\lambda^* = 1.936\times10^{7}\lambda V^{2/3}(M/RT)^{1/2}$$

$$= F(V/V_0) \qquad (5.62)$$

should be a function only of the ratio (V/V_o) , where V is the molar volume of the liquid, and V_o is the characteristic molar volume only weakly dependent on temperature, and is defined as the close-packed volume of the hard-sphere system.

5.6.3 N-Pentane.

The thermal conductivity of the liquid n-pentane [186], has been measured within the temperature range of 306K to 360K and pressures up to 500MPa; the experimental accuracy associated with this set of data is one of $\pm$0.3%. Whereas the correlation of the pressure dependence of the thermal conductivity by means of equation (4.2) is suitable for interpolation, it has little or no value for extrapolation and prediction. For such purposes, it has been mentioned earlier that a correlation in terms of density or molar volume, V, is much more meaningful. The isotherm 305.8K was adopted as a reference and assigned a characteristic molar volume, V_o, which was:

$$V_o(305.8K) = 62.56 \times 10^{-5}\ m^3 mol^{-1} \qquad (5.63)$$

chosen to be approximately consistent with those established for other normal alkanes [195]. Subsequently, the values of V_o for the isotherms 322.8K and 342.5K which secure the optimum degree of superposition of lines of λ^* versus $\ell n(V/V_o)$ for all three isotherms, have been determined and are included in table 5.1(a). The resulting single line has been represented by the equation:

$$\lambda^* = 4.6022 - 2.0602 \ell n V^*$$

where $V^* = V/V_o$ (5.64)

which provides a simple method of correlating the experimental data. Figure 5.ii gives the thermal conductivity ratio, λ^*, for n-pentane, as a function of the reduced molar volume (V/V_o), and it can be seen that the data lie in a smooth curve. Figure 5.iii contains a plot of the deviations of the experimental data from this correlation. The maximum deviation of any datum from the values generated by equation (5.46) is one of $\pm$3.8%, whereas the standard deviation is one of $\pm$1.3%. These deviations exceed the estimated uncertainty of the experimental data, and a closer examination of figure 5.iii reveals that the three isotherms exhibit marked different and systematic deviations from a common correlation. This situation is similar to that observed for n-hexane [183]. Thus, whereas the temperature independence of the function F_λ in equation (5.46) suggested by the hard-sphere theory of a dense fluid, is confirmed within limits suitable for correlations of modest accuracy, there is distinct evidence of its failure under a more rigorous test.

Consequently, in order to provide a better representation of the density dependence of the present thermal conductivity data, they have been represented along each isotherm by means of an equation of the form:

$$\ell n\lambda^* = a_o - a_1 \ell n(V/V_o) \qquad (5.65)$$

in which a_o and a_1 are allowed to be temperature dependent. The values

T(K)	$10^5 V_o (m^3.mol^{-1})$
305.8	6.256
322.8	6.213
342.5	6.188

Table 5.1(a) Characteristic Volumes, V_o, for Normal Pentane.

T(K)	a_0	a_1
305.8	4.6883	2.2138
322.8	4.6020	2.0580
342.5	4.4731	1.8470

Table 5.1(b) Coefficients of equation (5.61) for Normal Pentane.

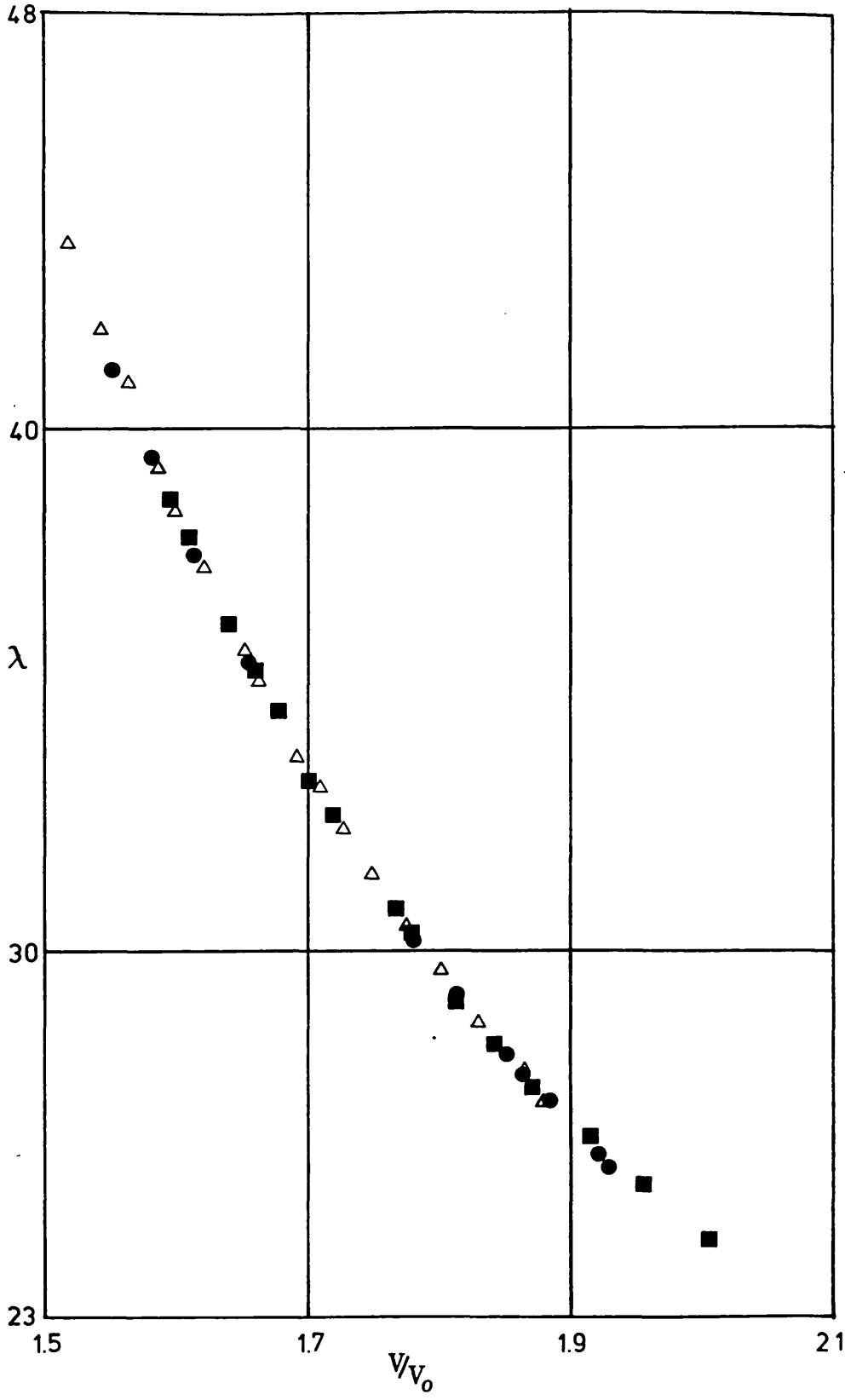


Figure 5.ii. The thermal conductivity ratio, λ , for n-pentane as a function of reduced molar volume.

△ 305.80 K; ● 322.80 K; ■ 342.50 K.

Figure 5.iii. Deviations of the experimental thermal conductivity from equation (5.64), as a function of density.

○ 305.80 K; ● 322.80 K; △ 342.50 K.

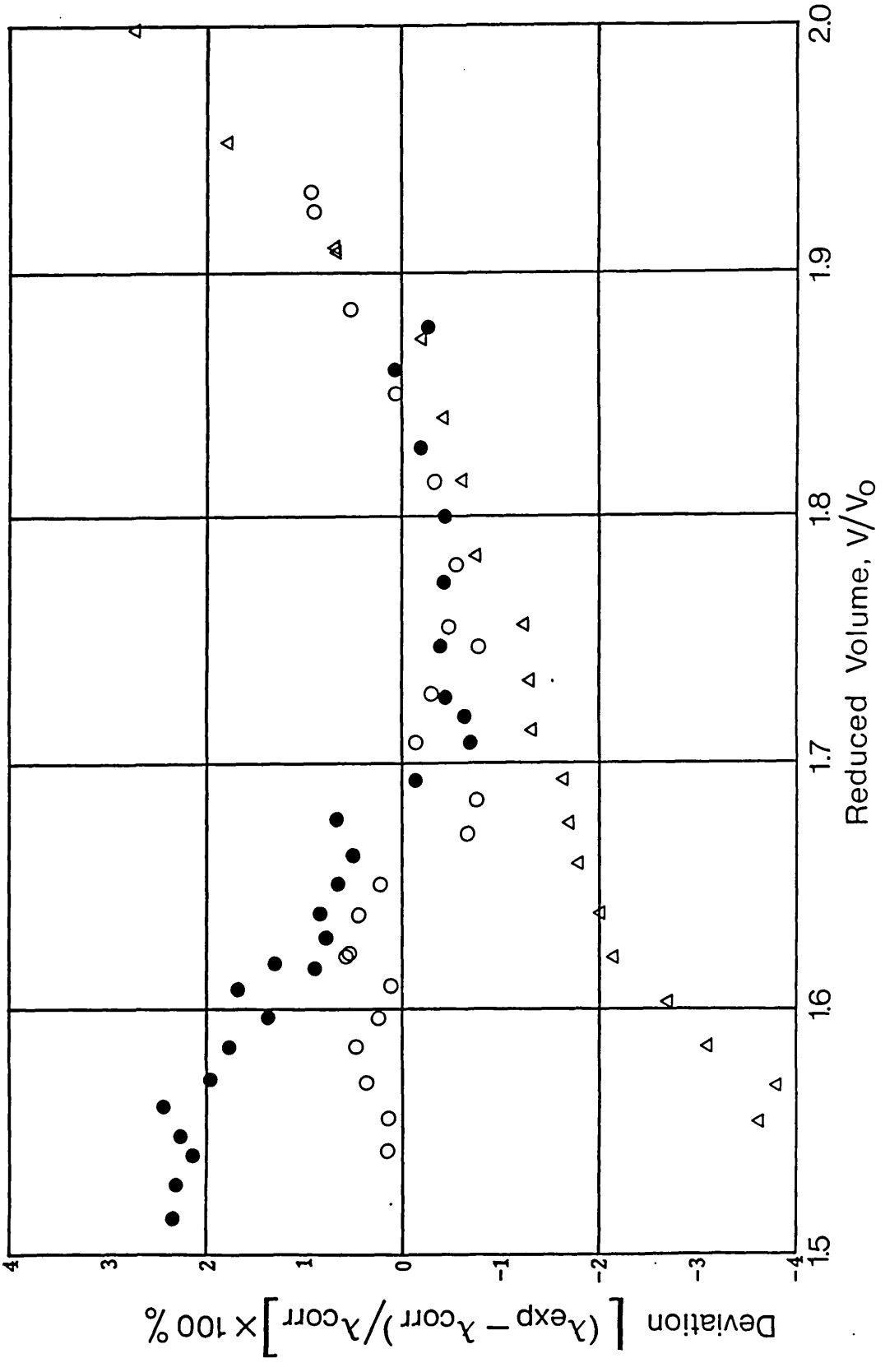
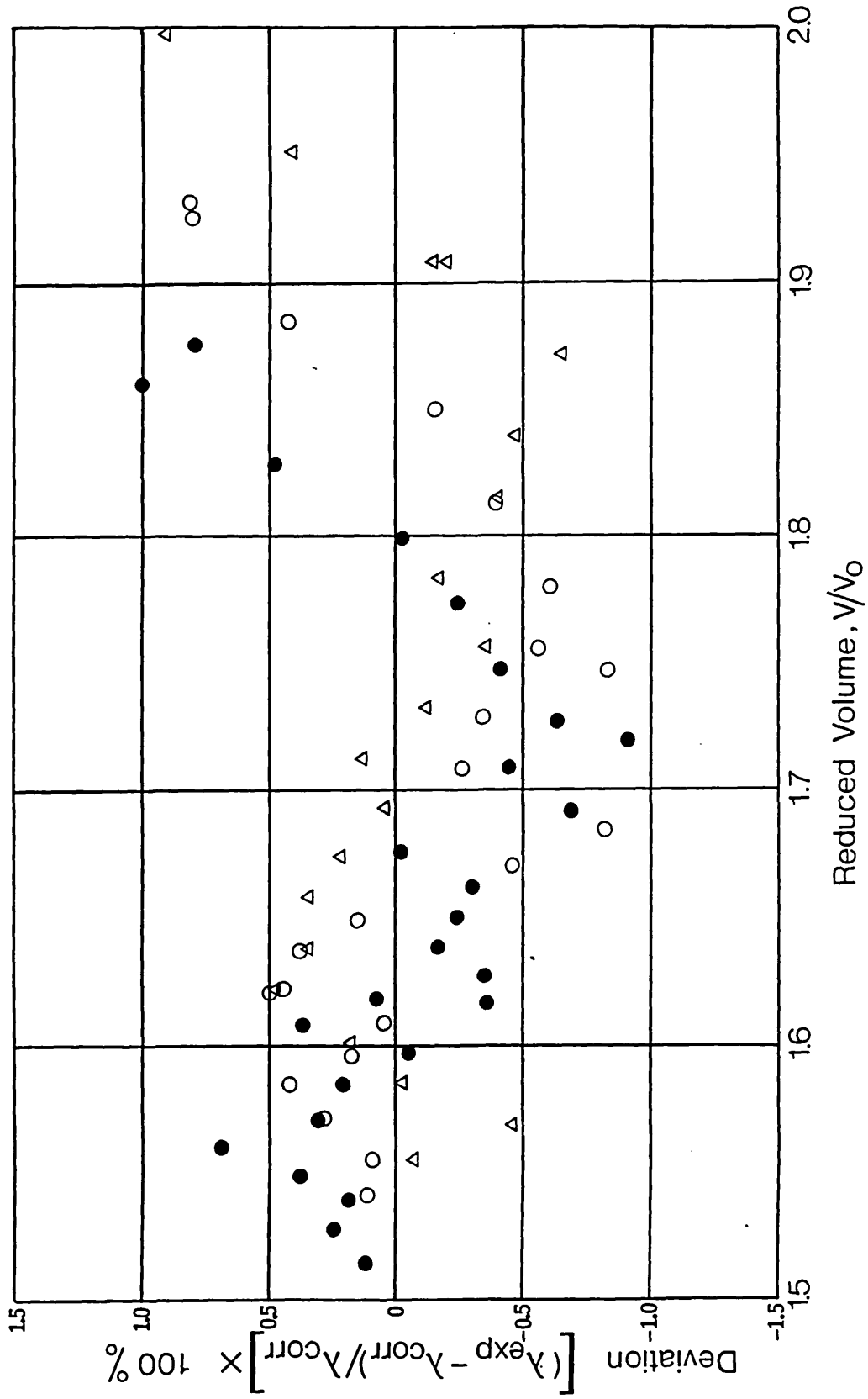


Figure 5.iv. Deviations of the experimental thermal conductivity data from individual correlations, using equation (5.65).

○ 305.80 K; ● 322.80 K; △ 342.50 K.



of V_o adopted in these representations are given in table 5.1(b) the same table includes the optimum values of the coefficients a_o and a_1. Figure 5.iv contains the deviations of the thermal conductivity for the three isotherms from the correlations of equation (5.65). In this case, the deviations amount to no more than $\pm$1.0%, whereas the standard deviation is one of $\pm$0.25%. These departures are much more nearly consistent with the combined uncertainty in the thermal conductivity and density.

5.6.4 Oct-1-ene.

In the case of oct-1-ene, which not a normal alkane, a similar analysis was applied to the experimental thermal conductivity [188], initially without reference to the results of earlier work for alkanes. The analysis was begun by adopting an essentialy arbitrary value for V_o at the lowest isotherm. This allowed the construction of the function λ^* versus $\ell n(V/V_o)$ for that isotherm (307.65K). Subsequently, if equation (5.62) is obeyed by the fluid, it should be possible to superimpose plots of λ^* vesus $\ell n(V)$ for other isotherms on that for the reference isotherm, merely by selecting a suitable value for V_o. In this way, values of V_o for all the isotherms have been determined, and they are listed in table 5.2. It has been found that the best representation of the single, composite curve λ^* versus (V/V_o) is given by the simple equation, and is illustrated in figure 5.v:

$$\ell n\, \lambda^* = 4.9339 - 2.3458 \ell n(V/V_o) \qquad (5.66)$$

Figure 5.vi gives a plot of the deviations of the present experimental

data from this correlation, which contains just one adjustable parameter. It can be seen that, with the exception of one point, the deviations do not exceed $\pm$0.8%. The standard deviation of the fit is one of $\pm$0.4%. Although this exceeds the uncertainty in the thermal conductivity alone, it is consistent with the combined uncertainty in the thermal conductivity and density. The correlation can therfore be employed for extrapolation of the present data to regions of state not covered in the present study.

Because the thermal conductivity of oct-1-ene is represented by a form of equation which proved successful for a variety of alkanes, it is worthwhile to examine this correspondence more closely. For this purpose, we have attempted to fit the thermal conductivity of oct-1-ene to the equation best describing the data for the alkanes [184]:

$$\ell n\ \lambda^{*} = 4.8991 - 2.2595\ell n(V/V_o) \qquad (5.67)$$

It is by means of such a fit for the lowest isotherm alone, that the value of V_o(307.65K) has been determined for the preceding analysis. Figure 5.vii shows the deviations of the thermal conductivity data for oct-1-ene from this universal correlation, using V_o values listed in table 5.2, and althiugh there is some evidence of systematic deviations of the data from the universal correlation, they never exceed $\pm$1.0%. This observation suggests that prediction of the thermal conductivity of other liquid alkenes may be possible over a wide range of states, provided that it is possible to determine the core volume V_o from just a few measurements.

T(K)	$10^5 V_o (m^3.mol^{-1})$
307.65	9.9435
320.65	9.9286
344.15	9.8988
360.15	9.8840

Table 5.2 Characteristic Volumes, V_o, for Oct-1-ene.

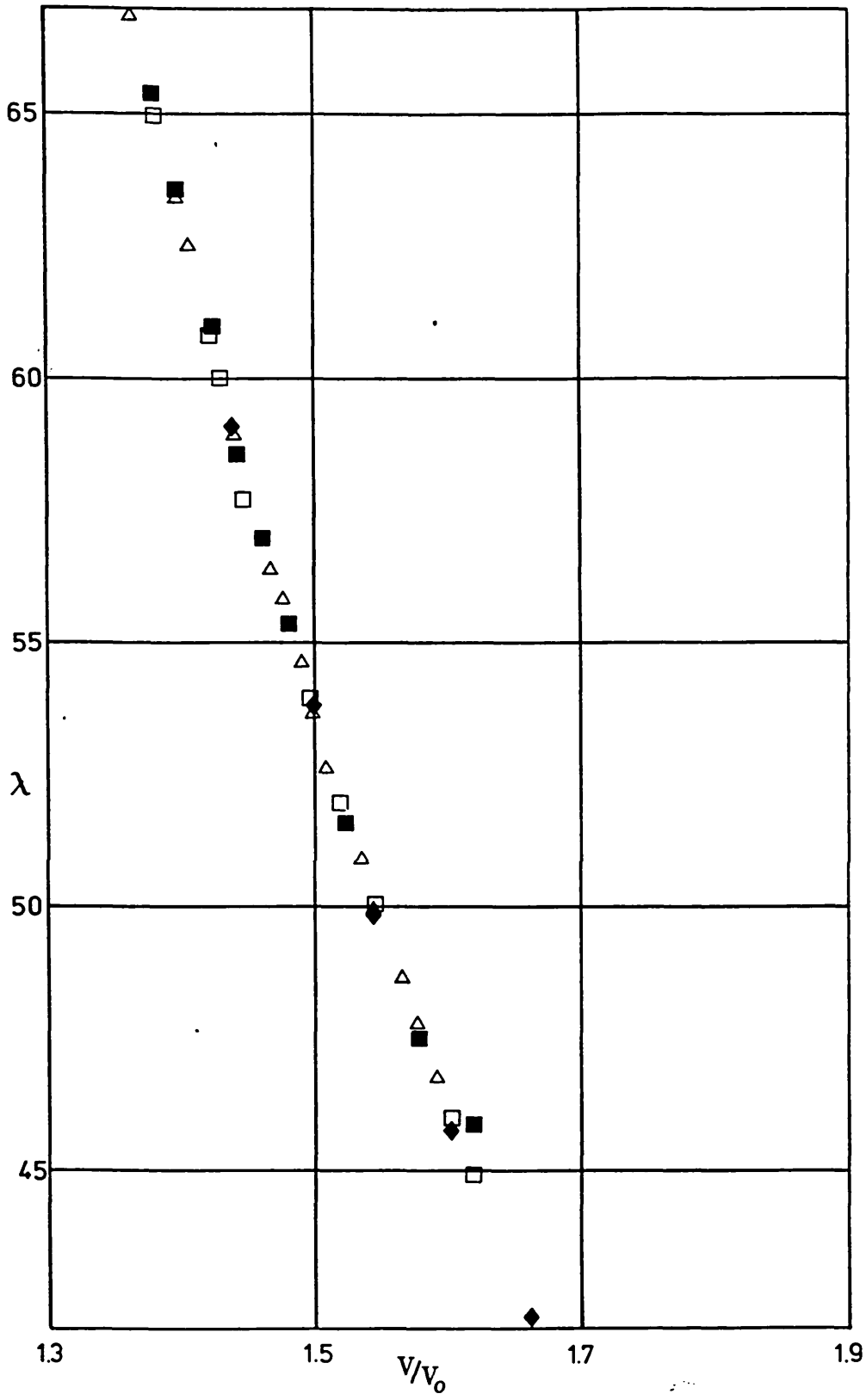


Figure 5.v. The thermal conductivity ratio, λ, as a function of the reduced molar volume for oct-1-ene.

△ 307.65 K; □ 320.65 K; ■ 344.15 K; ◆ 360.15 K.

Figure 5.vi. Deviations of the thermal conductivity of oct-1-ene from the correlation of equation (5.66).

● 307.65 K; ■ 320.65 K; ▶ 344.15 K; ◆ 360.15 K.

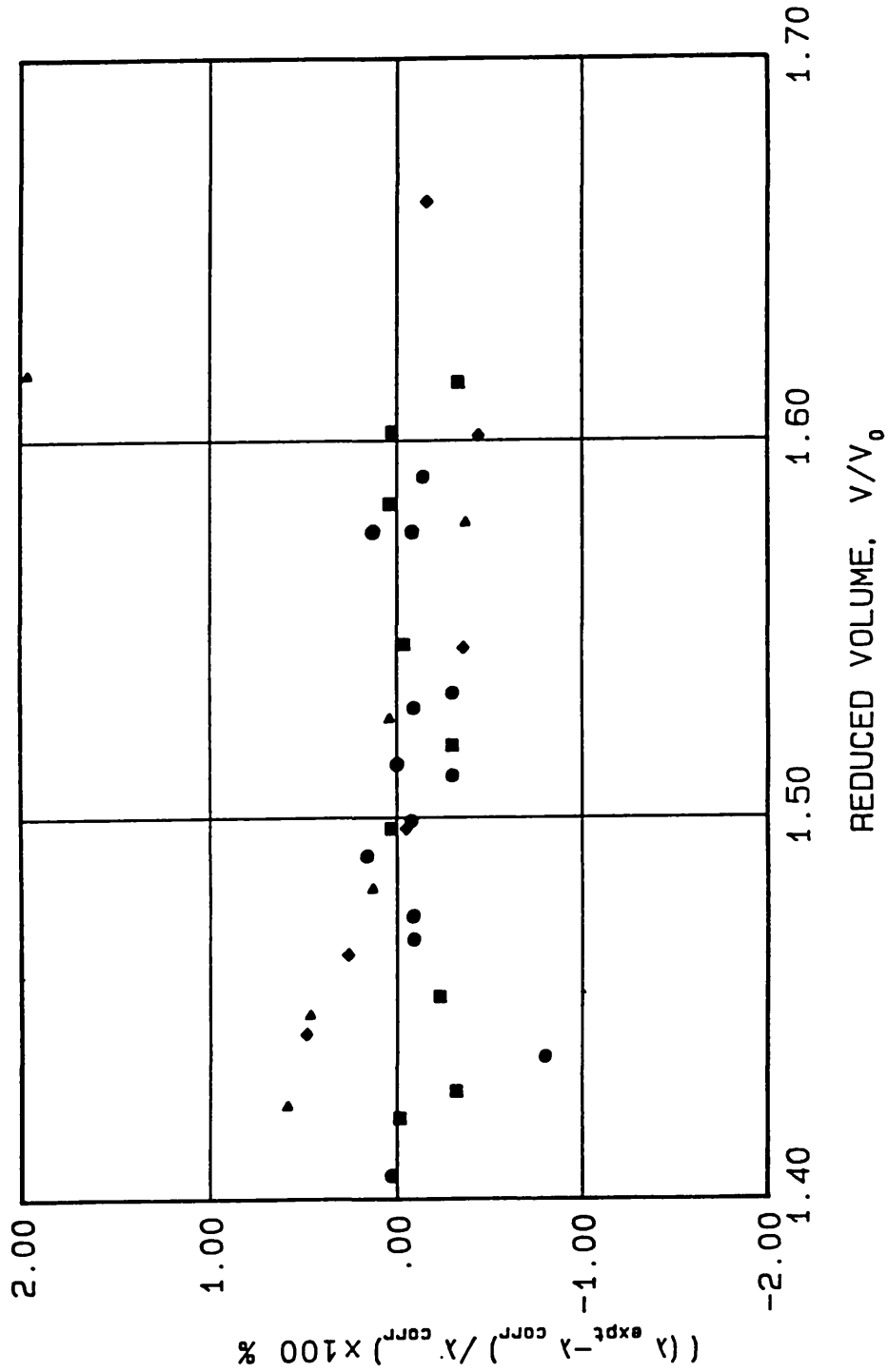
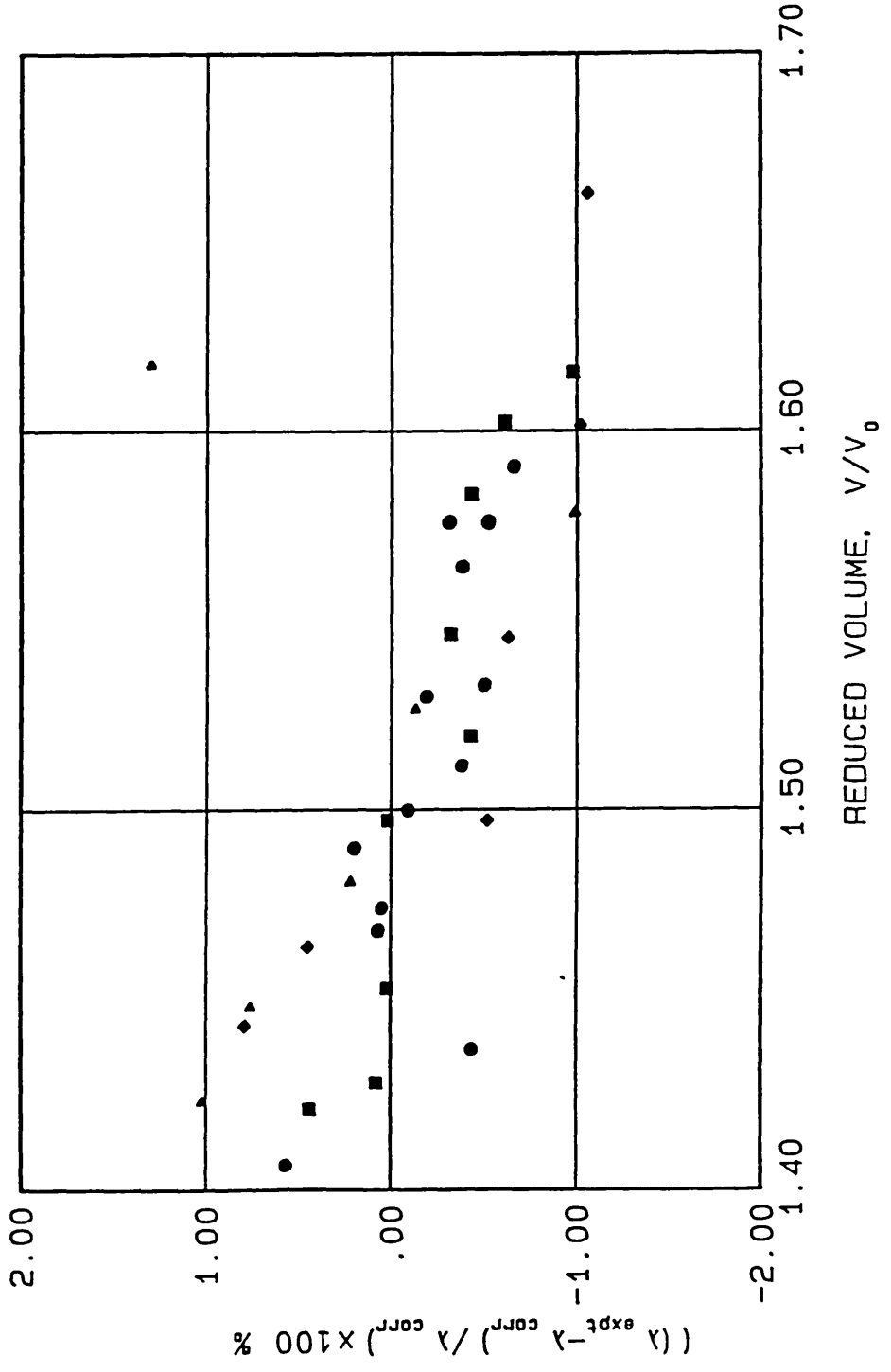


Figure 5.vii. Deviations of the thermal conductivity of oct-1-ene from the correlation of equation (5.67), universal among the alkanes.

● 307.65 K; ■ 320.65 K; ▶ 344.15 K; ◆ 360.15 K.



5.6.5 Carbon Tetrachloride.

It was interesting to see whether carbon tetrachloride, by virtue of it being a spherical molecule, would be capable of being represented in the same manner as for straight chain normal alkanes. A similar approach to that described above was applied to liquid carbon tetrachloride, and the scheme was well represented [187]. Therefore, it was necessary to assign a value for V_o to the isotherm 322.65K for the thermal conductivity measurements data performed on carbon tetrachloride. We have selected a value reported by Dymond [139] from an analysis of self-diffusion coefficient data so that:

$$V_o(322.65K) = 6.080 \times 10^{-5}\ m^3 mol^{-1} \qquad (5.68)$$

Subsequently, we have determined the values for the other two isotherms which secure an optimum representation of the thermal conductivity by means of a single, temperature-independent function $F_\lambda(V/V_o)$. The resulting values of V_o are:

$$V_o(310.65K) = 61.15 \times 10^{-5}\ m^3 mol^{-1} \qquad (5.69)$$

$$V_o(342.65K) = 60.56 \times 10^{-5}\ m^3 mol^{-1} \qquad (5.70)$$

and they are listed in table 5.3.

The corresponding single curve for λ^* as a function of (V/V_o), and illustrated in figure 5.viii, has been represented by the simple

equation:

$$\ell n\ \lambda^{*} = 4.4294 - 2.2162\ell n(V/V_o) \qquad (5.71)$$

Figure 5.ix contains a plot of the deviations of the experimental data from this correlation, and it can be seen that they do not exceed $\pm$0.4%, while the standard deviation amounts to $\pm$0.1%. These values are commensurate with the combined uncertainty in the density and the thermal conductivity, and the figure provides considerable support for the hypothesis contained in equation (5.62)

It now remains to be seen whether the same values of V_o provide a similar description of the other transport coefficients of carbon tetrachloride. For the viscosity, the analogue of λ^{*} is a quantity η^{*} as defined by the equation:

$$\eta^{*} = 6.035x10^{8}\eta V^{2/3}(MRT)^{1/2} \qquad (5.72)$$

Again, the hard-sphere theory leads to the result that:

$$\eta^{*} = F_{\eta}(V/V_o) \qquad (5.73)$$

where F_{η} is independent of temperature.

In order to test whether the values of V_o derived from the thermal

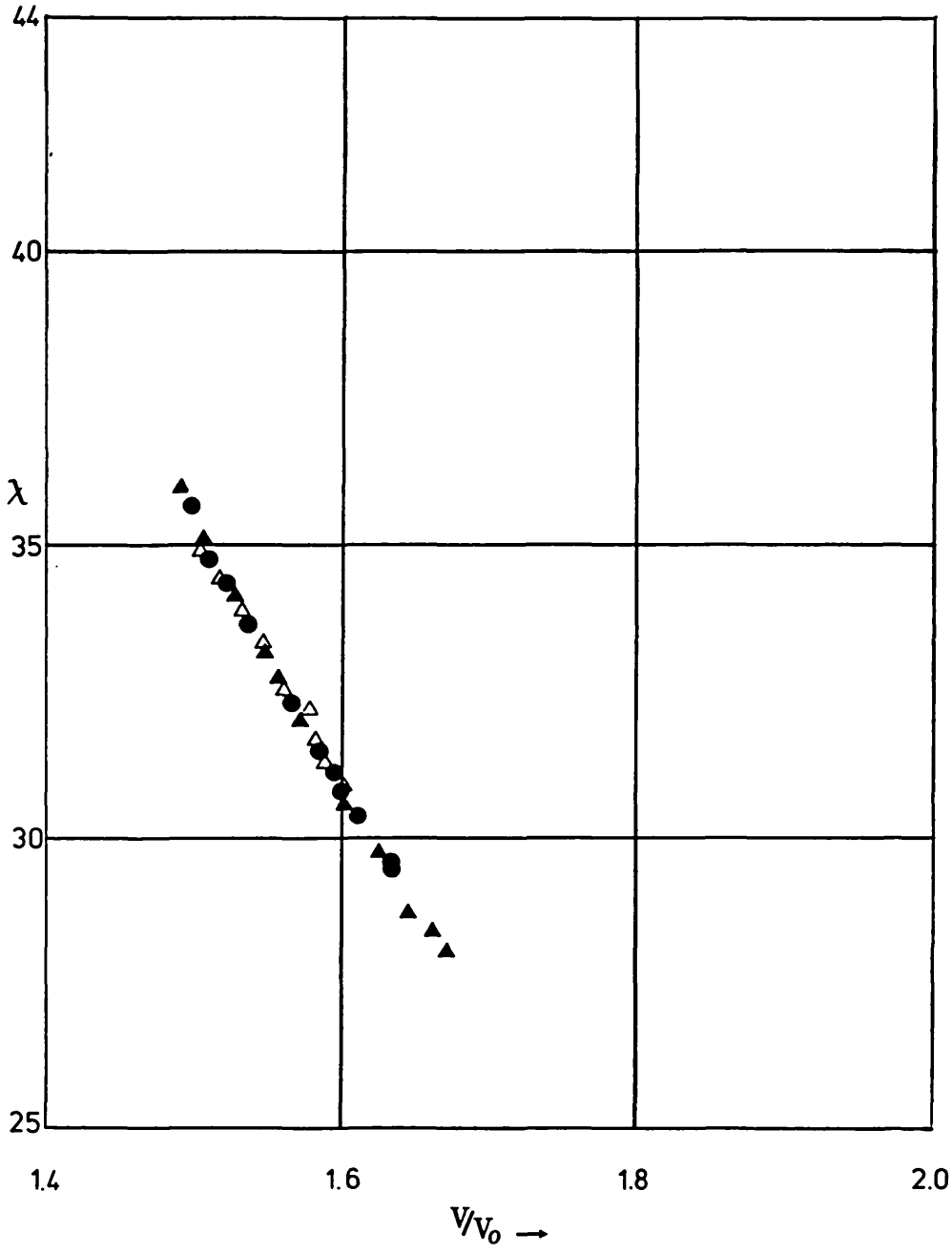


Figure 5.viii. The thermal conductivity ratio, λ, for carbon tetrachloride, as a function of reduced molar volume.

△ 310.15 K; ● 322.65 K; ▲ 342.65 K.

Figure 5.ix. The deviations of the thermal conductivity data from their correlation as a function of volume by equation (5.71).

● 310.15 K; ▲ 322.65 K; ■ 342.65 K.

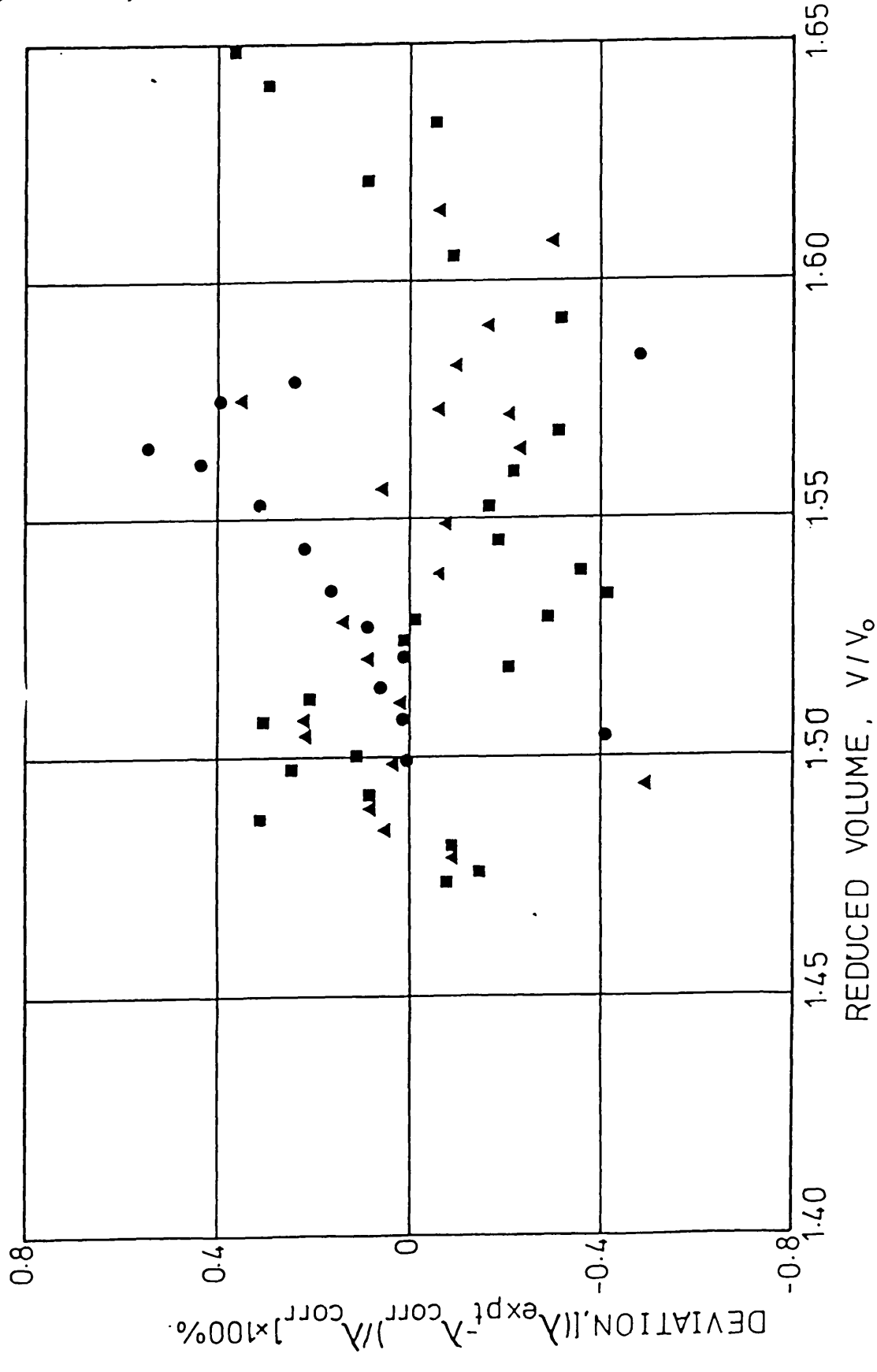


Figure 5.x. The function η^* for carbon tetrachloride.

Experimental data 173 : ● 311.55 K; ■ 323.15 K.

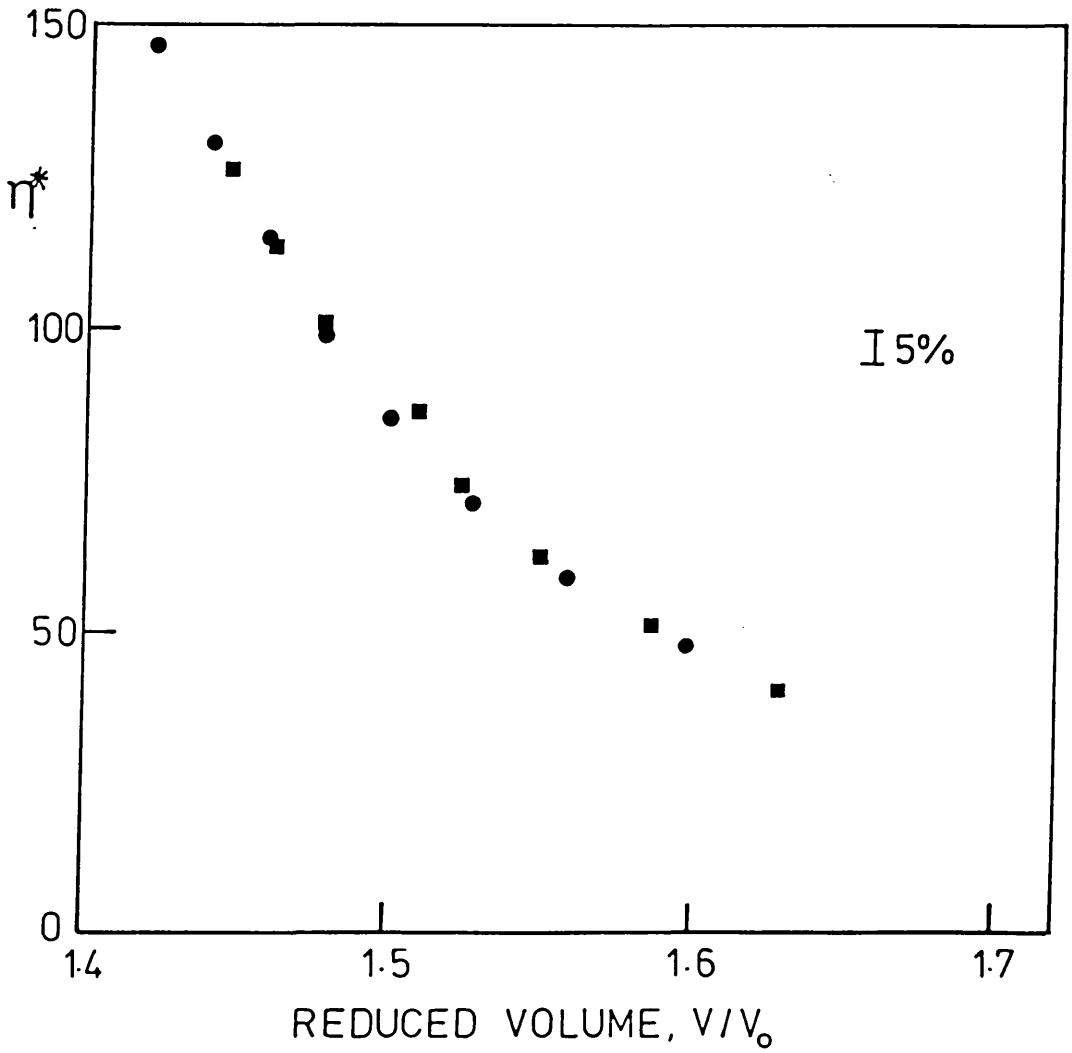
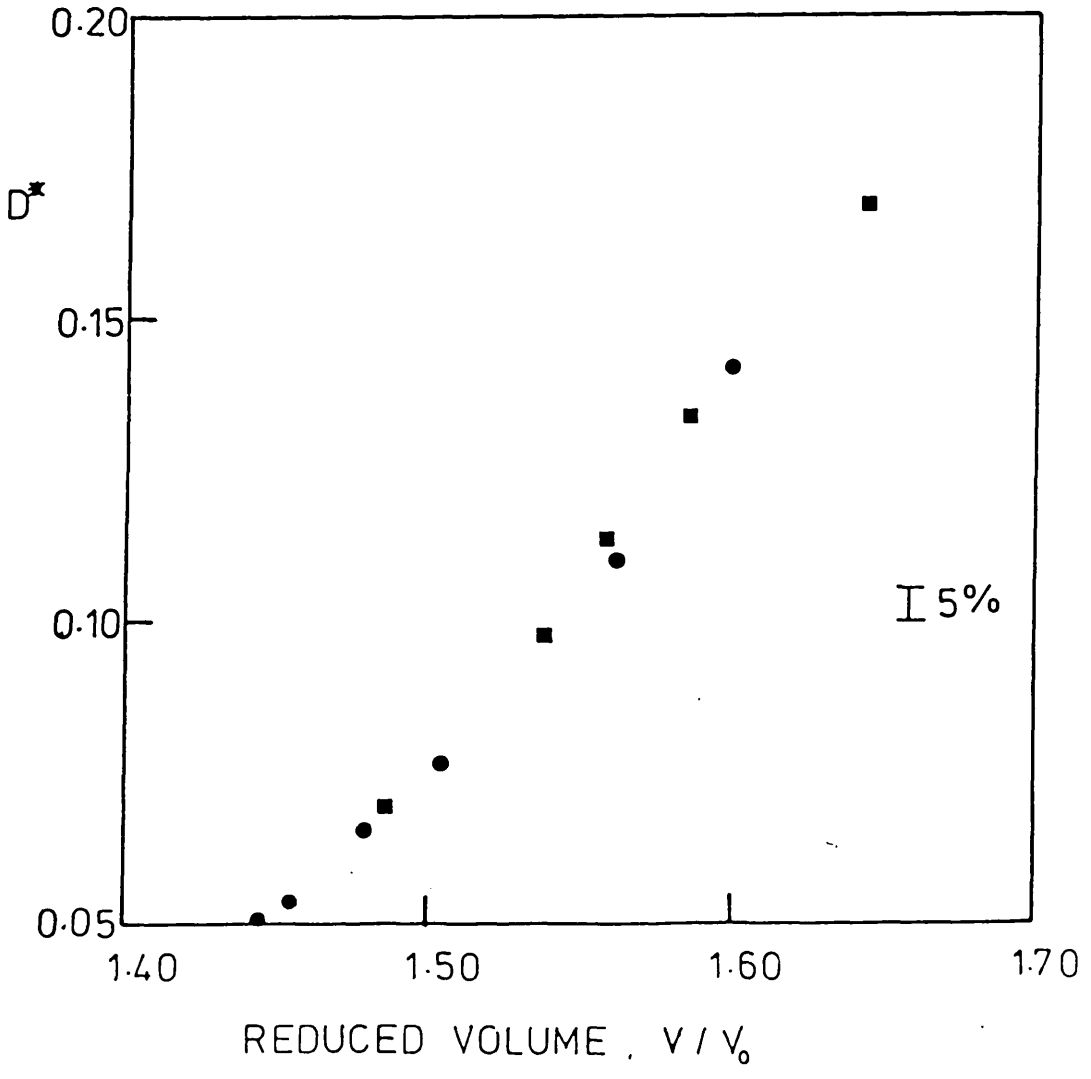


Figure 5.xi. The function D^* for carbon tetrachloride.

Experimental data 165 : ● 313.20 K; ■ 328.20 K.



T(K)	$10^5 V_o (m^3.mol^{-1})$
310.15	6.115
322.65	6.080
342.65	6.056

Table 5.3 Characteristic Volumes, V_o, for Carbon Tetrachloride.

T(K)	$10^5 V_o (m^3.mol^{-1})$
304.65	7.545
319.15	7.474
339.65	7.412
357.15	7.334

Table 5.4 Characteristic Volumes, V_o, for Ethylbenzene.

	$10^5 V_o (m^3.mol^{-1})$		
T(K)	o-xylene	m-xylene	p-xylene
308.15	7.9880	7.8714	7.9521
318.15	7.9473	7.8098	7.9185
337.65	7.8826	7.7739	7.8586
360.15	7.8282	7.7292	7.8178

Table 5.5 Characteristic Volumes, V_o, for the three isomers, o-xylene, m-xylene and p-xylene.

conductivity data are consistent with this result, we have employed the viscosity data of Collings and McLaughlin [173] to evaluate η^* along isotherms at 311.55K and 323.15K. Values for V_o for these temperatures have been interpolated from the value quoted earlier. Figure 5.x contains a plot of η^* versus (V/V_o) for these two isotherms, and it can be seen that the data conforms to a single curve within the uncertainty of the viscosity, which is estimated to be one of $\pm$2.0%.

An analogous treatment may be applied to the self-diffusion coefficient data of McCool and Woolf [169], for the two isotherms at 313.2K and 328.2K. In this case, we employ equation (5.26) for a test of the hypothesis that:

$$D^* = F_D(V/V_o) \qquad (5.74)$$

Again, the values of V_o have been interpolated from the analysis of the thermal conductivity data. Figure 5.xi contains a plot of D^* versus (V/V_o) for the two isotherms, and shows that the data fall on a single curve within their estimated uncertainty of $\pm$4.0%.

5.6.6 Ethylbenzene.

Earlier, measurements have been performed on benzene [196], and toluene [197] with the transient hot-wire instrument. The density dependence of the thermal conductivity was successfully applied to these two simple aromatic liquids.

In order to establish whether such a correlating scheme is equally applicable to accurately measured thermal conductivity data on ethylbenzene, which is a disk-shaped molecule, a similar approach of representing the density dependence was followed [175]. We first used the thermal conductivity and density data to construct lines of λ^* versus $\ell n(V)$ for each isotherm. Therefore, we adopted a reference value for V_o at 304.65K of:

$$V_o(304.65K) = 75.45 \times 10^{-6}\ m^3 mol^{-1} \qquad (5.75)$$

According to equation (5.62), it should be possible to superimpose the lines of λ^* against $\ell n(V)$ for other isotherms upon that for the reference isotherm, by a shift on the $\ell n(V)$ axis only; the amount of the shift yields V_o at each temperature. We have applied this analysis to all of the data within the range of the experimental densities ($p \leq$ 50MPa). Table 5.4 lists the V_o values for each isotherm. The single curve resulting from this process, as depicted in figure 5.xii, has been represented by the equation:

$$\ell n\ \lambda^* = 4.7533 - 2.1178 \ell n(V/V_o) \qquad (5.76)$$

and figure 5.xiii depicts a plot of the deviations of the experimental data from this fit. It can be seen that the thermal conductivity data of ethylbenzene are represented within a maximum deviation of $\pm$0.86%, with a standard deviation of $\pm$0.23%. These values exceed the estimated uncertainty in the thermal conductivity data alone, and it is possible to discern systematic deviations from a universal correlation, particularly at the highest temperature. Table 5.6 lists the

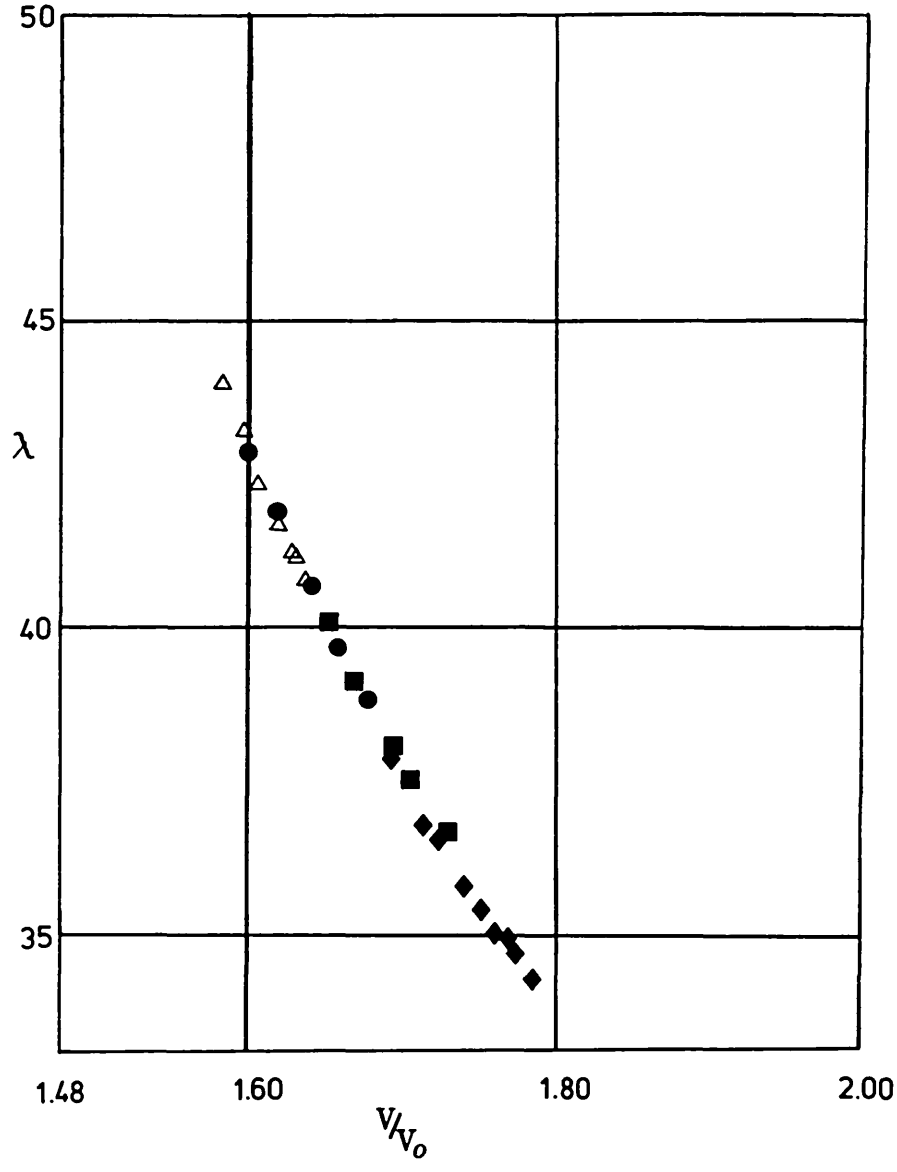


Figure 5.xii. The thermal conductivity ratio, λ, for ethylbenzene, as a function of reduced molar volume.

△ 304.65 K; ● 319.15 K; ■ 339.65 K; ◆ 357.15 K.

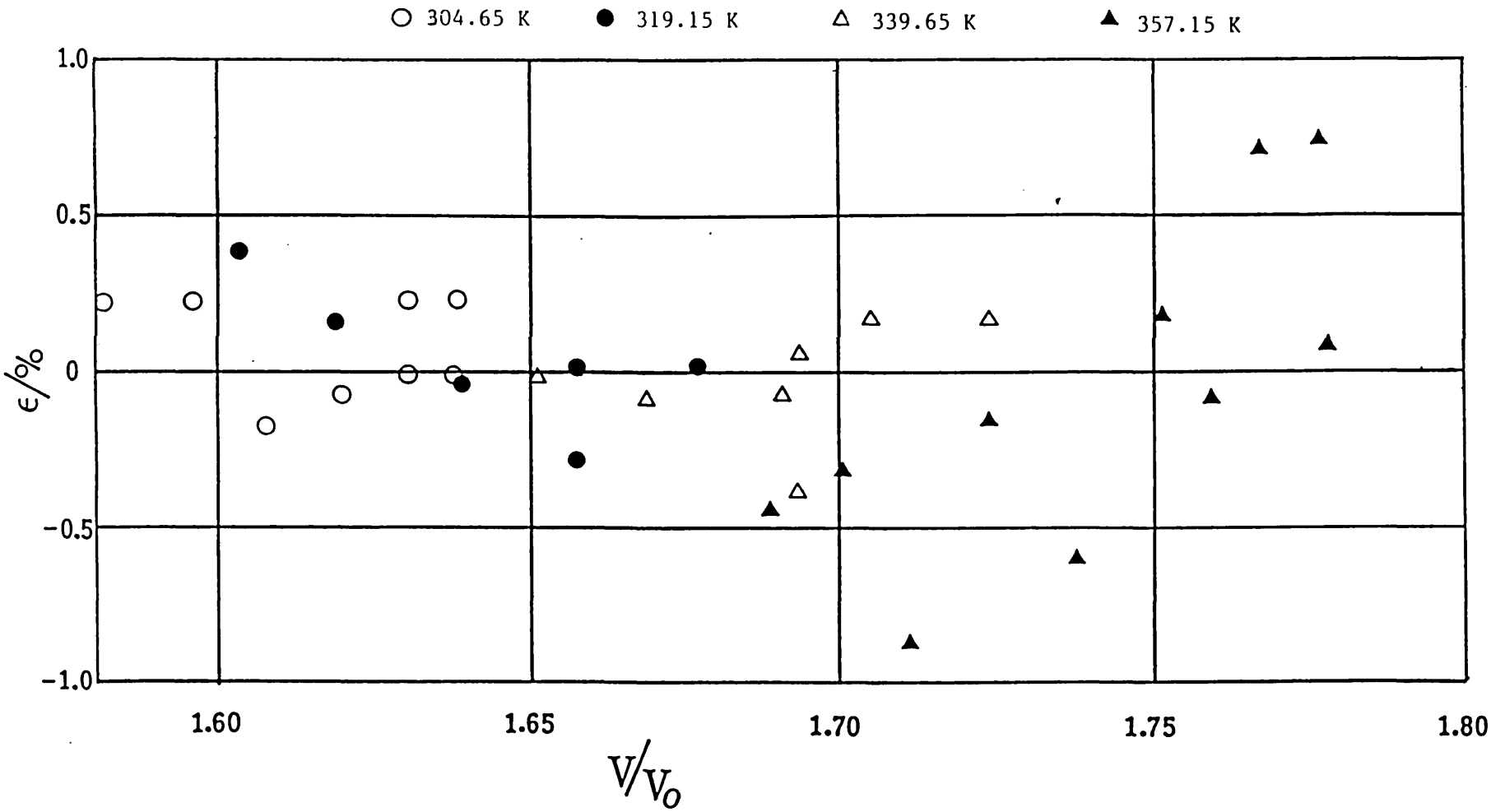


Figure 5.xiii. Deviation of experimental thermal conductivity data for ethylbenzene from the correlation of equation (5.76). $\epsilon = 100(\lambda_{exp} - \lambda_{corr})/\lambda_{corr}$.

T(K)	a_0	a_1	Deviation (%)
304.65	4.3112	2.1409	±0.26
319.15	4.3311	2.2118	±0.18
339.65	4.2879	2.0666	±0.12
357.15	4.2278	1.8965	±0.35

Table 5.6 Coefficients of the Correlation of Equation (5.61) for Individual Isotherms of Ethylbenzene.

coefficients of the correlation of equation (5.61) for individual isotherms of ethylbenzene.

5.6.7 The Xylene Isomers.

A similar study [70] was made on the representation of the density dependence of the thermal conductivity on the three xylene isomers, ortho-xylene, meta-xylene and para-xylene, which are essentially flat disk-shaped molecules. A reference value of V_o for o-xylene at T = 308.15K was adopted:

$$V_o(308.15K) = 79.88 \times 10^{-6}\ m^3 mol^{-1} \qquad (5.77)$$

which allows the experimental thermal conductivity for the other isomers and their measured isotherms, to be employed to determine the optimum values of the coefficients a_o and a_1 of the general equation (5.61). The coefficients are listed in table 5.5. In this way, the optimum correlation has been determined as:

$$\lambda^* = 4.675 - 2.234 \ell n(V/V_o(I)) \qquad (5.78)$$

for all the isotherms of xylene, because this study included the other two isotherms. Figure 5.xiv shows the resultant single curve for o-xylene only.

Figure 5.xv displays the deviations of all the experimental thermal conductivity data for the three xylenes, (within the range of

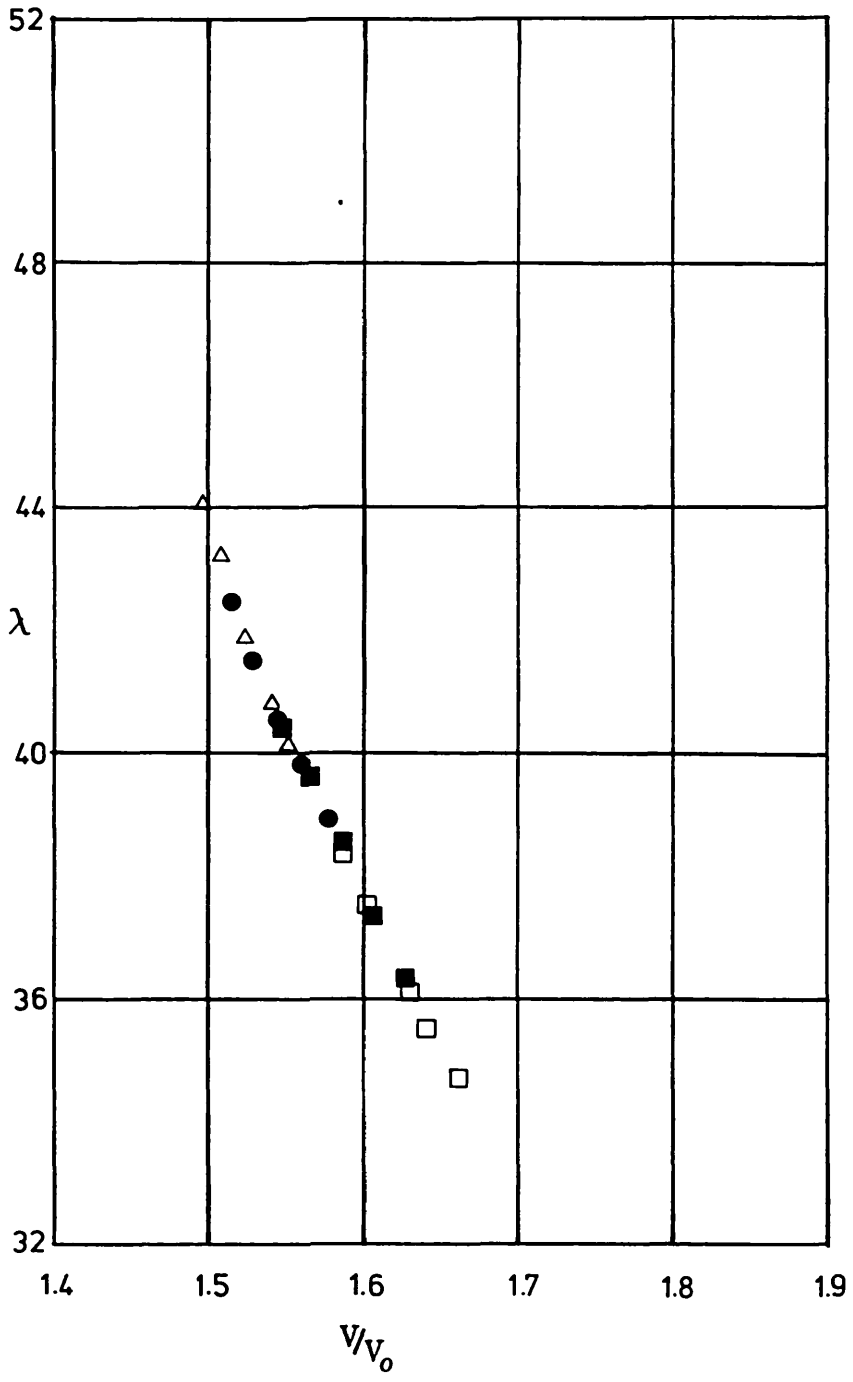
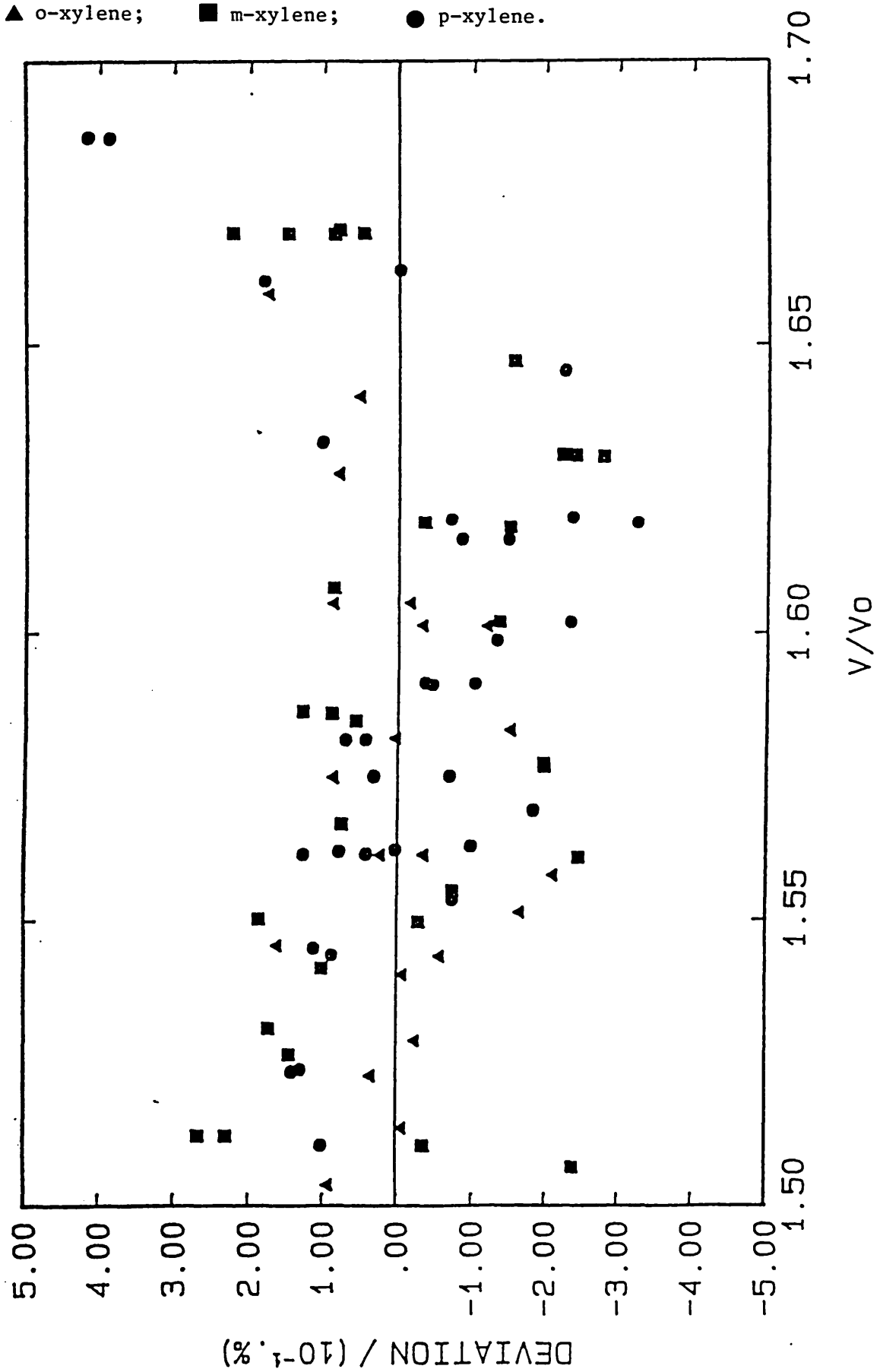


Figure 5.xiv. The thermal conductivity ratio, λ, for o-xylene as a function of reduced molar volume.

△ 308.15 K; ● 318.15 K; ■ 337.65 K; □ 360.15 K.

Figure 5.xv. Deviations of the thermal conductivity of the three isomers of xylene from the correlation of equation (5.78).

▲ o-xylene; ■ m-xylene; ● p-xylene.



the available density data) from the universal correlation of equation (5.61). It can be seen that the maximum deviation amounts to no more than $\pm$0.4%, while the standard deviation is one of $\pm$0.15%. This result provides ample confirmation of the universality of equation (5.61) among the three xylene isomers and, as usual, [195], permits ready and reliable interpolation and extrapolation of the present thermal conductivity data to other ranges of thermodynamic states.



Table 5.7 lists the coefficients of equation (5.61) for the individual fluids studied in this work.

5.7 The Universal Correlation.

A further feature of the results for the rough hard-sphere model may be utilized to extend the correlation procedure. It was mentioned in 5.5.4 that whereas the translational and internal contributions to the thermal conductivity of the rough hard-sphere fluid depended quite strongly on the value of K, the total thermal conductivity is almost independent of it. This result implies that the reduced thermal conductivity defined by equation (5.54) may be a nearly universal function of V/V_0 among the hydrocarbons studied. Again, this hypothesis is similar, but not identical, to the one made earlier [179].

In order to confirm the hypothesis, the curve of λ^* against $\ell n(V/V_0)$ for n-hexane at 307K was first adopted as a reference together with its corresponding value of V_0. Subsequently, the superimposition

of plots of λ^* versus ℓnV for other liquid hydrocarbons have been made, at several different temperatures, upon a reference curve along the ℓnV axis only.

The single curve resulting from the superposition process for each liquid studied earlier [184] has been represented by the single equation

$$\ell n\ \lambda^* = 4.8991 - 2.2595\ell n(V/V_o) \qquad (5.79)$$

with the coefficients a_o and a_1 securing the optimum representation of all the data. The success of this correlation procedure has the immediate advantage, that it allows the thermal conductivity to be evaluated outside the range of densities covered by direct measurement. In addition to that, it is possible to predict the thermal conductivity of any of the studied or correlated liquids, along an isotherm, from just one measurement at a particular density, for example, the density at saturation. It is worthwhile to add here, that the precision of these predictions should be only slightly inferior to that of direct measurements. Also, it should be mentioned that the temperature dependence of V_o follows a smooth curve, which lies very close to that obtained from the analysis of viscosity data, carried out by Dymond based upon the rough hard-sphere model.

These liquids, which have been included to obtain the correlation in equation (5.79), ranged from the simple straight chain molecules, such as n-propane to n-tridecane, the branched 2,2,4-trimethylpentane,

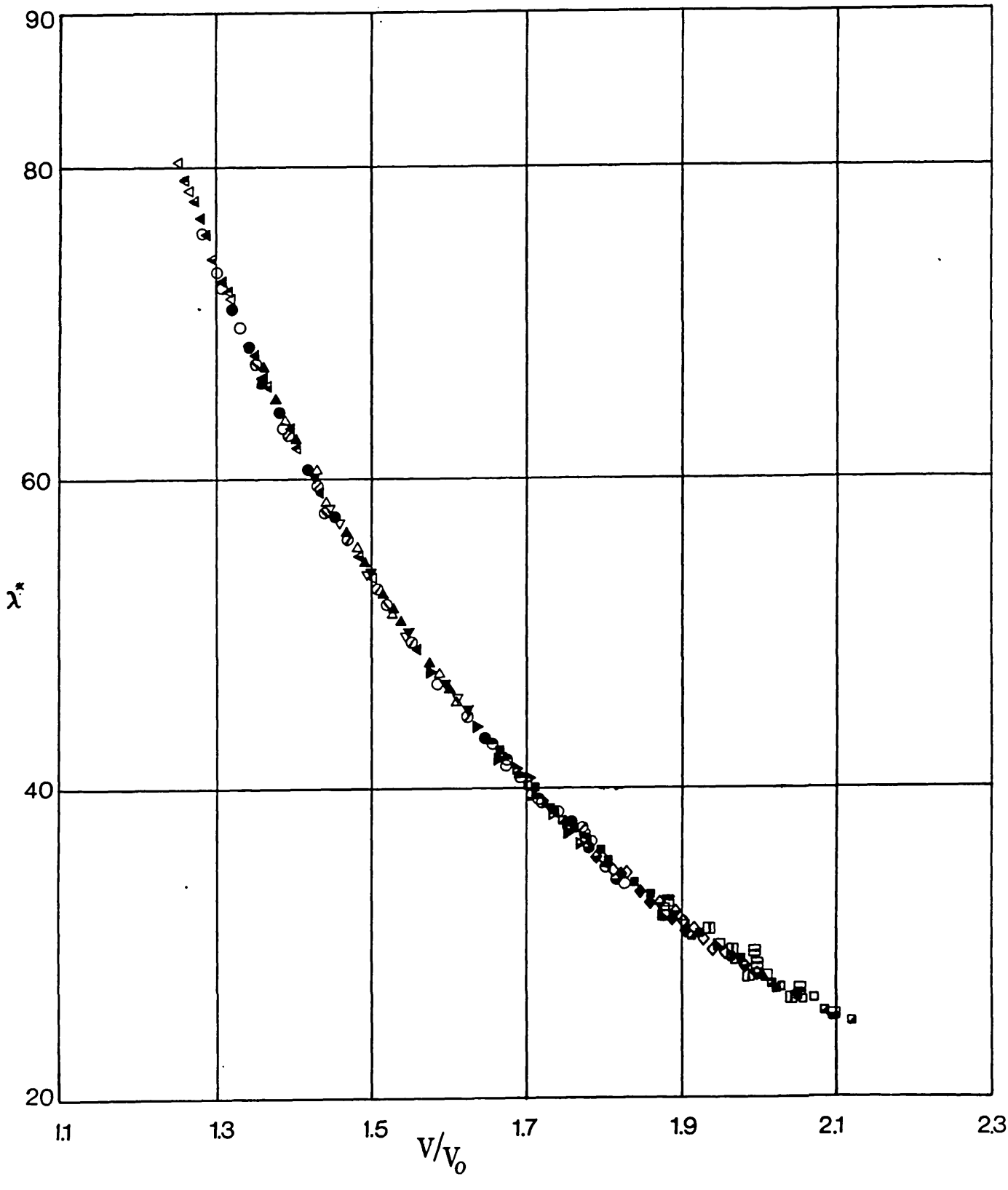
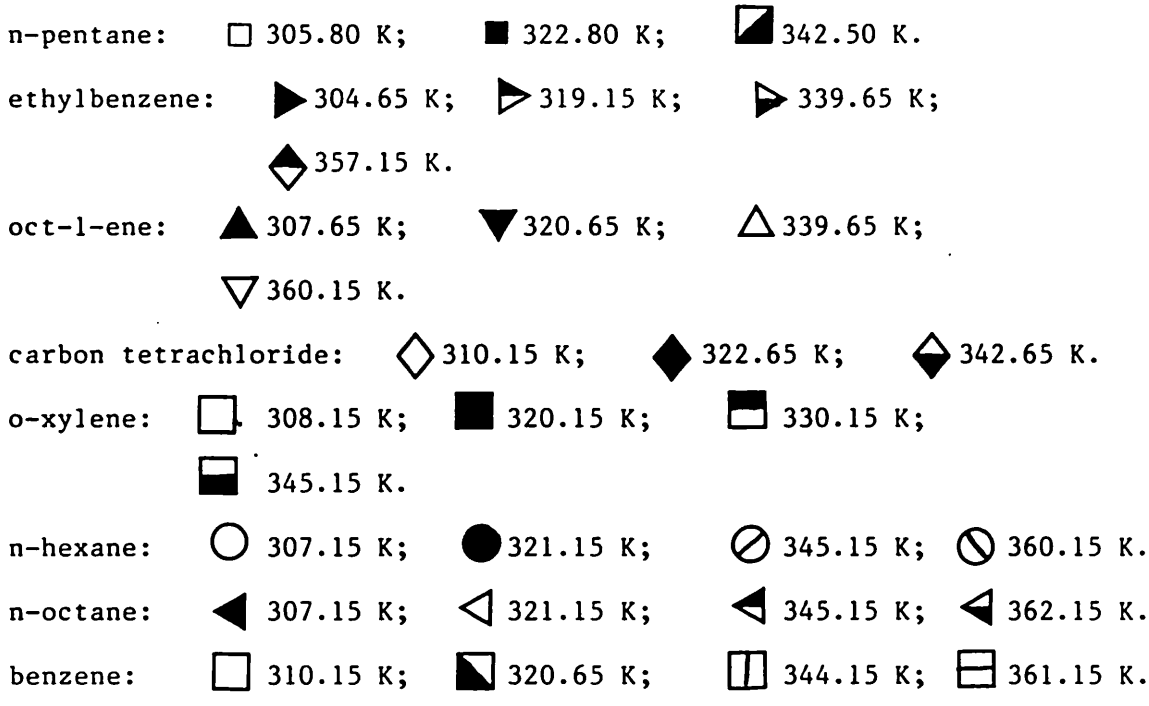


Figure 5.xvi. The thermal conductivity ratio, λ, as a function of reduced molar volume, for fluids studied in this work, in addition to some previously studied [71].

Liquid	a_0	a_1	Standard Deviation (%)
n-pentane	4.6022	2.0602	±1.30
oct-1-ene	4.9339	2.3458	±0.40
carbon tetrachloride	4.4294	2.2162	±0.10
ethylbenzene	4.7533	2.1178	±0.23
o-xylene m-xylene p-xylene	4.6750	2.2340	±0.15

Table 5.7 Coefficients of the Correlation of Equation (5.61) for Individual Liquids.

Figure 5.xvi. The thermal conductivity ratio, λ^*, for liquids studied in this work, as a function of reduced molar volume, V/V_o.
(Some points have been omitted for clarity.)
This plot contains data from previous work [71] for completeness.



and finally benzene and cyclohexane. The new liquids studied in this work was a logical continuation for extending the range and diversity of the systems studied. The liquids studied here, include n-pentane, carbon tetrachloride, oct-1-ene, ethylbenzene, and ortho-xylene. It is worthwhile noting here that all these measurements have an accuracy commensurate with the ones previous set. Figure 5.xvi displays the result of this superimposition of all the data points of all the systems studied, including the initial set that was instrumental in obtaining the universal correlation (some data points have been omitted for clarity). The striking feature of this procedure, is that the data points lie in a smooth curve, considering the fact that the systems investigated, lie within a wide density and temperature range, and that the molecular structures vary from the spherical for carbon tetrachloride, to the straight chain for n-pentane, and disk-shaped for ethylbenzene.

New values of V_o were adopted in order to enable the superimposition of the experimental thermal conductivity data, obtained for n-pentane, oct-1-ene, carbon tetrachloride, ethylbenzene and o-xylene, onto the previously derived correlation (equation 5.79), obtained from a regression analysis.

This equation is of the same form as those employed earlier, but a superscript 'u' on V_o is added, to signify that the basis for the derivation of the characteristic volume of each liquid for each isotherm, is somewhat different from that which was derived in the earlier sections. So that now we write:

Figure 5.xvii. Deviations of the experimental thermal conductivity data from the correlation of equation (5.80). The symbols used here are as in figure 5.xvi.

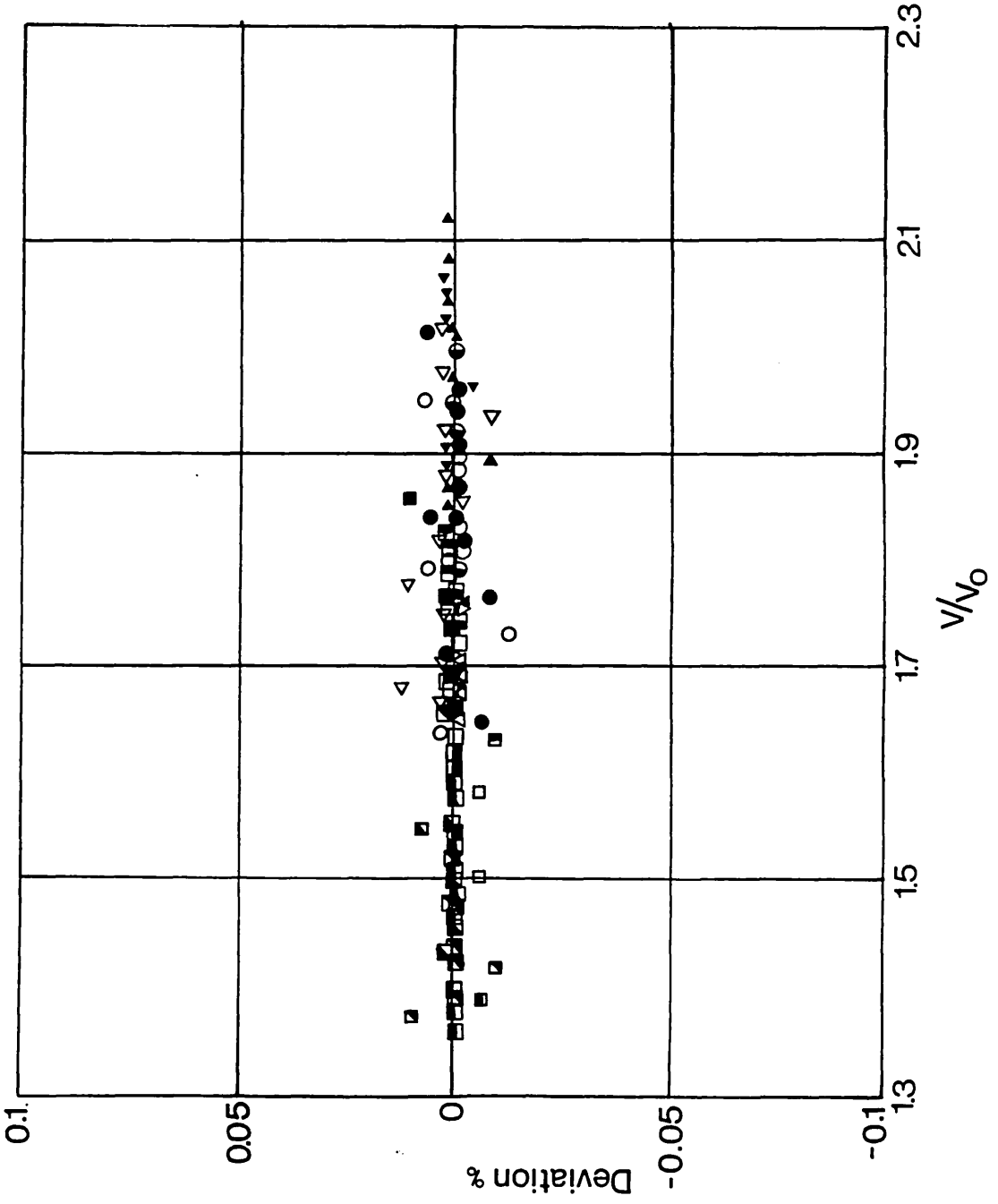


Table 5.8.

The Characteristic Volumes, V_o^u, for the Correlation of Equation (5.80) for All the Liquids Studied.

n-pentane

T(K)	305.80	322.80	342.50
$V_o^u x10^6$ m^3 mol^{-1}	57.50	57.13	56.80

oct-1-ene

T(K)	307.65	320.65	344.15	360.15
$V_o^u x10^6$	92.22	92.02	91.96	91.58

carbon tetrachloride

T(K)	310.15	322.65	342.65
$V_o^u x10^6$	51.04	50.69	50.50

ethylbenzene

T(K)	304.65	319.15	339.65	357.15
$V_o^u x10^6$	72.87	72.25	71.77	71.15

Table 5.8 (continued).

o-xylene

T(K)	308.15	318.15	337.65	360.15
$V_o^u \times 10^6$	71.56	71.02	70.95	70.45

$$\ell n\ \lambda^{*} = a_0 + a_1 \ell n\ (V/V_0^u) \qquad (5.80)$$

These values have been derived by employing the n-hexane curve at 307 K as the reference, and subsequently, fitting all the data for each liquid and its associated isotherms, onto that curve, simply by shifting along the ℓnV axis. Therefore, all the derived V_0 values are relative to the selected value for n-hexane, and should not be regarded as absolute. The values of V_0^u for each fluid for each experimental temperature are listed in table 5.8. Figure 5.xvii shows the deviation of the experimental thermal conductivity from the correlation of equation (5.80) Though the maximum deviation of some individual points from the best curve amounts to $\pm$0.05 %, and the standard deviation is about $\pm$0.01%, it is apparent that this near universality can provide a very good estimate of the thermal conductivity for the systems of interest. These deviations are in excess of the estimated uncertainty of the density and the thermal conductivity, and are somewhat larger than the corresponding values, when each liquid is considered on its own. The fact that it is possible to correlate all the data of the liquids studied with a single equation, with an associated accuracy of $\pm$0.1%, is remarkable, in view of the wide ranging thermophysical conditions.

The derived characteristic volume, V_0^u, of n-pentane has been represented in a plot of the number of carbon atoms of normal alkanes, against the characteristic molar volume. As can be seen in figure 5.xviii, the data for n-pentane fits well in the curve that was used earlier by Li [71] to illustrate the trend of the characteristic volume

Figure 5.xviii.

The characteristic volume (V_o^u) as a function of the number of carbon atoms of a series of normal alkanes

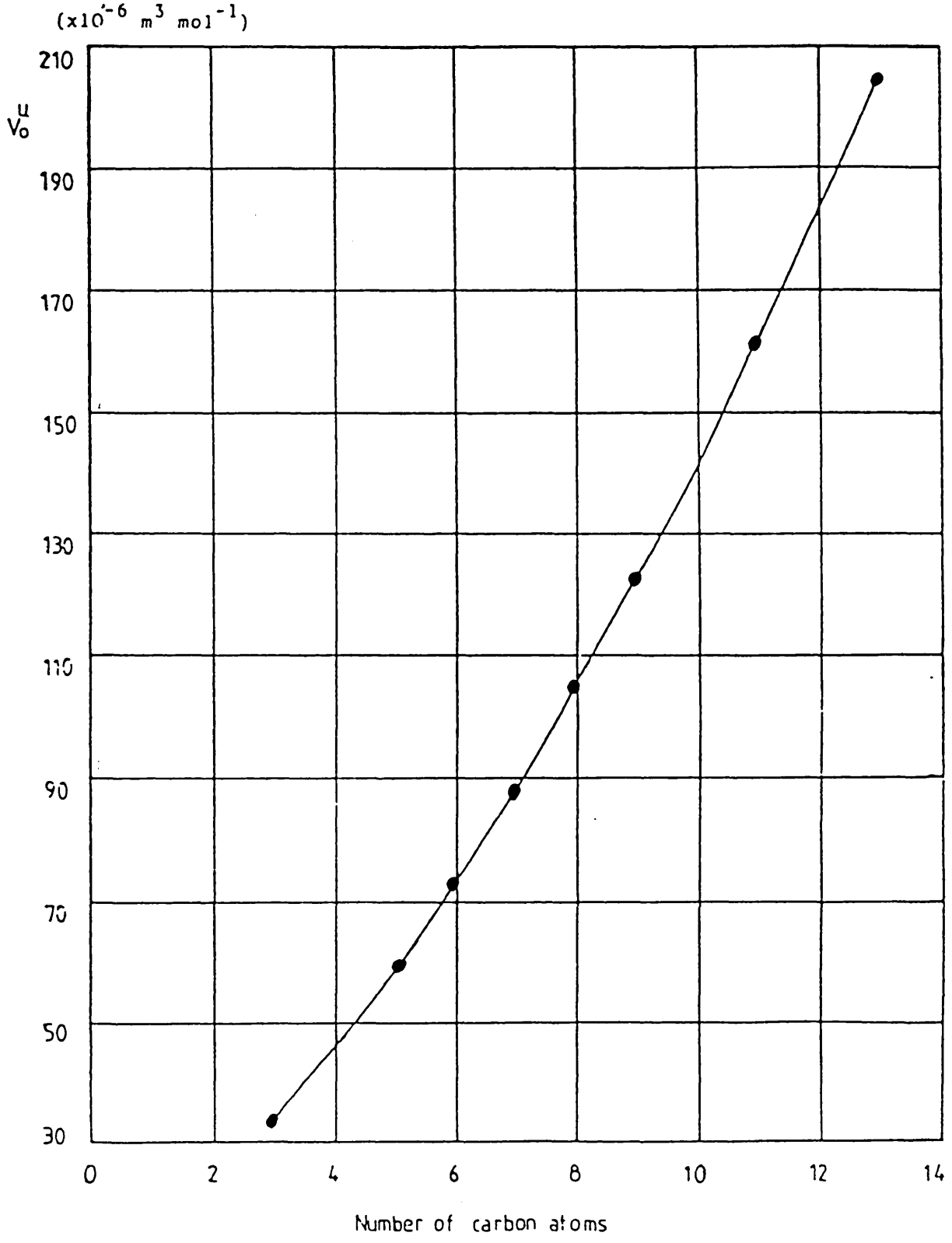


Figure 5.xix. The characteristic volume V_o^u for liquids studied in this work.

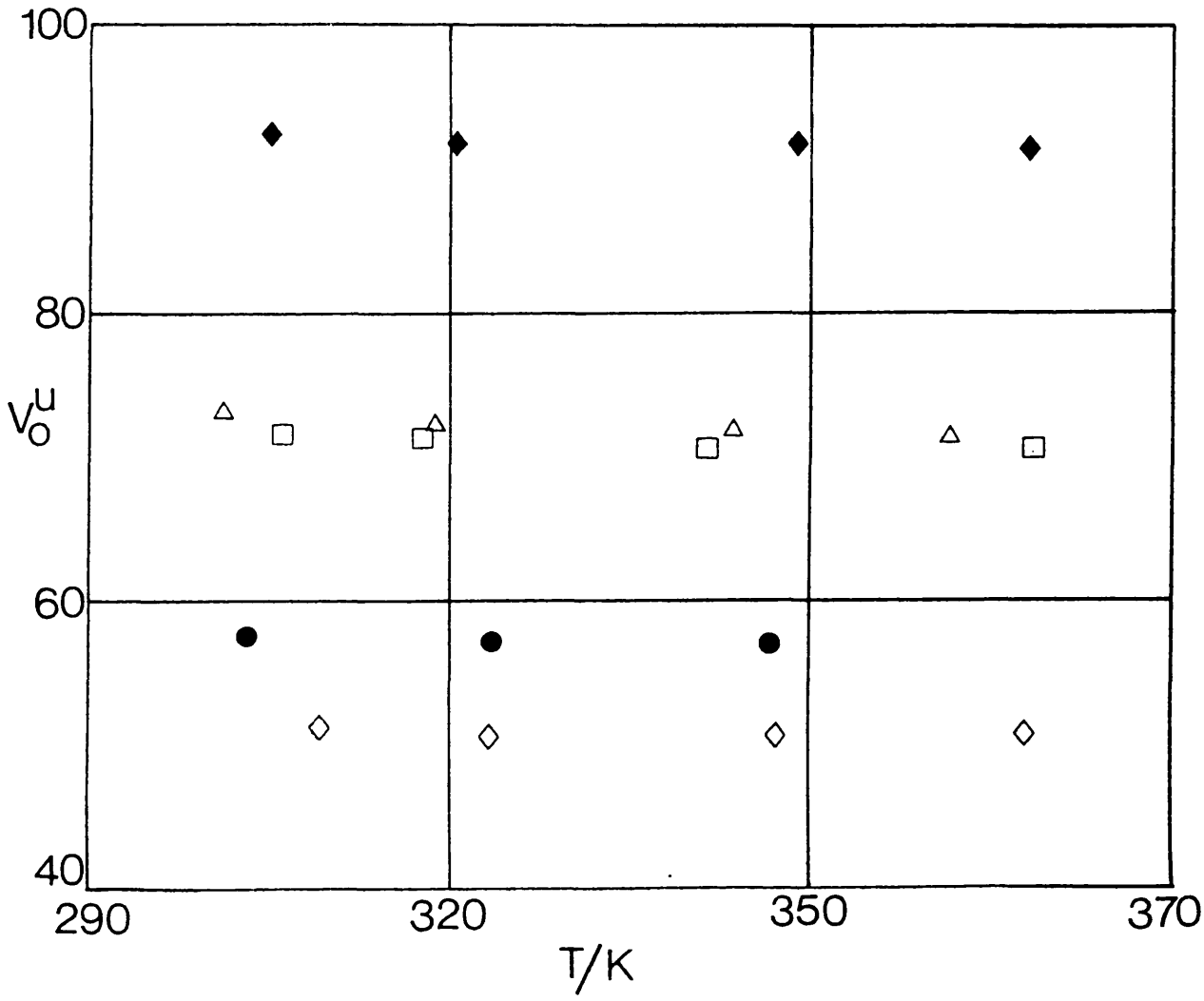
△ Ethylbenzene

● n-pentane

◆ Oct-1-ene

□ o-xylene

◇ Carbon tetrachloride



increasing with molecular weight.

It has been shown that the density dependence of the thermal conductivity of the fluids that have been included in this work, can be represented by a single universal equation, valid over a wide range of thermodynamic states. The form of the representation has been based upon a rough hard-sphere model, which contains many of the principal features of real polyatomic fluids. There is some evidence that such a model could provide a means of unifying the various transport properties of dense polyatomic fluids.

Further work is required to secure a means of embracing a much wider range of fluids, so as to make the process of predicting the thermal conductivity more powerful. The near universality of the relationship of the reduced thermal conductivity to the reduced characteristic molar volume, provides a reliable means of estimating the thermal conductivity of the liquids studied here, since all that is needed, is the characteristic molar volume V_o^u for the required temperature. This is easily obtained from a measurement of the thermal conductivity at one density at the temperature of interest. If this is not possible, then an interpolation or a modest extrapolation of the V_o^u value can be made by using the data given in table 5.8. Figure 5.xix illustrates the characteristic molar volume for each liquid as a function of temperature.

An alternative method of obtaining V_o^u would be from viscosity data, if the thermal conductivity has not been measured, as mentioned

for carbon tetrachloride, but at the expense of inferior accuracy. In view of the restricted range of the volumetric properties available for some of the fluids studied, this universal correlation could be systematically improved by extending the density range, so as to include a greater number of points in the statistical evaluations.

Chapter 6.

Conclusions.

A new instrument for the measurement of the thermal conductivity of electrically conducting liquids for use at the temperature range of 30° to 90°C and pressures up to 500 MPa has been constructed. This instrument is based upon the firmly established transient hot-wire technique, which has been suitably adapted to the special operating conditions that are demanded by the use of electrically conducting fluids. It was shown that the instrument was capable of operating with an accuracy of better than $\pm$0.3%, in common with the transient hot-wire instruments employed for gases and electrically insulating liquids. It is confidently believed that the thermal conductivity data obtained with this instrument, are the most accurate available at present. It is therefore hoped and recommended that further measurements on water and new measurements on saline solutions be undertaken to complement the high quality data accumulated so far with this instrument. The high accuracy of the experimental data obtained for the thermal conductivity of water, means that the results can be used in establishing a reference standard, and the possible calibration of other thermal conductivity instruments currently being constructed in various laboratories.

Some minor, but significant improvements have been implemented in

the thermal conductivity instrument for electrically insulating liquids. This apparatus continues to provide new thermal conductivity data for liquids of interest. This continuous quest for accurate data acquisition is fundamental in providing a firm foundation upon which molecular transport properties and theories can be modelled and tested with.

The preceding chapter dealt with the discussion of the Van der Waals theory, and its application to the smooth hard-sphere model, which in turn has been heurestically extended by Chandler and Dahler to encompass the rough hard-sphere model. The rough hard-sphere theory has been shown to provide a remarkbly successful means of predicting the thermal conductivity, as well as the thermal diffusivity and viscosity of dense fluids, over a wide range of thermodynamic states. This can be done by employing correlations that have been deduced from experimental results of one of the transport properties. This correlating scheme, can be reliably used for the interpolation and modest extrapolation of the limited - though highly accurate - available experimental data. Thus, the range of densities and temperatures can be extended to include conditions that have not been studied for various reasons, such as the limited time available in performing the measurements, or some physical constraints that are imposed on the experimental conditions, which are beyond the design capability of the instument.

It is imperative that the thermal conductivity instrument continue to yield highly accurate data of fluids. This is essential in

order to provide a rigorous means of testing the various theoretical approaches, such as the rough hard-sphere model, to explain the transport properties of real dense fluid systems. Significant progress is still needed to fully explain the transport properties of dense hard-sphere fluids with the same conciseness that is available for dilute monatomic fluids.

A P P E N D I C E S

Appendix 1

A1.1 Introduction.

A new method of operation of an automatic Wheatstone bridge for use in conjunction with a transient hot-wire thermal conductivity instrument, has been employed for the measurement of the thermal conductivity of electrically insulating and electrically conducting liquids. The new arrangement provides greater flexibility of operation by replacing the resistance network of previous versions [14,71] with a digital to analogue converter.

Figure A1.i contains a schematic diagram of the new bridge arrangement. The symbols R_L and R_S represent the long and short wires of the thermal conductivity cells respectively. The left-hand arm of the bridge is identical with that of previous arrangements [14,71]. However, the right-hand arms of the bridge used earlier have been replaced by a different arrangement in which V_E is a digital to analogue source of voltage, which can be arranged to provide preset values accurately to a programmed sequence. Elements R_9 and R_{10} are included in the circuit merely to simulate the input impedance of the null-detector (comparator) connected across A-B.

For details of bridge operation, see section §.3.8.

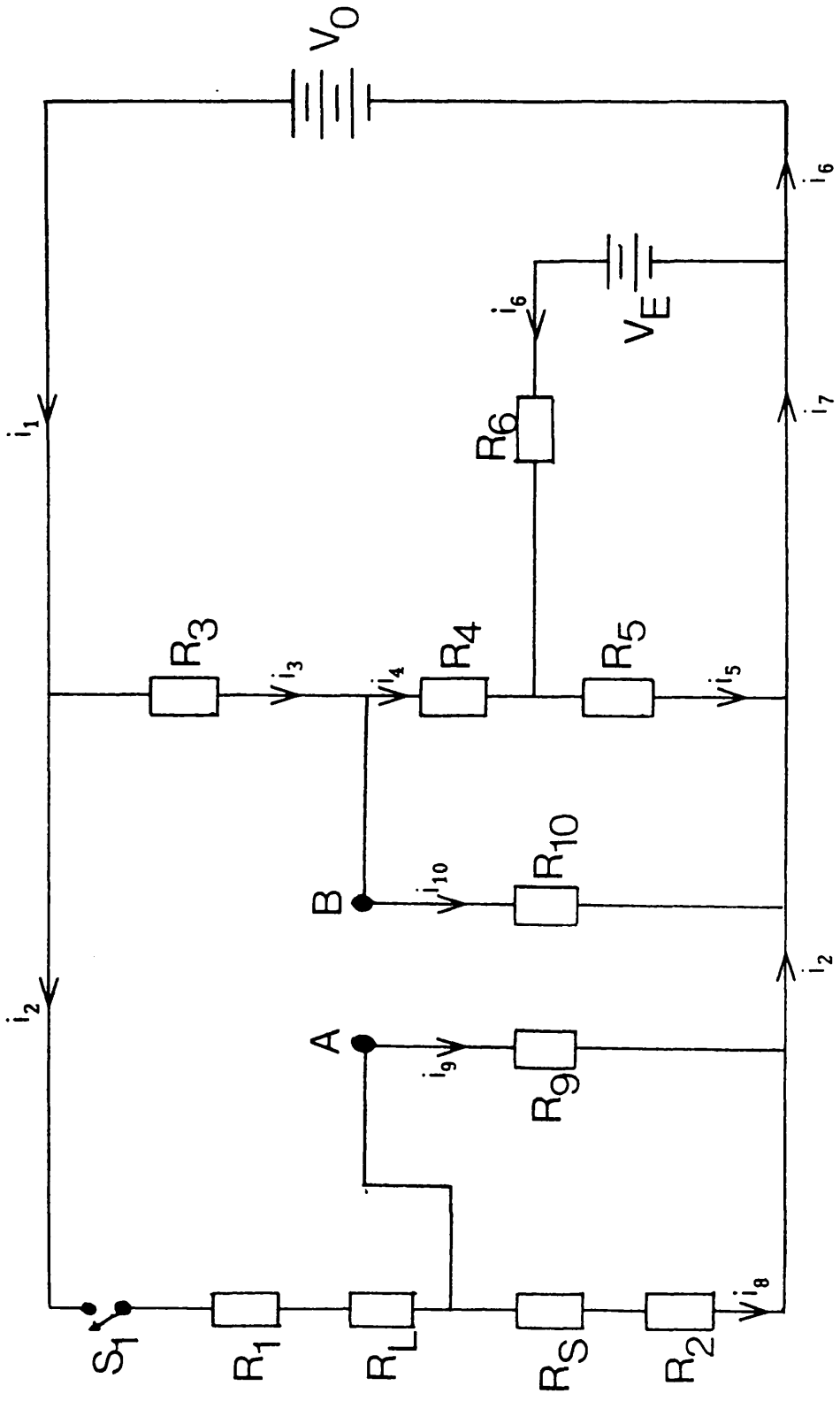


Figure A1.i. Diagram of the new automatic Wheatstone bridge, depicting the currents flowing in the circuits.

A1.2 Circuit Analysis in Detail.

With reference to figure A1.i, the following equations can be established:

$$i_1 = i_2 + i_3 \tag{A1}$$

$$i_1 = i_7 - i_6 \tag{A2}$$

$$i_2 = i_8 + i_9 \tag{A3}$$

$$i_3 = i_4 + i_{10} \tag{A4}$$

$$i_5 = i_6 + i_4 \tag{A5}$$

$$i_7 = i_5 + i_{11} \tag{A6}$$

$$i_{11} = i_2 + i_{10} \tag{A7}$$

$$V_o = i_3R_3 + i_4R_4 + i_5R_5 \tag{A8}$$

$$V_o = i_2(R_1 + R_L) + i_8(R_2 + R_S) \tag{A9}$$

$$V_E = i_6R_6 + i_5R_5 \tag{A10}$$

$$V_o = i_3R_{10} + i_{10}R_{10} \tag{A11}$$

These equations may be solved to give the across A-B as follows:

$$\frac{V_{AB}}{V_o} = \frac{R_1 + R_L + \dfrac{(R_2 + R_S)(R_1 + R_L)}{R_9}}{(R_1 + R_L + R_2 + R_S) + \dfrac{(R_2 + R_S)(R_1 + R_L)}{R_9}}$$

$$- \left[\left[\frac{R_3}{R_5} + \frac{R_3}{R_6}\right]\left[1 + \frac{R_5R_6}{(R_5 + R_6)(R_3 + R_{10})} + \frac{(R_3+R_4)}{(R_3+R_{10})}\right]\right]$$

$$- \frac{\dfrac{V_E}{V_o}\cdot\dfrac{R_3}{R_6}\left[1 - \dfrac{R_3}{(R_3+R_{10})}\left\{1 + \dfrac{2(R_3+R_4)(R_5+R_6)}{R_5R_6}\right\}\right]}{\left[1 + \dfrac{(R_5+R_6)(R_3+R_{10})}{R_5R_6} + \dfrac{(R_5+R_6)}{R_5R_6}\cdot\dfrac{R_3^2}{(R_3+R_{10})}\right]}$$

(A12)

At balance, $V_{AB} = 0$, this leads to the result:

$$\frac{R_1 + R_L + \dfrac{(R_2 + R_S)(R_1 + R_L)}{R_9}}{R_1+R_2+R_L+R_s+\dfrac{(R_2 + R_S)(R_1 + R_L)}{R_9}} =$$

$$\frac{\left[\frac{R_3}{R_5}+\frac{R_3}{R_6}\right]\left[1+\frac{R_5R_6}{(R_5+R_6)(R_3+R_{10})}+\frac{R_3+R_4}{R_3+R_{10}}\right]}{\left[1+\frac{(R_5+R_6)(R_3+R_4)}{R_5R_6}+\frac{R_5+R_6}{R_5R_6}\cdot\frac{R_3^2}{(R_3+R_{10})}\right]}$$

$$-\frac{\frac{V_E}{V_o}\cdot\frac{R_3}{R_6}\left[1+\frac{R_3}{(R_5+R_6)(R_3+R_{10})}\left\{1+\frac{2(R_3+R_4)(R_5+R_6)}{R_5R_6}\right\}\right]}{\left[1+\frac{(R_5+R_6)(R_3+R_4)}{R_5R_6}+\frac{R_5+R_6}{R_5R_6}\cdot\frac{R_3^2}{(R_3+R_{10})}\right]}$$

(A13)

Solving this equation for the resistance difference of wires, $R_L - R_S$, we obtain:

$$R_L - R_S =$$

$$\frac{\left[\frac{R_L}{R_S}-1\right]\left[CR_2-(1-C)R_1-(1-C)\frac{(R_1+R_L)(R_2+R_L)}{R_9}\right]}{\frac{R_L}{R_S}(1-C)-C}$$

(A14)

where

$$C = \frac{\left[\frac{R_3}{R_5} + \frac{R_3}{R_6}\right] - \frac{V_E}{V_o}\cdot\frac{R_3}{R_6}}{\left[1 + \left[\frac{R_3}{R_5} + \frac{R_4}{R_5}\right]\left[1 + \frac{R_5}{R_6}\right]\right]} \qquad \text{(A15)}$$

A1.3 Leakage Currents and Their Effects.

A phenomenon has been observed in the thermal conductivity instrument for electrically insulating liquids, and this had a significant effect on the measurements being made with the instrument. An attempt to explain the phenomenon is thereby given. Leakage between the wires and the cell walls can occur in two ways: By conduction through the liquid itself, or possibly by conduction through contaminated insulatiog cones at the ends of the hot-wires. In either case, some current is taken from one or both arms of the bridge, into the ground circuit, thereby disturbing the balance of the bridge.

The circuit of the bridge during operation is shown in figure A1.ii. The power supply, V_o is centre tapped and decoupled to earth by the resistors, R_1 to R_5 , and capacitors C. The cell walls are also returned to the same earth point. R_{LK} represents the spurious leakage resistances.

It can be seen that if the leakage currents from the top and bottom arms of the bridge are similar, then the symmetry and balance are not greatly affected. But, as the resistances of the wires and the

bridge conditions change during an experiment, the leakage current may also change, and the relative effect on the balance point may be more or less significant. Such conditions would give rise to a curvature of the deviation plot.

To rectify this observation, a bias battery, V_B, was introduced into the earth circuit, so that the potential difference between the wires and the cell walls, could be varied. (A capacitor was included across the battery, to ensure high frequency noise decoupling.) These conditions were tried:

(a) Battery voltage = 0 Volts.

Result was a slight curvature.

(b) Battery voltage = +9 Volts.

Severe curvature was obtained. Steady state values show inflexion. Therefore, leakage current having a dynamic effect on balance.

(c) Battery voltage = -9 Volts.

Much reduced curvature. Steady state values linear,but shifted.

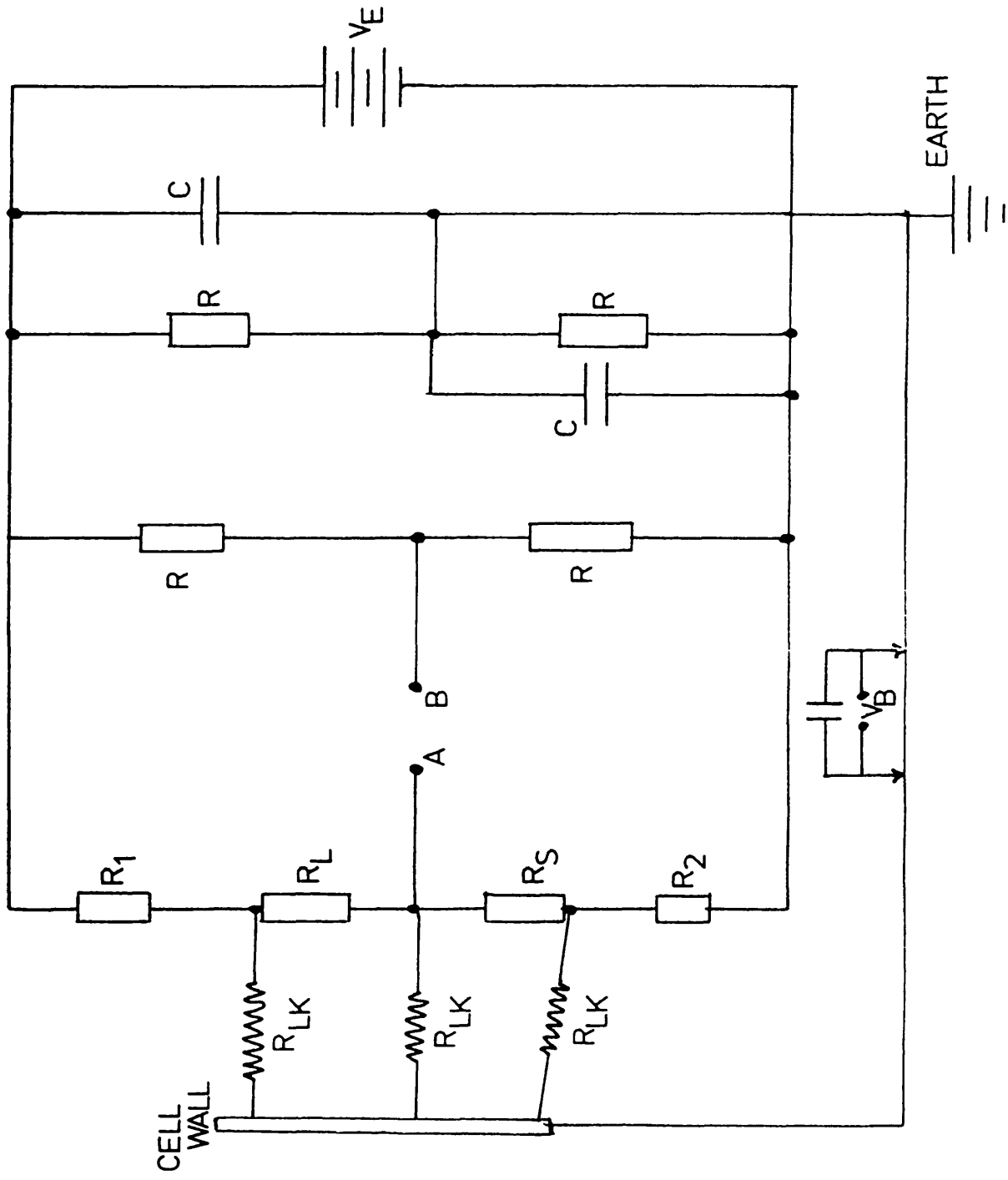
Condition (c) would appear to be the best for the transient run, as a deliberate leakage current is introduced at a level which remains substantially constant throughout the experiment, and therefore has little effect on the slope.

To get the best reading of the steady state condition, it might be

best to remove the battery, and allow the cell to find its own bias level, at which point no current would be flowing out of the bridge into the earth circuit. The maximum allowable leakage current is probably that at which the heating effect in the wire is significantly compromised in terms of the accuracy of the experiment.

****

Figure Al.ii. An illustration of the leakage currents encountered in the bridge for electrically insulating liquids, from the bridge to the cell walls.



Appendix 2.

A2.1 Introduction.

The bridge balance equations derived in section § 3.8, assumed that the lead resistances did not contribute significantly to the resistance difference, used to evaluate the temperature rise of the tantalum wires, employed in the transient hot-wire instrument for the measurement of the thermal conductivity of electrically conducting liquids.

It was necessary to reanalyse the derivation of the bridge balance equations in order to obtain the correct thermal conductivity for the test liquid. It was found that the lead resistances in the circuit had a profound effect in the evaluation of the thermal conductivity, because the calculation of the temperature rise is very dependent on the resistance of the difference of the long and short wires, $R_L - R_S$, and each contributing element in the circuit had, therefore, to be taken into consideration in the calculations.

Figure A2.i presents a schematic diagram of the various resistive elements that form part of the bridge circuit. The various components had each to be ascribed a suitable symbol to make it easier to analyse the problem.

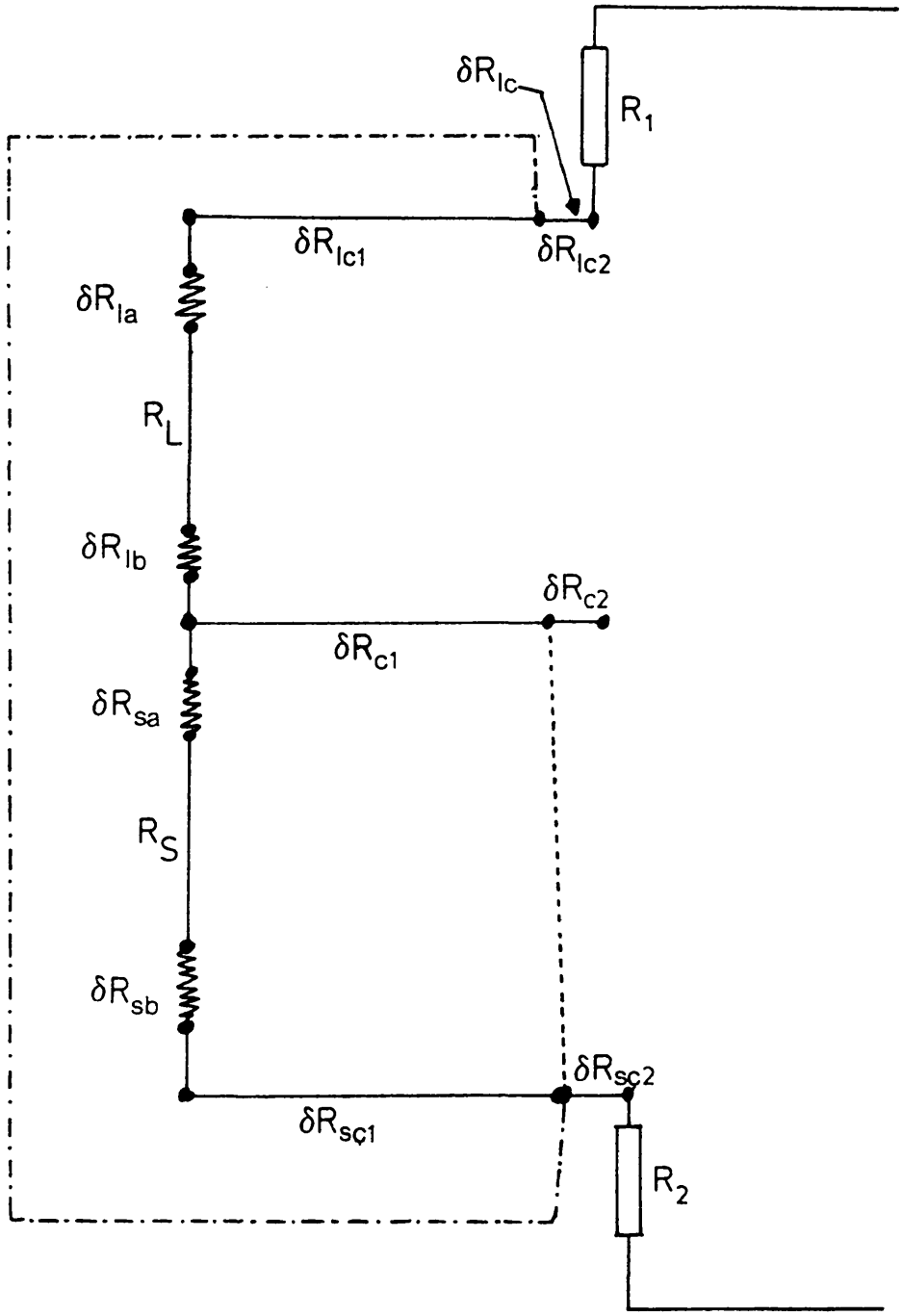


Figure A2.i. The bridge circuit with the various resistive elements.

Referring to figure A2.i,

The long wire and its connecting leads to the bridge:

$$\text{Let } \delta R_{La} + \delta R_{Lb} = \delta R_L \qquad \text{(B1)}$$

The short wire and its connecting leads to the bridge:

$$\text{Let } \delta R_{Sa} + \delta R_{Sb} = \delta R_S \qquad \text{(B2)}$$

$$\text{with } \delta R_{Lc} = \delta R_{Lc_1} + \delta R_{Lc_2} \qquad \text{(B3)}$$

$$\text{and } \delta R_{Sc} = \delta R_{Sc_1} + \delta R_{Lc_2} \qquad \text{(B4)}$$

being the contributions from the selector box present in the circuit. The selector box has a function of replacing the long and short wires in the arms of the bridge in order to evaluate the absolute resistances of each wire in turn. Thus, the wires connected to it contribute to the overall resistances. Therefore the current flowing through the arm of the bridge is:

$$i' = \frac{V}{R_1 + R_2 + R_L(t) + R_S(t) + \delta R_L + \delta R_S + \delta R_{Lc} + \delta R_{Sc}} \qquad \text{(B5)}$$

So, the heat generation in the long wire is:

$$i'^2\sigma_L = i'^2 \frac{R_L}{l_1} \qquad \text{(B6)}$$

where l_1 is the long wire length and σ_L is the resistance per unit length of the long wire.

In a transient run, where we are concerned with (R_L-R_S), the total resistances are:

$$[\ R_L + \delta R_L + \delta R_{Lc}\ ] - [\ R_S + \delta R_S + \delta R_{Sc}\ ] \qquad \text{(B7)}$$

$$\text{Therefore } \Delta R = (R_L-R_S) + (\delta R_L+\delta R_{Lc}) + (\delta R_S+\delta R_{Sc}) \qquad \text{(B8)}$$

And at equilibrium:

$$\Delta R = [R_L(0) - R_S(0)] + (\delta R_L+\delta R_{Lc}) + (\delta R_S+\delta R_{Sc}) \qquad \text{(B9)}$$

$$\text{Now } R_L + R_S = \frac{R_L - R_S}{l_1-l_2}.(l_1+l_2) - \frac{2\sigma_1\Sigma}{l_1-l_2}\, l_1.l_2 \qquad \text{(B10)}$$

$$\text{where } \Sigma = 1 - \sigma_2/\sigma_1 \qquad \text{(B11)}$$

Therefore the current flowing is:

$$i' = \frac{V}{R_1+R_2+\frac{(R_L-R_S)}{l_1-l_2}.(l_1+l_2)-\frac{2\sigma_1\Sigma.l_1.l_2}{l_1-l_2}+\delta R_L+\delta R_S+\delta R_{Lc}\delta R_{Sc}} \qquad \text{(B12)}$$

So $\Delta R = (R_L - R_S)_{measured} = (R_L + \delta R_L + \delta R_{Lc}) - (R_S + \delta R_S + \delta R_{Sc})$ (B13)

and $(R_L - R_S)_{measured} = \Delta R - (\delta R_L - \delta R_S) - (\delta R_{Lc} - \delta R_{Sc})$ (B14)

In greater detail, the current is:

$$i' = \frac{V}{R_1 + R_2 + \left[\frac{\Delta R - (\delta R_L - \delta R_S) - (\delta R_{Lc} - \delta R_{Sc})}{(l_1 - l_2)}\right].(l_1 - l_2) - \frac{2\sigma_1 \Sigma . l_1 . l_2}{(l_1 - l_2)}}$$

$$\ldots \frac{1}{+\delta R_L + \delta R_S + \delta R_{Lc} + \delta R_{Sc}} \quad \text{(B15)}$$

Note: l_1 = long wire length and l_2 = short wire length.

Now heat generated q is:

$$q = i'^2 \sigma_1 \quad \text{(B16)}$$

and $$\frac{\Delta R}{l_1 - l_2} = \sigma_w \quad \text{(B17)}$$

Therefore:

$$\frac{R_L - R_S}{l_1 - l_2} = \frac{l_1\sigma_1 - l_2\sigma_2}{l_1 - l_2} \quad \text{(B18)}$$

$$= \sigma_1 . \left[\frac{l_1 - l_2\sigma_1/\sigma_2}{l_1 - l_2} \right] \qquad \text{(B19)}$$

$$\text{So} \quad \sigma_1 = \frac{R_L - R_S}{[l_1 - l_2(1-\Sigma)]} \qquad \text{(B20)}$$

and with

$$R_L - R_S = l_1\sigma_1 - l_2\sigma_2 \qquad \text{(B21)}$$

giving

$$\sigma_1 = \frac{(R_L - R_S)}{l_1\left[1 - \frac{l_2}{l_1}.\frac{\sigma_2}{\sigma_1} \right]} \qquad \text{(B22)}$$

Rearranging yields:

$$\sigma_1 = \frac{(R_L - R_S) + l_2\sigma_2}{l_1} \qquad \text{(B23)}$$

To solve the bridge balance equations, we need $R_L(t)$ and $R_S(t)$, the resistances attained at time = t. It is necessary to evaluate $R_L(0)$ and $R_S(0)$ at the equilibrium conditions, that is prior to a transient run. This is done during the steady state measurement of the long wire and the short wire independently, using the selector box previousely mentioned. The selector is capable of substituting the long wire only, then the short wire only and then both wires together in order to evaluate the individual wires' resistances. Here, it is meant the absolute resistances of the wires R_L and R_S.

Therfore the measured long wire resistance at initial conditions is:

$$R_L(0)_{measured} = R_L(0)+\delta R_{Lc}+\delta R_{La}+\delta R_{Lb}+\delta R_{c_1} \qquad (B24)$$

and the measured short wire resistance at initial conditions is:

$$R_S(0)_{measured} = R_S(0)+\delta R_{Lc_2}+\delta R_{Sc_1}+\delta R_{Sb}+\delta R_{Sa}+\delta R_{c_1} \qquad (B25)$$

Therefore,

$$R_L = R_L(0)_{measured} - (\delta R_{Lc}+\delta R_L+\delta R_{c_1}) \qquad (B26)$$

and

$$R_S = R_S(0)_{measured} - (\delta R_{Sc_1}+\delta R_S+\delta R_{c_1}+\delta R_{Lc_2}) \qquad (B27)$$

with $\sigma_1 = \frac{R_L(0)}{l_1}$, and $\sigma_2 = \frac{R_S(0)}{l_2}$.

Note: The value of δR_{Sc_2} must be added to the R_2 value.

****

A2.3 Temperature Rise Evaluation.

The temperature rise of the wires can be calculated from the resistance difference of the long wire and the short wire during the

transient heating.

Therefore:

$$\Delta T' = \frac{\Delta R_{(t)} - \Delta R_{(0)}}{\alpha(T_o)\left[\Delta R_{(0)} - (\delta R_L - \delta R_s) - (\delta R_{Lc} - \delta R_{Sc})\right]} \tag{B28}$$

ΔT_w is evaluated from $\Delta T'$ as before (see section 3.8.6)

ΔR is the directly measured resistance difference,

$$R_L - R_S = \Delta R - (\delta R_L - \delta R_S) - (\delta R_{Lc} - \delta R_{Sc}) \tag{B29}$$

Now for the single wire measurement when the long wire only is in the circuit, the current is:

Long wire:

$$i' = \frac{V}{R_1 + R_2 + R_L(t) + \delta R_L + \delta R_{Lc} + \delta R_{c_1} + \delta R_{Sc_2}} \tag{B30}$$

$R_L(t)$ is found from the balance equations.

$$\Delta R_L = R_L + \delta R_L + \delta R_{c_1} + \delta R_{Lc} + \delta R_{Sc_2} \tag{B31}$$

Therefore

$$R_L = \Delta R_L - (\delta R_L + \delta R_{c_1} + \delta R_{Lc}) \tag{B32}$$

and the temperature rise is

$$\Delta T = \frac{\Delta R_L(t) - \Delta R(0)}{\alpha . R_L} \qquad \text{(B33)}$$

When the short wire only is in the circuit, that is substituted in place of the long wire, we get:

$$i' = \frac{V}{R_1+R_2+R_S(t)+\delta R_{Lc_2}+\delta R_{Sc_1}+\delta R_S+\delta R_{c_1}+\delta R_{Sc_2}} \qquad \text{(B34)}$$

and

$$\Delta R_S = R_S + \delta R_S + \delta R_{Lc_2} + \delta R_{c_1} + \delta R_{Sc_1} + \delta R_{Sc_2} \qquad \text{(B35)}$$

A2.4 Values of the Various Resistive Elements.

The resistances of the individual components in the resistance network were measured accurately with a very sensitive Ohmeter. The values of each resistance is included in the table below.

Component	Resistance (Ω)
δR_{Lc_1}	0.067
δR_{Lc_2}	0.073
δR_{c_1}	0.062
δR_{c_2}	0.061
δR_{Sc_1}	0.064
δR_{Sc_2}	0.068

****

Appendix 3.

A3.1 Calibration of Pressure Gauges.

The pressure gauges employed in the new instrument for the measurement of the thermal conductivity of electrically conducting liquids, were calibrated against a dead-weight tester. The dead-weight tester was described in detail elsewhere [14,71], and is accurate to better than 1MPa at 700MPa, and has been calibrated by the National Physical Laboratory.

A3.2 Calibration Constants.

The effective area of the piston A_p is given by:

$$A_{PT} = A_p(a + \Delta bT) \qquad (C1)$$

where

$$A_p = A_o(a + aP) \qquad (C2)$$

and

$$\Delta T = T - 293.15 \qquad (C3)$$

$$A_o = 3.227477 \times 10^{-6}\ m^2 \ \pm 1.29 \times 10^{-10}\ m^2 \qquad (C4)$$

$$a = 2.973\times10^{-6}\ \text{MPa}^{-1} \pm 1.45\times10^{-7}\ \text{MPa}^{-1} \qquad (C5)$$

$$b \approx 23\times10^{-6}\ \text{K}^{-1} \qquad (C6)$$

The pressure, p is then obtained as:

$$p = \frac{M.g}{A_{pT}} \qquad (C7)$$

where M is the total mass of the piston, carrier and weights.

The calibrations of the preesure gauges obtained are presented in table A3.1, and the pressure of the test fluid in the autoclave can be deduced from the gauge readings by the interpolation of the calibration data.

Gauge { 1 }.

Temperature °C	Gauge Reading (bar)	Mass (Kg)	Absolute Pressure (MPa)
20.0	670.0	22.315846	67.8917
20.5	960.0	31.973597	97.28745
20.5	1249.0	41.614696	126.60883
20.5	1540.0	51.280947	156.01580
20.5	1830.0	61.000047	185.49638
20.5	2119.0	70.610946	214.70003
20.5	2406.0	80.233146	243.87694
20.5	2696.0	89.893247	273.21781
20.5	2985.0	99.540397	302.51709
20.5	3270.0	109.166800	331.47862
20.5	3562.0	118.789800	360.97212
20.5	3851.0	128.451800	390.28115
20.5	4140.0	138.063250	419.47318
20.5	4428.0	147.704900	448.68373
20.5	4716.0	157.351600	477.89816
20.5	5010.0	167.083950	507.47117
20.5	5294.0	176.700650	536.50068
20.5	5585.0	186.365050	565.78832
20.5	5818.0	194.170850	589.45713

Table A3.1 Calibrations for gauge number { 1 }.

The low range pressure gauges were calibrated against another dead-weight tester independently. The results of their calibrations are presented in table A3.2.

Dead Weight (bar)	Up (bar)	Down (bar)	Mean (bar)
70	73	77	75.0
210	210	214	212.0
350	348	351	349.5
490	485	488	486.5
630	625	629	627.0
770	762	765	763.5
910	900	904	902.0
1050	1040	1043	1041.5
1190	1178	1181	1179.5
1330	1314	1317	1315.5
1470	1457	1457	1457.0

Table A3.2 Calibration of lower range pressure gauge.

The simple linear fit gives this equation:

$$P = -4.559 + 1.0132Pg \quad (\pm 1.1) \text{ bar} \qquad (C8)$$

The quadratic fit represents the data more realisticaly.

$$P = -5.834 + 1.0182Pg - 3.2306 \times 10^{-6} Pg^2 \quad (\pm 0.9) \text{ bar} \qquad (C9)$$

REFERENCES.

[1] J.V. Sengers, NBS Special Publication Number 590,(1980).

[2] J.T. Adams, Fluid Phase Equilibria, 29,23(1986)

[3] M.J. Assael, C.A.N. de Castro, W.A. Wakeham, Proceedings of the Int'l Chem. Eng. Conf., CHEMFOR 78, Braga, Portugal, (1978).

[4] A.J.F. Mendonca, M.J. Assael, C.A.N. de Castro, W.A. Wakeham, Rev. Port. Quim. 23,7(1981).

[5] J.B. Armstrong, S.F.Y. Li, W.A. Wakeham, ASME Annual Winter Meeting, Pheonix, Arizona, USA,1982.

[6] M.L. Matos Lopes, C.A.N. de Castro, W.A. Wakeham, Proceedings of the Int'l Chem. Eng. Conf.,CHEMFOR 85, Coimbra, Portugal, (1985).

[7] C.A.N. de Castro, W.A. Wakeham, Proc. of the First CODATA Symp. on Chem. Thermodyn. and Thermophys. Data Bases, Paris, France, (1985).

[8] A.H. Harrison, Fluid Phase Equilibria,29,47(1986).

[9] S. Machietto, G. Maduabeuke, R Szcepanski, Fluid Phase Equilibria, 29,59(1986).

[10] E.E. Shpil'rain, A.S. Umanski, Yu.A. Gorshov,High Temp.-High Pressures, 7,361(1975).

[11] M. Smoluchowski, Ann. Phys. u. Chem. 35,983(1911)

[12] J.J. de Groot, J. Kestin, H. Sookiazian, W.A. Wakeham, Physica, 92A,117(1978).

[13] J.J Healy, J.J. de Groot, J. Kestin, Physica, 82C,392(1976).

[14] J. Menashe. Ph.D. Thesis, London University, 1980

[15] M.J. Assael, M. Dix, A. Lucas, W.A. WAkeham, J. Chem. Soc. Faraday Trans. I.,77,439(1981).

[16] J.A.A. Snell, N.J. Trappeniers, A Botzen, Proc. Kon. Ned. Akad. Wet.,82B,303(1979).

[17] R. Tufeu, Ph.D. Thesis, University of Paris IV, 1971.

[18] H.M. Roder, D.E. Diller, J. Chem. Phys., 52,592 (1970).

[19] R. Siegel, Trans. ASME 80,347(1958).

[20] J.A. Schetz, R.J. Eichorn, J. Heat Transfer,Trans ASME, 84, ser. C,334(1962).

[21] R.J. Goldstein, D.G. Briggs, J. Heat Transfer, Trans ASME, 86, ser. C,490(1964).

[22] A. Michels, J.V. Sengers, P.S. Van der Gulik, Physica, 28,586(1962).

[23] C.A.N. de Castro, W.A. Wakeham, Proc. 1st Nat. Cong. on Pure and Applied Maths., Lisbon (1974).

[24] H.S. Carslow, J.S Jaeger, Conduction of Heat In Solids, 2nd Edition, Oxford University Press, (1959), p 261.

[25] J. Menashe, W.A. Wakeham, Int. J. Heat and Mass Transfer, 25,661(1982).

[26] H. Poltz, Int. J. Heat and Mass Transfer, 8,515(1965).

[27] H. Poltz, Int. J. Heat and Mass Transfer, 8,609(1965).

[28] H. Poltz, R. Jugel, Int. J. Heat and Mass Trans.10,1075 (1967).

[29] W. Liedenfrost, paper presented at Thermal Conductivity Conference, Gattingberg, Tennesse, USA (1963).

[30] I. Rhyming, Int. J. Heat and Mass Transfer, 9,315(1960).

[31] R.G. Diessler, J. Heat Transfer, Trans-ASME, 86,240(1960).

[32] R. Grief, G.P. Clapper, Appl. Sci. Res.,(15)A.

[33] S. Rosseblad, Astrophysik und Atom-Theoretische Grundlage Springer Verlag, Berlin, 41(1931).

[34] M. Perlmutter, J.R. Howell, J. Heat Transfer, Trans-ASME 86,69(1964).

[35] E.F.M. Van der Held, Appl. Sci. Res.3A,237(1952)

[36] E.F.M. Van der Held, Appl. Sci. Res.4A,77(1952).

[37] A Saito, N. Mani, J.E.S. Venart, Proc 16th Nat. Heat Transfer Conf. 76-CSME/CSChE-6 (1976).

[38] A. Saito, J.E.S. Venart, Proc. 6th Int. Heat Tran. Conf. 3,79(1978).

[39] A. Saito, Bull. of the JSME, 23,1459(1980).

[40] C.A.N. de Castro, J.C.G. Calado, W.A. Wakeham, 6th European Thermophys. Props. Conf., Yogoslavia (1978).

[41] C.A.N. de Castro, S.F.Y. Li, G.C. Maitland, W.A. Wakeham, Int. J. Thermophys. 4,311(1983).

[42] B. Taxis., DIC Thesis, (1987).

[43] E.N. Haran, W.A. Wakeham, J. Phys.E.15,839(1982).

[44] J.W Haarman, Ph.D. Thesis, Technische Hogeschool, Delft, The Netherlands, (1959).

[45] J.J. de Groot, J. Kestin, H. Sookiazian, Physica,75,454 (1974).

[46] J. Kestin, W.A. Wakeham, Physica, 92A,102(1978).

[47] C.A.N. de Castro, J.C.G. Calado, W.A. Wakeham, M. Dix, J. Phys. E: Scient. Instrum. 9,1073(1976).

[48] J. Kestin, R. Paul, A.A. Clifford, W.A. Wakeham, Physica, 100A,349(1980).

[49] J.H. Haarman, Physica, 52,605(1971).

[50] J.H. Blackwell, Can. J. Phys. 34,437(1917).

[51] J. Fischer, J. Ann. Phys. 34,669(1939).

[52] M. Smoluchowski, Phil. Mag. 21,11(1911).

[53] Y. Nagasaka, A. Nagashima, J. Phys. E: Scient. Instrum. 14,1435(1981).

[54] Y. Nagasaka, Ph.D. Thesis, Keio University, Japan (1982).

[55] Y. Nagasaka, A. Nagashima, Thermal Conductivity of Liquids, Physics Abstracts 44.50 (1981).

[56] T.N. Vezuroglu, Prog. Astro. Aero. 879(1967).

[57] J. Menashe, W.A. Wakeham, Ber. Bunsengesell. Phys Chem, 85,340(1981).

[58] J.C.G. Calado, U.V. Mardolcar, C.A.N. de Castro, H.M. Roder, W.A. Wakeham, Physica, 143A,314(1987)

[59] B. Stolhane,S. Pyle, Teknisk Tidskrift, 61,38(1931).

[60] Y. Nagasaka, A. Nagashima, Rev. Sci. Instrum. 52,229(1981).

[61] P.G. Knibbe, R.D. Raal, Int. J. of Thermophys. 8,181(1987).

[62] J.R. Parson Jr, J.C. Muuligan, Rev. Sci. Instrum.49,1460 (1978).

[63] O. Nilsson, O. Sandberg, G. Backstrom, Rev. Sci. Instrum. (in press).

[64] J.M.N.A. Fareleira, C.A.N. de Castro, (To be Published).

[65] C.A.N. de Castro, B. Taxis, W.A. Wakeham (in press).

[66] W.A. Wakeham, M. Zalaf, Fluid Phase Equilibria, 36,183 (1987).

[67] C.A.N. de Castro, S.F.Y. Li, R.D. Trengove, W.A. Wakeham, J. Chem. Ref. Data, 15,1097(1986).

[68] H. Kashiwagi, T. Hashimoto, Y. Tanaka, H. Kubota, T. Makita, Int. J. of Thermophys., 3,3(1982).

[69] N.B. Vargaftik, ed., Tables on the Thermophysical Properties of Liquids and Gases, 2nd Edition, Wiley, New York (1975).

[70] B. Taxis, W.A. Wakeham, M. Zalaf, Int. J. of Thermophys., 9(1),21(1988).

[71] S.F.Y. Li, Ph.D. Thesis, London University,(1984)

[72] A.A. Clifford, J. Kestin, W.A. Wakeham, Physica, 100A,370 (1980).

[73] G.C. Maitland, M. Mustafa, M. Ross, R.D.Trengove, W.A. Wakeham, M. Zalaf, 9th ASME Symposium on Thermophys. Props., Boulder, Colorado, USA (1985)

[74] C.A.N. de Castro, R.D. Trengove, W.A. Wakeham, Rev. Port. Quim. (in press).

[75] A.M.F. Palavra, W.A. Wakeham, M. Zalaf, High Temp-High Pressures, 18,405(1986).

[76] D.A. Vermilyea, J. of Electrochem. Soc. 101(8), 389(1954).

[77] D.A. Vermilyea, Acta Metallurgica, 1,282(1953).

[78] A. Alloush, W.B. Gosney, W.A. Wakeham, Int. J. Thermophys., 3(3),225(1982).

[79] International Practical Temperature Scale of 1968, (NPL), HMSO, London, (1968).

[80] M.J. Assael, Ph.D. Thesis, London University, (1980).

[81] W.A. Wakeham, M. Zalaf, Physica, 139,140B,106(1986).

[82] K.N. Marsh, ed. Pure and Applied Chem., 53,1863(1981).

[83] C.A.N. de Castro, J.C.G. Calado, W.A. Wakeham, Proc. 7th Symp. Thermophys. Props., 730(1970).

[84] C.A.N. de Castro, W.A. Wakeham, Thermal Cond. 18,65(1984).

[85] Y. Nagasaka, A. Nagashima, Ind. Eng. Chem. Fundam. 20,216 (1981).

[86] A. Easteal, L.A. Woolf, J. Chem. Eng. Data, 31,265(1986).

[87] P.W. Bridgman, Proc. Am. Acad. Arts Sci. 66,182(1932).

[88] H. Kratske, S. Muller, H. Bohn, R. Kohler, J. Chem. Thermodyn. 17,283(1985).

[89] M. Gehrig, H. Lentz, J. Chem. Thermodyn., 11,291(1979).

[90] A.M. Mamedov, T.C. Alchendov, A. Abdullaev, Izh. Fiz. Zh., 30,705(1976).

[91] J.D. Isdale. (to be published).

[92] L.T. Carmichael, J. Jacobs, B.H. Sage, J. Chem. Eng. Data, 14,31(1969).

[93] G.Kh. Mukhamedzyanov, A.G. Usmanov, Inzh-fiz Zh., 13,177 (1967).

[94] G.F. Bogatov, Yu.L. Rastorguev, B.A. Grigor'ev, Khim. Tekhn. Topl. Masel, 9,31(1969).

[95] Y.L. Rastorguev, V.V. Pugach, Izv. Vyssh. Uchebn. Zaved. Neft'i Gaz, 13(8),69(1970).

[96] Ya. M. Naziev, A.A. Abasov, Izv. Vyssh. Uchebn. Zaved. Neft'i Gaz, 12,65(1969).

[97] L. Haar, J.S. Gallagher, G.S. Kell, Proc. of the 8th Symp. on Thermophys. Props., ed. J.V.Sengers, ASME, New York, II,298(1982).

[98] L. Haar, J.S. Gallagher, G.S. Kell, NBS/NRC Steam Tables, Washington DC, USA, (1984).

[99] W.D. Westwood, N. Waterhouse, P.S. Wilcox, Tantalum Thin Films.

[100] J.V. Sengers, J.T.R. Watson, R.S. Basu, B. Kamgar-Parsi, R.C. Hendricks, J. of Phys. and Chem. Ref. Data, 13(3), 893(1984).

[101] IAPS " The Provisional IAPS Formulation 1982 for the Thermodynamic Properties of Ordinary Water Substance for Scientific and General Use "(1984)

[102] J.H. Dymond, Physica, 75,100(1974).

[103] J.H. Dymond, T.A. Brawn, The Transport Properties of Fluids, Theory, Estimation, and Use. HMSO, Edinburgh, (1979).

[104] M. Assael, C.A.N. de Castro, W.A. Wakeham, Proc. of Chem. Port. (University of Braga, 1978)I, p161.

[105] G.C. Maitland, E.B. Smith, Chem. Soc. Rev., 2,181(1973).

[106] L.A. Viehland, E.A. Mason, S.I. Sandler,J. Chem. Phys., 68,5277(1978).

[107] S. Chapman, T.G. Cowling, Mathematical Theory of Non-Uniform Gases, Cambridge, (1952).

[108] P. Pesibois, M. De Leener, Classical Kinetic Theory of Liquids, Chapter IV, Wiley, New York, (1977).

[109] S.A. Rice, P. Gray, The Statistical Mechanics of Simple Liquids, (Interscience), New York, (1977)

[110] G.C. Maitland, M. Rigby, E.B. Smith, W.A. Wakeham, Intermolecular Forces-Their Origin and Determination, Clarendon Press, Oxford, (1981).

[111] P. Gray, Physics of Simple Liquids, H.N.V. Temperley, J.S. Rowlinson, G.S. Rushbrooke, North Holland, Amsterdam, (1968).

[112] N.A. Metropolis, A.W. Rosenbluth, M.N. Rosenbluth, A.H. Teller, J. Chem. Phys., 21,1087(1953).

[113] W.W. Wood, F.R. Parker, J. Chem. Phys.,27,720(1957).

[114] E.M. Gosling, I.R. McDonald, K. Singer, Mol. Phys. 26,1475 (1973).

[115] W.T. Ashurst, W.G. Hoover, Phys. Rev. A, 11,658(1975).

[116] D.J. Evans, Phys. Rev. A, 23,1988(1981).

[117] D. Fincham, D.M. Heyes, Chem. Phys.,78,425(1983)

[118] B.J. Alder, T. Einwohner, J. Chem. Phys., 43,3399(1965).

[119] T. Einwohner, B.J. Alder, J. Chem. Phys., 49,1458(1968).

[120] B.J. Alder, D.M. Gass, T.W. Wainwright, J. Chem. Phys., 53,3813(1970).

[121] B.J. Alder, T.W. Wainwright, J. Chem. Phys., 27,1208(1957).

[122] B.J. Alder, T.W. Wainwright, J. Chem. Phys., 31,459(1959).

[123] S. Glasstone, K.J. Laidler, H. Eyring,The Theory of Rate Processes, McGraw-Hill Book Co. Inc., New York, (1941).

[124] S.A. Rice, A.R. Allnott, J. Chem. Phys., 34,2210(1961).

[125] T. Kihara, Rev. Mod. Phys., 24,45(1952).

[126] A. Einstein, The Papers are Collected in Investigations on the Theory of the Brownian Movement, Dover, New York, (1956).

[127] R.E. Eisenschitz, Statistical Theory of Irreversible Processes, (1958).

[128] P. Chandrasekhar, Rev. Mod. Phys., 15,1(1943).

[129] R.E. Powell, W.E. Roseveare, H. Eyring, Ind. Eng. Chem., 33,430(1941).

[130] H.T. Davis, S.A. Rice, J.V. Sengers, J. Chem. Phys., 35,2210,(1961).

[131] E.B. Smith, B.J. Alder, J. Chem. Phys. 30,1190(1959).

[132] B.J. Alder, T.E. Wainwright, Transport Processes in Statistical Mechanics, I. Prigogoine Ed., Interscience Pub. Inc., New York, p 97, (1959).

[133] H.L. Frisch, B. Berne, J. Chem. Phys., 43,250(1965).

[134] D. Enskog, Kungl. Svenska Net-Ak Handl., 4,63(1922).

[135] N.F. Carnahan, K.E. Starling, J. Chem. Phys., 51,635(1969).

[136] J.H. Dymond, B.J. Alder, J. Chem. Phys., 45,2061(1966).

[137] B.J. Alder, T.E. Wainwright, The Many-Body Problem, S.K. Percus Ed., Interscience Pub. Inc. New York, (1963).

[138] B.J. Alder, T.E. Wainwright, Phys. Rev. Letters, 18,988 (1967).

[139] J.H. Dymond, Chem. Soc. Reviews, 14,317(1985).

[140] J.H. Dymond, B.J. Alder, J. Chem. Phys., 48,343(1968).

[141] J.H. Dymond, B.J. Alder, Ber. Bunsenges. Phys. Chem. 75,394(1971).

[142] P.H. Oosting, N.J. Trappeniers, Physica, 51,418(1971).

[143] K.R. Harris, Physica, 94A,448(1978).

[144] K.R. Harris, N.J. Trappeniers, Physica, 104A,262(1980).

[145] J.H. Dymond, T.A. Brawn, Proc. Symp. of Transp. Props. of Fluids, NEL, East Kilbride, HMSO(1979)

[146] B. Arends, K.O. Prins, N.J. Trappeniers, Physica, 107A,307 (1981).

[147] A.J. Easteal, L.A. Woolf, D.C. Jolly, Physica, 121A,286 (1983).

[148] A.J. Easteal, L.A. Woolf,Physica, 124B,286(1984).

[149] N.J. Trappeniers, A. Botzen, H.R. Van Ven Berg, J. Oosten, Physica, 30,985(1964).

[150] A. Michels, A. Botzen, W. Shuurman, Physica, 20,1141 (1954).

[151] E.G. Reynes, G. Thodos, Physica, 30,1529(1964).

[152] J.A. Grachi, G.P. Flynn, J. Ross, Chem. Phys. 51,3856 (1969).

[153] N.J. Trappeniers, A. Botzen, J.Van Oosten, H.R. Van Den Berg, Physica, 31,945(1965).

[154] J.H. Dymond, T.A. Brawn, "Molecular Theories of Transport in Dense Fluids" in Transport Properties of Fluids and Fluid Mixtures, HMSO, Edinburgh, (1980).

[155] U.V. Mardolcar, C.A.N. de Castro, Ber. Bunsenges. Phys. Chem., 91,152(1987).

[156] A. Michels, J.V. Sengers, L.J.M. Van de Klundert, Physica, 29,149(1963).

[157] R. Tufeu, D. Vidal, M. Lallemand, B. Le Neindre, High Temp-High Pressures, 11,587(1979).

[158] J.P.J. Michels, N.J. Trappeniers, Physica, 107A,299(1979).

[159] H.M. Roder, C.A.N. de Castro, U.V. Mardolcar, Int. J. Thermophys., 8(5),521(1987).

[160] B.A. Younglove, H.J.M. Handley, J. Chem. Ref. Data, 15,1323(1986).

[161] J.H. Dymond, Physica, 79A,65(1975).

[162] C.A.N. de Castro, H.M. Roder, J. Reo. Nat. Bun. Stand., 86,293(1981).

[163] D. Chandler, J. Chem. Phys., 60,3500(1975).

[164] D. Chandler, J. Chem. Phys., 62,1358(1975).

[165] M.A. McCool, L.A. Woolf, J. Chem. Soc. Faraday Trans, 68,1971(1972).

[166] J.H Dymond, J. Chem. Phys., 60,969(1974).

[167] W. Condiff, W. Lu, J.S. Dahler, J. Chem. Phys., 42,3445 (1965).

[168] B.J. McCoy, S.I. Sandler, J.S. Dahler, J. Chem. Phys. 45,3485(1966).

[169] M. Theodosopulu, J.S. Dahler, J. Chem. Phys.,60,3567(1974).

[170] M. Theodosopulu, J.S. Dahler, J. Chem. Phys.,60,4048(1974).

[171] K.R. Harris, Physica, 93A,593(1978).

[172] J.H. Dymond, T.A. Brawn, Proc 7th Symposium Thermophys. Properties, ASME, NewYork, p 660, (1977).

[173] A.F. Collings, E. McLaughlin, Trans. Faraday Soc. 67,340 (1971).

[174] H.J. Parkhurst Jr, J. Jonas, J. Chem Phys., 63,2705(1975).

[175] M.A. McCool, A.F. Collings, L.A. Woolf, J. Chem. Soc. Faraday I, 68,1489(1972).

[176] J.H. Dymond, T. Robertson, J.D. Isdale, Int. J. Thermophys. 2,133(1981).

[177] J.D. Isdale, J.H. Dymond, T.A. Brawn, High Temp-High Pressures, 11,571(1979).

[178] J.H. Dymond, T. Robertson, J.D. Isdale, Int. J. Thermophys. 2,223(1981).

[179] J. Menashe, M. Mustafa, M. Sage, W.A. Wakeham, Proc. 8th Symp. on Thermophys. Properties, p254, ASME, New York, (1981).

[180] H.M. Roder, Int. J. Thermophys. 6,119(1985).

[181] J.H. Dymond, Physica, 85A,175(1976).

[182] J.H. Dymond, Chem. Phys., 17,101(1976).

[183] S.F.Y. Li, G.C. Maitland, W.A. Wakeham, Ber. Bunsenges. Phys. Chem., 83,32(1984).

[184] S.F.Y. Li, G.C. Maitland, W.A. Wakeham, High Temp-High Pressures, 17,241(1985).

[185] J.H. Dymond, K.J. Young, J.D. Isdale, Int. J. Thermophys., 1,347(1980).

[186] A.M.F. Palavra, W.A. Wakeham, M. Zalaf, Int. J.Thermophys., 8(3),305(1987).

[187] A.M.F. Palavra, W.A. Wakeham, M. Zalaf, Int. J.Thermophys., 6,5(1985).

[188] S.F.Y. Li, W.A. Wakeham, M. Zalaf, Int. J. Thermophys., 8(4),407(1987).

[189] D.E. Diller, J. Chem. Eng. Data, 27,240(1982).

[190] D.E. Diller, L.J. Van Poolen, Int. J. Thermophys. 6(1),43 (1985).

[191] D.E. Diller, J.M. Saber, Physica, 108A,143(1981)

[192] H.M. Roder, C.A.N. de Castro, J. Chem. Eng. Data, 27,12 (1982).

[193] H.M. Roder, C.A.N. de Castro, High Temp-High Pressures, 17(4),453(1985).

[194] C.A.N. de Castro, R. Tufeu, B. Le Neindre, Int. J. Thermophys., 4,11(1983).

[195] S.F.Y. Li, R.D. Trengove, W.A. Wakeham, M. Zalaf, Int. J. Thermophys., 7,273(1986).

[196] S.F.Y. Li, G.C. Maitland, W.A. Wakeham, Int. J.Thermophys., 5,351(1984).

[197] C.A.N. de Castro,S.F.Y. Li, G.C. Maitland, W.A. Wakeham, Int. J. Thermophys., 4,311(1983).

****

List Of Publications.

1. Thermal conductivity of electrically-conducting liquids at high pressure.

W.A. Wakeham, M. Zalaf.

Physica, 139 & 140B,105(1986).

2. The thermal conductivity of carbon tetrachloride in the temperature range 310 to 364 K at pressures up to 0.2 GPa.

A.M.F. Palavra, W.A. Wakeham, M. Zalaf.

Int. J. Thermophys., 6,5(1985).

3. The transport properties of polyatomic fluids.

S.F.Y. Li, R.D. Trengove, W.A. Wakeham, M. Zalaf.

Int. J. Thermophys., 7(2),273(1986).

4. Transient hot-wire measurements of the thermal conductivity of gases at elevated temperatures.

G.C. Maitland, M. Mustafa, M. Ross, R.D. Trengove, W.A. Wakeham, M. Zalaf.

Int. J. Thermophys., 7(2),245(1986).

5. Absolute measurements of the thermal conductivity of helium and hydrogen.

M. Mustafa, M. Ross, R.D. Trengove, W.A. Wakeham, M. Zalaf.

Physica, 141A,233(1987).

6. Thermal conductivity of normal pentane in the temperature range 306-360 K at pressures up to 0.5 GPa.

A.M.F. Palavra, W.A. Wakeham, M. Zalaf.

Int. J. Thermophys., 8(3),305(1987).

7. Thermal conductivity of ethylbenzene in the temperature range 31-84°C at pressures up to 0.5 GPa.

A.M.F. Palavra, W.A. Wakeham, M. Zalaf.

High Temp.-High Press., 18,405(1986).

8. Thermal conductivity of oct-1-ene in the temperature range 307 to 360 K at pressures up to 0.5 GPa.

S.F.Y. Li, W.A. Wakeham, M. Zalaf.

Int. J. Thermophys., 8(4),407(1987).

9. The thermal conductivity of some electrically conducting liquids.

W.A. Wakeham, M. Zalaf.

Fluid Phase Equilibria, 36,183(1987).

10. The thermal conductivity of argon, carbon dioxide, and nitrous oxide.

J. Millat, M. Mustafa, M. Ross, W.A. Wakeham, M. Zalaf.

Physica, 145A,461(1987).

11. The thermal conductivity of neon, methane and tetrafluoromethane.

J. Millat, M. Ross, W.A. Wakeham, M. Zalaf.

Mol. Phys., 148A,124(1988).

12. The thermal conductivity of the xylene isomers.

B. Taxis, W.A. Wakeham, M. Zalaf.

Int. J. Thermophys., 9(1),21(1988).

List of Figures

		Page
2.i	The idealized experimental arrangement	14
2.ii	Temperature profile around the wire	20
2.iii	Effect of convection on temperature rise	22
2.iv	Hot wire arrangement for electrically conducting liquids	40
3.i	The thermal conductivity cells for electrically insulating liquids	63
3.ii	The new arrangement for the installation of the platinum wires in the thermal conductivity cells for electrically non-conducting liquids	65
3.iii	The thermal conductivity cells for electrically conducting liquids	68
3.iv	Spot-welding technique for the tantalum wires	70
3.v	The tantalum wires' assembly prior to placing in the Inconel thermal conductivity cells	74
3.vi	Postulated distribution of potential during anodic oxidation of tantalum	77
3.vii	The high pressure vessel, with the Inconel cells	80
3.viii	The pressurizing system	83
3.ix	Deviation of the measurement of the resistance of tantalum wire as a function of temperature from the correlation of equation (3.6)	90
3.x	A schematic diagram of the new bridge arrangement for the measurement of the thermal conductivity of liquids	95

3.xi	The automatic bridge for the measurement of the thermal conductivity, showing the currents for the circuit analysis	98
3.xii	The different earthing arrangements for both electrically conducting and insulating liquids	103
3.xiii	The comparator for the electronic bridge	106
4.i	The thermal conductivity of toluene as a function of pressure for three isotherms	123
4.ii	Comparison of the thermal conductivity data of toluene	124
4.iii	The deviations of the thermal conductivity data from their correlation as a function of pressure by equation (4.2) for liquid CCl_4	162
4.iv	The deviation of the experimental thermal conductivity of n-pentane from the correlation of equation (4.2)	164
4.v	The deviation of the thermal conductivity data from their correlation as a function of pressure by equation (4.2) for the xylene isomers	165
4.vi	The deviation of the experimental thermal conductivity data of oct-1-ene from the correlation of equation (4.2)	166
4.vii	The deviation of the experimental thermal conductivity of ethylbenzene from the correlation of equation (4.2)	167
4.viii	Deviation of the corrected, experimental temperature rise as a function of time from a linear fit in $\ell n\ t$ for a measurement in water at T = 302.65 K and P = 102.7 MPa	178

4.ix	Deviation of the experimentally measured temperature rise of the tantalum wire from a linear fit vs. ℓn t for a run in water at T =298K	179
4.x	Deviation of the present experimental data for thermal conductivity of water from the IAPS correlation	183
5.i(a)	Van der Waals model	198
5.i(b)	Realistic pair potential function	198
5.ii	The thermal conductivity ratio for n-pentane as a function of reduced molar volume	238
5.iii	Deviation of the experimental thermal conductivity of n-pentane from equation (5.64) as a function of density	239
5.iv	Deviation of the experimental thermal conductivity of n-pentane from equation (5.65) for individual isotherms	240
5.v	The thermal conductivity ratio as a function of the reduced molar volume for oct-1-ene	244
5.vi	Deviation of the thermal conductivity of oct-1-ene from the correlation of equation (5.66)	245
5.vii	Deviation of the thermal conductivity of oct-1-ene from the correlation of equation (5.67), universal among the alkanes	246
5.viii	The thermal conductivity ratio for CCl_4 as a function of reduced molar volume	249
5.ix	Deviation of the thermal conductivity data from their correlation as a function of molar volume by equation (5.71)	250
5.x	The function η^* for CCl_4	251

5.xi	The function D^* for CCl_4	252
5.xii	The thermal conductivity ratio for ethylbenzene as a function of reduced molar volume	257
5.xiii	Deviation of the experimental thermal conductivity data for ethylbenzene from the correlation of equation (5.76)	258
5.xiv	The thermal conductivity ratio for o-xylene as a function of reduced molar volume	261
5.xv	Deviation of the thermal conductivity data of the three isomers of xylene from the correlation of equation (5.78)	262
5.xvi	The thermal conductivity ratio as a function of reduced molar volume for the fluids studied in this work, in addition to some previously studied	266
5.xvii	Deviation of the experimental thermal conductivity data from the correlation of equation (5.80)	270
5.xviii	The characteristic volumes, V_o^u as a function of the number of carbon atoms of a series of n-alkanes	274
5.xix	The characteristic volumes, V_o^u for liquids studied in this work	275
A1.i	Diagram of the new automatic Wheatstone bridge, depicting the currents flowing in the circuits	283
A1.ii	An illustration of the leakage currents encountered in the bridge for electrically insulating liquids	290
A2.i	The bridge circuit with the various resistive elements	292

List of Tables

		Page
3.1	The characteristics of the thermal conductivity cells for electrically insulating liquids	66
3.2	The characteristics of the thermal conductivity cells for electrically conducting liquids	72
3.3	Bridge components	101
4.1	Summary of liquids employed for thermal conductivity measurements, their purity and sources	120
4.2	Thermal conductivity of toluene	121
4.3	Thermal conductivity of toluene with new bridge	125
4.4	Thermal conductivity of CCl_4 at T_{nom}= 310.15 K	130
4.5	Thermal conductivity of CCl_4 at T_{nom}= 322.65 K	131
4.6	Thermal conductivity of CCl_4 at T_{nom}= 342.65 K	132
4.7	Thermal conductivity of CCl_4 at T_{nom}= 359.65 K	133
4.8	Thermal conductivity of CCl_4 at T_{nom}= 364.50 K	134
4.9	Thermal conductivity of n-pentane at T_{nom}= 305.8 K	135
4.10	Thermal conductivity of n-pentane at T_{nom}= 322.8 K	137
4.11	Thermal conductivity of n-pentane at T_{nom}= 342.5 K	139
4.12	Thermal conductivity of n-pentane at T_{nom}= 359.5 K	141
4.13	Thermal conductivity of o-xylene at T_{nom}= 308.15 K	143
4.14	Thermal conductivity of o-xylene at T_{nom}= 318.15 K	144
4.15	Thermal conductivity of o-xylene at T_{nom}= 337.65 K	145
4.16	Thermal conductivity of o-xylene at T_{nom}= 360.15 K	146
4.17	Thermal conductivity of oct-1-ene at T_{nom}= 307.65 K	147
4.18	Thermal conductivity of oct-1-ene at T_{nom}= 320.65 K	148
4.19	Thermal conductivity of oct-1-ene at T_{nom}= 344.15 K	149

4.20	Thermal conductivity of oct-1-ene at T_{nom}= 360.15 K	150
4.21	Thermal conductivity of ethylbenzene at T_{nom}=304.65K	151
4.22	Thermal conductivity of ethylbenzene at T_{nom}=319.15K	152
4.23	Thermal conductivity of ethylbenzene at T_{nom}=339.65K	153
4.24	Thermal conductivity of ethylbenzene at T_{nom}=357.15K	154
4.25	Coefficients of the correlation for the pressure dependence of the thermal conductivity of CCl_4 from equation (4.2)	156
4.26	Coefficients of the correlation for the pressure dependence of the thermal conductivity of n-pentane from equation (4.2)	157
4.27	Coefficients of the correlation for the pressure dependence of the thermal conductivity of o-xylene from equation (4.2)	158
4.28	Coefficients of the correlation for the pressure dependence of the thermal conductivity of oct-1-ene from equation (4.2)	159
4.29	Coefficients of the correlation for the pressure dependence of the thermal conductivity of ethylbenzene from equation (4.2)	160
4.30	Thermal conductivity of water at T_{nom}= 302.65 K	173
4.31	Thermal conductivity of water at T_{nom}= 324.15 K	174
4.32	Thermal conductivity of water at T_{nom}= 341.65 K	175
4.33	Thermal conductivity of water at T_{nom}= 302.65 K up to 300 MPa	176
5.1(a)	Characteristic volume, V_o, for n-pentane	237
5.1(b)	Coefficients of equation (5.61) for n-pentane	237
5.2	Characteristic volumes, V_o, for oct-1-ene	243
5.3	Characteristic volumes, V_o, for CCl_4	253

5.4	Characteristic volumes, V_o, for ethylbenzene	253
5.5	Characteristic volumes, V_o, for three isomers of xylene	254
5.6	Coefficients of the correlation of equation (5.61) for individual isotherms of ethylbenzene	259
5.7	Coefficients of the correlation of equation (5.61) for individual liquids	267
5.8	The characteristic volumes, V_o^u , for the correlation of equation (5.80) for all the liquids studied	271
A3.1	Calibration gauge number {1}	302
A3.2	Calibration for the lower pressure range gauge	303

xxxxxxxxxxxxxxxxxxxxxxxxxxxxxxxxxxxxxxxxxxxxxxxxxxxxxxxx